國立交通大學

土木工程學系

博士論文

整合式無線感測網路之結構健康監測系統

於建築與土木結構之研發

DEVELOPMENT OF AN INTEGRATED WIRELESS SENSOR NETWORK-BASED STRUCTURAL HEALTH MONITORING SYSTEM FOR BUILDINGS AND CIVIL INFRASTRUCTURES

研 究 生:林 子 軒

指導教授: 洪 士 林 博士

中華民國一百年六月

整合式無線感測網路之結構健康監測系統於建築與土木結構之研發

DEVELOPMENT OF AN INTEGRATED WIRELESS SENSOR NETWORK-BASED STRUCTURAL HEALTH MONITORING SYSTEM FOR BUILDINGS AND CIVIL INFRASTRUCTURES

研 究 生：林 子 軒　　**Student: Tzu-Hsuan Lin**

指導教授：洪 士 林　博士　　**Advisor: Dr. Shih-Lin Hung**

國 立 交 通 大 學

土 木 工 程 學 系

博 士 論 文

A Dissertation

Submitted to Department of Civil Engineering

College of Engineering

National Chiao Tung University

In partial Fulfillment of the Requirements

for the Degree of

Doctor of Philosophy

in

Civil Engineering

June 2011

Hsinchu, Taiwan, Republic of China

中 華 民 國 一 百 年 六 月

整合式無線感測網路之結構健康監測系統

於建築與土木結構之研發

研究生：林子軒　　指導教授：洪士林 博士

國立交通大學

土木工程學系

摘要

本研究提出一整合式無線感測網路之結構健康監測系統架構並應用於建築與土木結構上。此架構主要包含了感測、資訊融合與管理以及決策診斷。在此架構目標下，本研究發展了一個整合式無線感測網路結構健康監測系統。此系統由多種無線節點所組成，包含感測結點、簇首節點、傳送節點與基地台。感測結點主要以 Imote2 平台為基礎，用來量測結構的動態反應或是環境參數。簇首節點為雙核心之設計結合了 Imote2 平台與額外之嵌入式系統。簇首節點含有額外之無線通訊模組與 GPS 來進行較長距離之資料接收、交換，並可以進行定位與同步之用。傳送節點可當作協調者並進行資料的跳躍傳送(Hopping)。基地台主要為接收所有回傳的感測資料與訊息，其硬體能力為所有結點中最高的。此系統亦包含了一個三層式的軟體架構，主要可以進行可靠的資料感測與傳輸、資料儲存、視覺化之使用者介面、資料分析與訊號處理等工作。在此軟體架構下，無線感測相關的結構健康監測的應用將可以很容易地被實行。此外，能源的消耗亦是無線感測的一個很重要的問題，因此，本研究發展了一個結合壓電、風車、與磁場的整合式能源擷取系統來改善能源消耗的問題。 結構健康監測可分為局部與全域之方法，然而，兩種方法各有其優缺點與應用之時機。因此本研究發展了一個整

合式的結構損害評估方法整合全域與局部之結構損害評估法，應用於結構健康監測上。在全域結構損害偵測方面，本文分別提出了新的子結構頻率響應函數法來對結構進行大範圍之損害評估。接著，以電機阻抗為主之局部損害評估法則可以用來進行小範圍局部損害之評估。

在實驗與數值模擬研究中，數值模擬的結果發現本文所提出之結構損壞評估方法可以成功地找出結構發生損壞的位置。另外無線感測網路結構健康監測系統亦於一縮尺之建築模型上進行驗證，其實驗結果證實此系統可進行高質量的感測與資料傳輸並可以精確地獲得結構的相關動態反應參數。為驗證所發展之無線感測網路結構健康監測系統應用於實際土木結構上之可行性，將此系統佈設於一橋梁上進行驗證。實驗結果顯示，此系統於實際土木之結構上依然可以獲得相當好的感測結果，無線傳輸也可以達到預期的效果。在實際土木結構監測的佈設上更可以發現本系統之優點，在實驗過程中，平均一個節點的建置小於 5 分鐘，比起傳統有線的監測系統來說，在時間成本的節省上更顯現出本系統的優勢。在六層樓縮尺模型試驗中，亦可以證實本研究所提出之整合式的結構損害評估方法可以識別出結構之全域與局部之損害。

DEVELOPMENT OF AN INTEGRATED WIRELESS SENSOR NETWORKS-BASED STRUCTURAL HEALTH MONITORING SYSTEM FOR BUILDINGS AND CIVIL INFRASTRUCTURES

Student: Tzu-Hsuan Lin **Advisor: Dr. Shih-Lin Hung**

Department of Civil Engineering

College of Engineering

National Chiao Tung University

ABSTRACT

The main purpose of this dissertation was to propose a framework for an integrated wireless sensor network (WSN)-based structural health monitoring (SHM) system in buildings and civil infrastructures. In this framework, three main parts were considered: the physical sensing; information fusion and management; and inference and decision making. To achieve this goal, an integrated WSN-based SHM system was developed. This system consists of sensing nodes, cluster head nodes, transfer node, and base station. The sensing node measures structural response or environmental parameters. Each sensing node is controlled by an Imote2 platform comprised of a microprocessor, sensor module, and communication device. To exchange information or to trigger sensing tasks, the cluster head node can communicate with sensing nodes or cluster heads of neighboring communities. The cluster head has a dual-core design that combines the Imote2 platform with a second embedded device. The cluster head has an extra wireless module and GPS. The extra wireless module provides additional RF power needed for long-range wireless

communication. The GPS is useful for synchronization and localization. The transfer node functions as a coordinating node for managing cluster heads and data hopping. The base station is the highest level end device and has the largest memory, the most powerful processor and the highest communication capability. The base station node is the gateway between smart sensor networks and the Host computer.

A three-tier software framework is also developed in this work serving as reliable data-sensing and transmission, data logging and data storage, user interface, data analyzing, and signal processing. Based on this software framework, a SHM application for specific purpose can be easily developed. Power sources and power consumption are the critical issue in WSN if batteries have to be periodically replaced. Hence, a novel windmill-magnet integrated piezoelectric (WMIP) energy harvesting system was also proposed.

Since local and global SHM have unique benefits and shortcomings, an integrated approach may be more effective than using either approach alone. This work developed a global-local-integrated damage detection approach for localizing damage. Substructure-based frequency response function approaches were proposed for global damage detection. Local damage was then identified by Electro-Mechanical-Impedance (EMI)-Based damage detection method.

Numerical and experimental study is also conducted to complete this study. Numerical results reveal that the proposed global damage detection approach can successfully locate damage at a single site and at multiple sites. Experimental analysis confirms the proposed integrated WSN-based SHM system provides excellent data sensing and transmission quality for determining the structural dynamic properties.

An experimental validation in building structure confirms that the proposed global SHM approach can indicate the approximate location of the damaged area in damaged floor and the EMI-based damage detection approach can check the component of building structure locally. Subsequently, the proposed WSN-based SHM system is employed in a bridge structure to test the feasibility in field. This experimental result confirms good-quality data collection by the proposed system. In experimental period, the system shows WSN-based SHM system outperforms conventional SHM system, especially in deploying sensors. Average time for deploying single node only takes within 5min.

ACKNOWLEDGEMENT

時間飛逝，轉眼間在交大也待了六個年頭了，學生生涯也在此畫下了句點。讀博士真是一個漫長的過程，其中辛酸只有經歷過的人才能夠體會吧。在博士期間，受到許許多多的幫助，在此獻上我最深的感謝。

當然最要感謝的是我的指導教授洪士林博士，他在研究上給予我非常大的自由，讓我可以進行我有興趣的研究，在論文的方向與內容給予我相當大的幫助，並在在其身上學到一個研究學者該有的風範。在生活方面，洪老師的國科會計畫也幫助了我減輕經濟上的壓力。感謝黃炯憲老師在我論文中很重要的理論部分給予我相當大的指導，在黃老師的身上也學到做研究嚴謹的態度。感謝廖德誠老師在電機領域相關的指導，讓我跨領域的學習能夠如此的順利。另外，在博士班期間很感謝東京大學的 Fujino 與 Nagayama 教授給我機會，讓我到東京大學訪問兩個月，這兩個月讓我學習到很多東西，是個難忘的經驗。感謝靜宜大學吳仁彰教授帶領我進入跨領域的研究，也感謝其時時為我禱告。感謝 Murthy 博士，無論是在研究或是 paper 的撰寫都給予我相當大的幫助，在他身上也學到很多。感謝中興工程科技研究發展基金會，中興工程顧問社，中華顧問工程司，給予我的獎學金。讓我能夠專心於研究上，不用為經濟擔心。

感謝研究室同學勇奇在我研究上有問題時可以互相討論，感謝研究室學弟們在我實驗上的幫忙，感謝一弘在我修習電機相關課程時給予我幫助，並在 WSN 的領域一起努力學習，感謝阿銘在天線上面的幫助，感謝秦飛在 Imote2 上給予的協助。還有許多在我博士班期間幫助過我的朋友，無法在此一一列出，在這一起獻上我的感謝。也要感謝女友珮茹這幾年來對我的鼓勵與關心。最後要感謝我的家人，沒有你們的支持，我沒有辦法專心地完成我的博士學位，感謝我的母親，您辛苦了。

CONTENTS

LIST OF TABLES

LIST OF FIGURES

CHAPHER 1 INTRODUCTION

1.1 Background of Structural Health Monitoring

Monitoring the structural health of buildings and civil infrastructure has received considerable interest recently. A low-cost, real-time monitoring system with high stability and robustness is required. A successfully implemented structural health monitoring (SHM) system has several benefits to the end user of a structural system. For example, a well designed SHM can reduce risk to operators and structural system, reduce risk through life-extending operation and control based on the use of health monitoring information and reduce cost for servicing structural systems based on condition-based maintenance scheduling [1].

Monitoring the structural health of a given structural system is a damage identification process that includes damage detection, damage localization, damage type evaluation, and damage severity estimation. Damage can be defined as changes to a structural system, such as its material and/or geometric properties, that alter its current or future performance [2, 3]. Structural health monitoring can be classified as local and global monitoring. Non-destructive evaluation (NDE) techniques are the most widely used methods for local health monitoring. Conventionally adopted global structural monitoring methods are vibration-based schemes. These methods identify damage by detecting modal property changes in, say, natural frequencies, modal damping, or mode shape [4].

The SHM problem is fundamentally one of statistical pattern recognition paradigm. This paradigm can be described as a four-part process [5]:

(1). Operational Evaluation:

Define damage for the system being monitored, realize the conditions, both operational and environmental, under which the system to be monitored, know the limitations on acquiring data in the operational environment.

(2). Data Acquisition, Fusion and Cleansing:

The data acquisition portion of the SHM process involves selecting the types of sensors, choosing the locations where the sensors should be placed, deciding the number of sensors to be used, and selecting the types of data acquisition/storage/transmittal hardware.

(3). Feature Extraction and Information Condensation：

Feature extraction is the process of the identifying damage-sensitive properties, derived from the measured system response, which allows one to distinguish between the undamaged and damaged structure.

(4). Statistical Model Development for Feature Discrimination.

The algorithms used in statistical model development usually fall into t fall into the general classification referred to as supervised learning, unsupervised learning, group classification and regression analysis.

After SHM was established, the next stage is a lead-in of damage prognosis. The damage prognosis is a process of predicting the future probable capability of a structural material or system in an online manner, taking into account the effects of damage accumulation and estimated future loading. Figure 1.1 illustrates the relation between usage monitoring, structural health monitoring, and damage prognosis [1, 6].

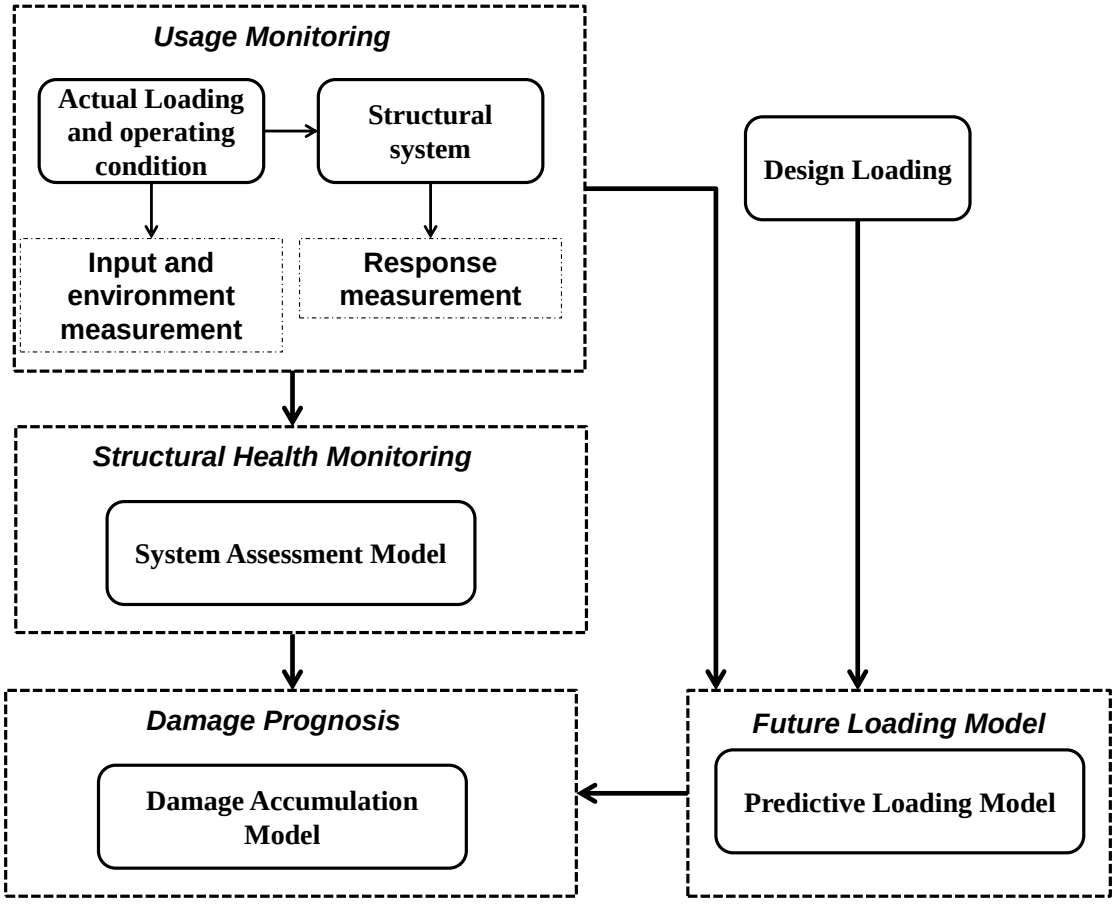

Figure 1.1 The relation between usage monitoring, structural health monitoring, and damage prognosis.

1.2 Motivation and Objective

In SHM, integration of cross discipline is essential for developing a flexible and robust system. For example, ***Civionics*** is currently the use of electronics for structural health monitoring (SHM) of civil structures. It is combination of electronic engineering with civil engineering, in a manner similar to avionics (aviation and electronics) and mechatronics (mechanical engineering and electronics) [7].

Generally, sensors comprise a significant portion of the SHM process. Recent developments in smart sensor technology enable new applications in structural health monitoring. The main features of a typical smart sensor are on-board microprocessor, sensing capability, data storage, wireless communication, battery power, and low cost.

Sensors are being deployed in civil infrastructures. Long term recorded data for monitoring are extensive. Smart sensors can process data before outputs are recorded, which reduces the quantity of data required and computing power [8].

When many sensors are implemented, wireless communication appears to be an attractive approach. Wired sensor systems can only deploy limited numbers of sensors because of cost constraints or excessive complexity. Wireless sensors are expected to minimize these problems by simplifying the installation of wired sensors [9-11]. Smart sensor-based wireless sensor networks (WSNs) are an attractive sensing technology for structural health monitoring applications because of their low manufacture costs, low power requirements, small size, and simple deployment (i.e., lack of cables) [12, 13].

Although numerous researchers have demonstrated the advantages of WSN [12-17], there are still existing many limitations. First, the wireless throughput is heavy to collect all of the measured information in SHM. The aggregation of dynamic measurement data consumes power- and time- consuming even when data are not collected in real time. For instance, Kim *et al.* [18] developed a multi-hop wireless sensor network to monitor the Golden Gate Bridge. They reported that transferring KB data from 64 nodes required over 12 hours. Moreover, sensor nodes are not synchronized with separate clocks. Packets may be lost in communication or sensing, and storage memory space is always limited. Therefore, an effective time-scheduling and data transmission protocol should be developed.

Additional, the processing ability of processor of node in WSN is slower than that of a PC. In SHM, a complex parameter identification-based embedded damage detection approach may not perform adequately when using resource-constrained

WSN hardware. Therefore, a non-parameter embedded damage detection approach such may be considered a appreciate approach.

Next, battery powered wireless nodes have limitations on consuming large amounts of power in packets delivering. Hence, power sources and power consumption are the critical issue if batteries have to be periodically replaced. Therefore, an intelligent self -powered wireless sensor networks via harvest and store ambient sources of energy should be considered to solve this barrier.

Furthermore, implementing an embedded algorithm in a complex development environment commonly involves hardware and software complexities, making the task quite challenging, especially for civil engineers with limited experience of WSN. Also, robust system development is problematic in a complex programming environment. Accordingly, a WSN-based SHM system should be developed based on an easy-to-use development environment. Related applications can be implemented efficiently in this the friendly environment.

The main purpose of this dissertation is to propose a framework of an integrated wireless sensor network-based structural health monitoring system in buildings and civil infrastructures. Figure 1.2 illustrates the proposed framework. In this framework, it is considered three main parts which are the physical sensing, information fusion and management, and inference and decision making. To achieve this goal, an integrated WSN-based SHM system is developed. This system consists of sensing nodes, cluster head nodes, transfer node, and base station. The purpose of sensing node is to measure the responses of structure or the environmental parameters. Cluster head node can communicate with the sensing nodes or other cluster heads of the neighboring communities to exchange information or triggering sensing task. The

transfer node is functions as coordinate node for managing the cluster heads and hoping the data. The base station is the highest level end device that has largest memory, most powerful processor and highest communication capability. The base station node is the gateway between smart sensor networks and the Host computer. The base station uploads the data to remote monitoring and control server via satellite, 3G telecommunication or WiMAX communication. A three-tier software framework is also developed in this work serving as reliable data-sensing and transmission, data logging and data storage, user interface, data analyzing, and signal processing. Based on this software framework, a SHM application for specific purpose can be easily developed. Power sources and power consumption are the critical issue in WSN if batteries have to be periodically replaced. Hence, a novel windmill-magnet integrated piezoelectric (WMIP) energy harvesting system was also proposed.

Both local and global SHM each has its own benefits and shortcoming, hence integrating aforesaid two approaches can obtain more effective damage detection result than only using one of them. This work proposed a global-local-integrated damage detection approach to localize damage. Substructure-based frequency response function approaches are proposed as global damage detection approach. Electro-Mechanical-Impedance (EMI)-Based damage detection method is used to identify local damage of structure in this study. In addition to theoretical developments in damage assessment approach and developing of wireless SHM system, experimental study is also conducted to complete this thesis.

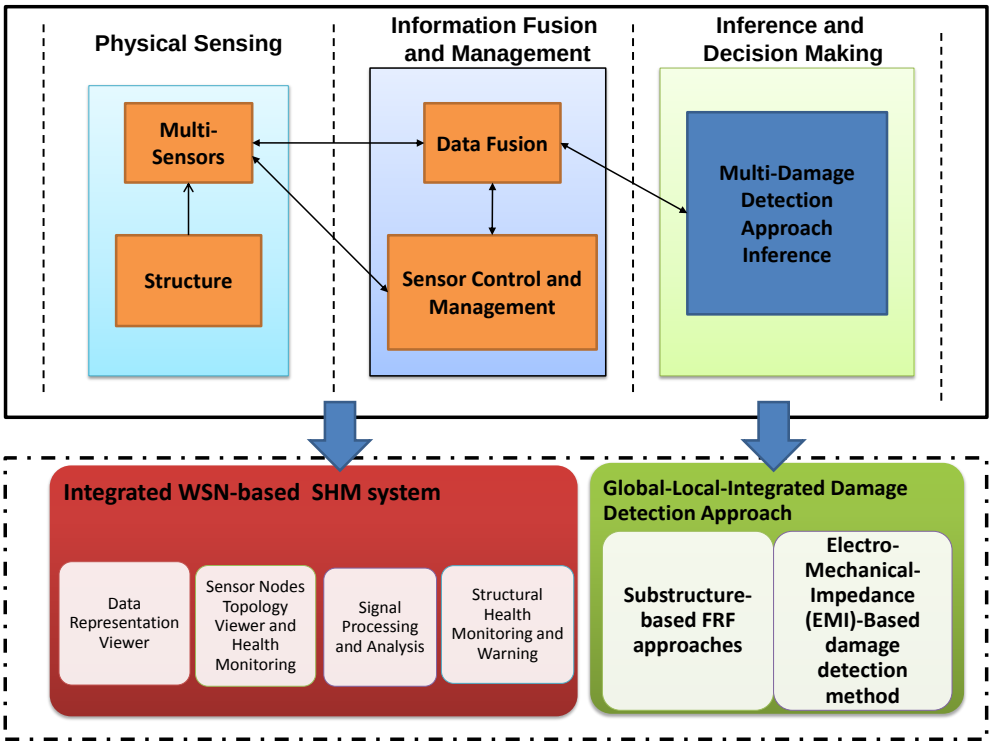

Figure 1.2 A framework of an integrated wireless sensor network-based structural health monitoring system.

1.3 Overview of Dissertation

This research focuses on realization of a vibration based SHM framework employing WSN based SHM system that can detect and localize damage. In addition to introduction in Chapter 1, Chapter 2 provides a review related to damage detection method and WSN-based SHM approaches that have been developed in literatures.

Since the WSN plays a significant role in this study, its basic theories and related techniques are briefly introduced in Chapter 3. In this Chapter, the basic wireless sensor technology would be introduced. WSN based architecture and protocol stack and operating systems for WSN then addressed. Time synchronization and related

applications are also included in this Chapter.

After the theoretical basis of WSN is established, the proposed integrated WSN-based SHM system then presented in Chapter 4. The architecture of this SHM system and wireless sensor nodes design are presented in Chapter 4. Chapter 4 also shows the proposed Windmill-magnet integrated piezoelectric (WMIP) energy harvesting system which is used to harvesting ambient energy. The software is also an important part in this system. The proposed three-tier software framework and reliable data-sensing and transmission service are hence included in this chapter.

Chapter 5 shows the proposed global-local-integrated damage detection approach. The theoretical basis and numerical study are presented in this chapter. The substructure-based frequency response function based global damage detection approaches are presented. Subsequently, the Electro-Mechanical-Impedance (EMI)-based local damage detection method is proposed herein to detect the local damage.

In Chapter 6, this dissertation focused on the experimental study. When the theoretical basis of damage detection method and wireless SHM system based measuring system are completed, series experimental study are conducted to verify the proposed algorithm and system. First off all, the wireless SHM system is verified involving sensor calibration, wireless communication quality, data losing, interference in material, power consumption. Subsequently, the proposed wireless SHM system is employed in a bridge structure to test the feasibility in field. Next, the proposed damage detection approach with proposed wireless SHM system then investigated in a ¼-scale six-storey steel structure that was designed by the National Center for Research on Earthquake Engineering (NCREE), Taiwan.

In the end of this dissertation, Chapter 7 summarizes the research detailed on the analytical and experimental study in this dissertation and presents possible directions for future research on SHM using wireless sensor networks.

CHAPHER 2 LITERATURE REVIEW

2.1 Introduction

This chapter provides a review related to SHM techniques and WSN-based SHM approaches that have been developed in literatures. Since the SHM can be classified as global and local monitoring, the global and local damage detection methods are briefly reviewed respectively. Moreover, this work focus on using WSN related techniques in developing SHM system. Some representative applications of WSN-based SHM, including theoretical developments, experimental validations, and practical applications, will be briefly reviewed in this chapter.

2.2 Structural Health Monitoring Approach

2.2.1 Global Damage Detection Method

Some global health monitoring methods are studied on either finding shifts in resonant frequencies or changes in structural mode shapes. Early works in health monitoring found that loss of a single member in a structure can result in changes in the fundamental natural frequency of one to as much as thirty percent. However, it is easy to see that some damage forms may not affect the frequency at low levels of vibration [8]. Although locating damage using frequency shifts requires either very accurate measurements or large damage extent, recent researches have shown that using resonant frequencies can get much less statistical variation from random error sources than other modal parameters [19, 20]. More detailed discussion related to damage detection using shifts resonant frequencies can be found in [21, 22]. West [23]

presented a efficient method using mode shape information for locating structural damage without the accurate FEM model. Mayes [24] developed a structural translational and rotational error checking (STRECH) method for locating model error by mode shape changes. Other studies provide instances of those mode shapes-based modal assurance criteria (MAC) and coordinate MAC (COMAC) values can be used to identify damage [25-27].

Early researchers [28] indicated that mode shape changes are not sensitive to locate local damage, an improved method for locating damage is to use the mode shape curvature. The using of mode shape curvature appears to be more sensitive for detecting damage due to losing stiffness of member than the mode shapes themselves [29]. Pandey [29] using the central difference operator to compute curvature values from the displacement mode shape. Their results demonstrate that changes in mode shape curvature can be a good damage index for the FEM beam structures. Topole and Stubbs [30] survey the practicality of using a limited set of modal parameters for detecting structural damage. Chance *et al*. [31] used measured strains instead to measure curvature directly, which dramatically improved unacceptable errors in calculating curvature from mode shapes.

Another class of damage detection method is based on the structural model matrices updating such as mass, stiffness, and damping. By solving the constrained optimization problem, this method updates model matrices using the structural equations of motion, the nominal model, and the measured data. Based on the various algorithms, the method can be classified as optimal matrix update methods [32-35], sensitivity-based update methods [36-39] and eigenstructure assignment method [40, 41]. These methods have some limitations such as the baseline of stiffness, mass, and damping matrices are probably inaccurate, and the solution of the optimization is not

unique [8].

Statistical pattern-recognition approaches are widely used in Global SHM. Sohn *et al*. [42] presented two pattern recognition techniques using time series method to analyze fiber optic strain gauge data obtained from two different structural conditions of a surface-effect fast patrol boat. The first technique combines Auto-Regressive (AR) and Auto-Regressive with eXogenous inputs (ARX) prediction models and the second technique employs outlier Mahalanobis distance measure-based analysis. These two methods were successfully employed to identify different structural damages by using data sets changes. The method in [42] is further applied to the damage detection of the benchmark problem designed by the ASCE task group [43]. The damage detection approach on the originally extracted damage-detection feature is modified to consider the influence of excitation variability and the orders of the ARX prediction model. Medium and severe damages are successfully detected and localized. This approach is investigated using various acceleration responses generated with different combinations of structural finite element models, excitation conditions and damage patterns in the benchmark study.

Artificial neural networks (ANNs) have been recently studied in SHM. Chen *et al.* [44] used ANNs to identify the structural dynamic parameters by using the structural responses in a building structure subjected to earthquake. The simulation results showed that the structural dynamic behavior can be well modeled by the trained neural networks. Wu *et al.* [45] employed ANNs for detecting structural damage in a three-story frame. The ANNs was used to recognize the frequency response characteristics of undamaged and damaged structures. The changing damage extents were simulated by changing the properties of individual members. Wen *et al*. [46] presented an ANNs-based approach for detecting structural damage. This work

adopts an unsupervised neural network which incorporates the unsupervised fuzzy neural network (UFN) to localized damage. The damage localization feature (DLF) is applied to locate structural damage by using the UFN. The analysis results indicated that the use of fuzzy relationship in UFN made the detection of structural damage more robust and flexible than the back-propagation network (BPN). In [47], ANNs has been used to training a set of strain measurements for different types of damage in a structure. Although ANNs can identify new damage type and location patterns, with a limited set of training examples, convergence is not guaranteed.

In addition to above method, wavelet-based damage detection method is also widely used in SHM [48-50]. The advantage of using wavelets is the capability to perform local analysis of a signal. Hence, wavelet analysis can find hidden information in data that other signal analysis methods may fail to detect. This property is essential for effective damage detection [50]. The wavelet-based damage detection approach is widely used to identify modal parameters of structural systems [51, 52], to detect beam structure damage [49, 53, 54], and to de-noise of signals [55, 56]. The discrete wavelet transform (DWT) shows that the de-noising capability is sufficient for detecting drill fractures and bearing race faults [56-58].

2.2.2 Local Damage Detection Method

The Non Destructive Testing (NDT) technique is mostly used in local damage detection. There are many methods for NDT such as ultrasonic, infrared thermography, eddy current X–ray. Such methods can detect tiny or incipient damage; however, it is usually expensive, power hungry and bulky. Sansalone and Carino [59] developed an impact-echo method for flaw detection in relatively thin concrete structures. They indicated that use the impact-echo method with frequency analysis can successfully

detect flaw in thin concrete structures.

Another impact method is known as impulse response, transient dynamic response, or impedance testing [60]. In their approach, both force history of the impact and the response of the structure are measured. The typical impulse response spectrum of the structure can be acquired using measured response and force history by using a signal processing technique. The impulse response spectrum of a structure reflects to the characteristic of structure such as geometry, the support conditions, and the cracks on structure.

The use of eddy current method has been developed for detecting surface-breaking cracks in the area of welded connections. One advantage of this method is that it can detect surface cracks of steel without removing paint. Commercial sensors have been designed for detecting the cracks of welds in highway bridges in the field. This eddy current-based method has successfully been employed in detecting the crack [61, 62].

Ultrasonic time of flight diffraction (TOFD) method has been developed to detecting and quantifying eye bars cracking. Compare to pulse-echo methods used the specular reflections from the crack face, this method is based on using the wave diffraction from a crack tip. Washer [63] applied this technology in the detection of eye bar cracks.

Electro-Mechanical-Impedance (EMI)-Based damage detection method is a new method of performing NDT by analyzing the electromechanical coupling property of piezoelectric materials. The EMI-based damage detection approach uses active surface-bonded PZT (Lead zirconate titanate) patches to sense structural-mechanical impedance changes. Liang *et al.* [64] first proposed an electrical admittance model of

the a PZT bar connected to a structure. Sun *et al*. [65] then experimentally used electrical impedance method to acquire FRF for a single location and to transfer FRF between two locations on a structure. This technique has proven effective in several experimental applications, including aircraft structures [66], temperature-variable applications [67], civil structural components [68], concrete structures [69], and PSC girder bridges [70]. Impedance methods also continue to attract the attention of researchers and field engineers. Park *et al*. [71] summarized future issues of the impedance method from hardware and software standpoints. Such issues include the difficulties in handling the crisp PZT sensors and in bonding them to the structure, the bulky and expensive analyzers required for impedance testing, the difficulties and complexities of acquiring and processing data in large-scale complex structures, and high power consumption.

2.3 Wireless Sensor Networks-Based Structural Health Monitoring Applications

Recently, smart sensor-based WSN has been considered as an alternative technology for SHM. In this section, available wireless sensor platforms developed in the academia and industries are reviewed, and applications of WSN to SHM of civil structures are also reviewed.

Mascarenas *et al*. [72] developed a mobile host-based WSN monitoring system. The mobile host transmitted energy to power the sensor node wirelessly. When the sensor node has received adequate energy for sensing, the sensor node then start sensing and wirelessly transmits the measurement to the mobile host. They used a commercially available radio-controlled helicopter to deliver microwave energy to wireless sensor nodes located on a decommissioned overpass in southern New

Mexico. The helicopter successfully delivered sufficient microwave energy to charge a wireless sensor node to get displacement measurements and transmit the data back to the helicopter. The results of this experiment show that a mobile-based wireless sensor network can feasibly be used to SHM.

Kim *et al*. [73] proposed a WSN SHM system which was deployed and tested on the 4200ft long main span and the south tower of the Golden Gate Bridge (GGB). 64 nodes are distributed deployed in the GGB deployment, over the main span and the tower, collecting ambient vibrations synchronously at 1kHz rate, with less than 10μs jitter, and with an accuracy of 30μG. The sampled data is collected via a 46-hop wireless network, with a bandwidth of 441B/s at the 46th hop. The collected data agrees with theoretical models and previous studies of the bridge. The deployment is the largest WSN for SHM.

Cho *et al*. [74] presented a structural health monitoring (SHM) system using a dense array of scalable smart wireless sensor network on a cable-stayed bridge (Jindo Bridge) in Korea. 70 sensors and two base station computers have been deployed to monitor the bridge. This autonomous SHM application is consideration with harsh outdoor surroundings. The performance of the system has been tested in terms of hardware stability, software reliability, and power consumption. 3-D modal properties were extracted from the measured 3-axis vibration data using output-only modal identification methods.

Potential of WSNs for using in bridge management has been evaluated in [75].In their study, a network of seven sensor nodes was installed on the Ferriby Road Bridge, a three-span reinforced concrete bridge. Three displacement sensor nodes were placed across cracks on the soffit of the bridge to measure the change in crack width. Three

inclinometer sensor nodes were mounted on two of the elastomeric bearing pads to measure the change in inclination of the bearing pads. Another node was used to monitored temperature in the box that contained the gateway. They suggest that the sensors are stable enough for long-term use. Sensor networks represent a useful tool that can be used to supplement, but not replace, visual inspection.

Recently, a mobile wireless sensor network is proposed for installation on a heavy truck to capture the vertical acceleration, horizontal acceleration and gyroscopic pitching of the truck as it crosses a bridge [76]. The vehicle-based wireless monitoring system is designed to interact with a static, permanent wireless monitoring system installed on the bridge. Specifically, the mobile wireless sensors time-synchronize with the bridge's wireless sensors before transferring the vehicle response data. Vertical acceleration and gyroscopic pitching measurements of the vehicle are combined with bridge accelerations to create a time-synchronized vehicle–bridge response dataset. In addition to observing the vehicle vibrations, Kalman filtering is adopted to accurately track the vehicle position using the measured horizontal acceleration of the vehicle and positioning information derived from piezoelectric strip sensors installed on the bridge deck as part of the bridge monitoring system. Using the Geumdang Bridge (Korea), extensive field testing of the proposed vehicle–bridge wireless monitoring system is conducted. Experimental results verify the reliability of the wireless system and the accuracy of the vehicle positioning algorithm.

CHAPHER 3 WIRELESS SENSOR NETWORKS

3.1 Introduction to Wireless Sensor Networks (WSN)

Recently, advanced micro-electro-mechanical systems (MEMS) technology, wireless communications, and electronics engineering have improved the development of WSN. WSN is based on wireless sensor nodes. These tiny wireless sensor nodes, which consist of sensing, processing, and communicating components, collaborate with each other via wireless communication.

WSN have great potential for many applications in different scenarios such as natural disaster monitoring [77], military target tracking and surveillance [78], biomedical health care [14], and hazardous environment investigation and seismic sensing [79]. In military target tracking and surveillance, a WSN can assist army to detect and identify enemy target such tank movements as spatially-correlated and coordinated troop. With natural disasters, wireless sensor nodes were used to sense and detect the environment to forecast disasters before they occur. In biomedical care applications, the wireless sensors can help monitor a patient's health in surgical. For seismic sensing, deployment of large numbers of wireless sensors along the volcanic area can detect the development of earthquakes and eruptions.

A wireless ad hoc network is a kind of wireless technology. It is decentralized type of wireless network. The network does not rely on a preexisting infrastructure. Instead, each node forward data dynamically based on the network connectivity. Ad hoc networks can use flooding for forwarding the data. There are differences between WSN ad hoc networks. The differences between WSN and ad hoc networks was

illustrate below [80]:

i. The number of sensors in a WSN can be several orders of magnitude higher than an ad hoc network.

ii. Sensor nodes are densely deployed in field.

iii. Sensor nodes are expected to failures in WSN.

iv. The topology of a sensor network changes when sensor node failure.

v. WSN mainly use broadcast or tree communication paradigm whereas most ad hoc networks are based on point-to-point communications.

vi. WSN are limited in power, computational capacities, and memory.

Yick [81] classified the WSN into five types: terrestrial WSN, underground WSN, underwater WSN, multi-media WSN, and mobile WSN. Terrestrial WSNs typically consist of hundreds to thousands of inexpensive wireless sensor nodes deployed in a application area. For deploying WSN, sensors can generally either deterministically or randomly be placed in an area of interest [82]. The type of sensors determines the choice of the deployment scheme rely on application and the environment. A viable controlled node deployment is necessary when sensors are expensive or when their operation is significantly affected by their position. Such scenarios include underwater WSN applications, highly precise seismic monitoring, and placing imaging and video sensors. Moreover, in some applications random distribution of wireless sensor nodes is the necessary option. This is chiefly fact for harsh environments such as a battle field or a disaster region. Depending on the node distribution and the level of redundancy, random node deployment is considered a good approach that can achieve the required performance goals.

3.2 Subsystem of Smart Wireless Sensor Node

In this section, the subsystems of a smart wireless sensor are discussed. Figure 3.1 shows the composition of wireless sensor node. Generally, a smart wireless sensor is composed of three or four functional subsystems: on-board micro-processor unit, sensing unit, wireless communication unit, and power unit [12, 83]. The computational micro-processor was generally used for the computational tasks. For SHM application, to convert analogue sensor outputs to a digital format, the ADC with a resolution of 16 bits or higher is needed. The sensing unit always includes an ADC to connect sensors. For capturing low-order global response modes of a civil structure, the wireless sensing unit should be designed to record response data at sample rates at least 100 Hz. To capture high-order response modes of structural components of civil structure, the wireless sensing unit should therefore need relatively as high as possible sample rates (greater than 500 Hz) [12, 84]. The random access memory (RAM) was used to stack the measured and processed data. A flash memory with software programs was used for the system operation and data processing [85]. A 16 bit digital sensor data could be stored at one time, at least 256 KB of RAM is required for a WSN application. For the simultaneous multiple tasks application, at least approximately 256 KB of flash memory would be provided for that purpose [84]. The wireless communication unit is used to communicate with other wireless sensor nodes and to transfer the sensing data using a RF radio modem and antenna Lower data loss rate is necessary for the highly reliable wireless communication in the conditions of channel interference, multi-path reflections and path losses. Radio signals always decrease as they propagate through structural materials such as reinforced concrete or steel material and the large scale civil structures require wireless communication ranges of at least 100 m. [12, 84, 86].

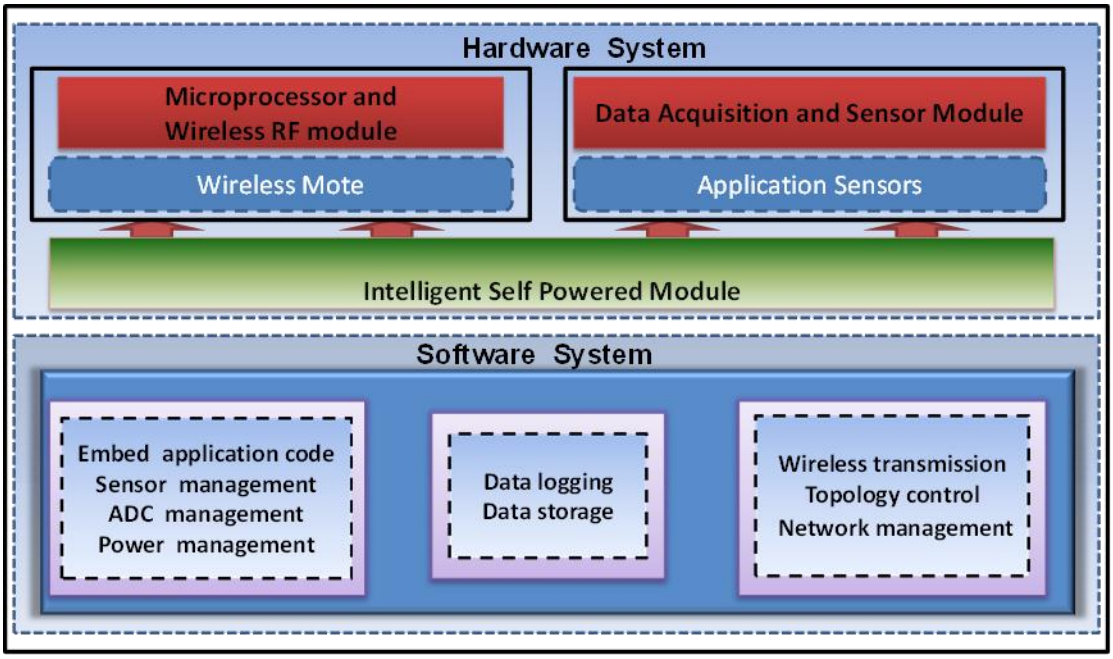

Figure 3.1 Composition of wireless sensor node

3.3 Wireless Sensor Platforms

A number of smart wireless sensor platforms have been developed in academia and industries. Straser and Kiremidjian [87] first proposed a design of a low-cost wireless modular monitoring system (WiMMS) for monitoring the civil structures by integrating a microcontroller and a wireless radio. Lynch *et al*. [88] used more powerful computational unit to improve the WiMMS. The WiMMS platform has been improved further by Wang *et al*. [89] with a software service which utilize the computational power of the wireless sensor for multiple tasking (e.g. processing or transmitting data while collecting data). The tasks can be executed simultaneously. Aoki *et al*. [90] have developed remote intelligent monitoring system (RIMS) for structural health monitoring of bridges and infrastructures. The RIMS consists of high-clock microcontroller, 3-axis MEMS piezoresistive accelerometer, and internet-based wireless modem. This system can be controlled via ethernet protocol. Chung *et al*. [91] have developed a wireless sensor platform named DuraNode for

monitoring bridges and buildings. DuraNode not only has a special feature for wireless sensing but also allows the wired internet data communication for building structures using an established Local Area Network (LAN). Farrar and Allen [92] have developed a smart wireless sensor platform, called Husky. This platform performs a series of damage detection algorithms by embedding a Java-based damage detection algorithm package (DIAMOND II). Chen and Liu [93] presented a mobile agent approach for enhancing the flexibility and reducing raw data transmission in wireless structural health monitoring sensor networks. In their approach, they developed an integrated wireless sensor network consisting of a mobile agent-based network middleware and distributed high computational power sensor nodes. A mobile agent system called Mobile-C was embedded this mobile agent middleware. The mobile agent middleware allows a sensor network moving dynamically to the data source. With mobile agent middleware, a sensor network is able to be implemented in newly developed diagnosis algorithms and can be adjusted in response to operational or task changes.

Besides the smart wireless sensor platforms developed in the academia, a number of commercial smart wireless sensor platforms have been also developed for SHM applications in the industries. Mica Motes, which is initially developed at the University of California-Berkeley and subsequently commercialized by *Crossbow Inc*., may be the most famous commercialized wireless sensor platform. The Mote is an open source wireless sensor platform with both its hardware and software. Motes is very popular to the public [12]. The Wisden was design for structural data acquisition. The Wisden perform wavelet-based compression techniques to overcome the bandwidth limitations based on Mica2 motes platform [94]. Mica mote and piezoelectric sensors then integrated for a parallel distributed structural health

monitoring system. The developed system can successfully monitor the concentrated load position or a loose bolt position [95]. The performance of the mica mote was investigated through a two story steel structure testing on shaking table. The results shows that Mica mote can get the sufficient performance for the intended purpose [96]. Mote has been successively revised to Imote and Imote2 by Intel. The Imote2 may be the most powerful and promising smart wireless sensor platform for SHM. It built with 32 bit XScale processor with a RAM of 32 MB and a flash memory of 32 MB, and an integrated radio with a built-in 2.4 GHz antenna. Nagayama *et al.* [11] successfully implemented a decentralized computing strategy in a wireless smart sensor networks that used Imote2 for system identification. In their study, the measured data was aggregated locally by a selected sensor node within the communication distance in sensor group, and only limited pre-processed data was sent back to the base station to locate the health of the structure.

3.4 Factors Influencing Sensor Network Design

Based on lacking of power, having physical damage or environmental interference, some sensor nodes may fail or be blocked. The failure of sensor nodes should not affect the overall task in WSN. Therefore, the reliability or fault tolerance issue should be considered. Robust fault tolerance is the ability to endure sensor network functionalities without any interruption due to sensor node failures [97].

In studying a different phenomenon, the hundreds or thousands number of sensor nodes may be deployed. Depending on the application, the number may reach an extreme value of millions. The new WSN approaches must be able to deal with this number of nodes. The high density nature of the sensor networks can be less than 10 m in diameter for some specific applications [98].

The cost of a single node is very important to influence the overall cost in WSN with a large number of sensor nodes. If the cost of the WSN is more expensive than deploying traditional sensors, then the WSN is out of its benefit. It is why the cost of each sensor node has to be kept low. For example, the novel technology allows a Bluetooth radio system to be less than 10$ [99]. Also, the cost of a sensor node should be much less than 1$ in order for the WSN to be feasible in the future.

The size of sensor node may be another important issue in some WSN applications. The required size may be smaller than even a cubic centimeter which is light enough to remain suspended in the air [100]. Apart from the size, there are also some other constraints for designing a sensor node. These nodes must [101]

i. Consuming in extremely low power,

ii. Operating in high volumetric densities,

iii. Having low production cost and be dispensable,

iv. Operating unattended,

v. Be adaptive to the environment.

Sensor nodes are densely deployed to record different phenomenon. Therefore, they usually work isolated in remote geographic areas. They may be working

i. in busy intersections,

ii. in the interior of a large machinery,

iii. at the bottom of an ocean,

iv. inside a twister,

v. on the surface of an ocean during a tornado,

vi. in a biologically or chemically contaminated field,

vii. in a battlefield beyond the enemy lines,

viii. in a home or a large building,

ix. in a large warehouse,

x. attached to animals,

xi. attached to fast moving vehicles, and

xii. in a drain or river moving with current.

3.5 The 802.15.4 and Zigbee Standards

The ZigBee Alliance [102] is an association of companies working together to develop reliable, cost-effective, low-power wireless networking standard. ZigBee technology was applied in a wide range of products and applications across consumer, commercial, industrial and government markets worldwide. ZigBee builds upon the IEEE 802.15.4 standard which defines the physical and MAC layers for low cost, low rate wireless application. ZigBee defines the network layer specifications for star, tree and peer-to-peer network topologies and provides a framework for application programming in the application layer. Figure3.2 shows the 802.15.4 and Zigbee Architecture. The following subsections give more details on the IEEE and ZigBee standards.

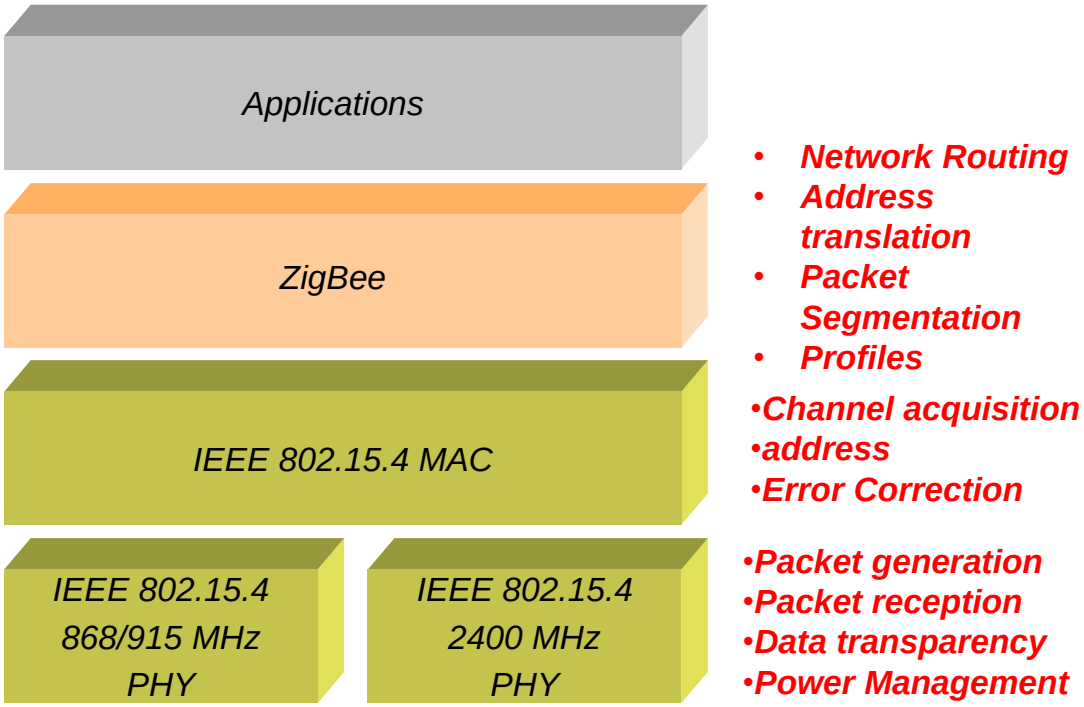

Figure 3.2 802.15.4 and Zigbee Architecture

IEEE 802.15.4 standard

The IEEE 802.15.4 standard [103] defines the protocol of the physical and MAC layers for Low-Rate Wireless Personal Area Networks (LR-WPAN). The advantages of an this standard maintaining a simple and flexible protocol stack that are ease of installation, reliable data transfer, short-range operation, extremely low cost, and a reasonable battery life.

The physical layer supports three frequency bands and 27 channels with Direct Sequence Spread Spectrum (DSSS) access mode: a 2450 MHz band (with 16 channels), a 915 MHz band (with 10 channels) and a 868 MHz band (1 channel), all using the. The 2450 MHz band employs Offset Quadrature Phase Shift Keying (O-QPSK) for modulation. The 868/915 MHz bands rely on Binary Phase Shift Keying (BPSK). In addition to radio on/off operation, the physical layer supports functionalities for channel selection, link quality estimation, energy detection

measurement and clear channel assessment.

The MAC layer defines two types of nodes: Reduced Function Devices (RFDs) and Full Function Devices (FFDs). The FFDs node are equipped with a full set MAC layer functions can act as a network coordinator or a network end-device. When acting as a network coordinator, FFDs using beacons for synchronization, communication and network join services. RFDs can only act as end-devices which equipped with sensors/actuators. They may only interact with a single FFD. Two main types of network topology are considered in IEEE 802.15.4, namely, the star topology (Fig3.3)and the peer-to-peer topology (Fig3.4).

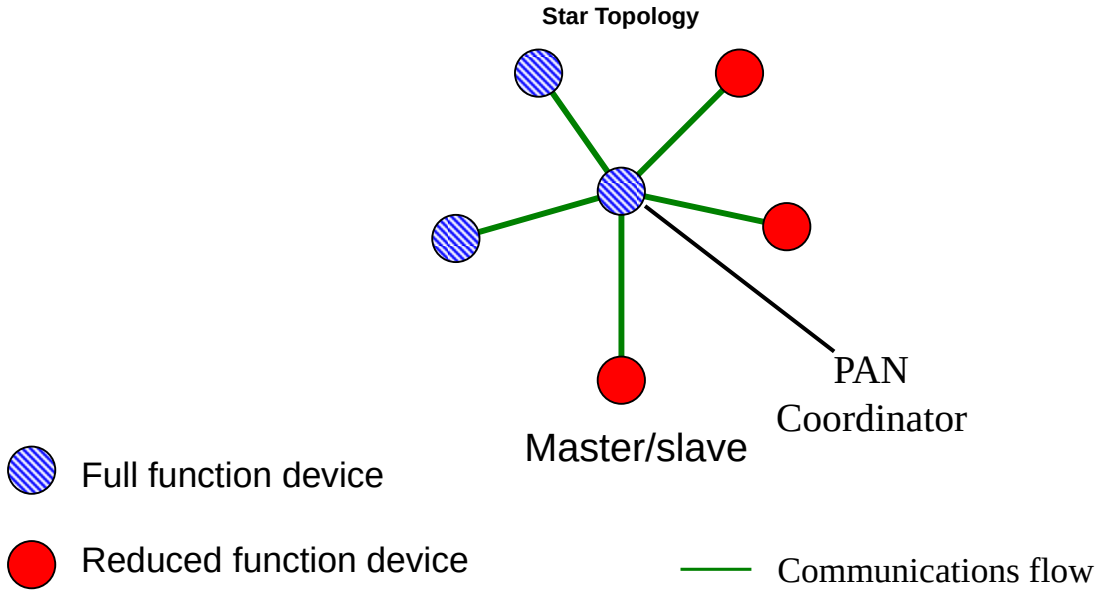

Figure 3.3. Star topology

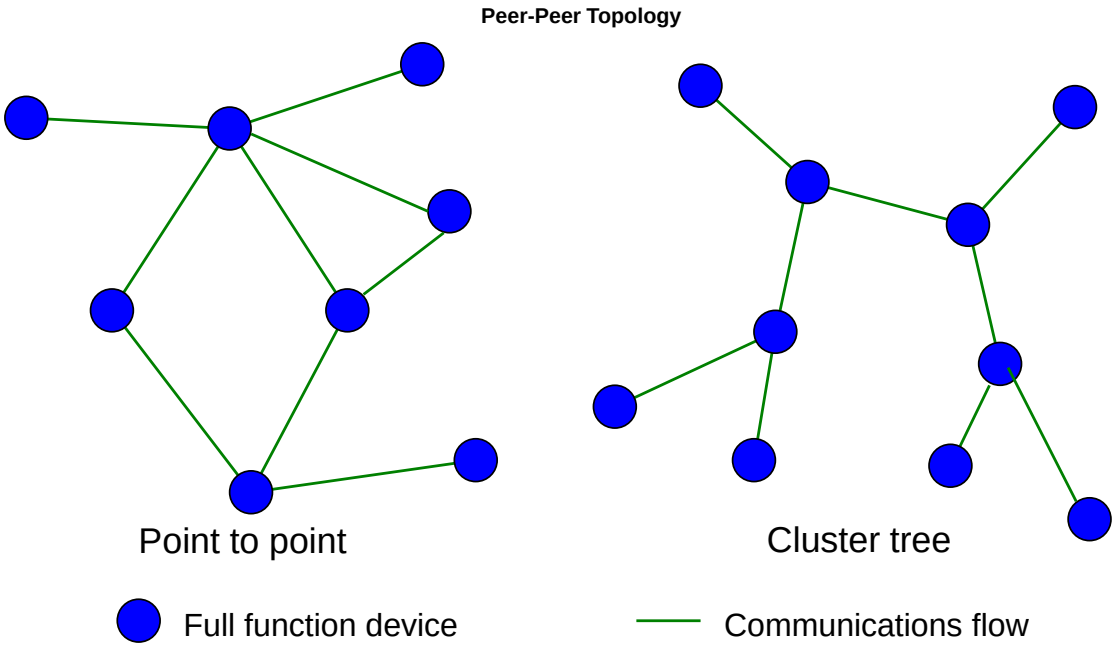

Figure 3.4. Peer-to-peer topology

The ZigBee standard

ZigBee [102] deals with the higher layers of the protocol stack. The network layer (NWK) organizes and provides routing over a multihop network (built on top of the IEEE 802.15.4 functionalities). The Application Layer (APL) provide a interface for distributed application development and communication. The APL comprises the Application Framework, the ZigBee Device Objects (ZDO), and the Application Sub Layer (APS). In the Application Framework, user can defined have up to 240 Application Objects of a ZigBee application. The ZDO provides services that allow the application objects to discover each other and to organize into a distributed application. The APS offers an interface to data and security services to all application objects and ZDO.

ZigBee identifies three device types. A ZigBee end-device is corresponding to an IEEE RFD or FFD for a simple task. A ZigBee router is an FFD with routing capabilities. The ZigBee coordinator is an FFD for managing the whole WSN. The

ZigBee network layer supports more complex topologies like the tree and the mesh while the IEEE 802.15.4 naturally uses the star topology. Multihop routing, route discovery and maintenance, security and joining/leaving a network are among the functionalities provided by the network layer with consequent short (16-bit) address for assigning to newly joined devices.

3.6 Operating Systems for Wireless Sensor Networks

As the technology moving on, from its root in the Computer Science and Electronic Engineer community, TinyOS has been adopted as an easy used WSN operation system in more and more application fields, like Civil Engineering.

TinyOS is designed for low power, ad-hoc, and embedded sensor networks; it is a component based and event driven operation system which make it a very flexible and easy to use. These features make TinyOS easy to deploy in different WSN platforms like Mica, TelosB, Imote2, EYES, BTNode, also Gains and Hawk platform from China. Although the low level hardware devices are different, researchers who work on it could use similar environment and share their work results by the component mechanism.

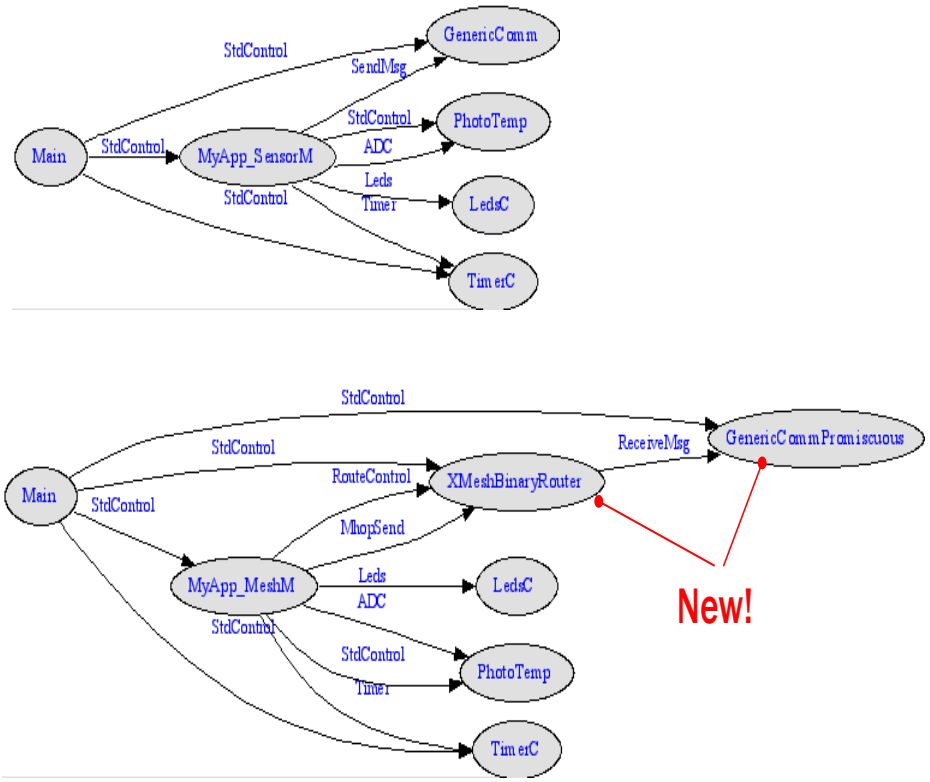

Figure 3.5 Schema of TinyOS (Crossbow)

This is a great advantage for the WSN users. Researcher can use as much as existed code like the multi-hop algorithm due to the absence of embedded programming skill. Just as the Figure 3.5 shows, when the researcher wants use the Multi-hop protocol in his application based on TinyOS, the only thing is to find the Xmesh Component then adds it to extent the application. Therefore, researchers could focus on the key problems like data flow, analyses model etc, instead of paying too much time on the WSN tools itself.

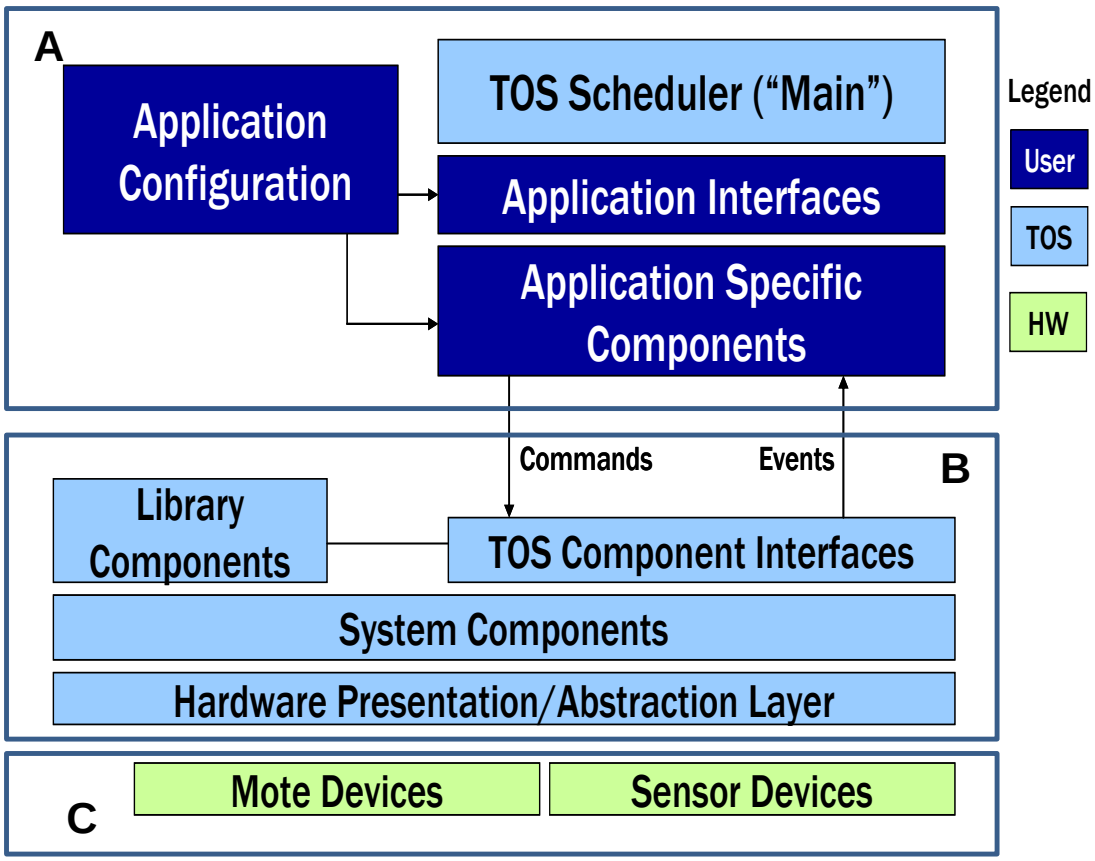

Figure 3.6 Architecture of TinyOS (Crossbow)

The Figure 3.6 shows the architecture of TinyOS. The architecture divide into three parts, are represented by function A, B and C. The function C means the hardware device provided by industry, basically consisted with MCU, radio chip, storage chip, and sensors. The function B means the TinyOS core and Firmware, this part is also usually provided along with hardware device. The function A is the user definition part, should be modified by researchers. Also the share of components is realized in this part.

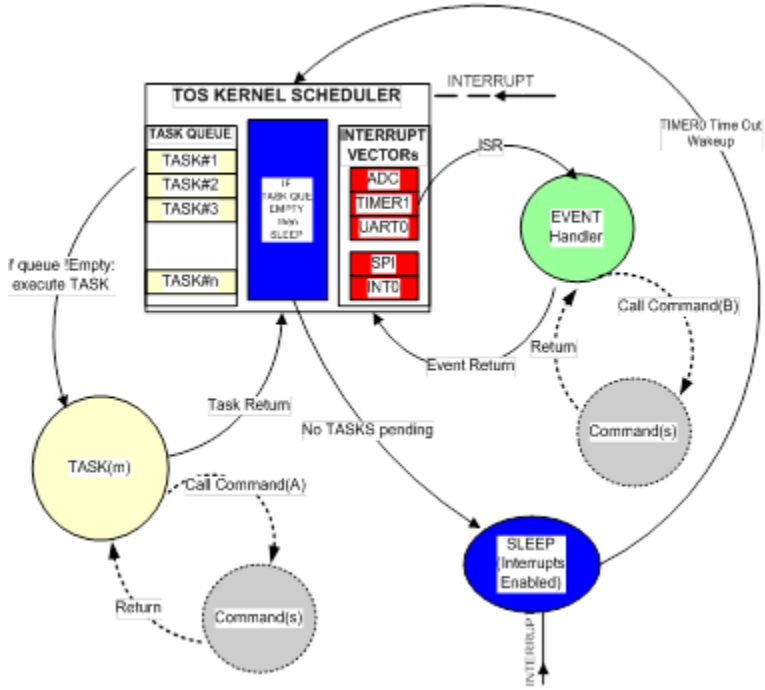

Figure 3.7 The process in TinyOS(Crossbow)

The process in TinyOS could be generally dived into two categories: event and task. Event represents a completed sensor reading, or a RF message received, or any other user specified event. When the event fired, a pre-defined function will be carried out to process this event. This kind of process should be as quick as possible to avoid interference among different events. So some long time desired process are classify as Task will be active when CPU is free, like some data reconstruction and signal process work should be done in Task.

The regular steps of a TinyOS process are as follows:

i. Physical event fired.
ii. Event handler signaled.
iii. Event parsed and Task posted according to different Event.
iv. Event finished
v. Task active
vi. Carried Task
vii. Task Finished

There are two types of component; module and component. Components is written with code and wired together as a Configuration to create a Mote application. The interface provides two methods, “provide” and “use”, to wire the components. The table 3.1 shows all description of keywords in TinyOS.

Table 3.1 Description of keywords in TinyOS.

Keword	Description
interface	A collection of event and command definitions
module	A basic component implemented in nesC.
configuration	A component made from wiring other components.
implementation	Contains code & variables for module or configuration.
components	List of components wired into a configuration.
provides	Defines interfaces provided by a component.
uses	Defines interfaces used by a module or configuration.
as	Alias an interface to another name.
command	Direct function call exposed by an interface.
event	Callback message exposed by an interface.

Due to the limited memory, the memory usage and memory space need to be managed. The TinyOS uses the static memory model to manage the memory. The components of static memory model are statically linked together and size required determined at compile time. The global variables are used to conserve memory and the pointers are also using here.

TinyOS, the innovation operation system enables researchers to implement their own WSN research easily, enables researchers share their code and research result all over the world instead of building everything by oneself, enables an entry level researcher build up a prototype system very easily and quickly. Plenty of component based libraries, supporting mesh protocols, distributed services, data acquisition tools and QoS service, which makes user easy to construct the individual application with high efficiency and reliability. However, for civil engineers, students and researchers, using TinyOS to develop the individual SHM application are not very easily. A new WSN development environment should be developed.

3.7 Time Synchronization

In wireless sensor networks, the data fusion is a basic operation. Data from each sensor is collected by a data fusion center [104]. The fusion of individual sensor uses exchanging messages that are time stamped by each sensors local clock. This task needs an exact time among the sensors. Protocols that provide exact time clock are synchronization protocols. Over the past few decades, researchers have developed successful clock synchronization protocols for wired networks. However, these protocols are unsuitable for a WSN because the challenges posed by WSN are different and manifold from wired networks.

There is several facts influence synchronization in WSN. The major error in time synchronization schemes is the message delivery delay with non-determinism in the latency estimating. A description of sources of synchronization error was first described by Koeptz [105] and extended recently by Horauer et. al. [106].

The main time synchronization errors are shown below [106]:

(1). Send Time: The delay in the packet traversal from the message assembly

at the application layer all the way down to MAC layer. Highly non-deterministic.

(2). Access Time: Is the channel contention time, that in dense broadcast medium such as ours can be in the order of hundreds of milliseconds. Least deterministic part of the message delivery.

(3). Interrupt Handling Time: The delay between the radio chip raising and the microcontroller responding to an interrupt. Can be an issue if interrupts are disabled on the microcontroller.

(4). Transmission and Reception Time:The delay in sending or receiving the entire length of the packet over the channel. Largely deterministic, is a function of bandwidth and packet size.

(5). Propagation Time: The delay, for a particular symbol of the message, in traversing all the way to the receiver. The propagation time can be deterministic if the speed of propagation is assumed constant, and endpoint location is known, or if synchronization exchange is performed with assumption of path symmetry. This delay can be significant in the underwater acoustic channel since assuming clocks will not skew over packet exchanges would be incorrect.

Basically, there are two schemes to synchronize clocks: Sender-Receiver and Receiver- Receiver. All synchronization schemes developed within these two basic frameworks. Network Time Protocol (NTP) is widely used in the Internet. It is approach works well with high latency and high variability [107]. The NTP protocol estimates both offset and skew using long-term, bi-directional exchange of time information. Unfortunately, NTP is a poor match for WSN for several reasons. First, it

assumes communications are relatively inexpensive. However theWSN are bandwidth and energy constrained. Next, NTP is designed for constant low rates operation in the background. (At a maximum polling rate of 16 sec, NTP took around an hour to reduce error to about 70us). On the other hand, TSHL (Time Synchronization for High Latency)[108] exchanges number of broadcast beacons to compute skew and then perform one bidirectional exchange to compute a skew-corrected offset. Generally, TSHL and NTP synchronize clock using the same time information, however TSHL reduces energy consumption using a smaller number of broadcast beacons by replacing long-term bidirectional communication.

CHAPHER 4 INTEGRATED WSN-based SHM SYSTEM

4.1 Introduction

Characterized by its low manufacturing cost, low power requirement, miniaturized size, and no need for cabling, the wireless sensor networks (WSN) has emerged as an attractive sensing technology for deploying dense distributed sensors[12, 13]. Among the various wireless monitoring techniques [12-17], the MICA mote is a commercially available product that has been used extensively by researchers and developers. It utilizes an Atmel ATmega 128L processor that runs at 4 MHz. The 128L is an 8-bit microcontroller that has 128 kilobytes of onboard flash memory to store the mote's program. MICA motes have certain limitations, including limited sampling rate, processing ability, storage, and transmission ability. In comparison, the advanced wireless sensor platform Imote2 is considered as a better choice for developing and deploying customized wireless sensor networks efficiently [109, 110]. While the WSN-based sensing system is accessible and achievable, development beyond a prototype towards full-scale structure applications often incurs hardware and software complexities, making it quite challenging, especially for civil engineers with limited WSN experience. Also, robust system development is problematic under a complex programming environment. To this end, this thesis presents an easy-to-use development environment based on the .NET Micro Framework (NETMF). Applications can be implemented efficiently under the NETMF. Evidently, the accelerated development of the SHM techniques can be partly attributed to the user-friendly environment brought by the WSN.

This chapter discusses the architecture for proposed Integrated WSN-based SHM system. This system is developed based on NETMF platform, which is an advanced sensor platform compatible with NETMF. Architecture, wireless sensor node design, energy harvesting system, software framework, and WSN-Based SHM service to be employed in this thesis are described.

4.2 Architecture of Integrated WSN SHM System

The proposed integrated WSN-based SHM system is shown in Fig.4.1. This system is based on hybrid wireless communication, structural conditions will be assessed remotely. The proposed architecture consists of sensing nodes, cluster head nodes, transfer node, and base station. The purpose of sensing node is to measure the responses of structure or the environmental parameters. They are deployed in structure to perform specific tasks such as sensing, data processing, and acknowledgement. Each sensing node is based on Imote2 platform which is comprised of a microprocessor, sensor module, and communication device. All sensing data will be sent to a cluster head nodes in their own community using one hop transmission.

Cluster head node can communicate with the sensing nodes or other cluster heads of the neighboring communities to exchange information or triggering sensing task. The cluster head is a dule core design which combine Imote2 platform and second embedded device. The cluster head has extra wireless module and GPS. The extra wireless module has more powerful RF power can increase the wireless communication distance. The GPS is useful for synchronization and localization purposes. The transfer node is functions as coordinate node for managing the cluster heads and hoping the data. The sensing data will be sent to the base station, if needed,

using fast communication device such as WiFi. The base station is the highest level end device that has largest memory, most powerful processor and highest communication capability. The base station node is the gateway between smart sensor networks and the Host computer. The base station uploads the data to remote monitoring and control server via satellite, 3G telecommunication or WiMAX communication. A Host computer may be needed in this architecture as an interface to sends commands and parameters to smart sensor networks via the base station.

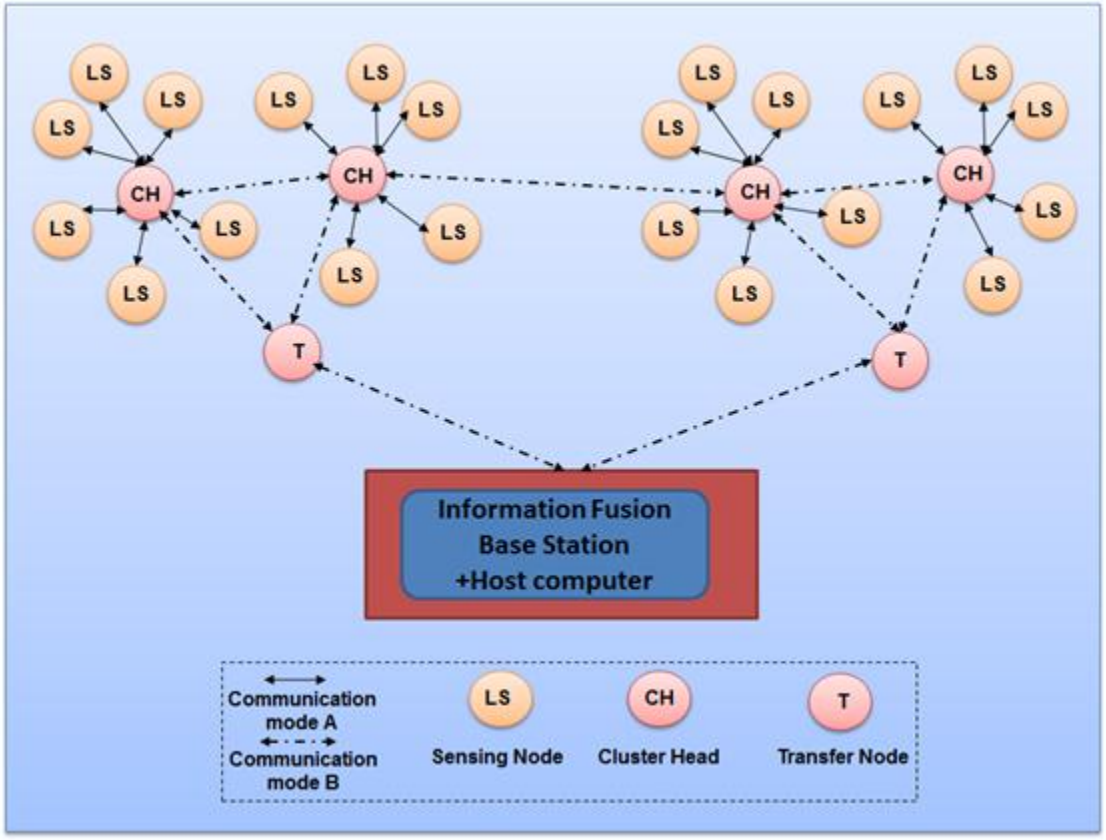

Figure 4.1 Integrated WSN-based SHM system architecture: different roles are assigned to nodes

4.3 Hardware Design

This section shows all hardware design of wireless sensor nodes which are proposed and employed in this study. The proposed wireless sensor nodes are sorted into sensing nodes, cluster head nodes, transfer node, and base station.

4.3.1 Sensing Node

The sensing node consists of mote component and sensor component, is shown in Fig. 4.2. Figure 4.3 indicates the block diagram of sensing node architecture. The "mote" usually contains Microprocessor, Memory storage, and RF chip. The Imote2 platform is chosen for mote component herein. The Imote2 platform is an advanced platform for wireless sensor network nodes. The Imote2 platform is suitable for application in a structural health monitoring system that typically requires signal pre-processing functions applied to sensing nodes [83].

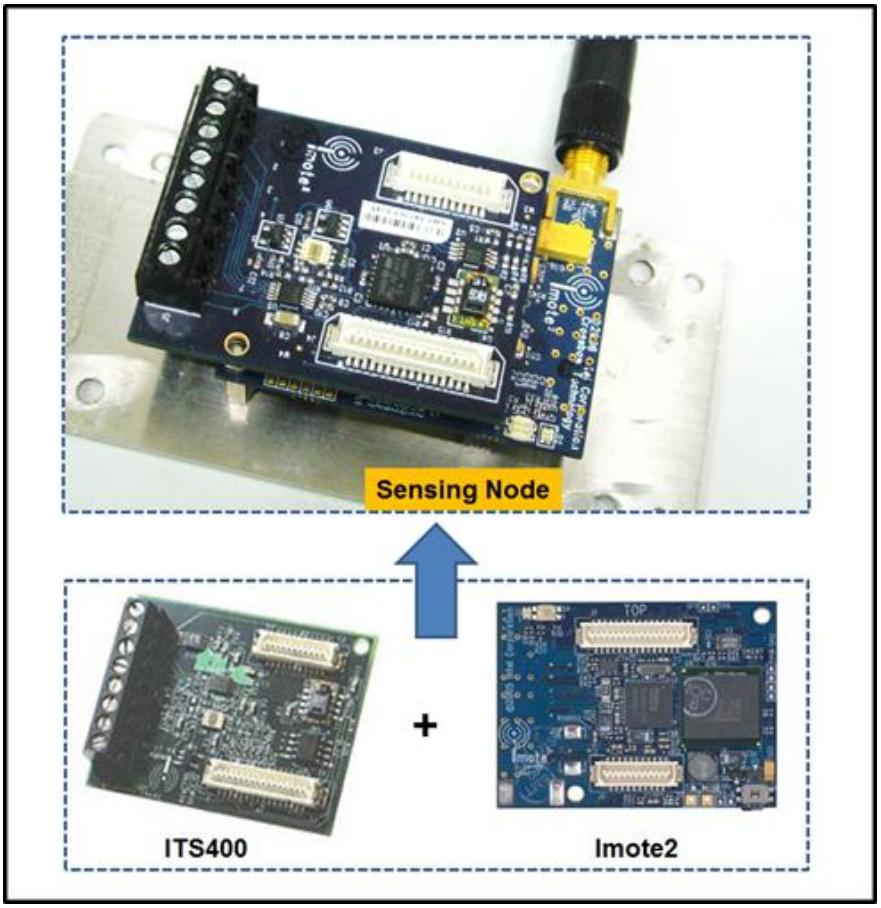

Figure 4.2 Photo of sensing node

The Imote2 platform contains the PXA271 (XScale) processor. This processor operates in the low-voltage (0.85V) and low-frequency (13 MHz) mode, thereby

enabling low-power operation. The processor can be scaled to 104 MHz at the lowest voltage and increased to 416MHz using dynamic voltage scaling. The Imote2 platform can perform complex signal processing functions, such as FFT and image compressing. The Imote2 platform contains 256 KB of SRAM divided into four equal 64KB banks. The PXA271 of the Imote2 platform is a multi-chip module that has three chips in a single package—the processor, 32 MB of SDRAM, and 32 MB of flash memory. Such a memory improvement is a significant advantage compared with the 4kB of RAM in Mica motes. The sensing task must store a massive amount of sample data in external flash memory. The write/read data rate is limited by one slow hardware device. However, the Imote2 platform stores sample data in RAM instead of the complex and slow flash write function. The processor integrates many I/O options, making it extremely flexible in supporting different sensors, A/Ds, and radio options. These I/O options are I2C, three synchronous serial ports, three high-speed UARTs, GPIOs, SDIO, USB client and host, AC97 and I2S audio codec interfaces, a fast infrared port, PWM, a camera interface, and high-speed bus. The Imote2 platform uses the CC2420 IEEE 802.15.4 radio transceiver, which supports a 250 Kbps data rate with 16 channels in the 2.4GHz band.

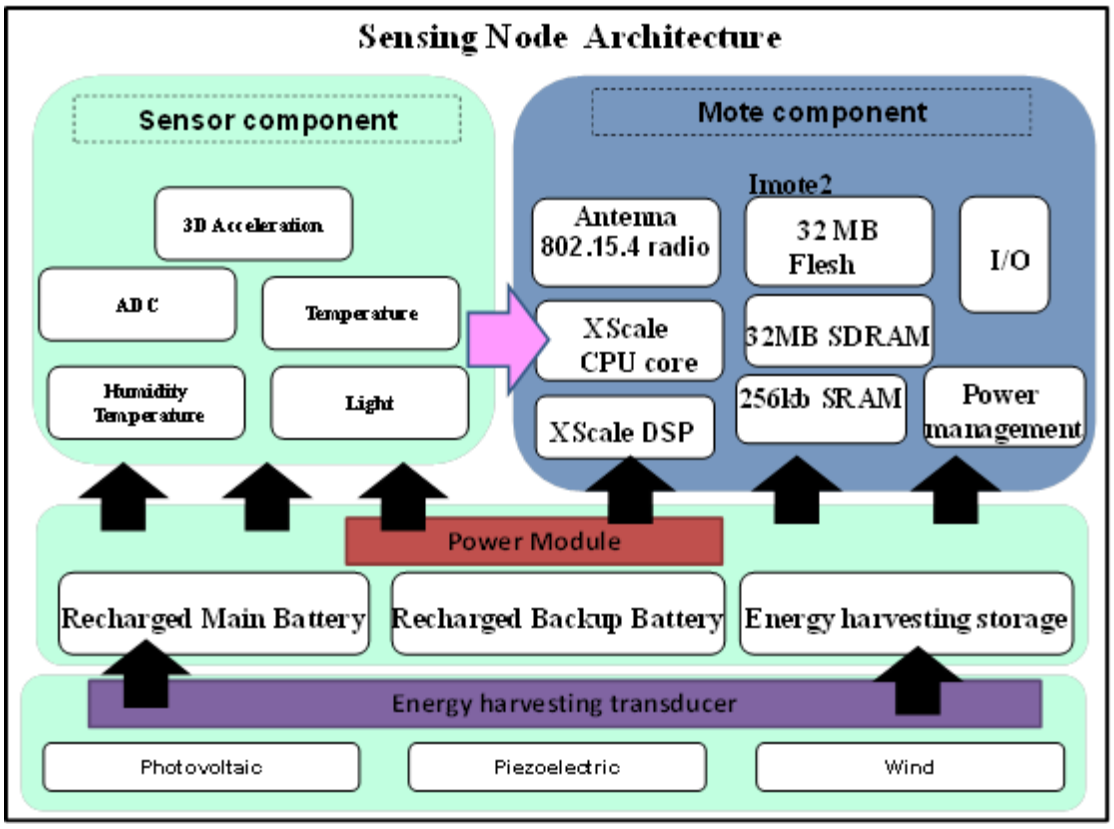

Figure 4.3 Block diagram of sensing node architecture.

Table 4.1 compares mote platforms which are widely used in many research groups. It can be seen in the table that the transmission range of RIRS is 300 m outdoor, two to three times than other motes. The power consumption of TelosB is much lower than other motes. For SHM application, high sampling rate sensing always get great amount of data. By comparison, although Imote2 does not outperform other motes in power consumption and transmission range, the larger memory is more suitable for SHM application. The larger memory is beneficial for smart sensor applications, which is require multiple tasks, such as wireless communication, data logging, data acquisition, and in-situ signal processing.

The sensor component is ITS400 herein. The ITS400 sensor board is designed to connect to the basic connectors on the Imote2. It contains a ST Micro LIS3L02DQ 3d accelerometer, SHT15 temperature/humidity sensor, TAOS TSL2651Light Sensor and

Maxim MAX1363 4 Channel General Purpose A/D. This Accelerometer board has a range of +/- 2g with 12 bit resolution. It communicates to Imote2 with two possible interfaces, SPI or I2C. By default, the sensor is connected to SSP1 on the Imote2.

On board SHT15 sensor can be used for requiring high accuracy temp reading (+/- 0.3 degC) and humidity. This sensor interfaces to the Imote2 through two GPIO pins. The data pin of the SHT11 is connected to GPIO 100, whereas the clock pin is connected to GPIO 98. The TAOS TSL2651 light sensor interfaces to the Imote2 through the I2C bus. The interrupt pin is connected to GPIO99 through a NAND gate. If GPIO 99 conflicts with another board, the BT_TXD pin can be used instead by loading R35. The board includes a Maxim MAX1363, 4 channel, 12 bit resolution general purpose ADC for quick prototyping. Each channel supports 0-3 V input signals. The ADC interfaces to the Intel Mote 2 through the I2C bus. The analog pins are brought out to a Molex PN-39357-0003 connector (J5).

Table 4.1 Comparison of mote platform

	MICA2	MICAZ	IRIS	TelosB	Imote2
Processor	ATmega128L	ATmega128L	ATmega128L	MSP430	XScalePXA271
Clock speed(MHz)	7.37	7.34	16	6.7	13-416
Bus size(bits)	8	8	8	16	32
Program Flash Memory(bytes)	128 k	128 k	128 k	48 k	32 M
EEPROM (bytes)	4 k	4 k	4 k	16 k	
RAM (bytes)	4 k	4 k	4 k	10 k	256 k+ 32 M external
ADC	10 bit	10 bit	10 bit	12 bit	N/A
Active power(mA)	8	8	8	1.8	31@13 MHz

Sleep power(*u*A)	15	15	8	5.1	390
Measurement Flash(bytes)	512 k	512 k	512 k	1024 k	32 M
RF Chip	CC1000	CC2420	At86rf230	CC2420	CC2420
Frequency(MHz)	2400-2483.5	2400-2483.5	2400-2483.5	2400-2483.5	2400-2483.5
Data rate (kbps)	38.4	250	250	250	250
Transmission power (dbm)	-20-5	-24-0	3	-24-0	-24-0
Outdoor range	150 m	100	300	100	100
Indoor range	30 m	30	50	30	30
Typica supply voltage	3.3 V	3.3 V	3.3 V	3.3 V	4.5 V
Size (mm)	58 x 32 x 7	58 x 32 x 7	58 x 32 x 7	65 x 31 x 6	36x 48 x 9
Weight (g)	18	18	18	23	12

4.3.2 Cluster Head and Transfer Node

The cluster head node is a dule core design which combines Imote2 platform and second embedded device FEZ domino platform, which contains extra wireless module and GPS. Figure 4.4 and 4.5 show the Block diagram of Cluster Head node architecture and photograph of Cluster Head node on a box. Cluster head nodes are in charge of collecting data from sensing nodes and managing data; these nodes have

features such data storage on SD card or USB memory devices, database support, Runtime Loadable Procedure (RLP), which is used to implement intensive data processing function and time-critical routines such as FFT. The Transfer node has the same hardware design to cluster head node without Imote2.

Domino is a tiny open-source board based on ARM7 microcontroller from NXP running Microsoft NETMF. With this sophisticated combination, a developer can easily control this microcontroller IOs and interfaces such as SPI, UART (Serial Port) and I2C with simple unified managed code (C# code). Many libraries have already included similar FAT file system, threading, USB Client, USB Host, UART, SPI, I2C, GPIO, PWM, ADC, DAC, and many more.

The extra wireless module used herein is Digi XBee modules. XBee is a wireless communication module that Digi built to the 802.15.4/ZigBee standard. These modules communicate with the microcontroller using the UART. Table 4.2 gives the specification of Xbee models. It can be seen in the table that the transmission range can be designated by choosing specific model. It is useful for deploying WSN in large scaled structure.

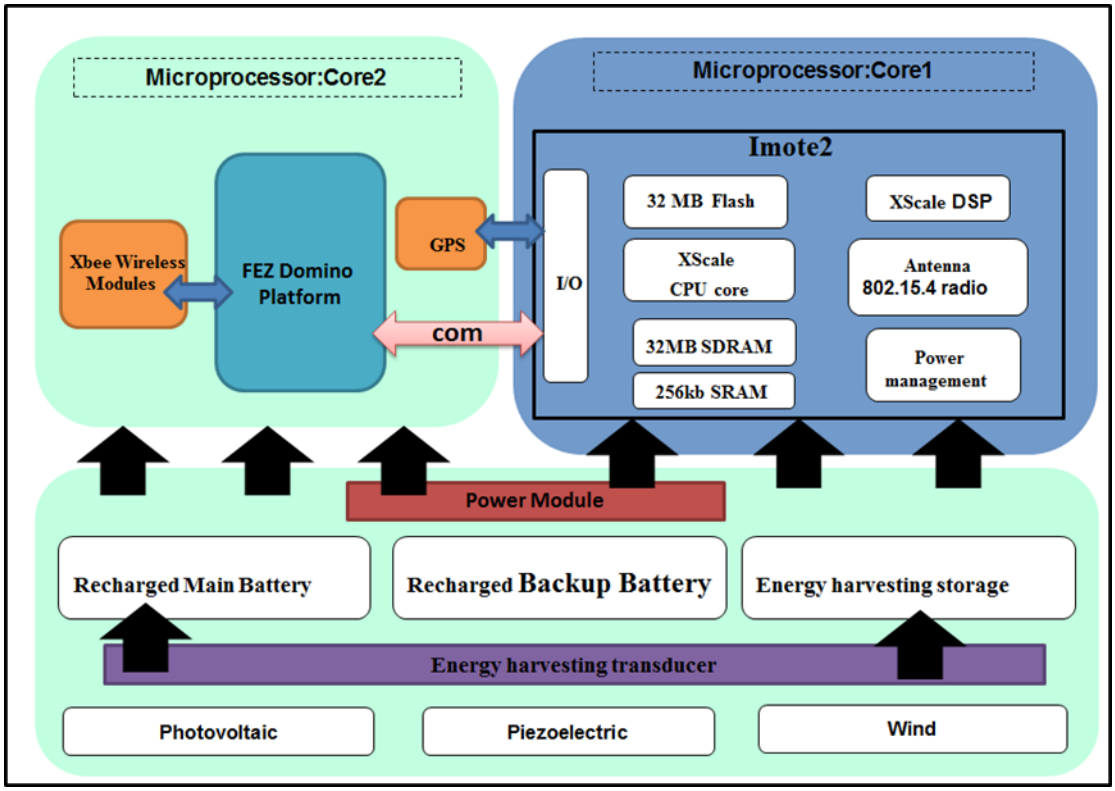

Figure 4.4 Block diagram of Cluster Head node architecture.

Table 4.2 Specification of Xbee models.

Model	XB	XB-Pro	XB-ZB	XB-ZB-Pro	XB-868	XB-900	XB-XSC
Protocol	802.15.4	802.15.4	Zigbee-Pro	Zigbee-Pro	RF	RF	RF
Frequency	2.4GHz	2.4GHz	2.4GHz	2.4GHz	868MHz	900MHz	900MHz
Tx power	1mW	100mW	2mW	50mW	315mW	50mW	100mW
Sensitivity	-92dB	-100dBm	-96dBm	-102dBm	-112dBm	-100dBm	-106dBm
Range	500m	7000m	500m	7000m	40Km	10Km	24Km

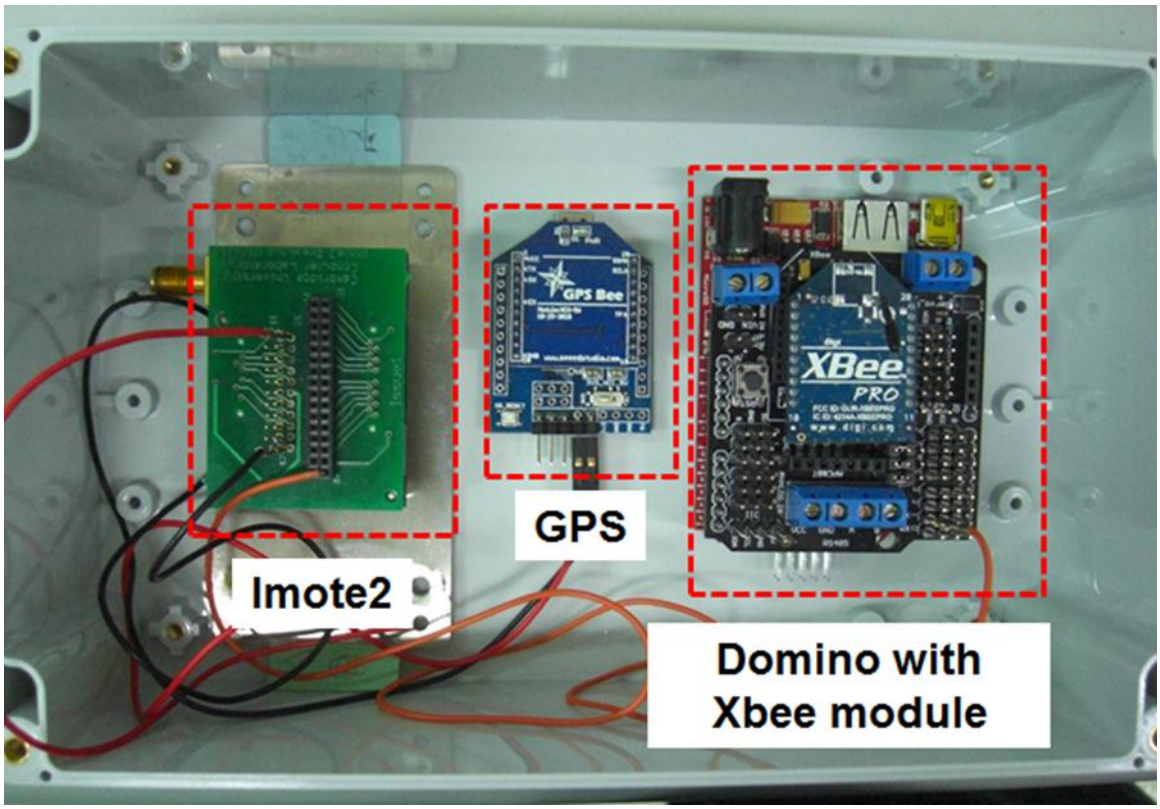

Figure 4.5 Photograph of Cluster Head node on box

4.3.3 Base Station

The base station is the highest level device that can store a mass of data and upload to remote center. The base station is based on ChipworksX Module. ChipworkX Module is a small (67.6mmx47mm) ARM9 processor based board with SO-DIMM200 slot interface and a very high performance. ChipworkX Module supports a complete set of features such as FAT, USB device and many more. In addition, it supports many other exclusive features, for example, USB host, PPP, GPRS, 3G...etc. The sensing data can store and access using SD/MMC cards and USB memory devices such as Thumb Drives and Hard Disks. Moreover, the USB host function can access other devices like mice, keyboards, joysticks, printers, USB modem and more. Furthermore, using SQLite database, allowing fast logging and retrieving of standard SQL quires. For real-time and high processing needs, Runtime

Loadable Procedures, allow users to load their own compiled native code (C or assembly).

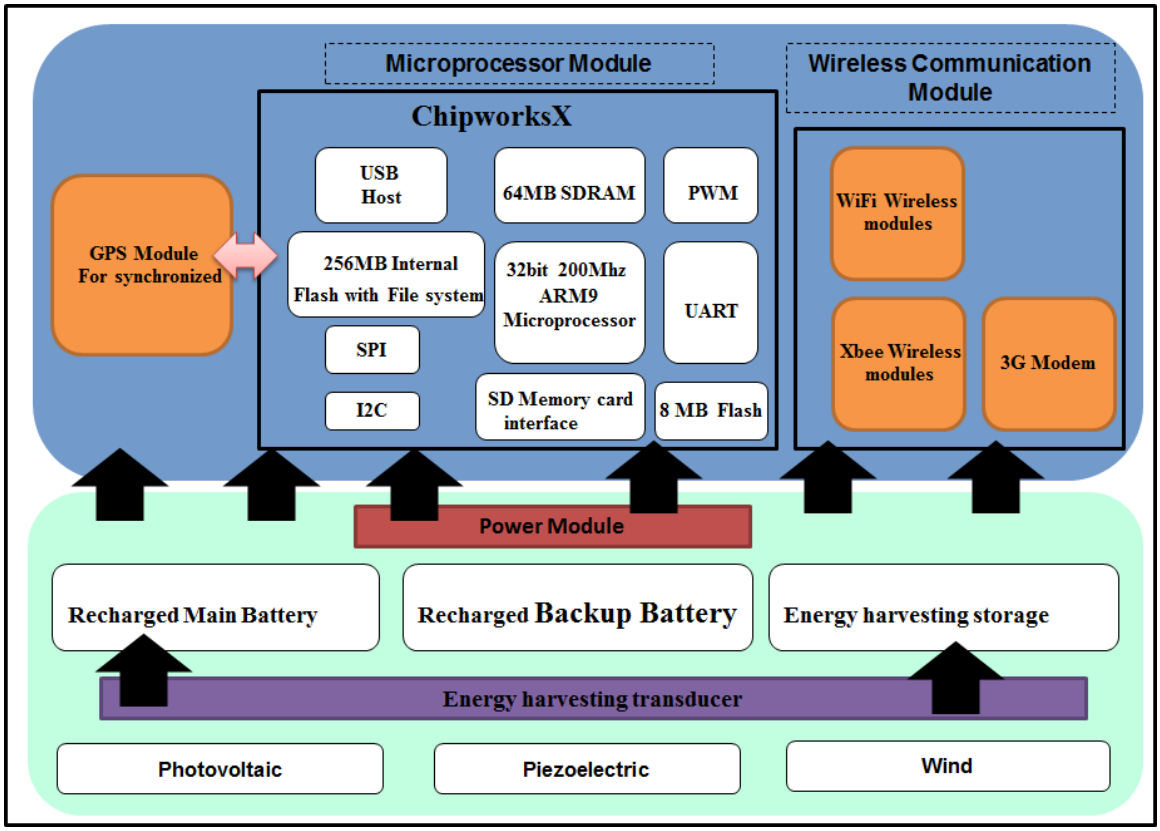

Figure 4.6 Block diagram of base station architecture.

4.3.4 Multi-Sensor Board Design

This study developed a new sensor board which integrates a six degrees of freedom inertial measurement unit (6 DoF IMU) SD746 sensor chip (*SensorDynamics Inc.*) and a GPS module. The SD746 is used to measure acceleration and the GPS is used to synchronize the sensing nodes. Figure 4.7 shows the simplified block diagram of proposed 6 DoF-GPS sensor board. The chosen 6 DoF IMU is a temperature-compensated and calibrated sensor that integrates functionality of 3-axis gyro sensor and 3-axis accelerometer in one small package. Exposing the module to accelerations and angular rates leads to small variations of the MEMS sensors

capacitances. Amplifier and ADC convert these changes in the gyro and accelerometer capacitances into digital signals and then processed by dedicated Digital Signal Processing (DSP) units. The DSP applies filtering, bias and sensitivity adjustment, temperature compensation. Individual sensor configuration data are stored into a non-volatile memory which contains also the individual serial number for production and traceability. SPI and I2C communication interfaces share the same digital IOs. A set of internal monitoring signals, continuously available though both SPI and I2C interface allows the user to check the correct functionality of the entire module. Figure 4.8 presents the photograph of the developed multi-sensor board. Table 4.3 and 4.4 shows the physical and electrical characteristics of gyro and accelerometer sensor.

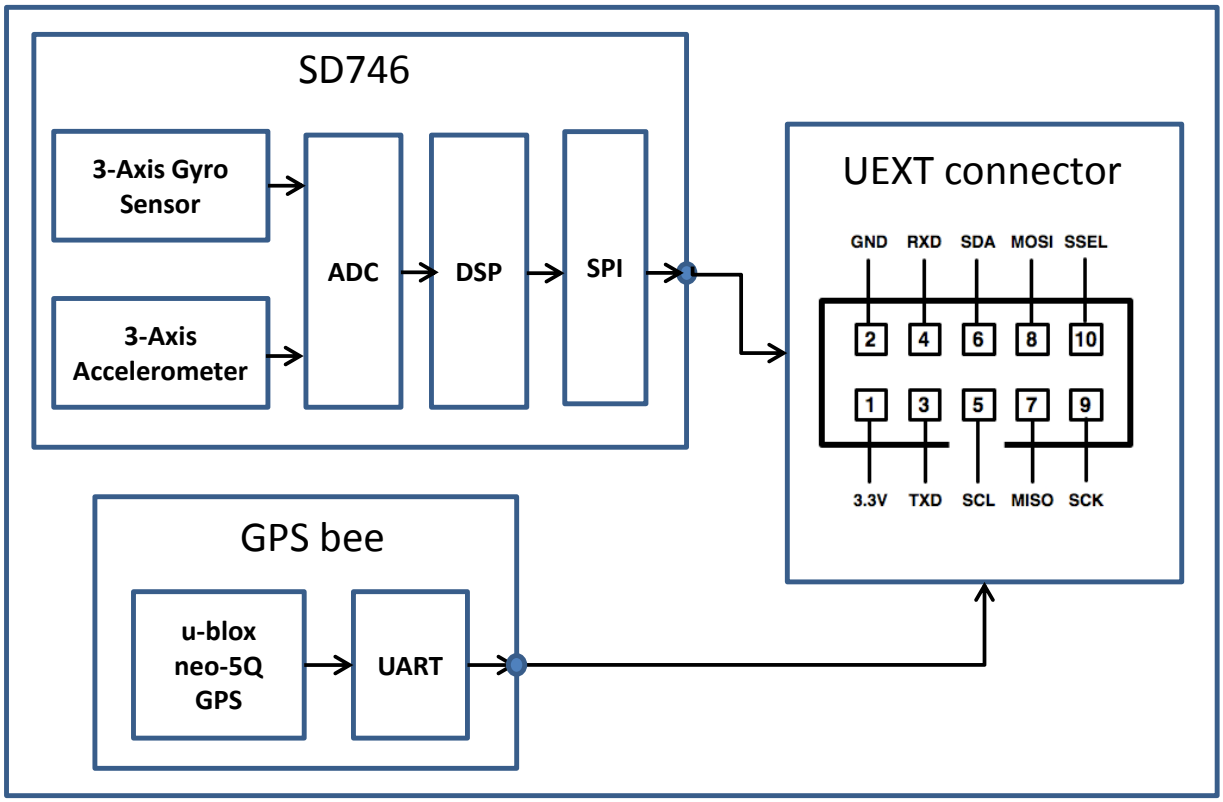

Figure 4.7 Simplified Block Diagram of Multi-sensor board

Figure 4.8 Photography of developed Multi-sensor board

Table 4.3 Physical and Electrical Characteristics of Gyro Sensor

PARAMETER	UNIT	MIN	TYP	MAX
Full Scale Range	°/s	-	±20481	-
Resolution	°/s/LSB	-	0.0621	-
Digital Resolution	bit	-	16	-
Noise Density	°/s/√Hz	-	0.06	-
Nominal Bandwidth (programmable)	Hz	10	-	80
Bandwidth Accuracy	%	-10	-	10
Bias at Room Temperature	°/s	-	±5	-
Bias Variation Over Temperature2	°/s	-	±5	-
Sensitivity Error at Room Temp.	%	-	±2	-
Sensitivity Error Over Temperature3	%	-	±5	-
Linearity Error	%	-	±0.2	-
Cross Axis Sensitivity1	%	-	±2	-
Signal Update Rate	KHz	10	-	-

Table 4.4 Physical and Electrical Characteristics of Accelerometer Sensor

PARAMETER	UNIT	MIN	TYP	MAX
Full Scale Range	g	-	±84	-
Resolution	μg/LSB	-	244.1	-
Digital Resolution	bit	-	16	-
Noise Density	(mg)/√Hz	-	0.28	-
Nominal Bandwidth (programmable)	Hz	10	-	80
Bandwidth Accuracy	%	-10	-	10
Bias at Room Temperature	g	-	±0.05	-
Bias Variation Over Temperature2	g	-	±0.2	-
Sensitivity Error at Room Temp.	%	-	±2	-
Sensitivity Error Over Temperature3	%	-	±5	-
Linearity Error	%	-	±0.5	-
Cross Axis Sensitivity	%	-	±2	-
Signal Update Rate	KHz	10	-	-

The GPS module is designed based on NEO-5Q GPS chip (*Ubox Inc.*) and used to synchronize the sensing nodes. The accuracy of timepulse signal is 40ns RMS. The NEO-5Q has a 32-channel acquisition engine with over 1 million effective correlators and is capable of massive parallel searches across the time/frequency space. This enables a Time To First Fix (TTFF) of less than 1 second while long correlation/dwell times make possible the best-in-class acquisition and tracking sensitivity. An available functionality is KickStart, a new feature enabling accelerated acquisition of weak signals. Once acquired, satellites are passed on to a power-optimized dedicated tracking engine. This arrangement allows the GPS engine to simultaneously track up to 16 satellites while searching for new ones. It has several features that are shown below:

i. 50-channel u-blox 5 engine with over 1 million effective correlators
ii. <1 second Time To First Fix for Hot and Aided Starts
iii. -160dBm acquisition and tracking sensitivity
iv. Accelerated startup at weak signals for modules with KickStart feature

v. Supports AssistNow Online and AssistNow Offline A-GPS services; OMA SUPL compliant
vi. 4 Hz position update rate
vii. Miniature 2.0mm pitch header, compatible with Xbee socket

4.3.5 Power Module

Power sources and power consumption are the critical issue in WSN if batteries have to be periodically replaced. Hence, this study proposed a power module with energy harvesting system and energy storage unit. The proposed theory is harvesting the ambient energy like the vibration of the bridge to power the sensor device or to recharge the primary battery. A novel energy harvesting based on piezoelectric transducer was developed. Next section completed describes the proposed energy harvesting system in detail.

4.4 Windmill-Magnet Integrated Piezoelectric (WMIP) Energy Harvesting System

Although a wireless sensor network based structural health monitoring system has many benefits, power sources and power consumption are the critical issue if batteries have to be periodically replaced. Therefore, harvesting and storing the ambient sources of energy to supply the sensor node seems to be an agreeable approach. The sources of ambient energies typically include thermal, sunlight, wind, RF and vibration energy. This study only considered the vibration based piezoelectric energy harvesting approach. Several researches proposing and reviewing the possible energy harvesting schemes can be found in the literature [111-114].

4.4.1 General Theory of Vibration-Based Energy Harvesting Method

A single degree of freedom lumped spring mass system is mostly utilized to model a vibration-based energy harvesting system. A diagram of a piezoelectric cantilever beam with a proof mass at the end and a model of equivalent lumped spring mass system is shown in Fig.4.8. The equation of motion of a single degree of freedom (SDOF) system consisting of a mass *m*, a spring with spring constant *k*, and a damping coefficient *c* under external excitation is described as

$$m\ddot{z}(t)+c\dot{z}(t)+kz(t)=-m\ddot{y}(t) \tag{4.1}$$

where z is the net displacement. Assuming that the external excitation is harmonic given as $y(t)=Y\sin(\omega t)$, the steady –state solution for the mass displacement is given by

$$z(t)=\frac{\left(\frac{\omega}{\omega_n}\right)^2}{\sqrt{\left(1-\left(\frac{\omega}{\omega_n}\right)^2\right)^2+\left(2\xi\frac{\omega}{\omega_n}\right)^2}}Y\sin(\omega t-\phi) \tag{4.2}$$

where the ϕ is the phase angle given by

$$\phi=\tan^{-1}\left(\frac{\omega c}{k-\omega^2 m}\right) \tag{4.3}$$

The approximate mechanical power of a piezoelectric generator can be given by

$$P = \frac{m\xi Y^2 \left(\frac{\omega}{\omega_n}\right)^3 \omega^3}{\left[\left(1-\left(\frac{\omega}{\omega_n}\right)^2\right)^2 + \left(2\xi\frac{\omega}{\omega_n}\right)^2\right]} \tag{4.4}$$

The maximum energy can be extracted by setting the excitation frequency to match the natural frequency of the system and is given by

$$P = \frac{mY^2\omega_n^{\ 3}}{4\xi} \tag{4.5}$$

Observing Eq. (4.5), it provides evidence that power can be optimized by lowering damping, increasing natural frequency, mass, and amplitude of excitation.

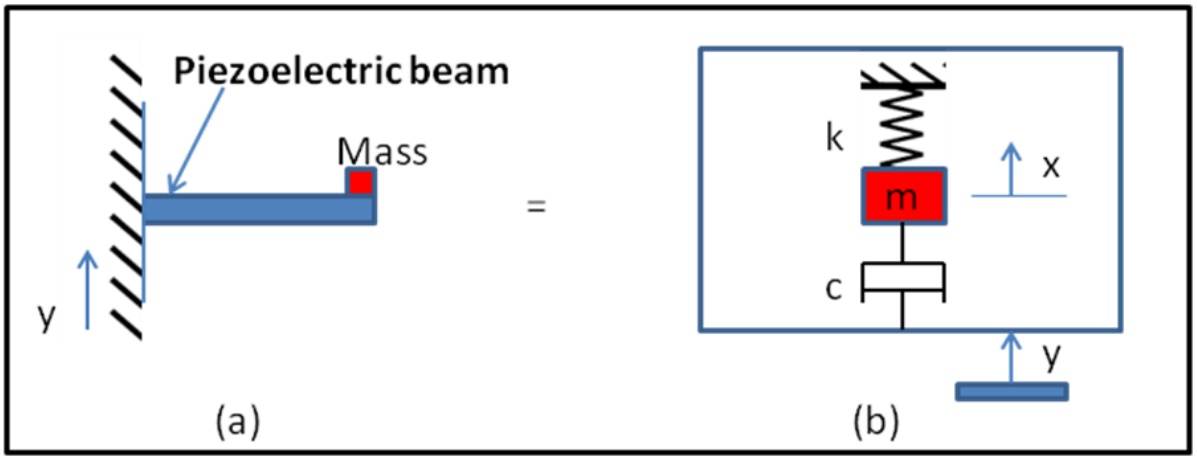

Figure 4.9 (a) Cantilever beam with tip mass, (b) model of equivalent lumped spring mass system

4.4.2 Energy Harvesting Circuits

A typical energy harvesting circuit, with piezoelectric generator, battery and

sensor, is shown in Fig.4.10. The piezoelectric material produces an ac voltage output when the piezoelectric deformed. Therefore, this voltage needs to be converted to a dc voltage before charging the capacitor. The four diodes form a bridge circuit to perform a rectifier. Energy harvesters typically produce small amounts of energy over long periods, therefore an energy storage component in the form of a supercapacitor usually contain in harvesters system. A larger capacitor provides power for a longer time for the same load but takes more time to charge it. Typical supercapacitor often has a much lower voltage than standard electrolytic capacitors, a zener diode usually used to prevent the voltage across the supercapacitor from increasing beyond its maximum voltage rating. When applying a load, the supercapacitor discharging immediately, and the voltage across the supercapacitor starts dropping. Hence, a dc/dc-voltage-converter IC is used to assurance a fixed voltage at the output.

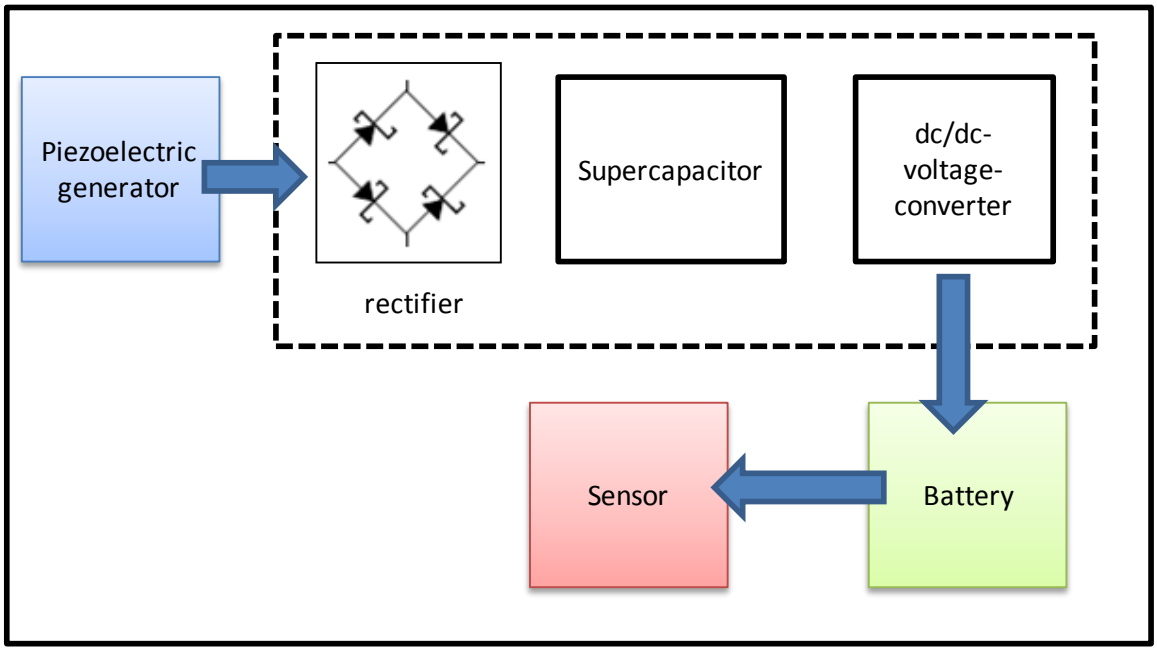

Figure 4.10 Typical piezoelectric harvesting circuit

The typical piezoelectric harvesting model can be improved via new energy harvesting IC, LTC3588-1 (*LINEAR TECHNOLOGY*). This IC combines a low-loss

full-wave bridge rectifier with a high efficiency buck converter to form a tiny energy harvesting component for an ambient energy harvesting. The peak load currents are much higher than a piezoelectric generator can produce. Thus the LTC3588-1 accumulates energy that released to the load to supply the sensor or controller. For the different purpose of applications, this IC provides four output voltages, 1.8V, 2.5V, 3.3V and 3.6V via two selectable pins. Typically, up to 100mA of continuous output current can be provided; however, a higher output current can be supplied by way of sizing the output capacitor. Base on this advanced energy harvesting IC, the architecture of energy harvesting based wireless sensor node was shown in Fig.4.11. A LTC3588-1 connects with piezoelectric generator and backup battery to supply the sensor. This architecture proposed that when ambient energy is obtainable, the battery is unloaded, but when the ambient source ceases, the battery initiates and serves as the backup power supply. The backup battery must connect with a series blocking diode connected to VIN pin to prevent reverse current flowing into the battery. Any stack of batteries can be used as long as the battery voltage does not exceed 18V. One should be considered that the peak voltage of piezoelectric generator should exceed the battery voltage. This approach not only decreases the replacing time of battery, but it also improves reliability and elasticity of sensing system. For instance, an energy harvesting sensor node is deployed on a structure such as a bridge, may gather energy when the vehicles pass through the bridge. However, in off-peak times the vehicles are rarely and vibration is also low, a battery backup can still supplies the sensor node.

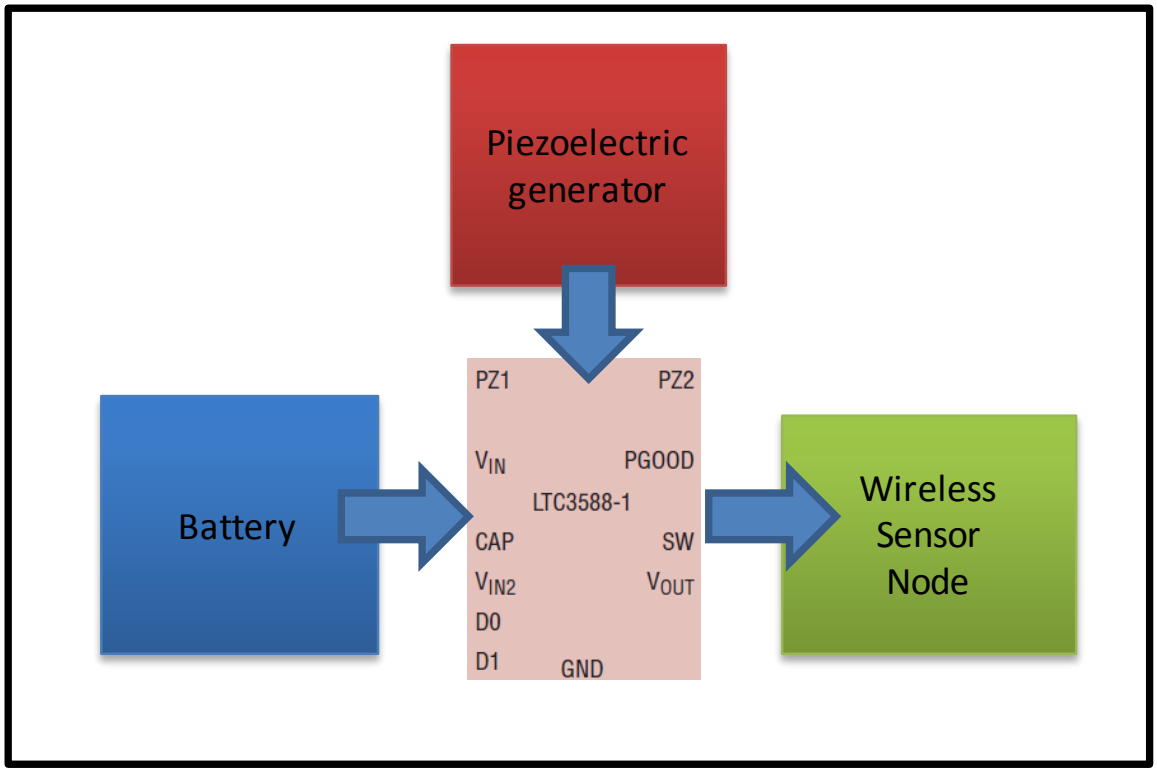

Figure 4.11 Architecture of energy harvesting based wireless sensor node

4.4.3 Windmill-Magnet Integrated Piezoelectric Energy Harvesting System

Most researchers tested piezoelectric energy harvesting device on machine or motor. The reason is the regular high frequency vibration of structure such as machine or motor can give maximum efficiency of energy harvesting. However, the low frequency vibration of civil structure such as bridge limits the energy harvesting efficiency. Therefore, this study proposed a scheme to solve this barrier. In first stage, the idea is to transfer the rotation of windmill to vertical vibrate the piezoelectric beam for energy harvesting. The proposed simple concept is shown in Fig. 4.12 Three piezoelectric materials were tested for the proposed concept shown in table 4.5.

Table 4.5 Different types of piezoelectric product

Type	Dimension(length X width)	Manufacturing Company
PZT	60X20mm	APC
MFC	85X28mm	Smart Material
Raw Volture	100X25.4mm	MIDE

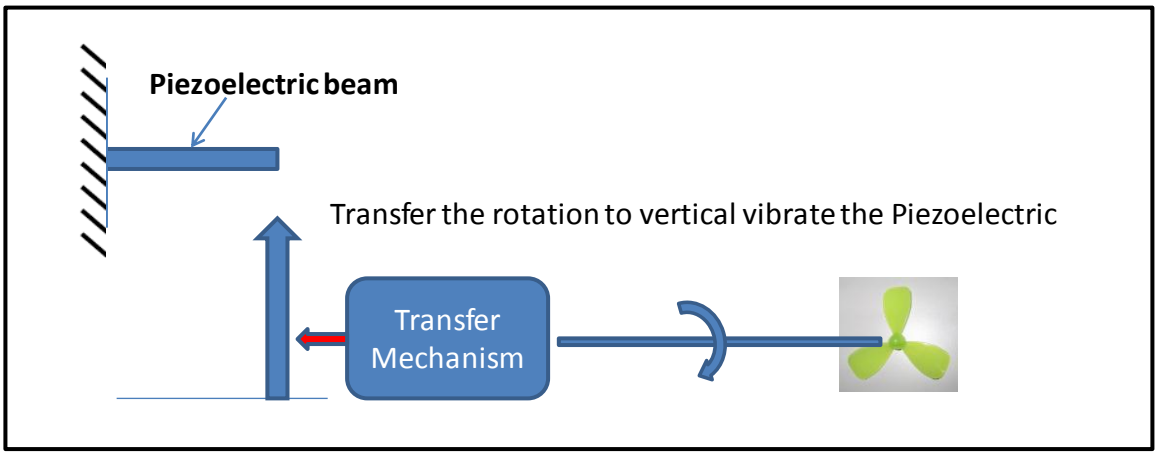

Figure 4.12 Schematic diagram of windmill based piezoelectric harvesting system

Fig. 4.13 shows the experimental setup on overpass in Tokyo University. A piezoelectric film was set as a cantilever beam mounted on a base which was fixed in the bridge. Wind can drive the windmill to beat the piezoelectric film to output the voltage. The Fig. 4.14 to 4.16 illustrates the output voltage of PZT, MFC and Raw Volture respectively. As shown in Figure, the peak voltage represents the high voltage output when the windmill beat the beam. The result also shows the MFC has high voltage under the same excitation. The result confirms that the proposed windmill based piezoelectric energy harvesting concept is practical. However, contact between windmill and piezoelectric beam might stop the whirling of blade. To solve this problem, a novel windmill-magnet integrated piezoelectric (WMIP) energy harvesting system was proposed in Fig. 4.17. The proposed WMIP harvesting system integrates a windmill, magnet and piezoelectric beam for energy harvesting. A magnet was

bonded on the tip of piezoelectric beam as a mass. A windmill was placed a proper distance from the piezoelectric beam and each blade was attached to a magnet. As the windmill turned, the magnetic force between the piezoelectric beam and windmill caused the beam to vibrate. Figure 4.18 is an example shows that the proposed WMIP energy harvesting system gives high frequency (close to 50Hz) and regular output voltage. This high frequency and regular output voltage provide efficient energy harvesting and storage.

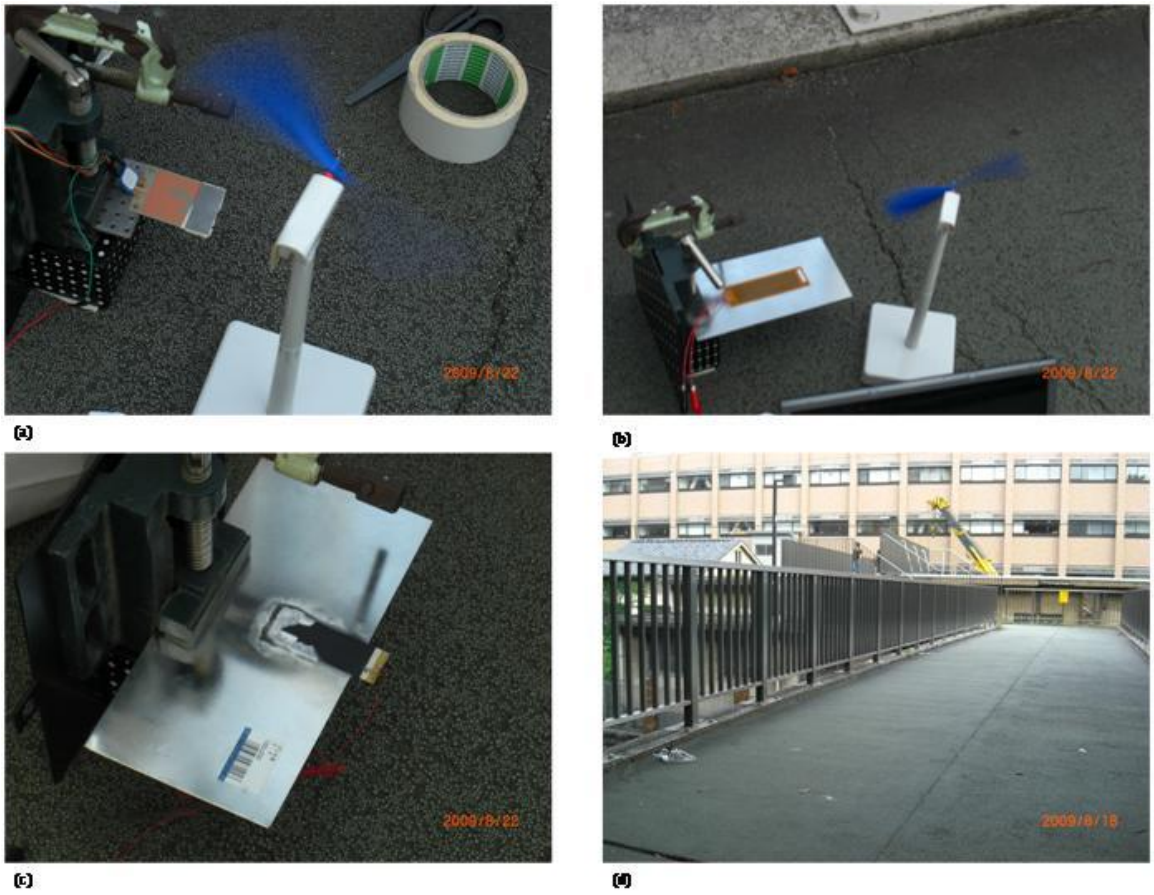

Figure 4.13 Experiment setup of windmill based piezoelectric harvesting system: (a) Raw Volture, (b)MFC, (c)PZT, (d) Overpass in Tokyo University.

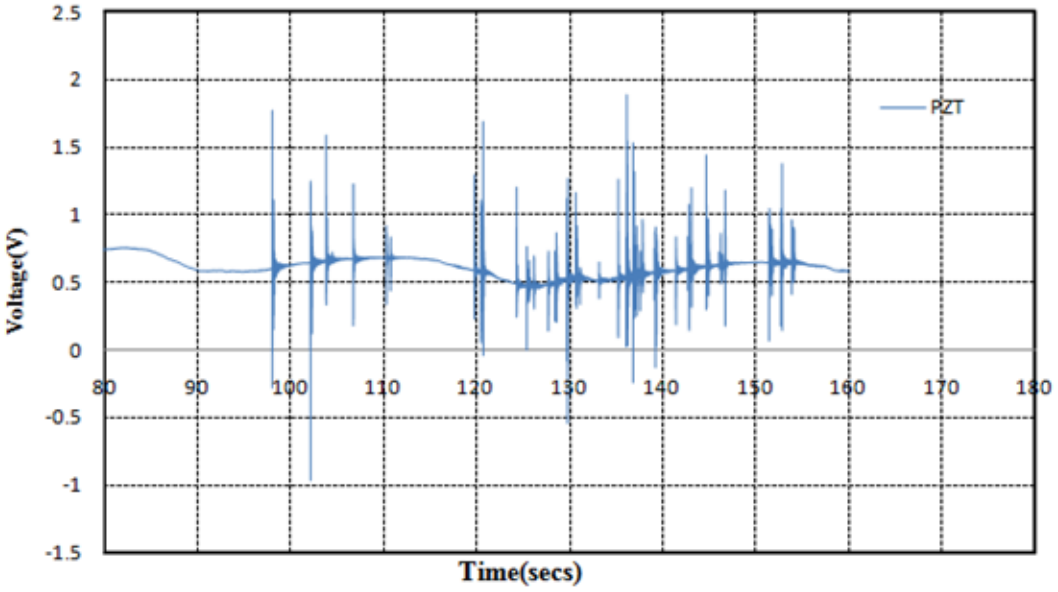

Figure 4.14 Output voltage of PZT

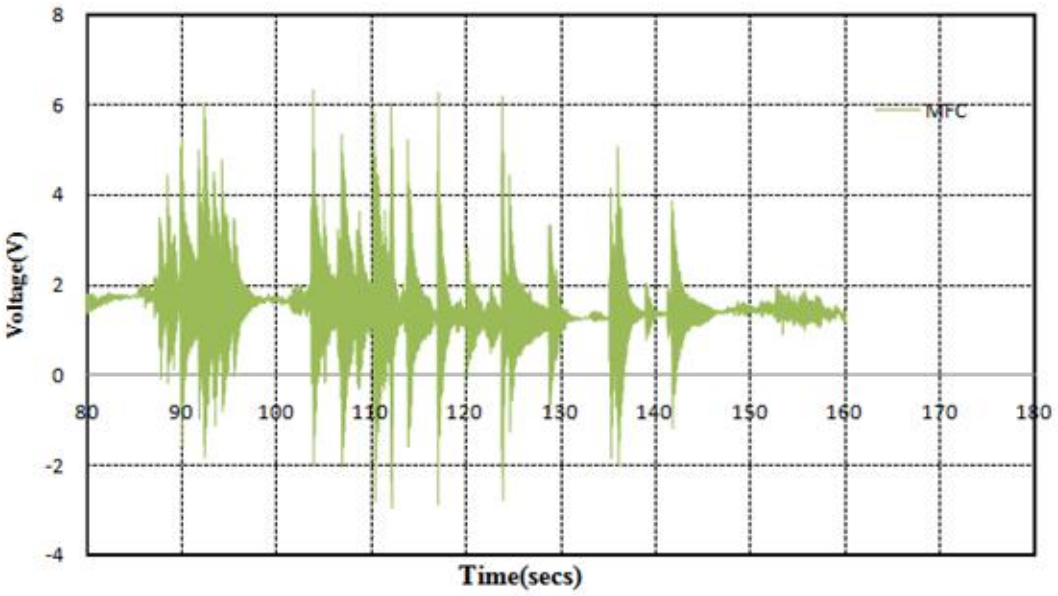

Figure 4.15 Output voltage of MFC

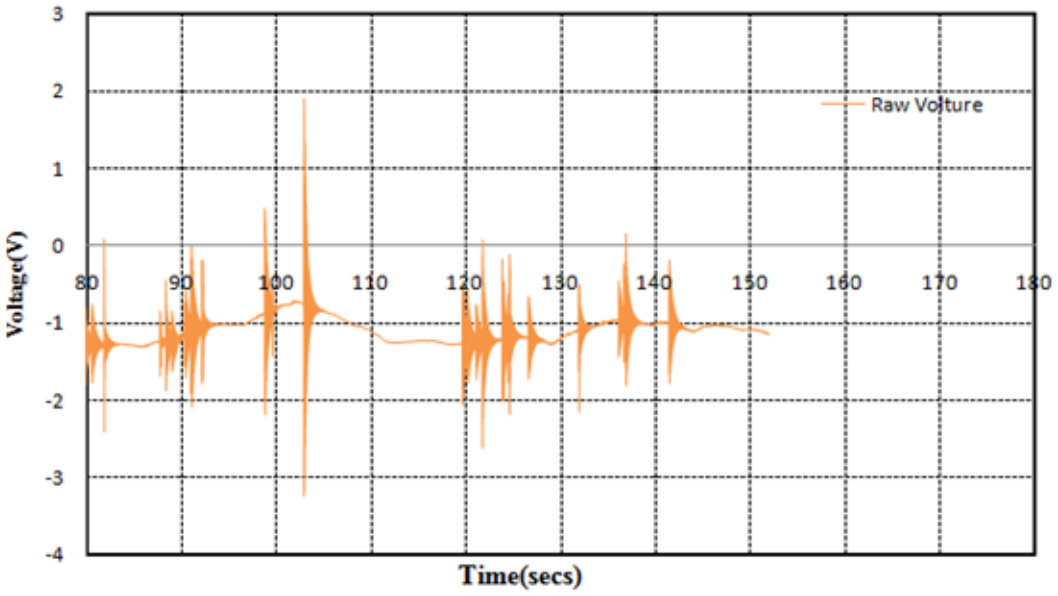

Figure 4.16 Output voltage of Raw Volture

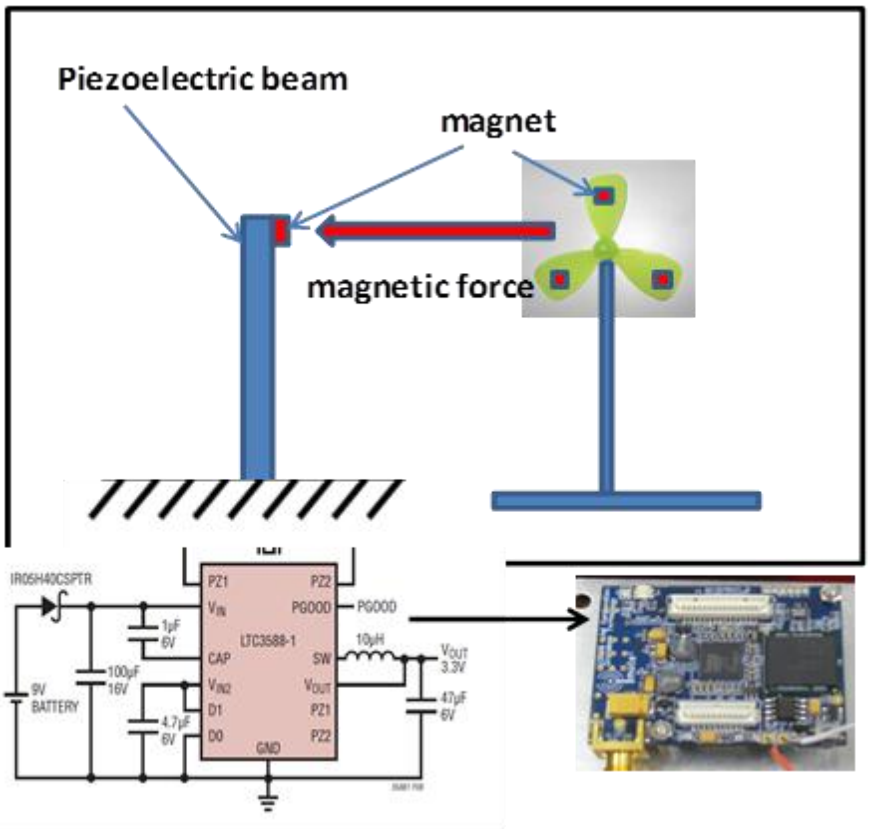

Figure 4.17 Windmill-magnet integrated piezoelectric (WMIP) energy harvesting system

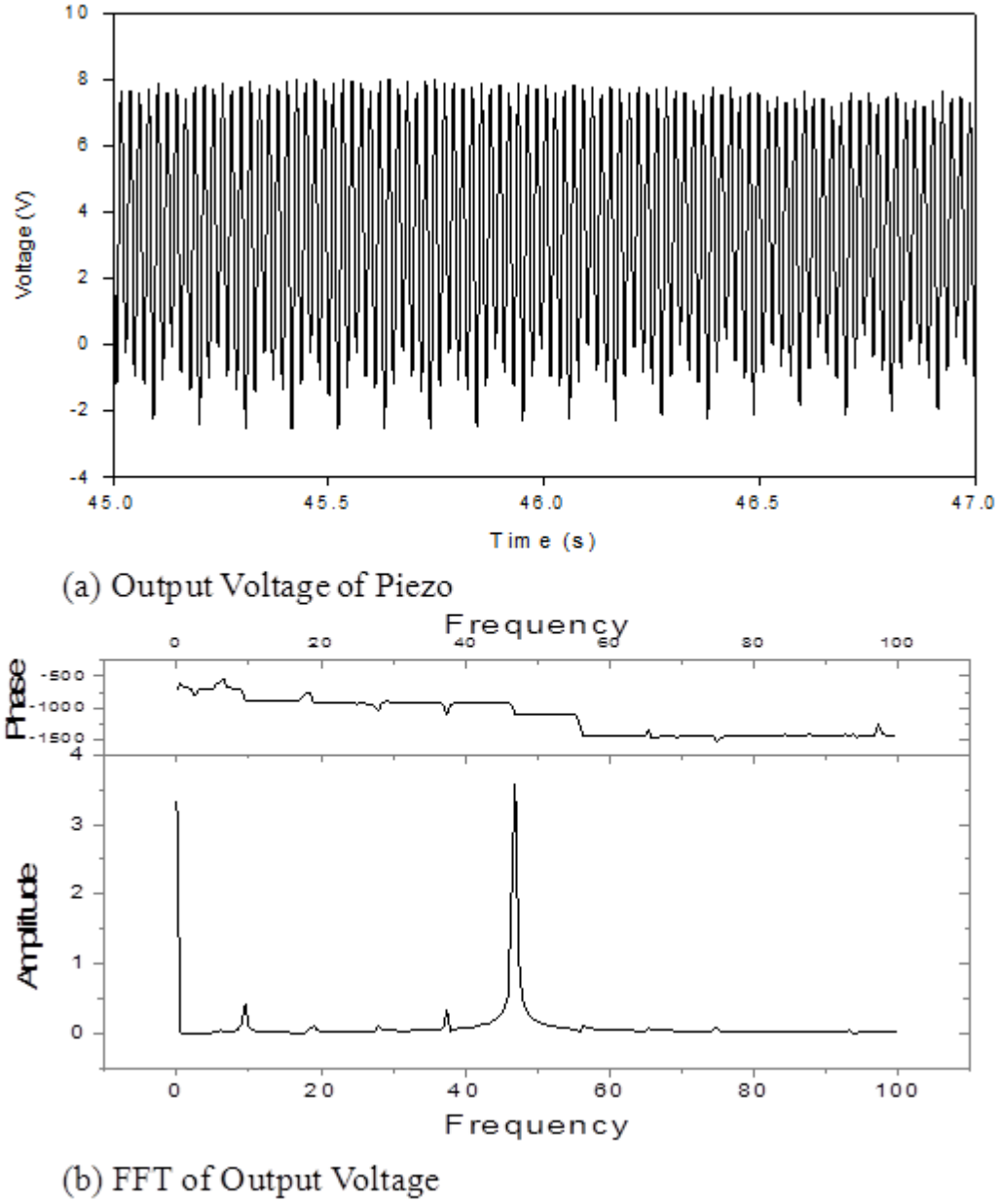

Figure 4.18 Output voltage and FFT of WMIP energy harvesting system

4.5 Three-Tier Software Framework

The proposed software system of integrated WSN-based SHM system is a three-tier-framework, i.e., node, logging and processing tiers. Herein, the node tier consists of developed application functions and is installed on all sensor nodes. The

application functions are developed in a Microsoft NETMF environment. The NETMF and Crossbow's API, i.e., application interface provided by manufacturing company of Imote2, assist most libraries in dealing with all peripherals and drivers, allowing us to develop individual applications for the SHM efficiently. The logging tier, implemented based on C# and NETMF, is installed on the cluster head node and base station and is intended for logging the data and data storage. The processing tier is developed using LabVIEW. This tier has several functions. First, raw data are converted into engineering units and then stored in a database. Next, a customized user interface is performed to select the desired sensor node from the data. The sensing data can also be analyzed by an advanced signal processing tool, e.g., filtering, smoothing, denoise, FFT, wavelet, and further data analysis.

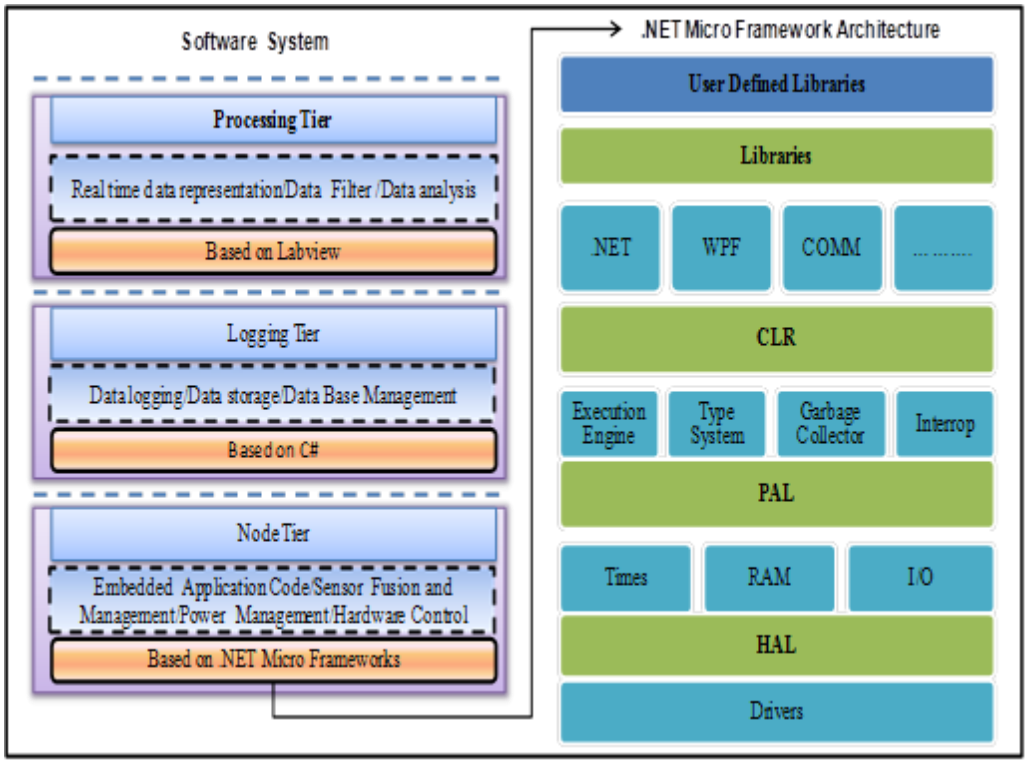

Figure 4.19 The proposed software architecture

4.5.1 Net Micro Frameworks-Based Embedded Development Environment

There are five layers in the basic architecture of NETMF. The platform adaptation layer (PAL) and hardware abstraction layer (HAL) layer deal with the hardware. The PAL supports higher-level integration, including asynchronous communication calls, high-level timers, and list and data structures. The HAL provides generic access to all peripherals and drivers. The NETMF's common language runtime (CLR) layer serves the purpose to load and execute managed code. By supporting managed code, the NETMF CLR allows for rapid development and safe execution of application code using modern programming languages and tools. Microsoft developed several basic application libraries in library layer, and then researchers can use it directly. As aforementioned description, the NET Micro Framework help for dealing all peripherals and drivers, the developer hence can focus on their individual application.

Figure 4.20 shows the structure of Class library which is branch out into three basic class of NETMF, basic class library of Imote2, and SHM class. The SHM class, a specialized class, is developed by this study for SHM application. Table4.6 gives a description of these three classes. Based on these three classes, a SHM application for specific purpose can be easily developed. Listing 4.1 presents an example code for periodical deep sleep and sampling. For example, the radio can be initialized via the constructor in `Radio` class: `public Radio (ushort freq, ushort power, ushort pan_address, ushort address)` where define the frequency, power, node address, and PAN address. After the parameters, such as the sampling rate, data types, and data length are declared, the sampling starts remaining 60 s with a sampling rate of 200 Hz.

The sampling data then writing to a packet. After sampling, the packet is sent using the `Send` method. Furthermore, for power saving, the mote can be put in deep sleep mode (drawing 525 uA) for 60 s just call the `DeepSleep` method. Therefore, by using above main functions and other fundamental APIs, the application can be developed rapidly.

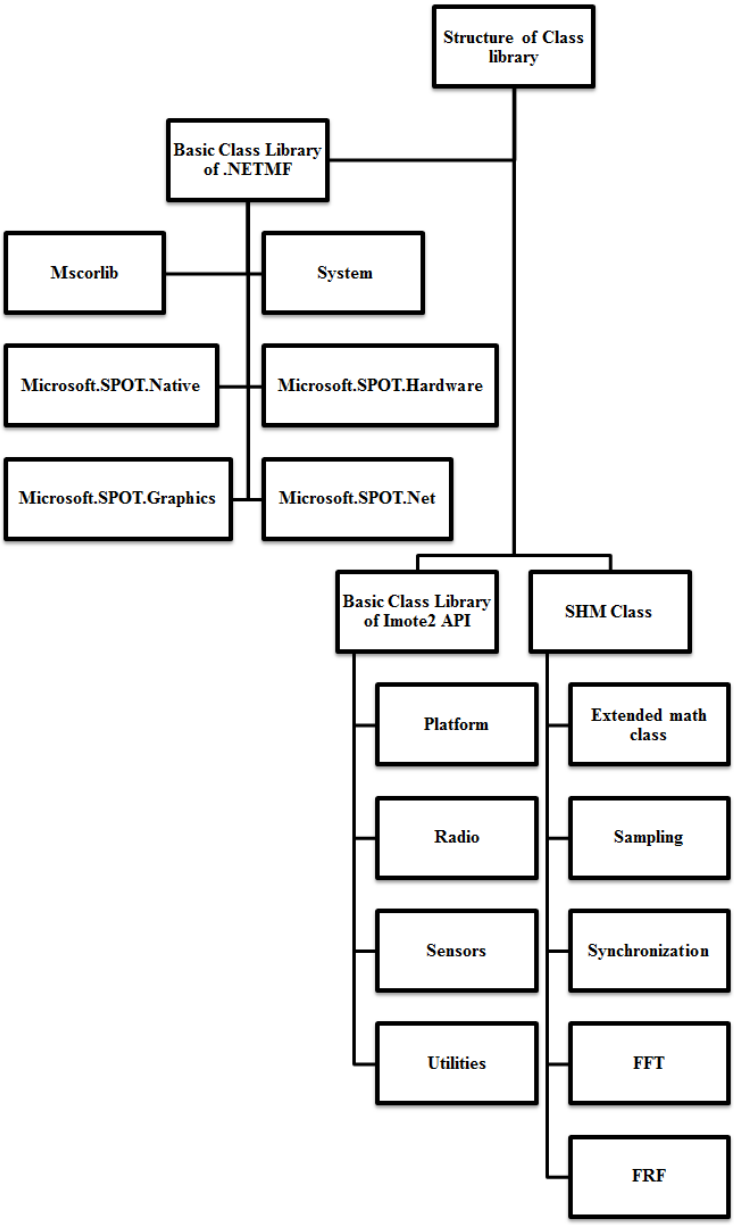

Figure 4.20 Structure of Class library

Table 4.6 Description of Class library

Namespace of class	Name of class	Description of class
Basic class of NETMF	Mscorlib	A subset of the core .NET classes.
	System	Only the System.Net namespace
	Microsoft.SPOT.Native	Core .NET Micro Framework classes.
	Microsoft.SPOT.Hardware	Managed hardware drivers.
	Microsoft.SPOT.Graphics	Low-level graphics classes.
	Microsoft.SPOT.Net	Internal socket drivers
basic class library of Imote2	Platform	For low-level access to the mote hardware
	Radio	To set various radio options
	Sensors	Various sensor drivers
	Utilities	Contains a number of utility classes
SHM class	Extended math class	Extend the basic math class
	Sampling	Sampling the sensor data
	Synchronization	Synchronizing the nodes
	FFT	To calculate FFT
	FRF	To calculate FRF

Listing 4. 1. Sample code for periodical deep sleep and sampling

```
public class XAccel
{
    public static void Main()
    {
        //Configurations
        const ushort _rfChannel = (ushort)RadioChannel.Ch15; // channel 11
        const ushort _rfPower = (ushort)RadioPower.M0DBM;  // -10dbm
        const int packet_length = 64;
        const int packet2_length = 30;
        Radio radio = new Radio(_rfChannel, _rfPower, 0xFFFF, 0xFFFF);
        byte[] packet = new byte[packet_length];
        byte[][] packetall = new byte[50000][];//
        short accelX, accelY, accelZ; //accel raw values
        int samplingrate = 5; //
        samplepakage = 1200;// pakegets
        int sendperiod = 50;
        //Sampling
        for (; ; )
        {
            while (pt < samplepakage)
            {

                        accelX = (short)(accelX + _sensor.AccelXRaw);
                        accelY = (short)(accelY + _sensor.AccelYRaw);
                        accelZ = (short)(accelZ + _sensor.AccelZRaw);

                    packetall[row][index++] = (byte)(Av_x1 & 0xFF);
                    packetall[row][index++] = (byte)((Av_x1 >> 8) & 0xFF);
                    packetall[row][index++] = (byte)(Av_y1 & 0xFF);
                    packetall[row][index++] = (byte)((Av_y1 >> 8) & 0xFF);
                    packetall[row][index++] = (byte)(Av_z1 & 0xFF);
                    packetall[row][index++] = (byte)((Av_z1 >> 8) & 0xFF);
                }
             }
        // sending data then go to deep sleep
            radio.SetRadioOption(RadioOption.LocalAddress, (ushort)_nodeid);
            for (row = 0; row < samplepakage; row++)
            {
                for (index = 4; index < packet_length; index++)
                {
                    packet[index] = packetall[row][index];
                }
                packet[1] = (byte)row;
                System.Threading.Thread.Sleep(sendperiod);
                     radio.Send((ushort)0xFFFF, (ushort)0xFFFF, packet);
            }
             pm.DeepSleep(600);
        }
      } //main
}
```

4.5.2 Data Logging and Data Storage

The logging tier, implemented based on C#, is installed on the cluster head node and base station and is intended for logging the data and data storage. The data is extracted from each packet and written to a text file or store in a database. The packet carries three parts, which are TosMsg header, sensor board header and data payload (Fig.4.21). The TosMsg header carries 5-byte TinyOS compatible header that provides Imote2 protocol compatibility with MICA and IRIS motes. Table 4.7 Shows the TosMsg header content. The next group in packet is the sensor board header that provides basic information of node. Next are the data payload that includes all the information serial number, timestamp, and sensor data. Herein, sensor data denotes 3 readings from X/Y/Z axis of the accelerometer sensor, each is 2 bytes. There are 10 groups in one packet. Table 4.8 and 4.9 present the content of sensor board header and data payload.

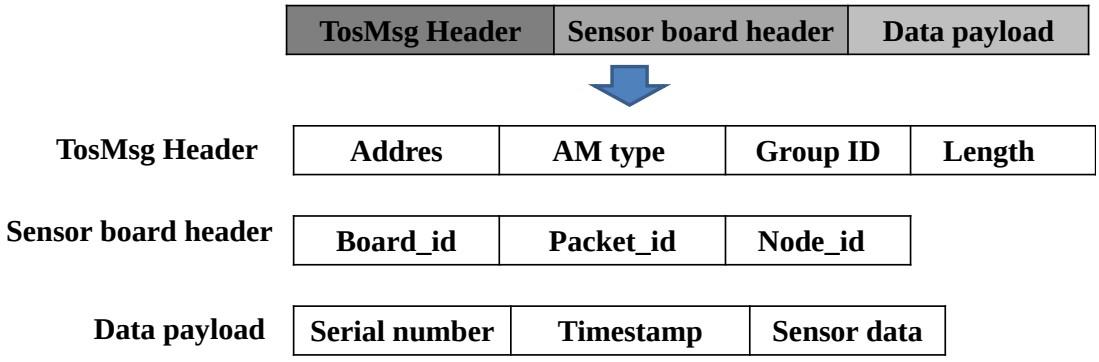

Figure 4.21. Packet format

Table 4.7 TosMsg header contents

Type	Field Name	Description
uint16_t	Address	Destination address of the packet
uint8_t	AM type	TinyOS Active Message ID
uint8_t	Group ID	TinyOS group ID
uint8_t	Length	Length of the packet

Table 4.8 Sensor board header content

Type	Field Name	Description
uint8_t	board_id	XSensor packet type field (Sensor streams are always a constant value of 0x11)
uint8_t	packet_id	XSensor packet sub-type field (XAccel is always a constant value of 0x01)
uint16_t	node_id	Network short address of sending node.

Table 4.9 Data payload

Type	Field Name	Description
uint16_t	serial number	Incrementing sequence number for yield calculation
uint16_t	timestamp	Timestamp information
uint16_t	accel_x	Accelerometer reading of X axis
uint16_t	accel_y	Accelerometer reading of Y axis
uint16_t	accel_z	Accelerometer reading of Z axis
	…	
uint16_t	accel_x	Accelerometer reading of X axis
uint16_t	accel_y	Accelerometer reading of Y axis
uint16_t	accel_z	Accelerometer reading of Z axis

4.5.3 User Interface and Visualized Signal Processing

The processing tier is developed using LabVIEW. This tier has several functions. First, raw data are converted into engineering units and then stored in a database. Next, a customized user interface is performed to select the desired sensor node from the data. The sensing data can also be analyzed by an advanced signal processing tool, e.g., filtering, smoothing, denoise, FFT, wavelet, and further data analysis. Figure

4.22 shows the functions of proposed user interface. Figure 4.23 shows how the sensor data can be represented in a Figure. Chart and nodes distribution can also be conveniently observed. Figure 4.25 presents the damage location in a visualization window which can indicate the location of damage visibly.

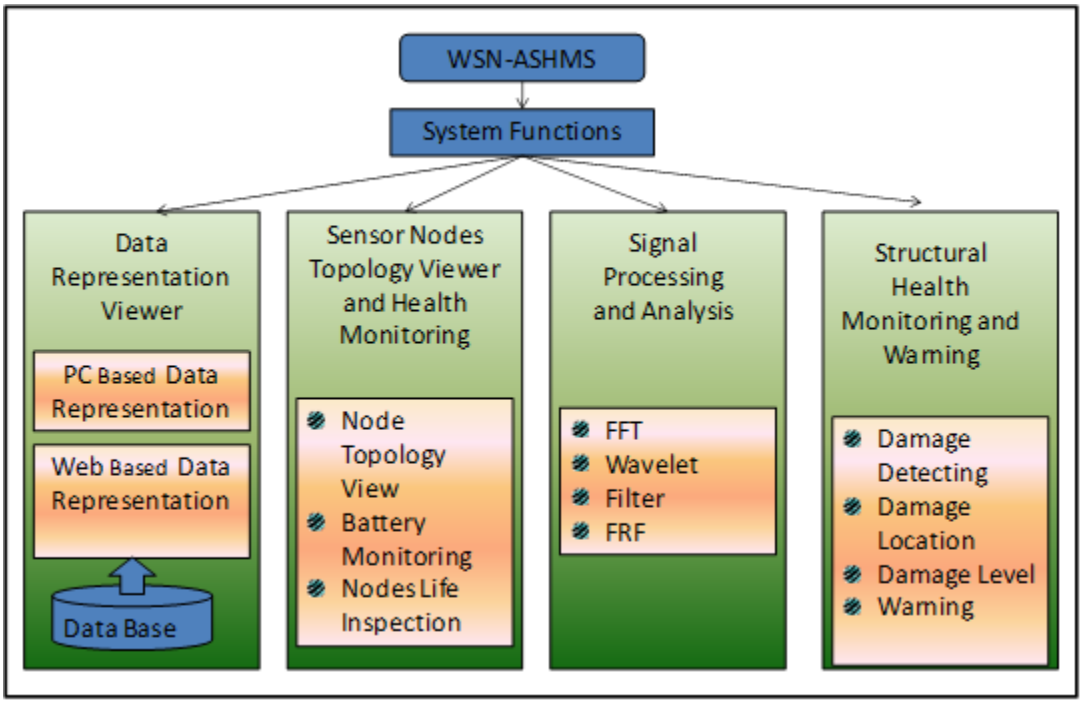

Figure 4.22 Functions of proposed user interface

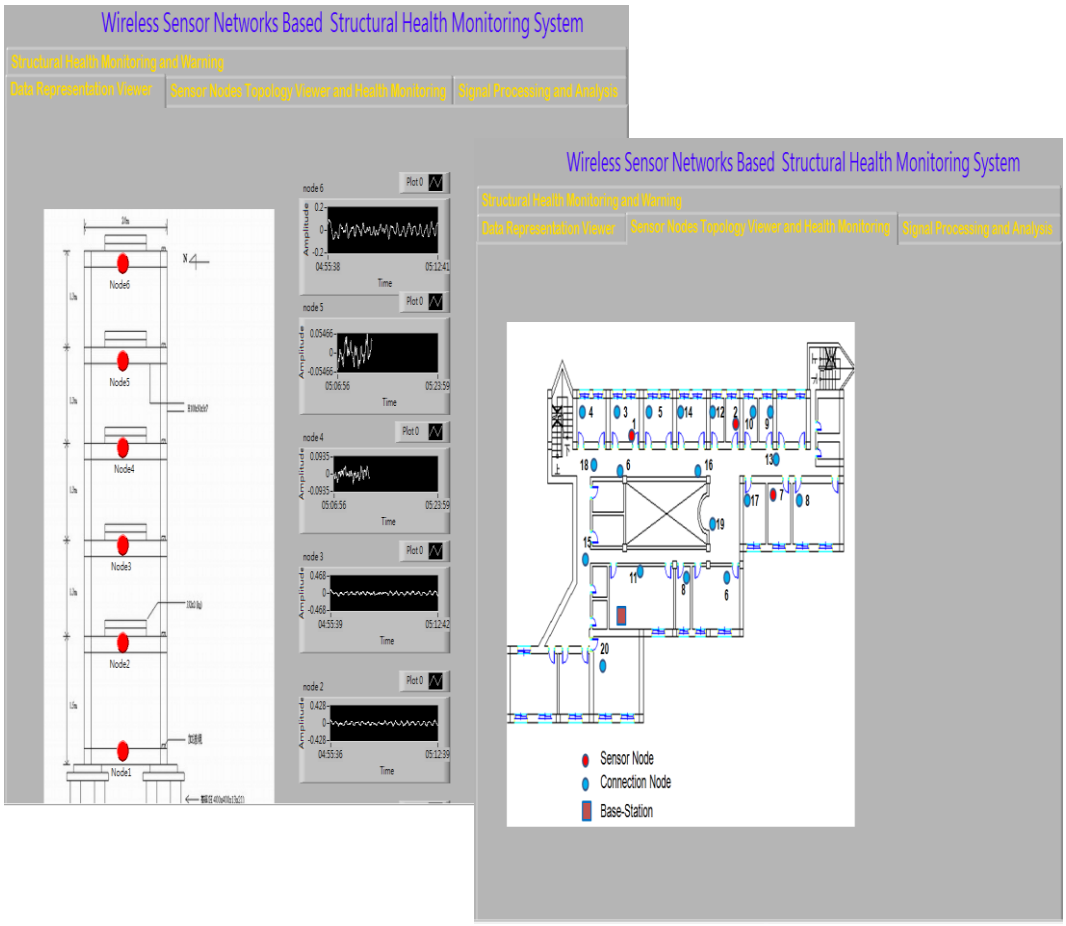

Figure 4.23 Sensor data representation and node distribution

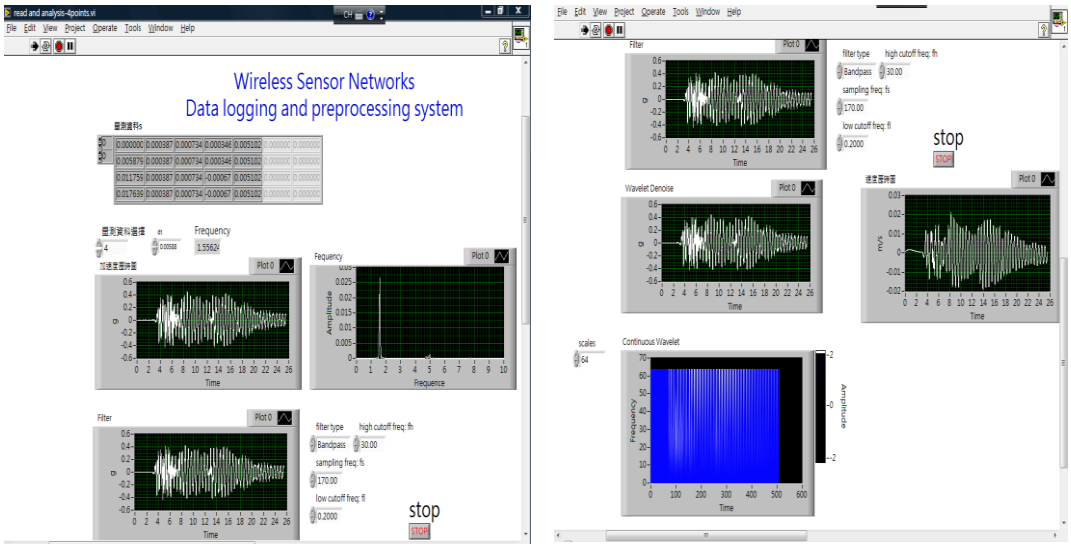

Figure 4.24 Signal processing interface

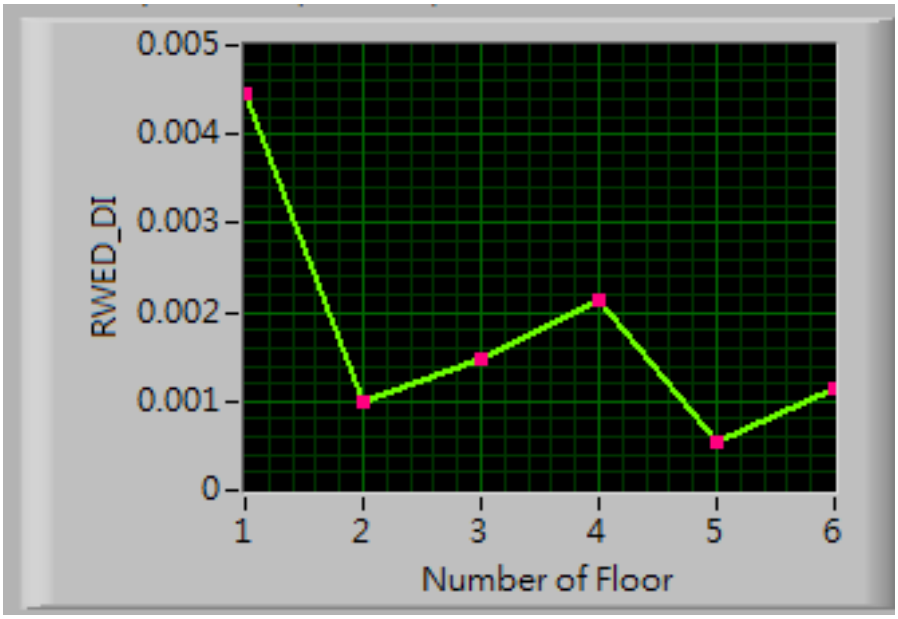

Figure 4.25 Damage location representation

4.6 Reliable Data-Sensing and Transmission Service

In this section, WSN-based middleware services for SHM application are developed. The middleware services include reliable data-sensing and transmission, which are data aggregation, reliable communication, and synchronized sensing. These middleware services are implemented on the nodes running .NETMF and are generally applicable to SHM application.

The reliable data-sensing and transmission service is presented in Figure 4.26. First, after the sensing nodes and cluster head node are initialized, the cluster head node sends an inquiring packet to confirm whether the sensing nodes are ready. The sensing nodes and cluster head node then exchange timestamp packets to synchronize together based on a two-phase synchronization scheme [108]. In general, two main clock errors must be corrected, i.e., skew and offset. In the first phase, the proposed protocol models the skew of all sensing node's clock; each node is then skew

synchronized. Next, the skew is estimated by performing linear regression over multiple timestamp packets from the cluster head node. Each timestamp packet P_i contains the transmit timestamp $t_{B,i}$ obtained at the MAC level, just before the packet leaves the cluster head node. The sensing nodes receive the packet at absolute time $t_{B,i} + D_{B \to S}$ where $D_{B \to S}$ refers to the unknown propagation delay between the cluster head node and the sensing nodes. The sensing nodes then record their local time $LT_S(t_{B,i} + D_{B \to S})$. Although the local time includes the error due to clock skew and offset in addition to propagation delay, the skew of the local clock can still be modeled with respect to the reference clock of the cluster head node by performing linear regression on the difference between $t_{B,i}$ and $LT_S(t_{B,i} + D_{B \to S})$. For *N* packets, the clock skew can be modeled by linear regression over the data set of (x_i,y_i) pairs, where x_i and y_i are $(t_{B,i} - LT_S(t_{B,i} + D_{B \to S}))$ and $LT_S(t_{B,i} + D_{B \to S})$, respectively.

In the second phase, the clock offset is corrected by the classical two-way synchronization exchange in a manner similar to that of the TPSN synchronization protocol [115]. Once a sufficient number of packets to estimate the skew are obtained, the sensing nodes send a packet with the skew-corrected local timestamp, $T1 = LT'_S(T1)$, to the cluster head node. The cluster head node records its received local time $T2 = LT_B(T1 + D_{S \to B})$, then replies with a packet to sensing nodes with *T2* and transmit timestamp *T3*. Upon receiving the packet, the sensing nodes record the skew-corrected local time $T4 = LT'_S(T3 + D_{B \to S})$. Finally, the sensing node can compute its clock offset as $Offset = \left[(T2 - T1) - (T4 - T3)\right] / 2$.

Following completion of the synchronization, all sensing nodes starts to sample data and write data to an array. The parameters, such as the sampling rate, data type,

and data length, are declared before the sampling starts. Following the sampling, the time-scheduling data transmission procedure is initiated to send data from the sensing nodes to the cluster head node. Initially, the sensing nodes wait until a *sending-delay* time is equivalent to (*total sampling time* + *total packet sending time*)* (*node ID*). For instance, if the *node ID* is 0, the sensing node 0 transmits the packet immediately since the *sending-delay* is zero. The data in each sensing node are then taken from the array, filled in a packet, and sent to the cluster head node. With this procedure, each node sequentially sends data to the cluster head node with a respective *sending-delay* to avoid packet collision. However, packets losses occur occasionally, even though the time-scheduling data transmission is designed to avoid packets collision. The base station thus continuously checks the number of packets in the sequence from the sensing nodes and records the number of each missing packet in the sequence. As a result, the base station can request a sensor node to rectify the missed packets.

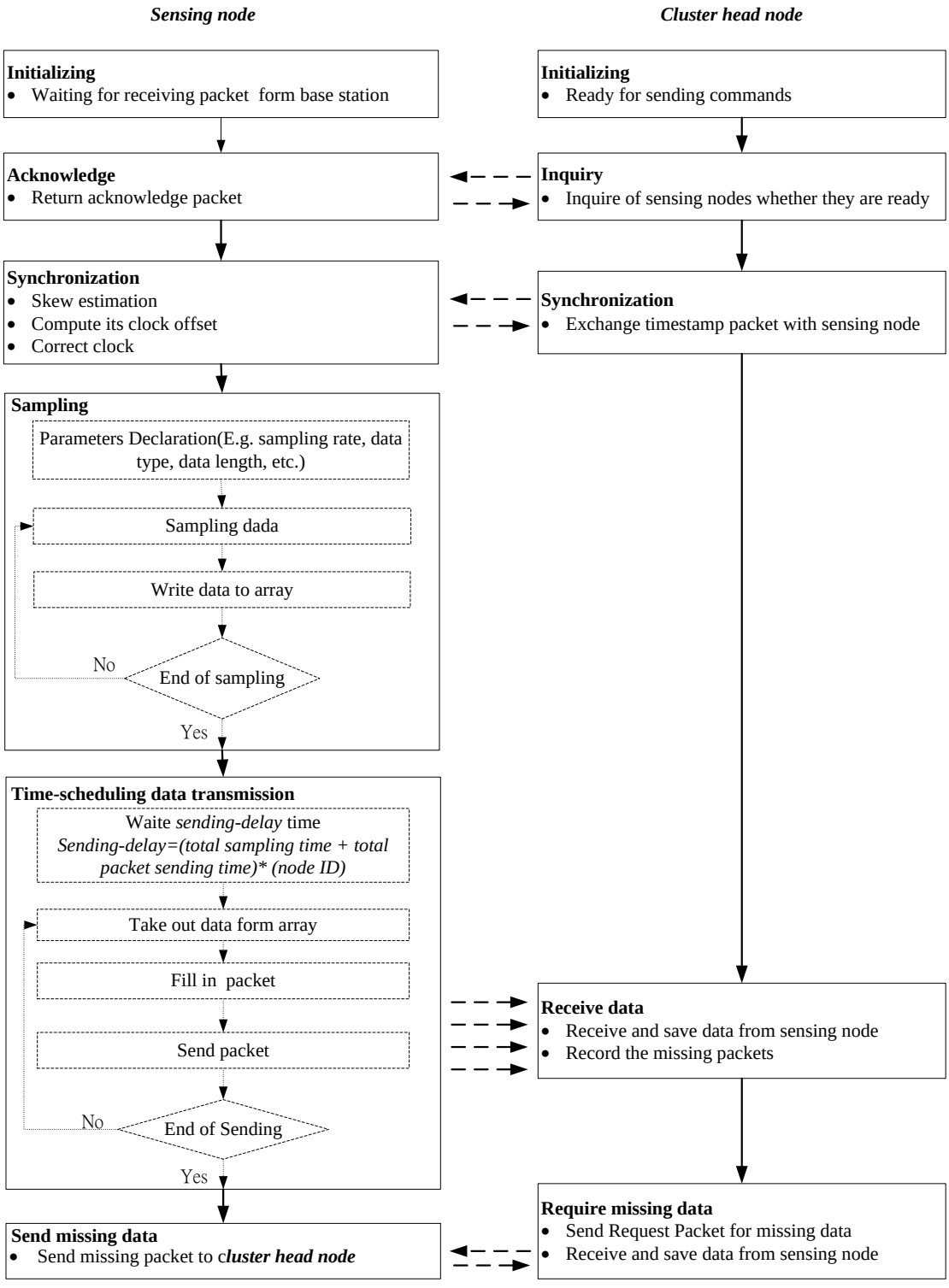

Figure 4.26. Reliable data-sensing and transmission service

CHAPHER 5 DEVELOPMENT OF GLOBAL-LOCAL-INTEGRATED DAMAGE DETECTION APPROACH

5.1 Introduction

Structural health monitoring (SHM) was broadly classified into local and global categories. The Non Destructive Testing (NDT) technique is mostly used in local damage detection. There are many methods for NDE such as ultrasonic, infrared thermography, eddy current X–ray. Such methods can detect tiny or incipient damage; however, it is usually expensive, power hungry and bulky. Global SHM, on the other hand, can discover damage large enough to influence the properties of the entire structure or large sections of it. Most existing global damage detection methods identified damage based on changes in basic modal properties that extract from structural response by low cost sensing systems.

Both local and global SHM each has its own benefits and shortcoming, hence integrating aforesaid two methods can obtain more effective damage detection result than only using one of them. This research proposed a global-local-integrated damage detection approach which is shown in Fig. 5.1.

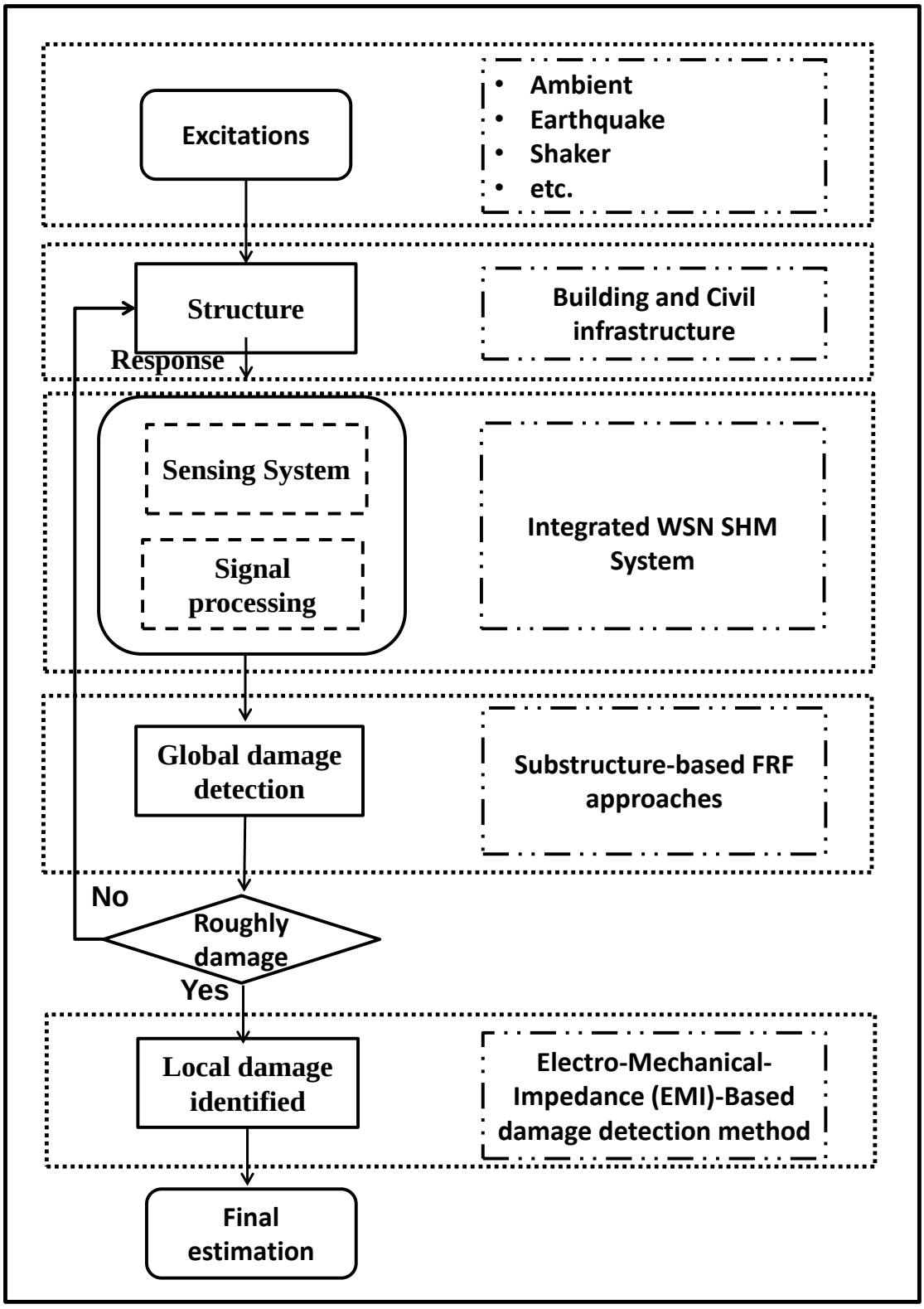

Figure 5.1 global-local-integrated damage detection approach

In the first stage, the global method is adopted to detect the change of characteristic of entire structure. Subsequently, roughly damage areas of structure are

identified. In stage two, after recognized the damage occurring and approximate location, a local method was developed to identify the detailed condition of damage. For instance, in a building structure, a global SHM can roughly indicate the location of damaged floor. The local SHM then check the component of building structure in detail. Substructure-based frequency response function approach was proposed as global damage detection approach. Electro-Mechanical-Impedance (EMI)-Based damage detection method is used to identify local damage of structure in this study.

5.2 Substructure-Based Frequency Response Function for Global Damage Detection

A frequency response function (FRF) expresses the structural response to an applied force as a function of frequency. This response may be represented in terms of displacement, velocity, or acceleration [116, 117]. Theoretically, FRF can be expressed in terms of system properties of mass, stiffness, damping, and modal properties. Moreover, using measured FRF-data has a major benefit that the measured FRF-data can provide much more damage information in a desired broadband frequency range than modal data because the modal data are identified mainly from a very limited number of FRF-data around resonance frequency [118, 119].Accordingly, an FRF scheme is reasonably expected to be feasible for detecting structural damage.

Several studies have applied the FRF to locate damage. Thyagarajan *et al*. [120] developed a method based on FRF data and an optimal number of sensors on a structure to identify damage locations, overcoming the former limitation of large number of computations required for high dof. structure. Lee and Shin[121] combined an FRF-based structural damage identification method (SDIM) with a reduced domain

approach to detect damage to beam structures. This method depends on data for the natural frequencies and mode shapes of the intact beams and the FRFs of damaged beams to identify structural damage. They demonstrated the feasibility of this SDIM using numerically simulated damage-identification tests. Their analytical results illustrated that the use of FRFs seems to be very promising for structural damage identification. Other investigations have extended FRF methods, such as the FRF curvature method or the FRF shape-based method, to improve the detection of damage locations. Sampaio *et al.*[122] developed a theoretical FRF curvature method and evaluated the efficiency of this method using numerically simulated data and experimental data for a real bridge. Their analytical results demonstrated that their FRF curvature method was effective in detecting damage on single site. Maia *et al.*[123] also presented an FRF curvature-based damage detection method and compared its performance with that of a conventional mode shape-based method. According to their results, methods based on FRF curvatures outperformed mode shape-based methods. Liu *et al.*[124] developed an FRF shape-based method. This method utilized the imaginary parts of FRF shapes of a beam structure to identify the damage location before and after damage. Their analytical results exhibited that this method was effective for a low-frequency range.

As well beam structures, FRF have been applied to detect damage in a building structure. By using measured FRF and neural networks (NNs), Ni *et al.*[125] identified the seismic damage of a 38-storey building model. That study determined FRFs for dimensionality reduction and noise elimination based on principal component analysis (PCA). According to their results, PCA is feasible for filtering unwanted measurement noise. Their damage identified results obtained after moderate earthquakes or super-strong earthquakes, in which considerable damage as identified

at the bottom portion of the building structure. Furukawa *et al*.[126] developed a damage detection method using uncertain FRFs based on a statistical bootstrap method and then applied it to a building structure. Their analytical results confirmed that the proposed statistical method to detect structural damage can determine whether the detected damage is a real damage or an identification error due to measurement noise. Kanwar *et al*.[127] demonstrated the feasibility of using FRF to the structural damage of reinforced concrete buildings. By using FRF, Hsu and Loh[128] detected damage of building structure subjected to earthquake ground excitation. This method required FRFs of intact and damaged systems as well as system matrices of the intact system to derive the damage identification equations. Their numerical results indicated that only the frequencies close to the natural frequencies of the damaged system need to be selected in order to solve the identification equations. Meanwhile, their experimental studies demonstrated the feasibility of the proposed algorithm in detecting the structural damage within an acceptable accuracy.

Accordingly, an FRF scheme is reasonably expected to be feasible for detecting structural damage. An novel substructure-based FRF approach with a damage location index (*SubFRFDI*) was proposed to localize damage to building structures from seismic response data.

5.2.1 Substructure-Based Frequency Response Function Approach

A frequency response function (FRF) is a transfer function, expressed in the frequency domain. FRF can be represented in terms of magnitude and phase with real and imaginary components. The response may be given in terms of displacement, velocity, or acceleration. Consider a linear system as represented by the diagram in Figure 5.2.

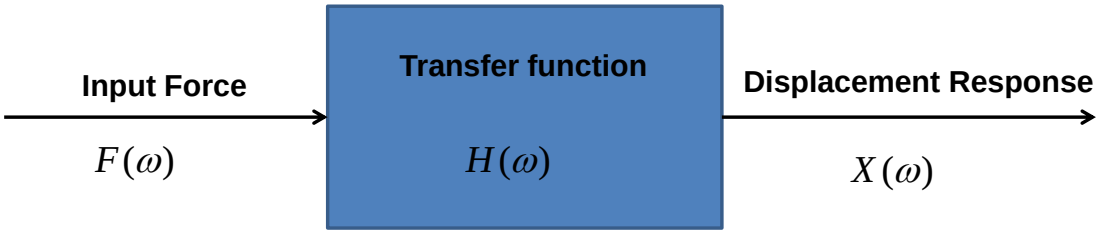

Figure 5.2 Frequency Response Function Model

The relationship in Figure 5.2 can be represented by the following equations

$$H(\omega) = \frac{X(\omega)}{F(w)} \tag{5.1}$$

where the $F(\omega)$ is the input force as a function of the angular frequency ω. $H(\omega)$ is the transfer function and $X(\omega)$ is the displacement response function. Each function is a complex spectral function, and considers each to be a Fourier transform for simplicity.

Consider a SDOF system which was subjected to a force excitation and the basic model of an SDOF system consists of a mass *m*, a spring with spring constant *k*, and a damping coefficient *c*. The equation of motion is

$$m\ddot{x}(t) + c\dot{x}(t) + kx(t) = f(t) \tag{5.2}$$

$$\ddot{x}(t) + \frac{c}{m}\dot{x}(t) + \frac{k}{m}x(t) = \frac{f(t)}{m} \tag{5.3}$$

By convention

$$\frac{c}{m} = 2\xi\omega_n, \frac{k}{m} = \omega_n^{\ 2} \tag{5.4}$$

where ω_n is the natural frequency in (radians/sec), and ξ is the damping ratio.

By substituting Eq.(5.4) in to Eq. (5.3),

$$\ddot{x}(t) + 2\xi\omega_n \dot{x}(t) + \omega_n{}^2 x(t) = \frac{\omega_n{}^2 f(t)}{k} \tag{5.5}$$

Takes the Fourier transform of each side of equation (5.5), the resulting FRF is

$$\frac{X(\omega)}{F(w)} = \frac{\omega_n{}^2}{k(\omega_n{}^2 - \omega^2 + j(2\xi\omega\omega_n))} \tag{5.6}$$

where the ω_n, k and ξ are the nature frequency, stiffness and damping ration, respectively. The defined FRF uses displacement as the response. It is known as receptance.

By replacing the displacement response $X(\omega)$ with velocity $\dot{X}(\omega)$ and acceleration $\ddot{X}(\omega)$, two different types of FRFs cane be defined as:

$$\frac{\dot{X}(\omega)}{F(w)} = \frac{j\omega\omega_n{}^2}{k(\omega_n{}^2 - \omega^2 + j(2\xi\omega\omega_n))} \tag{5.7}$$

$$\frac{\ddot{X}(\omega)}{F(w)} = \frac{-\omega^2\omega_n{}^2}{k(\omega_n{}^2 - \omega^2 + j(2\xi\omega\omega_n))} \tag{5.8}$$

where the Eqs.5.7 and 5.8 are Mobility FRF and Accelerance FRF, respectively.

The reciprocals of the three FRFs of an SDOF system also have useful physical significance and can be represented as

$$\text{Dynamic stiffness} = \frac{force}{displacement} = \frac{F(w)}{X(\omega)} \tag{5.9}$$

$$\text{Mechanical impedance} = \frac{force}{velocity} = \frac{F(w)}{\dot{X}(\omega)} \tag{5.10}$$

$$\text{Apparent mass} = \frac{force}{acceleration} = \frac{F(w)}{\ddot{X}(\omega)} \tag{5.11}$$

In a shear building, beams and floor systems are assumed to be rigid in flexure. Several factors, such as the axial deformation of beams and columns, and the effect of axial force on column stiffness, are neglected in analysis. Although an ideal shear building does not exist in practice, it is helpful for illustrating the use of substructure-based FRF to locate damage. For a damped multi-degree of freedom (MDOF) shear building with, say, *N* dofs., the equations of motion are

$$[M]\{\ddot{x}(t)\} + [C]\{\dot{x}(t)\} + [K]\{x(t)\} = \{f(t)\} \tag{5.12}$$

where $[M]$, $[C]$, and $[K]$ are $N \times N$ mass, viscous damping, and stiffness matrices, respectively; and $x(t)$ and $f(t)$ are $N \times 1$ vectors of the displacement functions and effective external excitation load, respectively. The mass matrix is diagonal, while $[C]$ and $[K]$ are tri-diagonal. Applying the Fourier transform to Eq. (1) and performing a simple arrangement yields

$$\{X\} = \left([K] + i\omega[C] - \omega^2[M]\right)^{-1}\{F\} \tag{5.13}$$

which can be written simply as

$$\left[H(\omega)\right]=\frac{\{X\}}{\{F\}} \tag{5.14}$$

where $\left[H(\omega)\right]$ is an FRF of the MDOF structure system as similar to the FRF of SDOF system.

The MDOF structure is divided herein into various substructures. Consider an *N*-storey shear building subjected to base excitations with acceleration a_g, which can be described by a simplified model (Fig. 5.3). *N* substructures of the original structure can be easily established. The first substructure has the 1st—N^{th} dofs. while the second has the 2nd—N^{th} dofs. Accordingly, the i^{th} substructure has the i^{th}—N^{th} dofs. (Fig. 5.3). The responses of any degrees of freedom of the i^{th} substructure are the same as those of the original complete structure.

When $i\neq 1$, considering an undamped sheer building model. For the i^{th} substructure, the balance of forces in the i^{th} floor can be written as

$$k_i\left(\tilde{x}_i(t)-\tilde{x}_{i-1}(t)\right)-k_{i+1}(\tilde{x}_{i+1}(t)-\tilde{x}_i(t))+m_i\ddot{\tilde{x}}_i(t)=0 \tag{5.15}$$

where $\tilde{x}_i(t)$ is the total displacement response of the i^{th} dof., and $\ddot{\tilde{x}}_i(t)=\ddot{x}(t)+a_g$.

For the $(i+1)^{th}$ to N^{th} floors, the balance of forces is

$$k_{i+1}\left(\tilde{x}_{i+1}(t)-\tilde{x}_i(t)\right)-k_{i+2}(\tilde{x}_{i+2}(t)-\tilde{x}_{i+1}(t))+m_{i+1}\ddot{\tilde{x}}_{i+1}(t)=0 \tag{5.16}$$

$$k_{i+2}\left(\tilde{x}_{i+2}(t)-\tilde{x}_{i+1}(t)\right)-k_{i+3}(\tilde{x}_{i+3}(t)-\tilde{x}_{i+2}(t))+m_{i+2}\ddot{\tilde{x}}_{i+2}(t)=0 \tag{5.17}$$

$$\ldots k_N\left(\tilde{x}_N(t)-\tilde{x}_{N-1}(t)\right)+m_N\ddot{\tilde{x}}_N(t)=0 \tag{5.18}$$

The Eqs. (5.15')~(5.18') can be written as

$$(k_i+k_{i+1})\tilde{x}_i(t)-k_{i+1}\tilde{x}_{i+1}(t)-m_i\ddot{\tilde{x}}_i(t)=k_i\tilde{x}_{i-1}(t) \tag{5.19}$$

$$-k_{i+1}\tilde{x}_i(t)+(k_{i+1}+k_{i+2})\tilde{x}_{i+1}(t)-k_{i+2}\tilde{x}_{i+2}+m_{i+1}\ddot{\tilde{x}}_{i+1}(t)=0 \tag{5.20}$$

$$-k_{i+2}\tilde{x}_{i+1}(t)+(k_{i+2}+k_{i+3})\tilde{x}_{i+2}(t)-k_{i+3}\tilde{x}_{i+3}+m_{i+2}\ddot{\tilde{x}}_{i+2}(t)=0 \tag{5.21}$$

$$\ldots -k_N\tilde{x}_{N-1}(t)+k_N\tilde{x}_N(t)+m_N\ddot{\tilde{x}}_N(t)=0 \tag{5.22}$$

Equations (5.19')~(5.22') can be written as a matrix equation.

$$\begin{bmatrix} m_i & \cdots & \cdots & 0 \\ \vdots & m_{i+1} & & \vdots \\ \vdots & & \ddots & \vdots \\ 0 & \cdots & \cdots & m_N \end{bmatrix}\begin{Bmatrix} \ddot{\tilde{x}}_i(t) \\ \ddot{\tilde{x}}_{i+1}(t) \\ \vdots \\ \ddot{\tilde{x}}_N(t) \end{Bmatrix}$$

$$+\begin{bmatrix} k_i+k_{i+1} & -k_{i+1} & & \\ -k_{i+1} & k_{i+1}+k_{i+2} & -k_{i+2} & \cdots\ 0 \\ & \vdots & \ddots & \vdots \\ & 0 & \cdots & k_N \end{bmatrix}\begin{Bmatrix} \tilde{x}_i(t) \\ \tilde{x}_{i+1}(t) \\ \vdots \\ \tilde{x}_N(t) \end{Bmatrix}=\begin{Bmatrix} k_i\tilde{x}_{i-1}(t) \\ 0 \\ \vdots \\ 0 \end{Bmatrix} \tag{5.23}$$

When damping is considered, Eq.(5.23') can be expressed as

$$\begin{bmatrix} m_i & \cdots & \cdots & 0 \\ \vdots & m_{i+1} & & \vdots \\ \vdots & & \ddots & \vdots \\ 0 & \cdots & \cdots & m_N \end{bmatrix}\begin{Bmatrix} \ddot{\tilde{x}}_i(t) \\ \ddot{\tilde{x}}_{i+1}(t) \\ \vdots \\ \ddot{\tilde{x}}_N(t) \end{Bmatrix} \tag{5.24}$$

$$+\begin{bmatrix} c_i + c_{i+1} & -c_{i+1} & & \\ -c_{i+1} & c_{i+1} + c_{i+2} & -c_{i+2} & \cdots\ 0 \\ & \vdots & \ddots & \vdots \\ & 0 & \cdots & c_N \end{bmatrix} \begin{Bmatrix} \dot{\tilde{x}}_i(t) \\ \dot{\tilde{x}}_{i+1}(t) \\ \vdots \\ \dot{\tilde{x}}_N(t) \end{Bmatrix} +$$

$$\begin{bmatrix} k_i + k_{i+1} & -k_{i+1} & & \\ -k_{i+1} & k_{i+1} + k_{i+2} & -k_{i+2} & \cdots\ 0 \\ & \vdots & \ddots & \vdots \\ & 0 & \cdots & k_N \end{bmatrix} \begin{Bmatrix} \tilde{x}_i(t) \\ \tilde{x}_{i+1}(t) \\ \vdots \\ \tilde{x}_N(t) \end{Bmatrix} = \begin{Bmatrix} c_i \dot{\tilde{x}}_{i-1}(t) + k_i \tilde{x}_{i-1}(t) \\ 0 \\ \vdots \\ 0 \end{Bmatrix}$$

where $\tilde{x}_i(t)$ is the total displacement response of the i^{th} dof., and $\ddot{\tilde{x}}_i(t) = \ddot{x}(t) + a_g$.

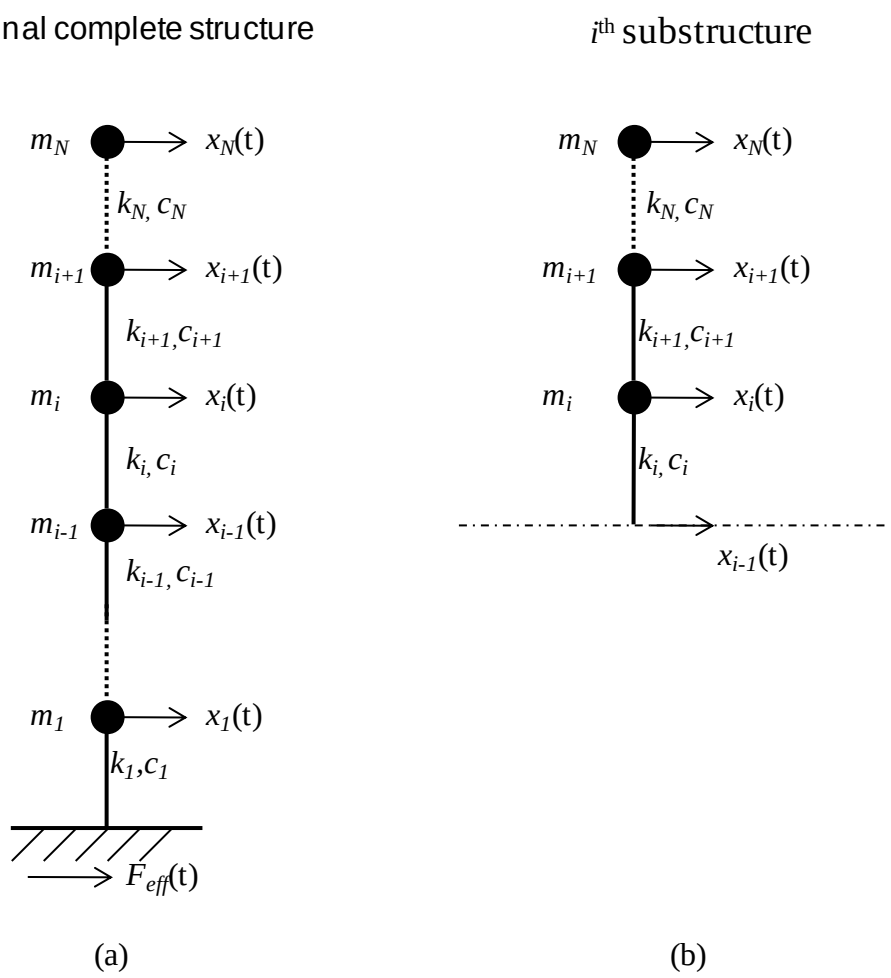

Figure 5.3. (a) Original complete structure, (b) the i^{th} substructure.

Equation (5.24) represents a single input/multiple output system. Clearly, the substructure-based FRFs of the j^{th} dof. in the i^{th} substructure are

$$H_j^{(i)}(\omega) = \frac{\tilde{X}_j}{(i\omega c_i + k_i)\tilde{X}_{i-1}} \quad , \quad j = i \text{ to } N \tag{5.25}$$

where $\tilde{X}_j$ and $\tilde{X}_{i-1}$ are the Fourier transforms of $\tilde{x}_j(t)$ and $\tilde{x}_{i-1}(t)$, respectively. The substructure-based FRF given by Eq. (5.25) depends on the properties of the i^{th}—N^{th} dofs. To estimate $H_j^{(i)}(\omega)$ from Eq. (5.25), c_i and k_i must be known. Unfortunately,

c_i and k_i are usually unknown in the damage diagnosis process. Moreover, acceleration responses are normally measured in monitoring the responses of a structure in an earthquake. Therefore, the measured acceleration responses of the original complete structure are used herein and these substructure-based FRFs are further simplified as

$$\tilde{H}_j^{(i)}(\omega) = \frac{\ddot{\tilde{X}}_j}{\ddot{\tilde{X}}_{i-1}}, \quad j = i \text{ to } N \tag{5.26}$$

where $\ddot{\tilde{X}}_j$ and $\ddot{\tilde{X}}_{i-1}$ are the Fourier transforms of $\ddot{\tilde{x}}_j(t)$ and $\ddot{\tilde{x}}_{i-1}(t)$, respectively. A specified substructure-based FRF, $H_j^{(i)}(\omega)$, can be estimated from measured acceleration of the $(i\text{-}1)^{\text{th}}$ and j^{th} dofs. Notably, when i =1, referring to the original complete structural system, these substructure-based FRFs are given by

$$\tilde{H}_j^{(1)}(\omega) = \frac{\ddot{\tilde{X}}_j}{A_g}, \quad j = 1 \text{ to } N \tag{5.27}$$

where A_g is the Fourier transform of a_g.

Theoretically, when the damage is assumed to have occurred in the column(s) between the i^{th} and $(i\text{-}1)^{\text{th}}$ dofs. (such that k_i is reduced *and* c_i is increased), the substructure-based FRF is significantly altered in the i^{th} dof., as described by, $\tilde{H}_i^{(i)}(\omega)$. Likewise, if stiffness k_i and k_l decline simultaneously, then the change in the corresponding FRFs, $\tilde{H}_i^{(i)}(\omega)$ and $\tilde{H}_l^{(l)}(\omega)$, is greater than what would typically be observed in $\tilde{H}_j^{(i)}(\omega)$. Consequently, damage can be identified as having occurred at

a single or multiple sites. For efficiency, only one substructure-based FRF, $\tilde{H}_i^{(i)}(\omega)$, is determined herein for each substructure to reduce the computational time. Damage of the shearing building structures is located based on the FRFs, $\tilde{H}_1^{(1)}(\omega)$, $\tilde{H}_2^{(2)}(\omega)$, …, $\tilde{H}_N^{(N)}(\omega)$, of all substructures.

Based on the aforementioned description, change in the substructure-based FRF is related to damage and can be utilized as an essential index to locate damage of the building structures. The operating conditions of this work are based on a known initial state, continuously measured seismic response data, and comparisons of before-and-after damage scenario for a shear building. Initially, sensors are deployed on the shear building and the corresponding response data are measured immediately after an earthquake excitation. The initial stiffness of the structure is then defined and the corresponding FRFs $\tilde{H}_{1,u}^{(1)}(\omega), \tilde{H}_{2,u}^{(2)}(\omega)$ …, $\tilde{H}_{N,u}^{(N)}(\omega)$ are computed as a known undamaged state, also referred to as a before-scenario state. Next, the sensors continuously collect seismic response data of the structure after each subsequent earthquake and the particular FRFs $\tilde{H}_{1,d}^{(1)}(\omega), \tilde{H}_{2,d}^{(2)}(\omega)$ …, $\tilde{H}_{N,d}^{(N)}(\omega)$ are obtained following, referred to as an after-scenario state. Before and after damage scenarios are compared to determine the damage location since a change in the substructure-based FRF is related to damage. A *dissimilarity* between the substructure-based FRFs in damaged and undamaged states can be used to identify the damage. The absolute dissimilarity $\bar{P}_i(\omega)$ is defined as

$$\bar{P}_i(\omega) = \left\| \left| \tilde{H}_{i,d}^{(i)}(\omega) \right| - \left| \tilde{H}_{i,u}^{(i)}(\omega) \right| \right| \tag{5.28}$$

where $\left| \tilde{H}_{i,d}^{(i)}(\omega) \right|$ and $\left| \tilde{H}_{i,u}^{(i)}(\omega) \right|$ are the magnitudes of $\tilde{H}_i^{(i)}$ in the damaged and undamaged states, respectively. These *N dissimilarities* $\bar{P}_1(\omega)$ — $\bar{P}_N(\omega)$ can be correspondingly calculated for a shear building with *N* floors. To locate conveniently and quantify the damage, a substructure-based FRF damage location index (*SubFRFDI*) for the i^{th} substructure is proposed. It is given by

$$SubFRFDI_i = 1 - Exp\left[-\rho^2 \left(\sum_{\omega=a}^{b} \left\{ \left(NDF_i(\omega) \right)^2 \right\} \right) / n \right] \tag{5.29}$$

where ρ, *a*, *b*, and *n* are working parameters and the $NDF_i(\omega)$ is expressed as

$$NDF_i(\omega) = \frac{\bar{P}_i(\omega)}{\max\left[\left| \tilde{H}_{i,d}^{(i)}(\omega) \right|_{\max}, \left| \tilde{H}_{i,u}^{(i)}(\omega) \right|_{\max} \right]} \tag{5.30}$$

The coefficient ρ is a control value that scales the index between zero and one and is set to five in this work. The range of selected frequencies for calculating *SubFRFDI* is set to *a*—*b*, where *a* is a starting frequency of zero and *b* is the end frequency, which equals the first modal frequency (undamaged state). The aforesaid a and b are determined by trial-and-error method. The value *n* equals (*b* - *a*) divided by sampling time, which is 0.005 s in this work. Figure 5.4 shows the FRF of substructure.

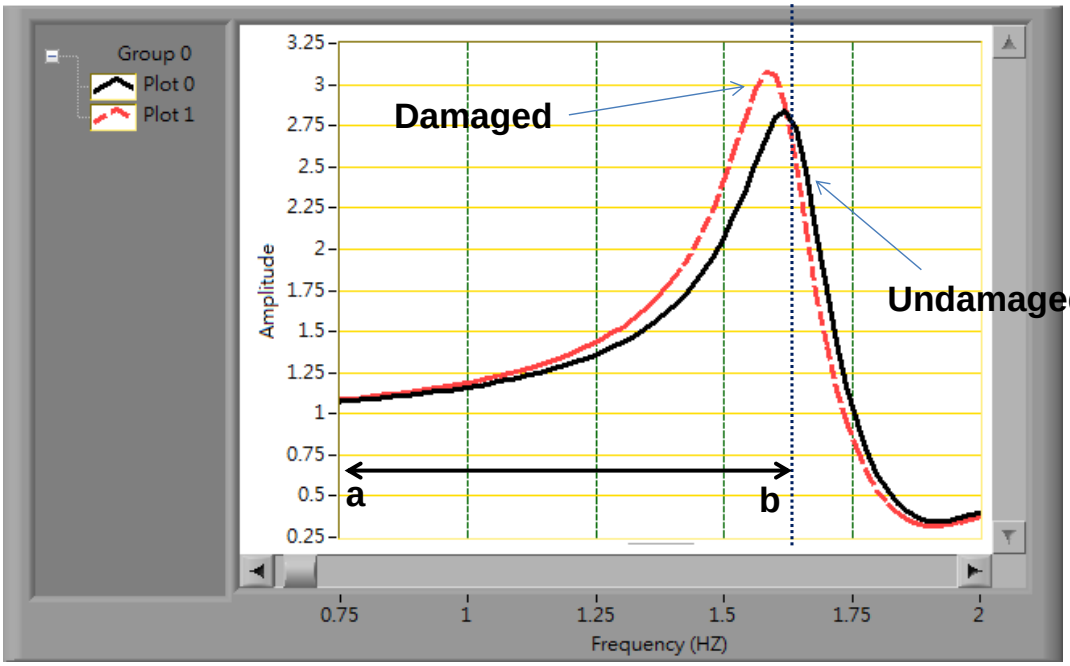

Figure 5.4. FRF of Substructure

If the properties of a structural system do not change, then the $SubFRFDI_i$ is close to zero. However, if the damage to storey *i* in a shear building is severe, then the value of $SubFRFDI_i$ is high. The resulting apparently significant peak value(s) of *SubFRFDI* indicate(s) that damage occurs at either a single site or at multiple sites. For instance, if damage occurs only in the i^{th} dof., then only the $SubFRFDI_i$ from all *SubFRFDI* has a significant peak value. If damage occurs at more than one site, such as in the i^{th}, j^{th}, and k^{th} dofs., then the corresponding *SubFRFDIs* will all have significant peak values.

5.2.2 Numerical Study

This section presents a numerical example of a six-storey shear plane frame structure that is subjected to base excitation, to evaluate the feasibility of the proposed damage-detection scheme. The structural parameters of each floor were the same -

mass m_i = 30 kg and stiffness k_i = 55.5 kN/m (i = 1—6). Numerical simulation was performed with 5% modal damping. The damage in this work was simulated as reduced storey stiffness. Single-site and multiple-site damage were studied. Table 5.1 presents the simulated damage cases: *Dam_*k_i (i = 1—6) denotes damage in the form of reduced stiffness k_i at a single site i; similarly, *Dam_*k_i&k_j ($i \neq j$) represents damages in the form of reduced stiffness k_i and k_j at multiple sites. Table 5.1 also presents the percentage reduction in k_i in parentheses.

Table 5.1 Descriptions of simulated damage cases.

Damage case	1	2	3	4	5	6	7	8
Notation	*Dam_*k_1	*Dam_*k_2	*Dam_*k_3	*Dam_*k_4	*Dam_*k_1	*Dam_*k_3	*Dam_*k_3 &k_5	*Dam_*k_1 &k_5
Damage level	k_1 (15%)	k_2 (15%)	k_3 (15%)	k_4 (15%)	K_1 (15%-30 %)	k_3 (15%-30 %)	K_3 (15%) and K_5 (15%)	k_1 (15%) *and* k_5 (15%)
Damage case	9	10	11	12	13	14	15	16
Notation	*Dam_*k_1 &k_3	*Dam_*k_1 &k_2	*Dam_*k_1 &k_2	*Dam_*k_1 &k_3	*Dam_*k_1 &k_3	*Dam_*k_1 &k_3&k_5	*Dam_*k_1 &k_3&k_5	*Dam_*k_1 &k_3&k_5
Damage level	k_1 (15%) *and* k_3 (15%)	k_1 (10%) and k_2 (20%)	k_1 (10%) and k_2 (20%)	k_1 (20%) and k_3 (10%)	k_1 (10%) and k_3 (20%)	k_1 (15%) k_3 (10%) *and* k_5 (5%)	k_1 (5%) k_3 (15%) *and* k_5 (10%)	k_1 (10%) k_3 (15%) *and* k_5 (5%)

For damage case 1, Figure 5.5 compares the conventional FRFs of the structure in the undamaged and damaged states, while Fig. 5.6 compares the substructure-based FRFs for each substructure. These Fig.s present only the parts of an FRF that correspond to frequencies that are less than the second resonant frequency of the complete structure or each substructure. The reduction in stiffness in the first storey

markedly changed the conventional FRFs of each floor whereas significant changes were observed only in the substructure-based FRF of substructure 1. The substructure-based FRF characterized and located damage more effectively than the conventional FRF.

To apply the proposed substructure-based FRF approach to locate structural damage, the locations of damage were determined using the *SubFRFDI*. Figure 5.7-5.10 presents the identified damage locations in four single-damage cases, 1, 2, 3, and 4. When damage occurred only to the i^{th} storey, the value of the *SubFRFDI* that corresponds to the i^{th} substructure greatly exceeded those that correspond to the other substructures. The proposed index is verified to have located the damaged storey. Four different percentage reductions in stiffness were assessed for damage case 1 and 3. Figure 5.11 and 5.12 shows the identified damage locations and corresponding to damage extent. As shown in Fig., the damage can be correctly located and the value of *SubFRFDI* was increasing corresponding to damage extent.

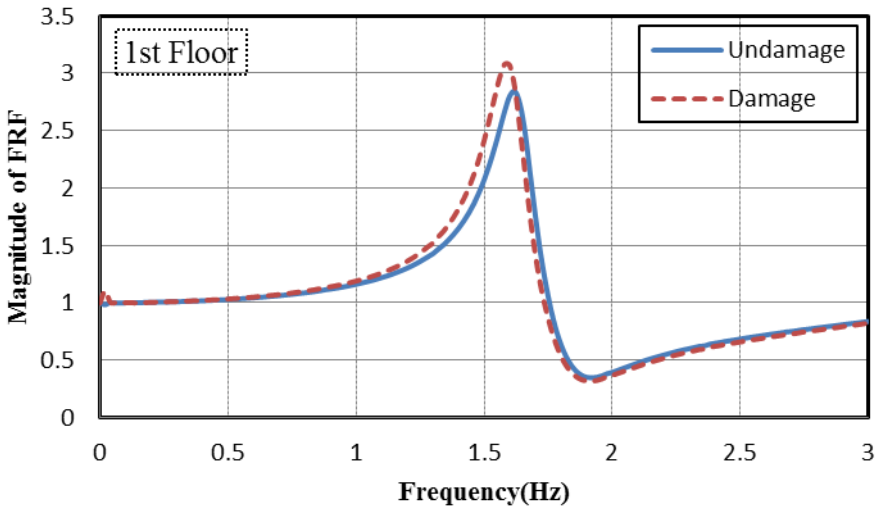
1st Floor
Undamage
Damage
Magnitude of FRF
Frequency(Hz)
0
0.5
1
1.5
2
2.5
3
3.5

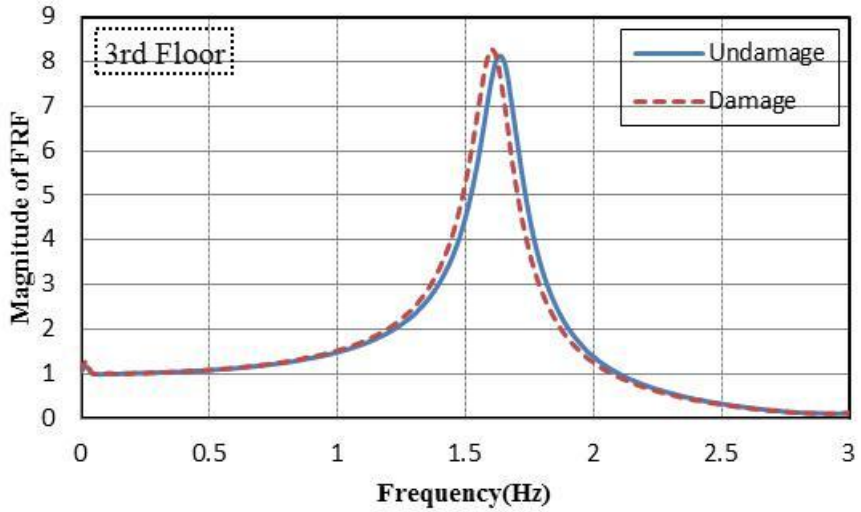
3rd Floor
Undamage
Damage
Magnitude of FRF
Frequency(Hz)
0
1
2
3
4
5
6
7
8
9

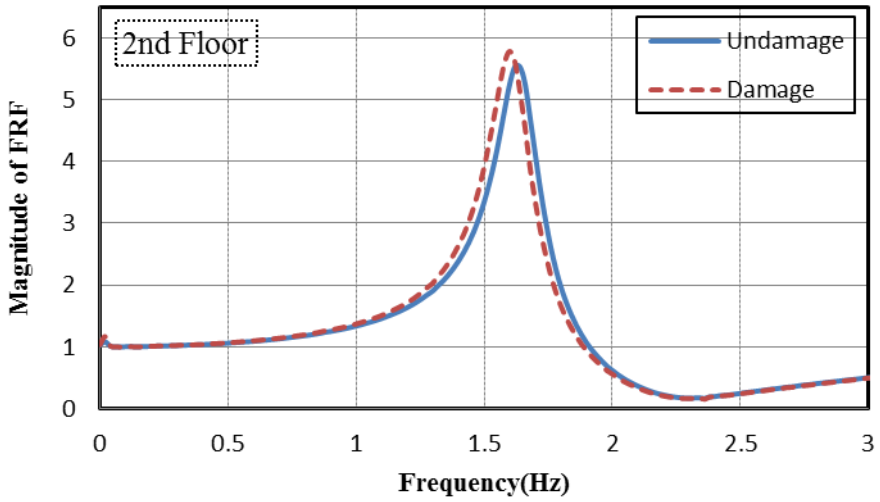
2nd Floor
Undamage
Damage
Magnitude of FRF
Frequency(Hz)
0
1
2
3
4
5
6

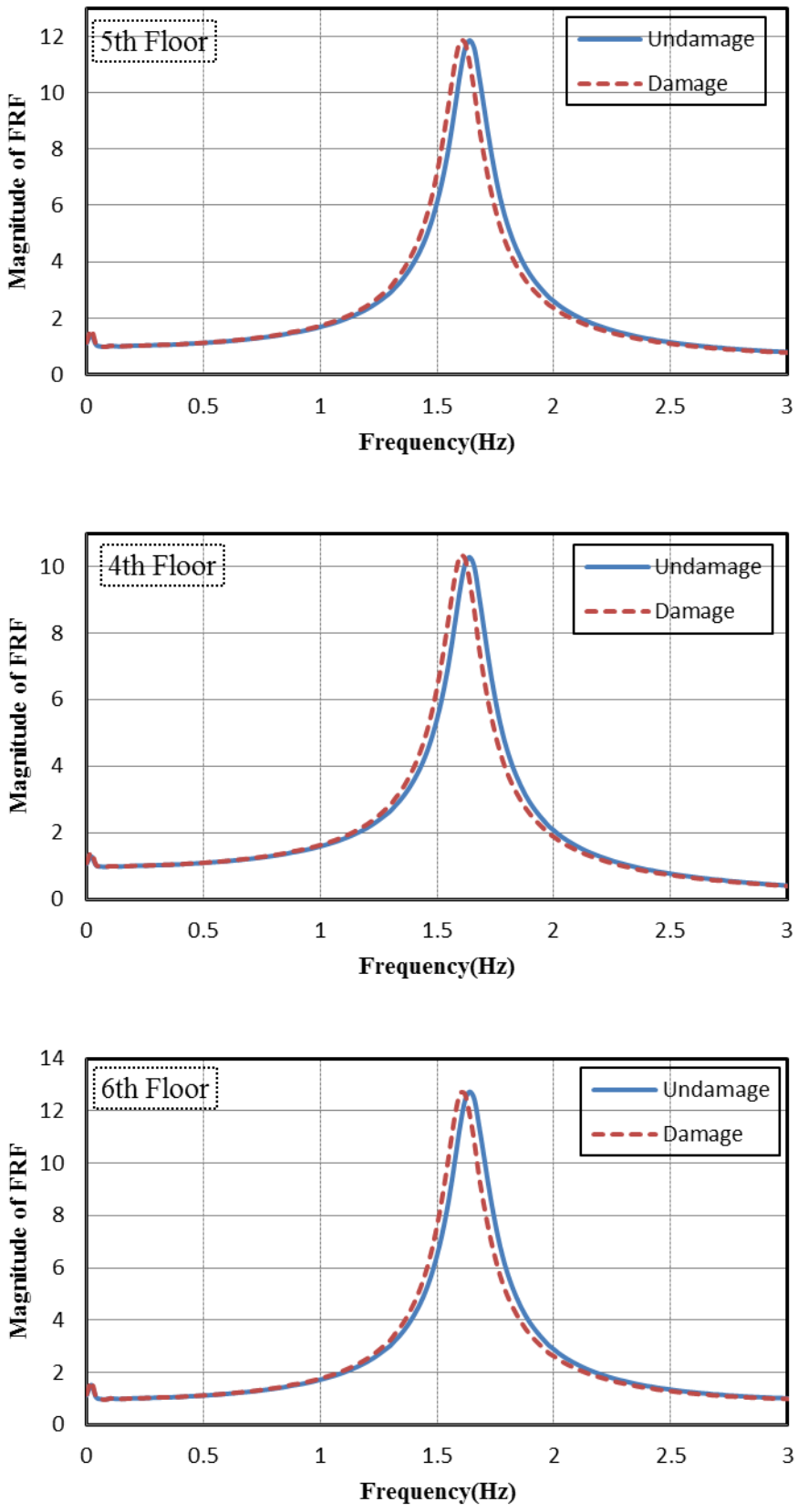

Figure 5.5 Comparisons of conventional FRFs of the structure in undamaged and damaged states for Case 1.

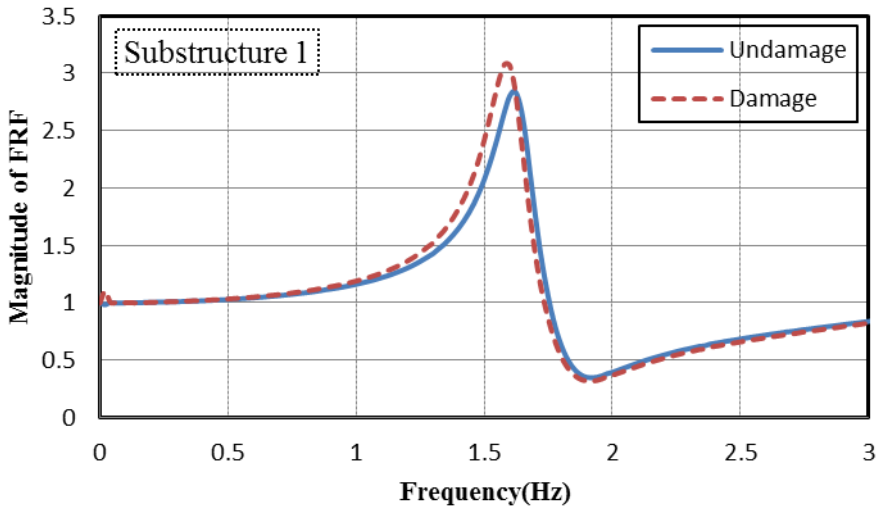
Substructure 1
Undamage
Damage
Magnitude of FRF
Frequency(Hz)
0
0.5
1
1.5
2
2.5
3
3.5

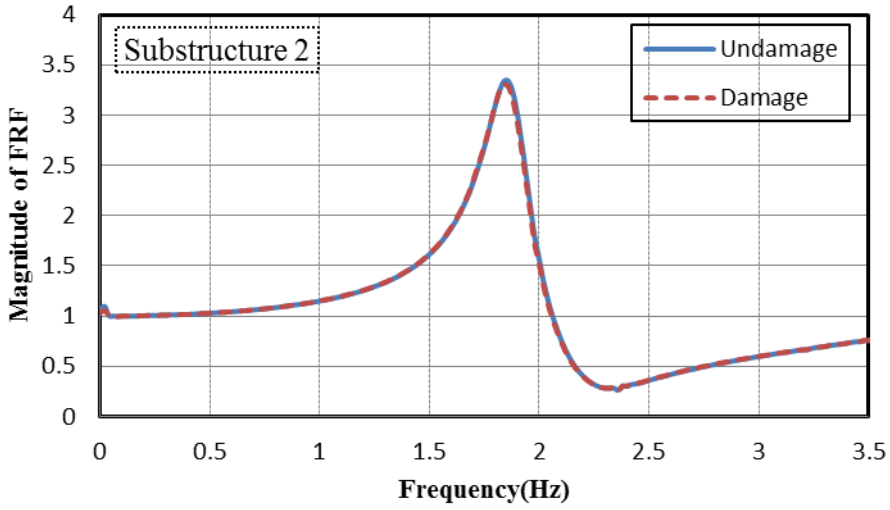
Substructure 2
Undamage
Damage
Magnitude of FRF
Frequency(Hz)
0
0.5
1
1.5
2
2.5
3
3.5
4

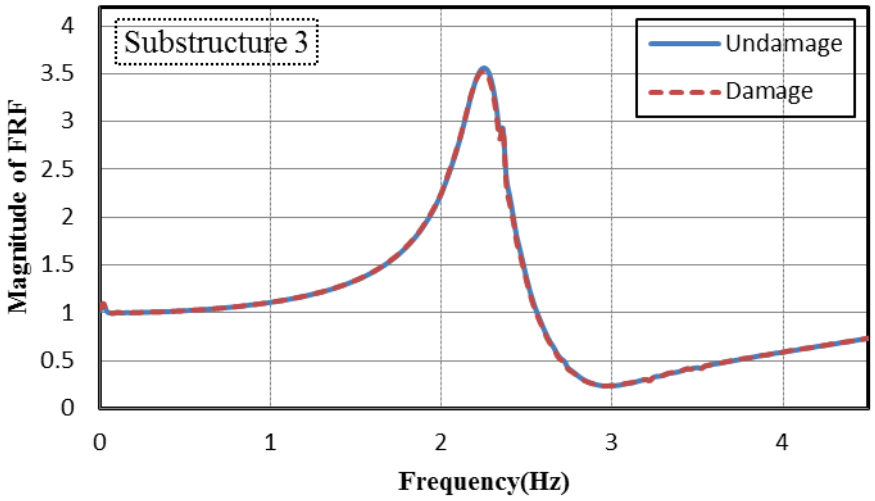
Substructure 3
Undamage
Damage
Magnitude of FRF
Frequency(Hz)
0
1
2
3
4
0.5
1.5
2.5
3.5

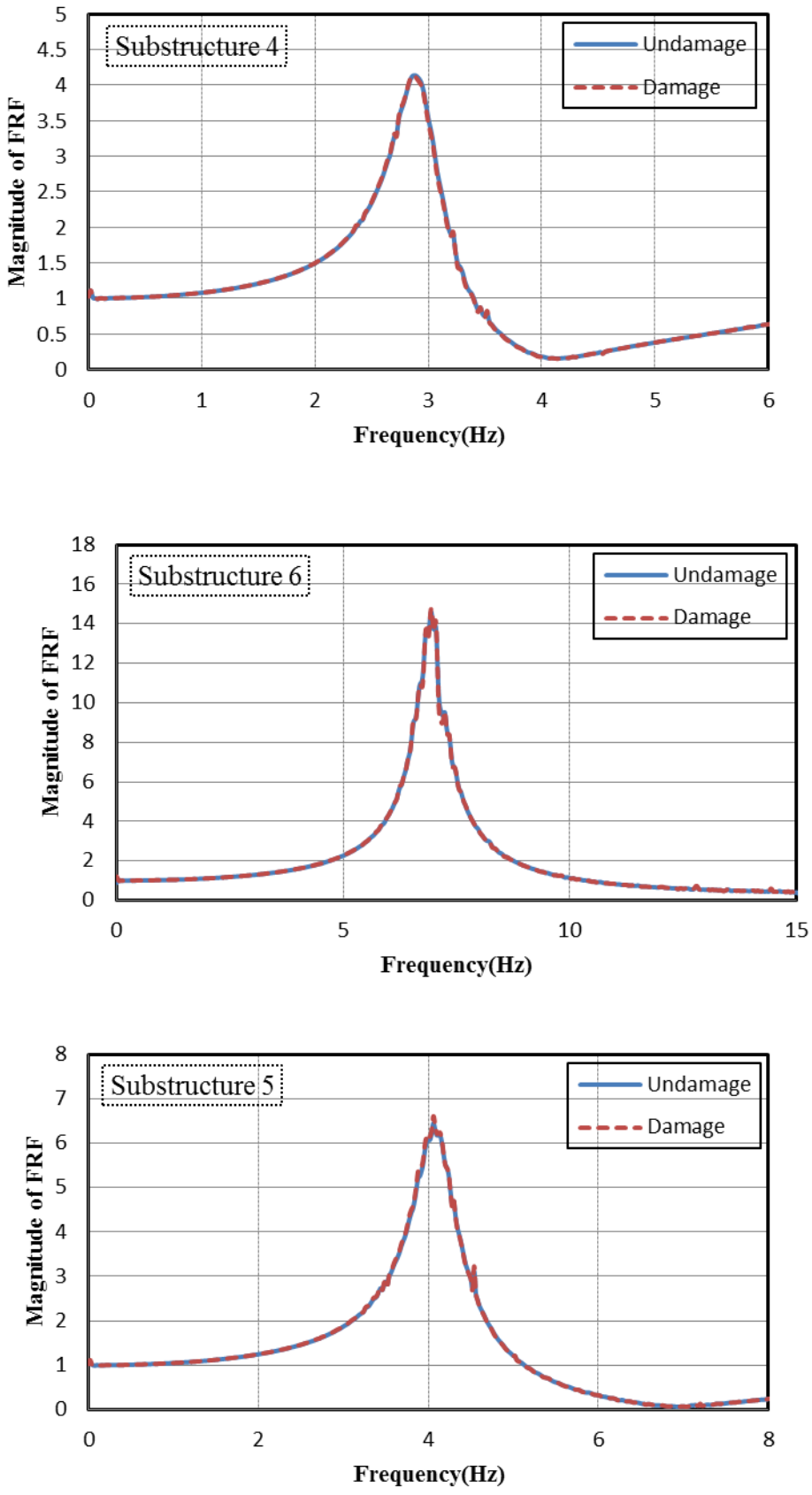

Figure 5.6 Comparisons of the substructure-based FRFs for each substructure for Case 1.

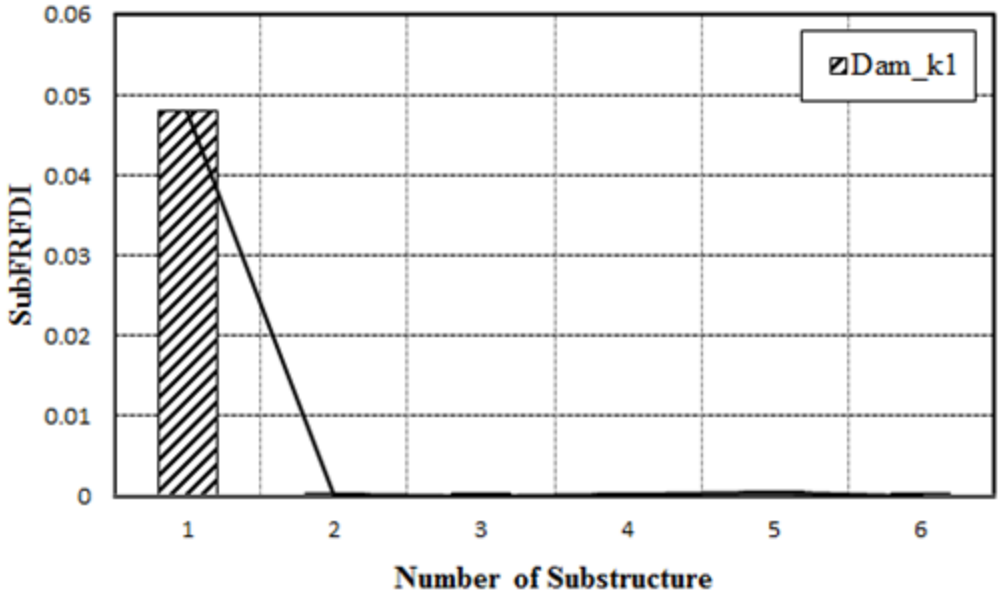

Figure 5.7 The identified damage locations in single-damage cases 1.

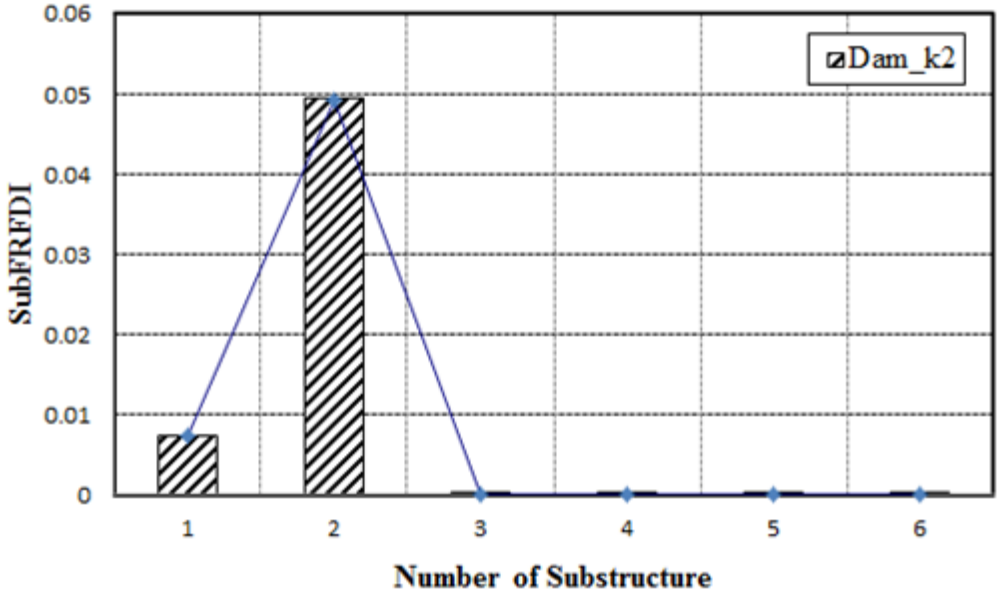

Figure 5.8 The identified damage locations in single-damage cases 2.

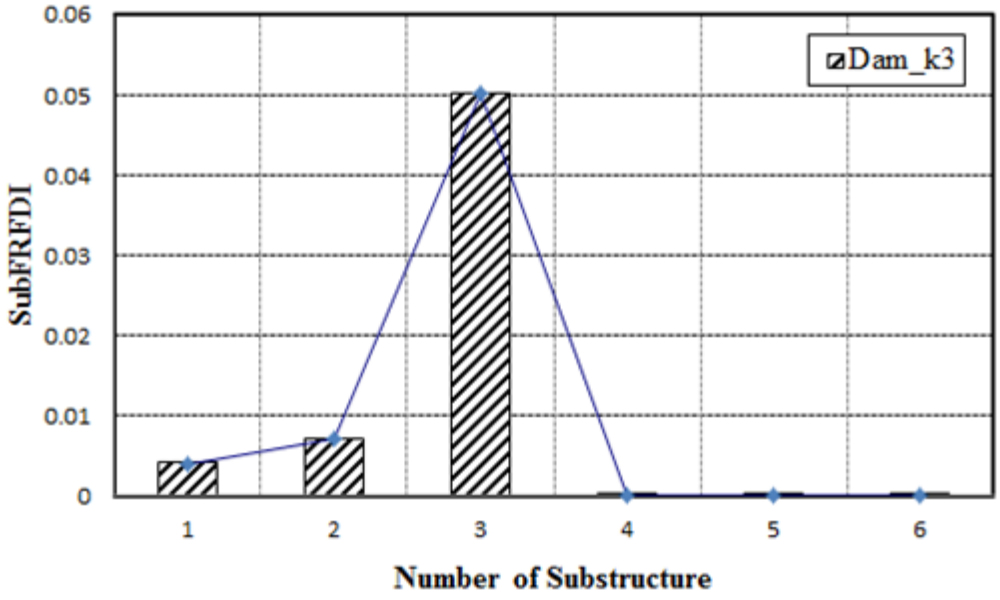

Figure 5.9 The identified damage locations in single-damage cases 3.

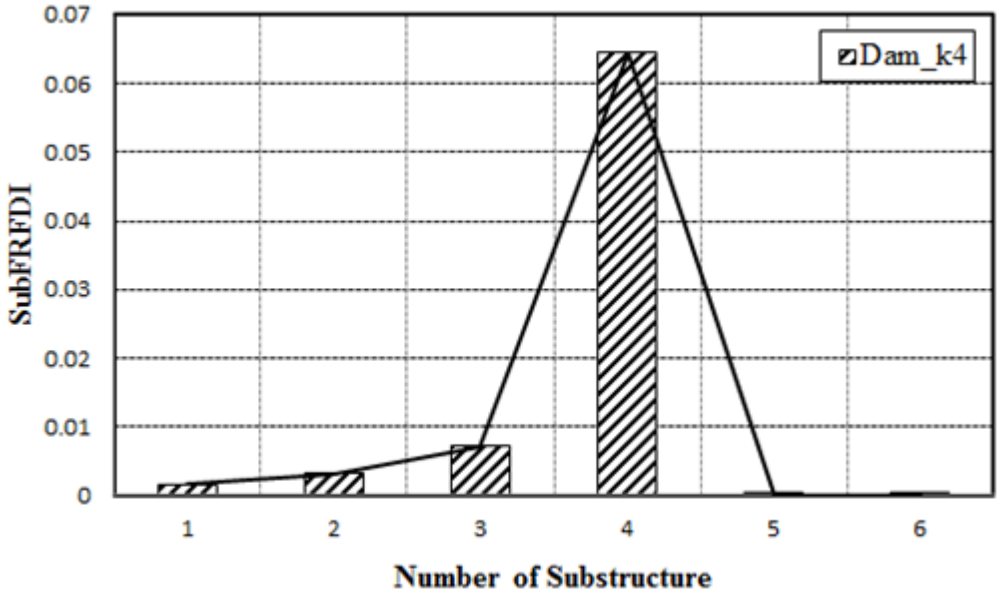

Figure 5.10 The identified damage locations in single-damage cases 4.

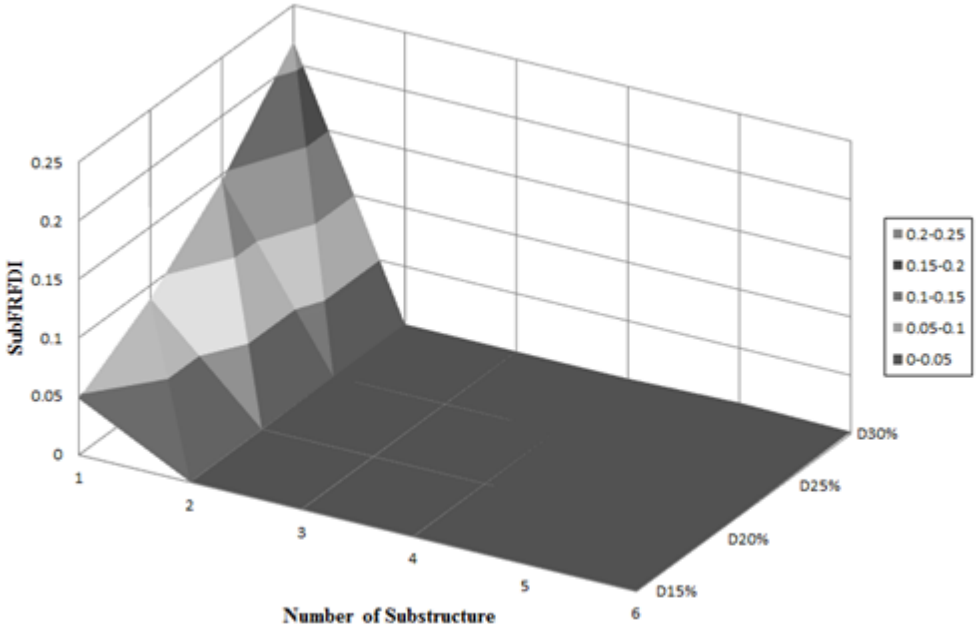

Figure 5.11 The identified damage locations in single-damage cases 1 for different damage extent.

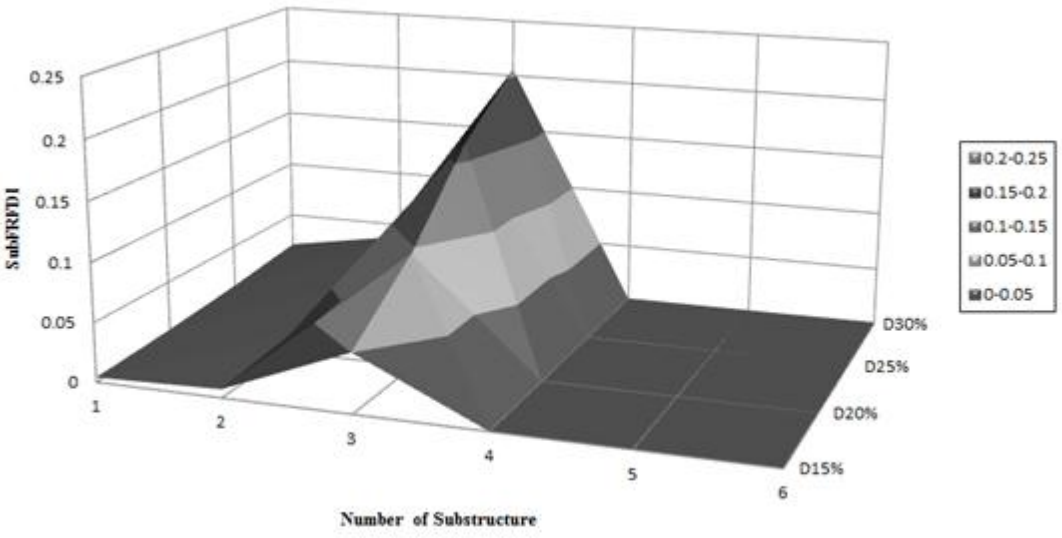

Figure 5.12 The identified damage locations in single-damage cases 3 for different damage extent.

To study the effects of the frequency range in the $SubFRFDI_i$, Fig. 5.13 presents

the values of the *SubFRFDI* of each substructure in damage case 3, obtained using two different frequency ranges. The frequency ranges, *a*—*b*, were set to 0—1.6 Hz and 0—2 Hz. The former range covers frequencies lower than the first modal frequency, while the latter range includes frequencies above the first modal frequency. The maximum value of the *SubFRFDI* for various substructures was normalized to one for comparison. The value of the *SubFRFDI* for substructure 3 was markedly larger than the others, when the values of *SubFRFDI* were computed using the two frequency ranges (Figure 5.13), indicating that the third storey was damaged. However, when the values of the *SubFRFDI* were obtained using the frequency range 0—2 Hz, the damage on the second storey may be mistakenly identified. Consequently, the damaged storey is easily identified when the *SubFRFDI* value is estimated using the substructure-based FRFs using frequency ranges below the first modal frequency. Those results further demonstrate that change-related information in the first model is adequate to identify the alteration between undamaged and damaged states, explaining why use of the first intact modal frequency in this work is acceptable.

To reflect the fact that measured data always contain noise, 5% and 10% white noise were respectively added to the numerically simulated responses and input acceleration in damage case 3. Figure 5.14 presents the effects of noise on substructure-based FRF. Figure 5.15 presents the effects of noise on $SubFRFDI_i$ estimations. Although noise influences $SubFRFDI_i$ values, especially for large *i*, the $SubFRFDI_i$ was still, correctly, greatest at $i = 3$.

To demonstrate that the proposed index is independent to responses to various input earthquakes and only reliant to the structural properties, the Kobe and El Centro

earthquakes were applied as input excitations. Figure 5.16 presents the *SubFRFDI* values of different substructures in damage case 4. The *SubFRFDI* values varied only slightly with the base excitations.

To compare the proposed *SubFRFDI* with an existing FRF-based damage location identification method, Fig. 5.17 presents the analytical results for damage case 3 obtained using the proposed method and the FRF curvature-method-based index (*FRFCDI*)[122]. The *FRFCDI* method is an extension of the mode shape curvature method for locating damage. The *FRFCDI* is given by

$$FRFCDI_i = \sum_{\omega} \left| \varphi_U''^i(\omega) - \varphi_D''^i(\omega) \right| \tag{5.31}$$

where $\varphi_U''^i(\omega)$ and $\varphi_D''^i(\omega)$ are the FRF curvatures of the i^{th} dof. of an undamaged structure and the corresponding damaged structure, respectively. Since $FRFCDI_i$ and $SubFRFDI_i$ have different values in a particular damage scenario, the maximum values of $FRFCDI_i$ and $SubFRFDI_i$ were normalized to one for comparison. The proposed *SubFRFDI* outperforms the *FRFCDI* method (Figure 5.17). The *FRFCDI* does not locate damage correctly, but the *SubFRFDI* does. Additionally, for the highest storey, *FRFCDI* has a larger error than the *SubFRFDI*.

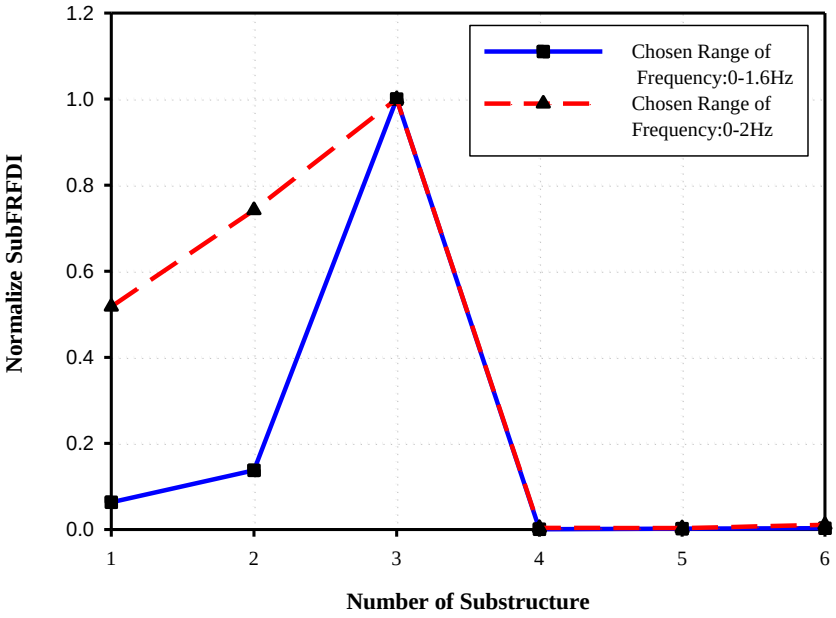

Figure 5.13 The values of the *SubFRFDI* of each substructure in damage case 3, obtained using two different frequency ranges.

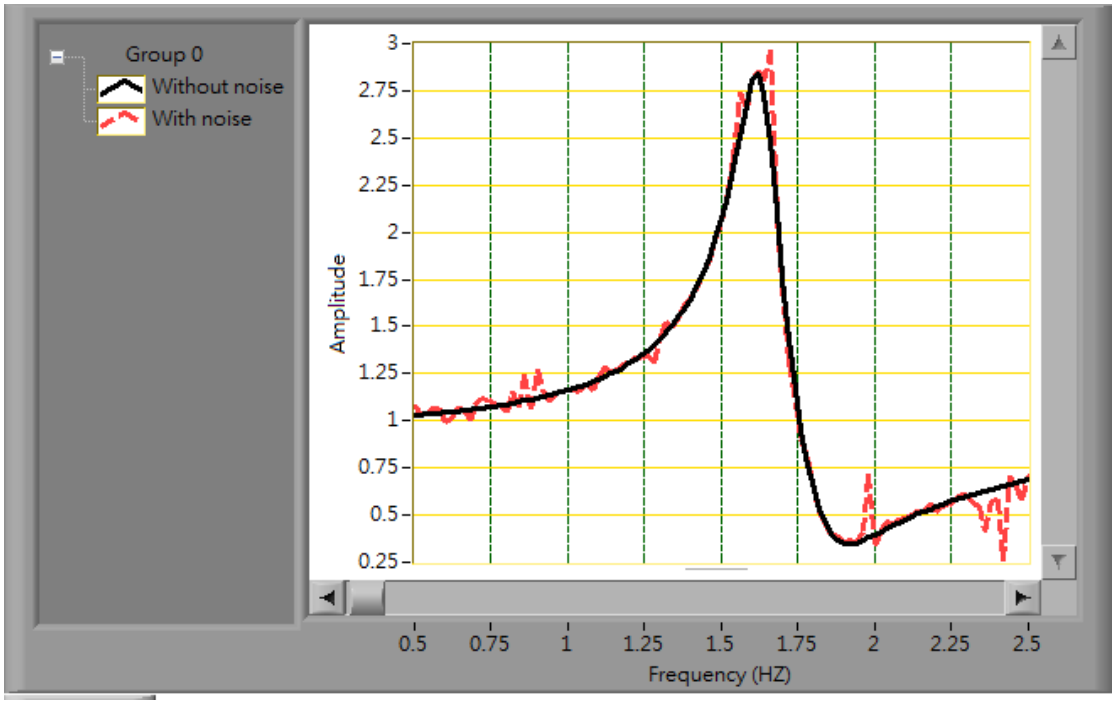

Figure 5.14. The FRF of substructure: With and without noise.

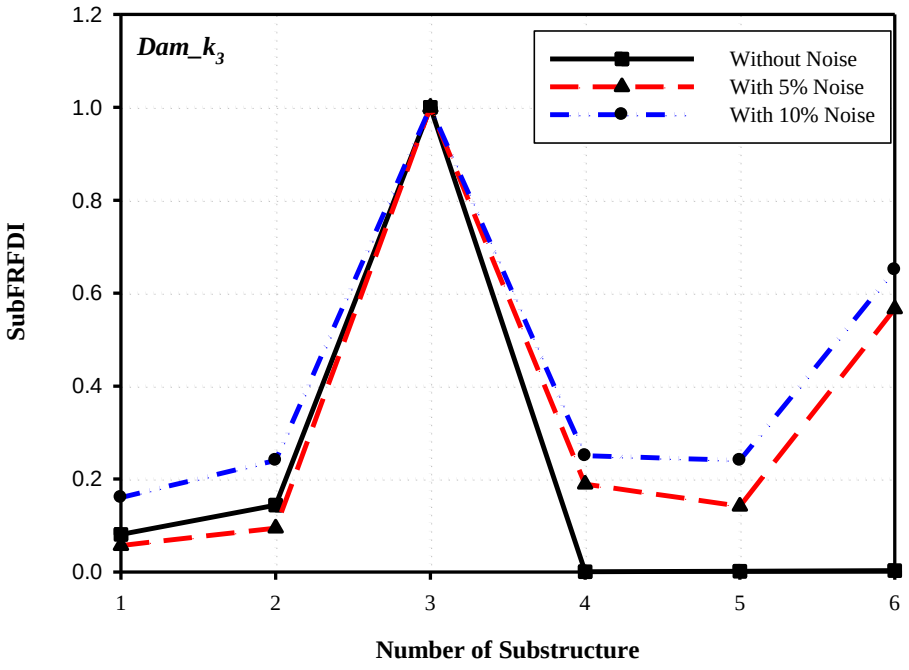

Figure 5.15 The effects of noise on *SubFRFDI*$_i$ estimations for Case 3.

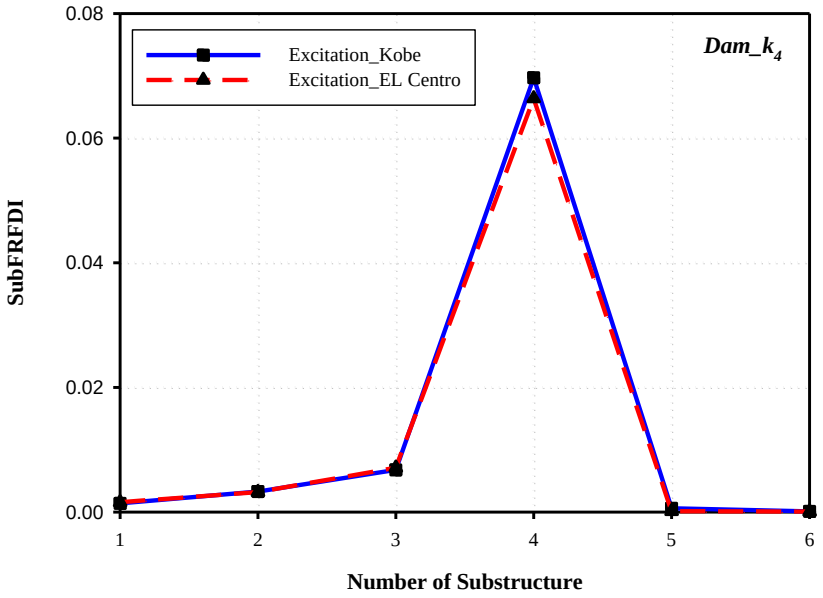

Figure 5.16 The *SubFRFDI* values of different substructures in damage case 4 with different earthquake excitations.

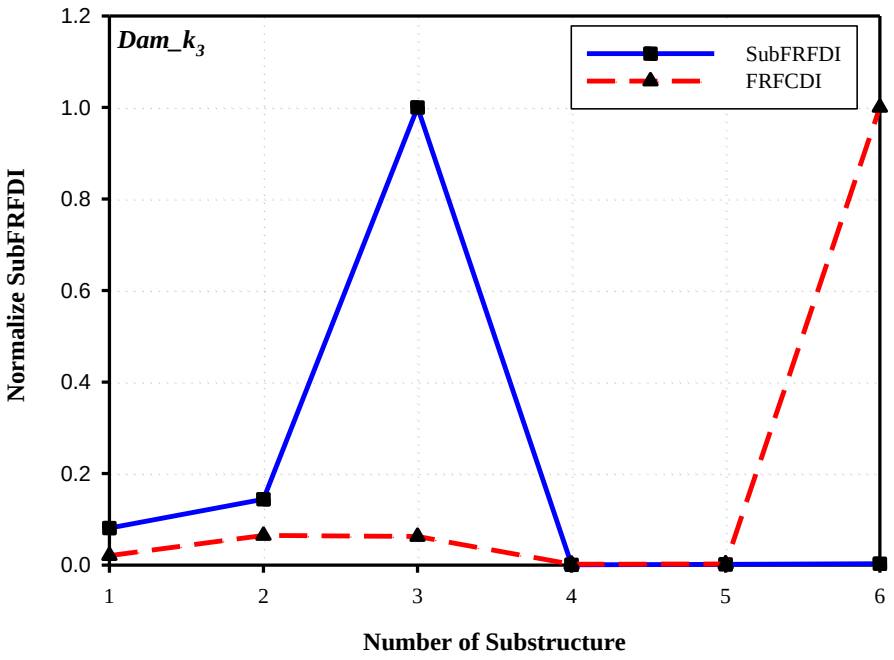

Figure 5.17 The analytical results for damage case 3 obtained using the proposed method (*SubFRFDI*) and the FRF curvature-method-based index (*FRFCDI*).

The proposed approach can identify damage locations at multiple sites and a single site. Figure 5.18-5.27 presents the *SubFRFDI* values for substructures in damage cases 7—16. The corresponding peaks reveal that even though multiple damage sites suffered damage of various degrees. Figures 5.18-5.27 present the proposed index accurately determined the locations of the damage in a multi-damage scenario.

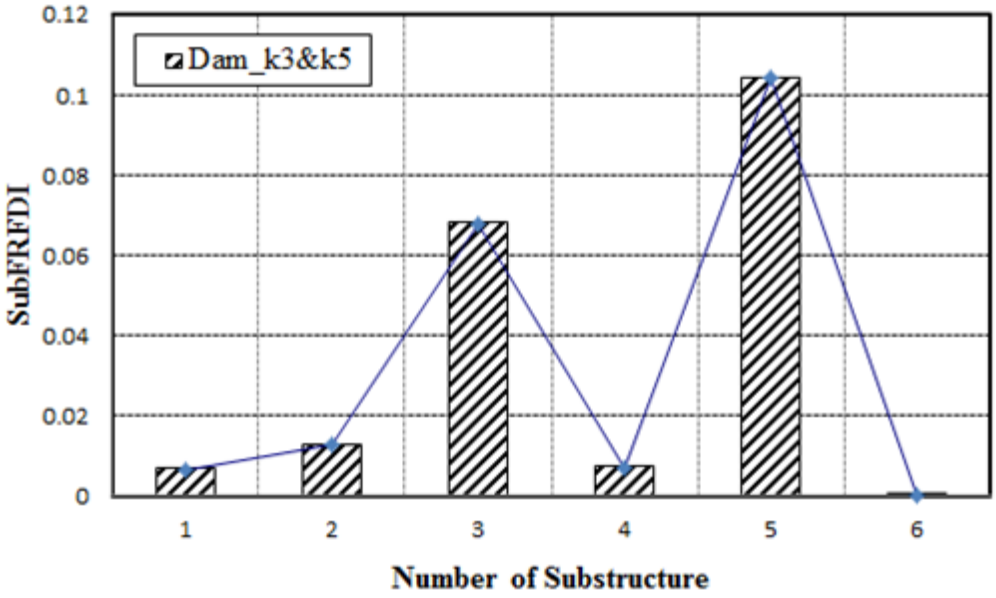

Figure 5.18 The *SubFRFDI* values for substructures in damage cases 7, multiple damage.

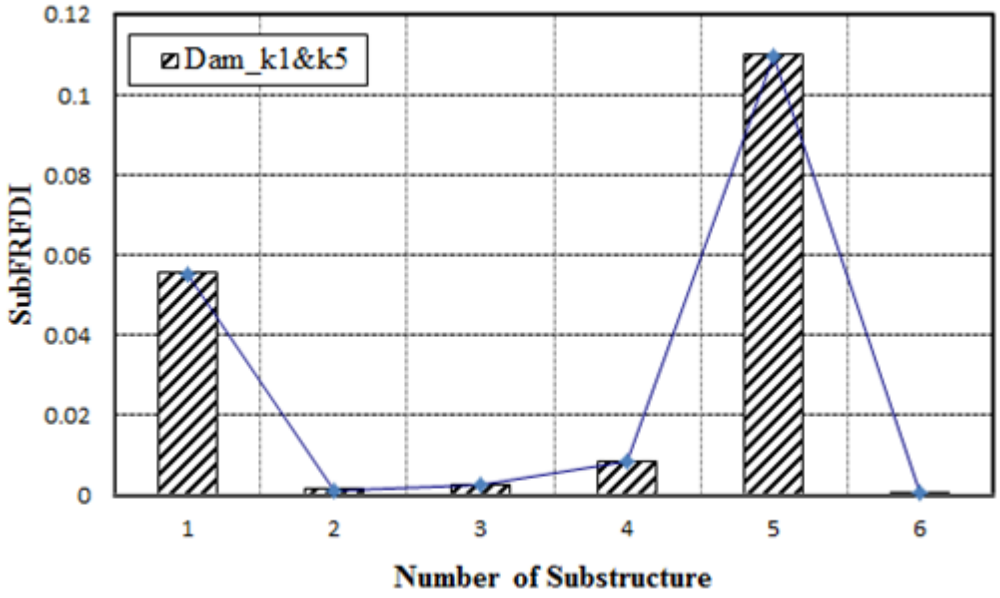

Figure 5.19 The *SubFRFDI* values for substructures in damage cases 8, multiple damage.

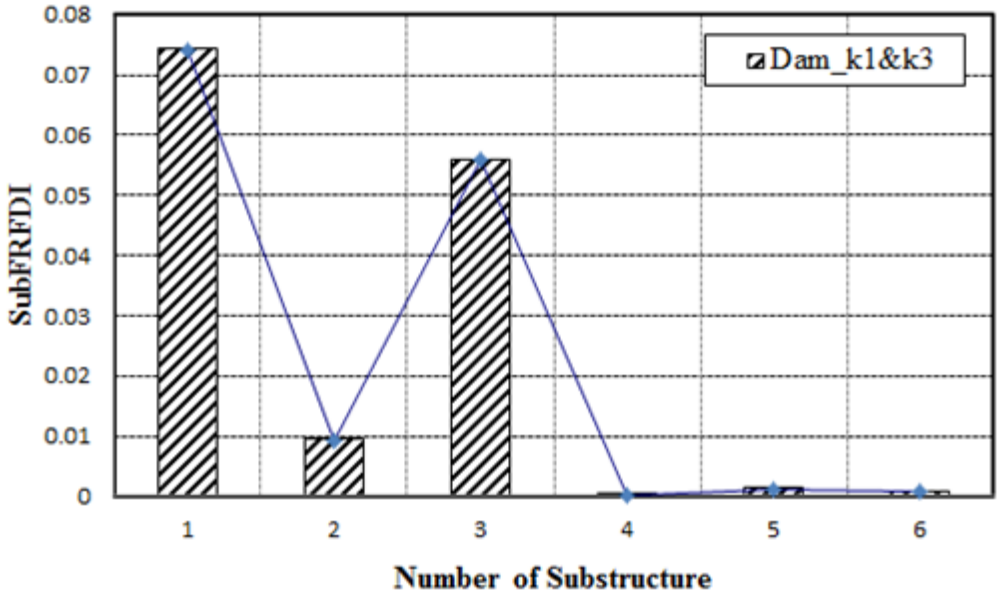

Figure 5.20. The *SubFRFDI* values for substructures in damage cases 9, multiple damage.

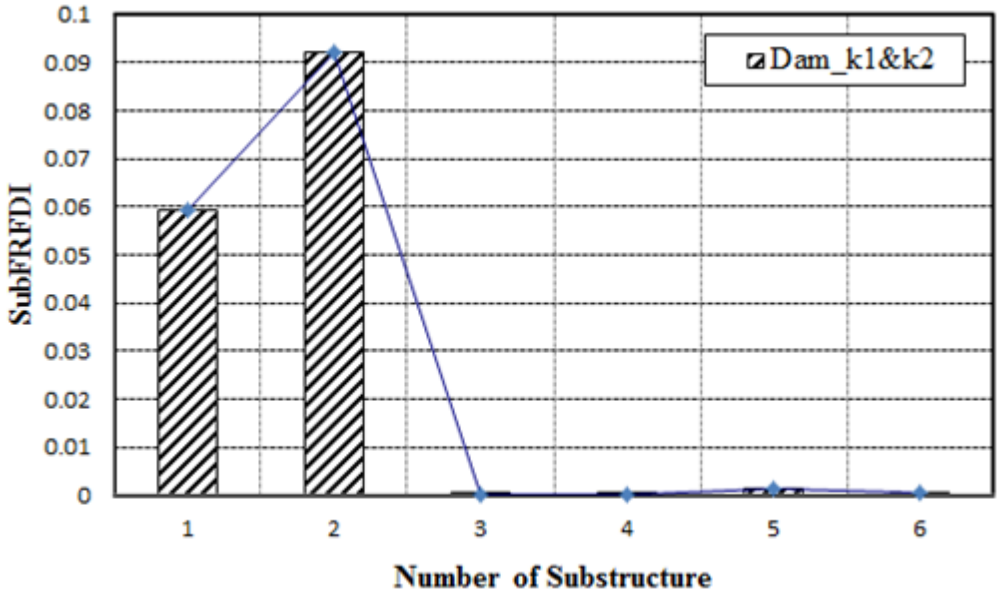

Figure 5.21 The *SubFRFDI* values for substructures in damage cases 10, multiple damage.

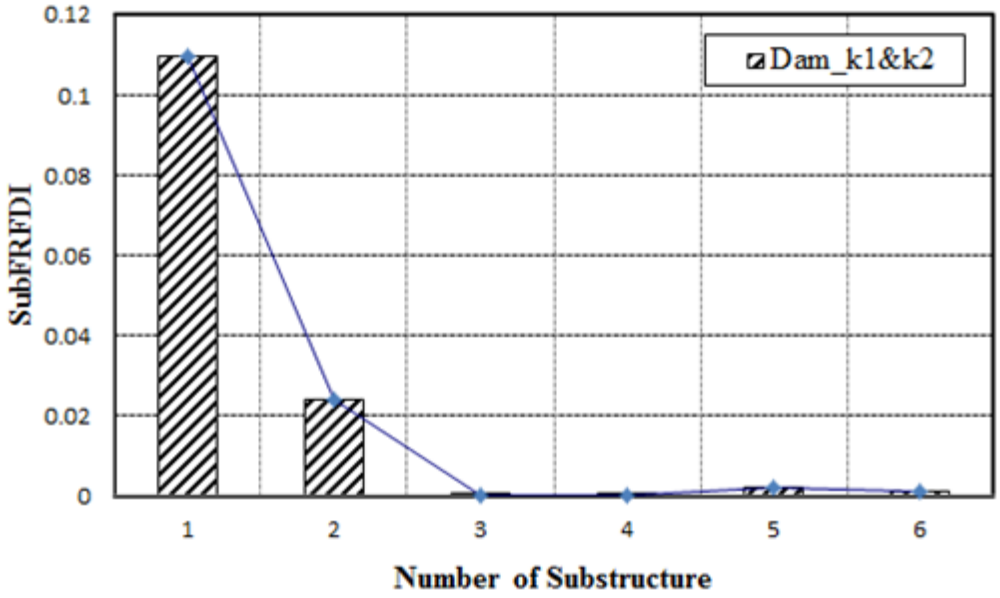

Figure 5.22 The *SubFRFDI* values for substructures in damage cases 11, multiple damage.

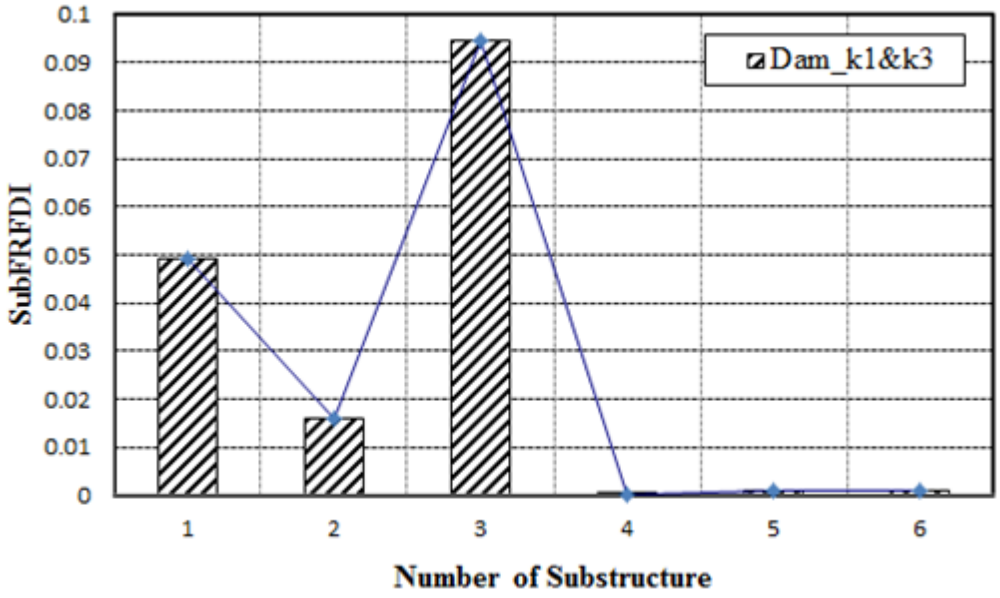

Figure 5.23 The *SubFRFDI* values for substructures in damage cases 12, multiple damage.

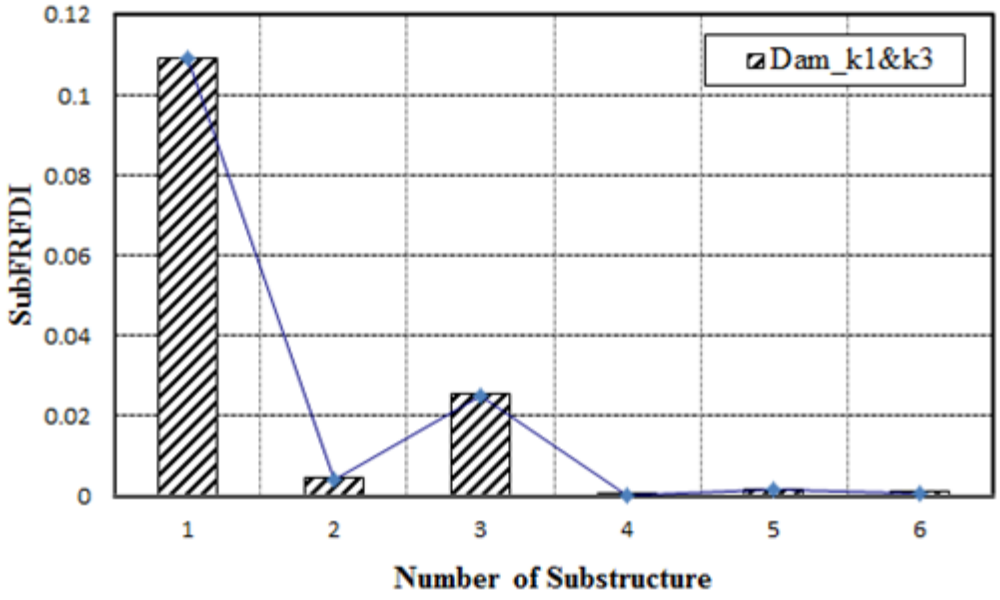

Figure 5.24 The *SubFRFDI* values for substructures in damage cases 13, multiple damage.

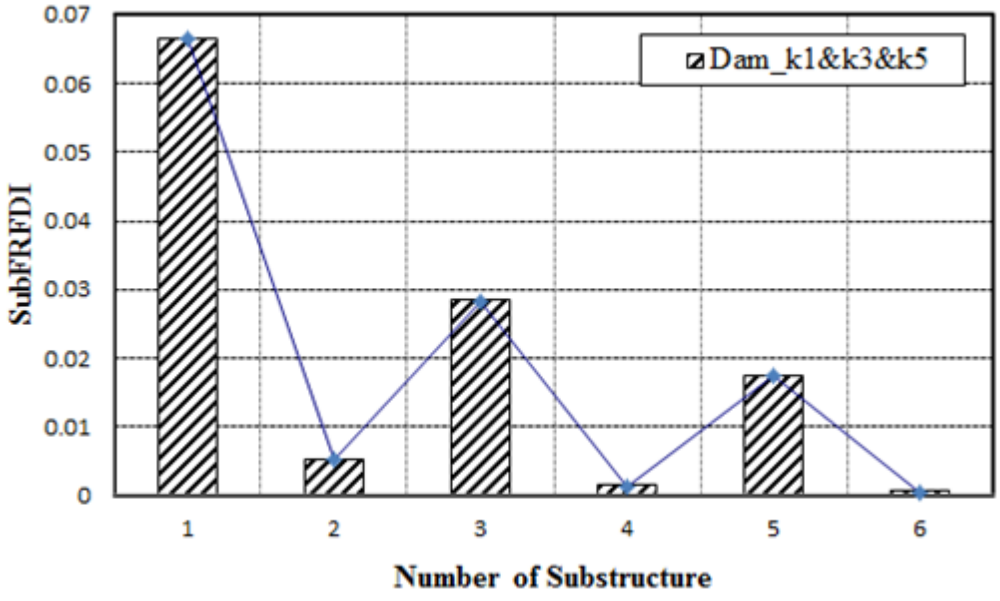

Figure 5.25 The *SubFRFDI* values for substructures in damage cases 14, multiple damage with various damage level.

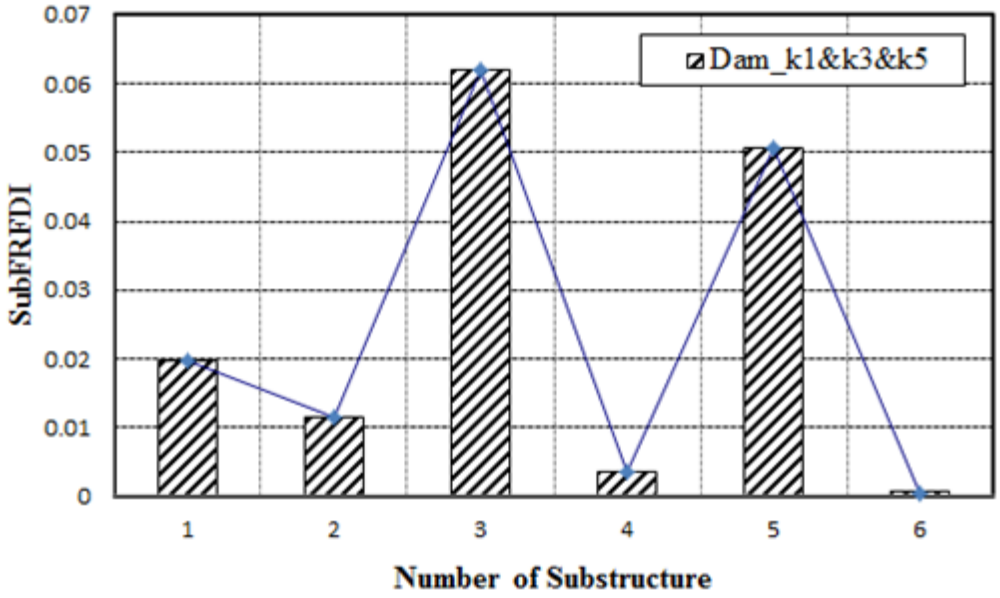

Figure 5.26 The *SubFRFDI* values for substructures in damage cases 15, multiple damage with various damage level.

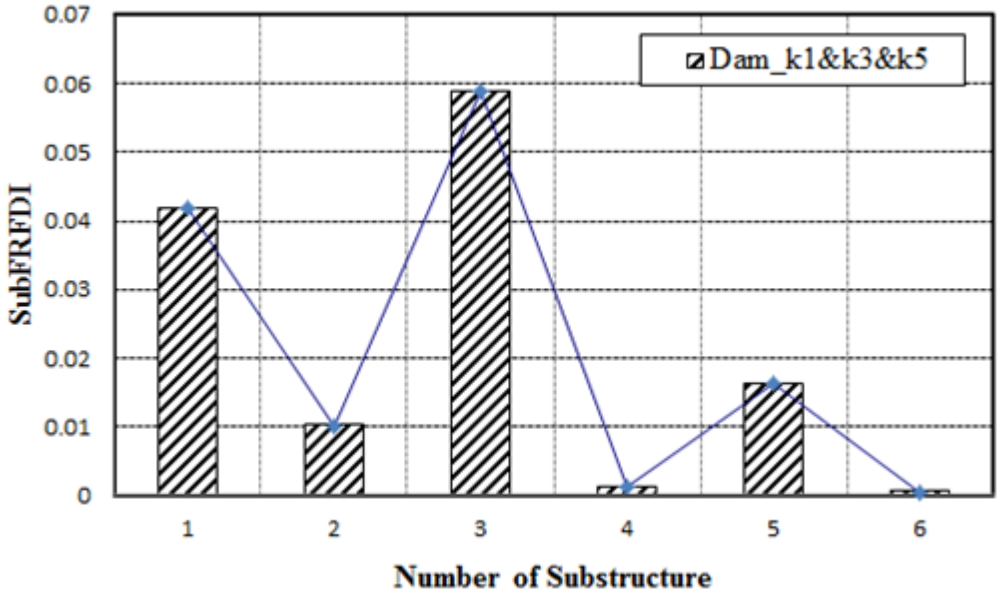

Figure 5.27 The *SubFRFDI* values for substructures in damage cases 16, multiple damage with various damage level.

5.2.3 Implement of SubFRFDI in Integrated WSN-Based SHM System

An SubFRFDI-based protocol was developed and embedded in the integrated WSN-based SHM System. Figure 5.28 presents the SubFRFDI-based protocol when using the WSN-based SHM System. Initially, the sensing nodes and base station exchange timestamp packets so that they can be synchronized using a two-phase synchronization scheme. The radio can be initialized via the constructor in *Radio* class of C# where define the frequency, power, node address, and PAN address. During the first phase, the proposed protocol models the skew in the clocks for all sensing nodes; each node is then skew synchronized. Next, the skew is estimated by performing linear regression over multiple timestamp packets from the base station. After synchronization, the sensing node waits for the fire command from event node. When the earthquake occurs, the event node immediately broadcasts a packet with a fire command to the sensing nodes. To send and receive the packet is easily using the classes *Send* and *ReceiveAny*. Finally, the sampling procedure for all sensing nodes starts performing sampling data and writing data to a response array. Corresponding parameters such as sampling rate, data type, and data length, are declared before sampling starts.

After sampling, the FRF calculation procedure is initiated. The sensing node *i*-1 then send FFT data to sensing node *i*. The FFT data are written to an input array. The FRF is next estimated by a FRF calculation function and is locally stored. Initially, the FRF is estimated as a known undamaged state. After each subsequent earthquake, the FRFs are referred to as a damage state. After the undamaged and damaged FRF are obtained, the SubFRFDI can then be estimated in all sensing nodes. Finally, all

sensing nodes send their SubFRFDI to the base station to evaluate the damage to the structure. In this protocol, the base station node and event node are powered by wall plug to be always waking. The sensing nodes are powered by rechargeable battery with energy harvesting system. All sensing nodes are set to be deep sleep mode and waking up by turns. At least one sensing node is waking on each floor for ensuring measuring. The mote can be put in deep sleep mode (drawing 525 uA) just call the *DeepSleep* class for a specified period of time.

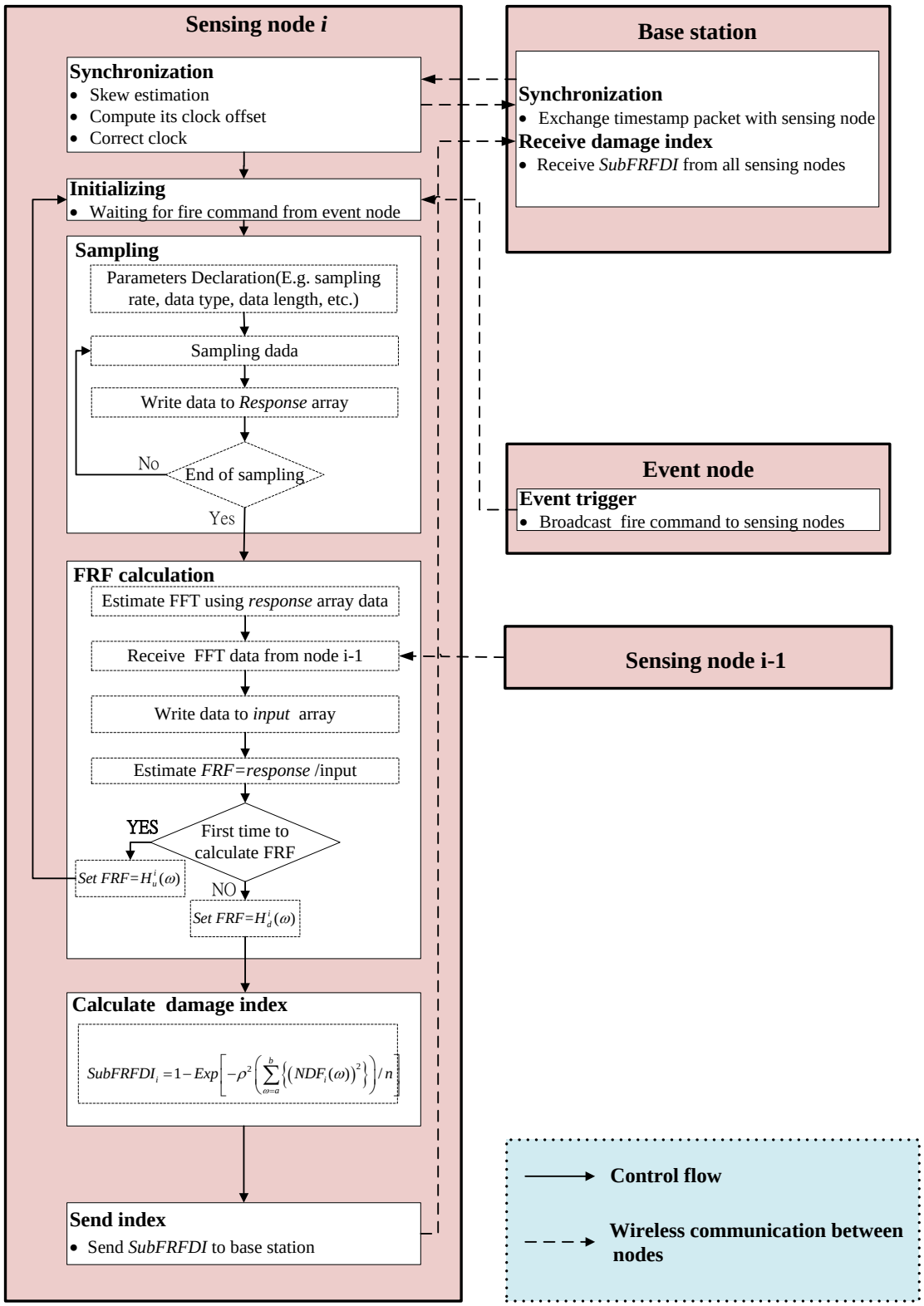

Figure 5.28 An SubFRFDI-based protocol

5.3 Electro-Mechanical-Impedance (EMI)-Based Local Damage Detection Method

5.3.1 Fundamental of EMI-Based Model

The EMI based damage detection approach use the EM coupling effect between active surface-bonded Piezoelectric patches and host structural. Researchers [64, 71] showed that the EMI is related to the mechanical impedance of a host structure, thus allowing monitoring the properties of the host structure using the measured electrical impedance. A piezoelectric patch-structure bonded system can be modeled as a circuit system [129], shown in Fig. 5.29. Herein, piezoelectric patch is modeled as a capacitor (C_p) and a self sensing-actuation voltage source (V_p) caused by input voltage (V_{in}). The output voltage, couple with V_p and V_{in}, can be expressed as

$$V_{out}(\omega) = \frac{Z_R(\omega)}{Z_R(\omega) + Z_p(\omega)} (V_{in}(\omega) + V_p(\omega)) \tag{5.32}$$

where Z_R is the electrical impedance of the resister and Z_p is electrical impedance of piezoelectric patch. Subsequently, the electrical impedance of piezoelectric patch can be written as

$$Z_p(\omega) = Z_R(\omega) \left(\frac{V_{in}(\omega) + V_p(\omega)}{V_{out}(\omega)} - 1 \right) \tag{5.33}$$

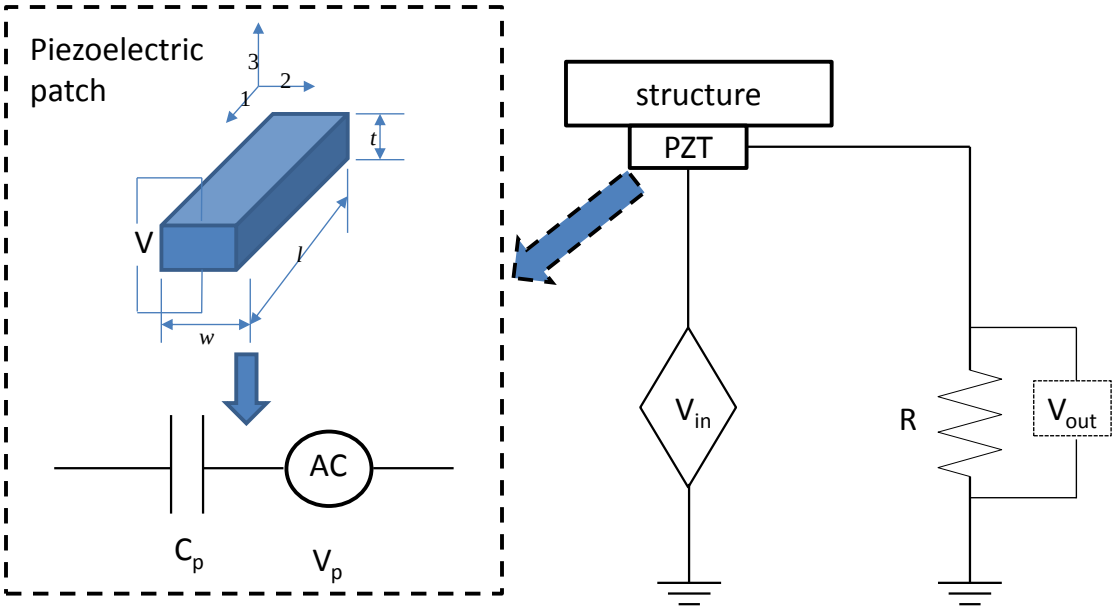

Figure 5.29. Diagram of PZT-structure bonded system

Since the self sensing-actuation voltage source (V_p) is related to structural mass, as confirmed by numerous researchers. Eq. 5.33 indicates that the Z_p has significant response to structural damage. A piezoelectric patch-structure bonded system can be further modeled as an electro mechanical admittance (EMA) model (Inverse of EMI). The electro mechanical admittance model can be expressed as [130]

$$Y(\omega) = j\omega \frac{wl}{t}\left(\left(\bar{\varepsilon}_{33}^{T} - d_{31}^{2}\hat{Y}^{E}\right) + \frac{Z_{pm}(\omega)}{Z_{pm}(\omega)+Z_{s}(\omega)} d_{31}^{2}\hat{Y}^{E}\left(\frac{\tan(kl)}{kl}\right)\right) \tag{5.34}$$

where w, l, and t are the width, length, and thickness of the piezoelectric patch; $\hat{Y}^{E}$ is the complex Young's modulus of the piezoelectric patch at zero electric field; $\bar{\varepsilon}_{33}^{T}$ is the complex dielectric constant of piezoelectric patch; d_{31}^{2} is the coupling piezoelectric constant in the x direction at zero stress; $k = \omega\sqrt{\rho / \hat{Y}^{E}}$ is the wave

number that is related to mass density ρ, $\hat{Y}^E$; and excitation frequency ω, respectively; Z_{pm} and Z_s are the mechanical impedances of the piezoelectric patch and the host structure, respectively. For a SDOF structure system, the mechanical impedances of structure is defined as

$$Z_s(\omega) = \frac{F_0}{\dot{v}} = \left|Z_s(\omega)\right| e^{i\theta} \tag{5.35}$$

in which

$$\left|Z_s(\omega)\right| = \sqrt{c^2 + \frac{\left(m\omega^2 - k\right)}{\omega^2}} \tag{5.36}$$

where the F_0 is a harmonic excitation force at angular frequency ω; $\dot{v}$ is velocity response in frequency domain; the *m*, *c* and *k* are mass, damping and stiffness of structure, respectively.

Equation (5.34) indicates that the EMI (or EMA) is directly related to the mechanical impedance of structure. As described in Eq. (5.34) and Eq. (5.35), when damage occurred to structure, the mechanical impedance of structure will be changed. Therefore, if the mechanical impedances of the piezoelectric patch remain undamaged, any changes in the EMI signal correlates with the damage in structure.

Although the EMI provides a qualitative method for detecting structural damage, the quantification approach need be established. A simple statistical algorithm, which is based on frequency-by-frequency comparisons, referred to Root Mean Square Deviation (RMSD), was used to develop the quantitative assessment of damage in previous research [69, 129, 131]. The RMSD is defined as

$$RMSD = \sqrt{\frac{\sum_{i=a}^{b}\left(I_i^D - I_i^U\right)^2}{\sum_{i=a}^{b}\left(I_i^U\right)^2}} \times 100 \qquad (5.37)$$

where I_i^U and I_i^D are the real part of impedance of piezoelectric patch at the i^{th} frequency point in undamaged and damaged structures, respectively. In a RMSD damage metric chart, the greater numerical value of the metric, the larger the difference between the baseline reading and the subsequent reading indicates the presence of damage in a structure.

5.3.2 Measurement of Piezoelectric-Impedance

The measurement of piezoelectric impedance is typically implemented by an impedance analyzer. The disadvantages of using impedance analyzer are relatively bulky size, expensive, and no portable. The Peairs *et al*. [132] developed an effective device using a digital signal analyzer with an FFT function that can measure and record the electric impedance of a PZT. Advantages of the new impedance-measuring device include its low cost, greater accessibility, and smaller size.

Credit to the progress of Micro Electronic Mechanical System (MEMS), the new single-chip impedance measurement device, AD5933 has been developed by Analog Device Inc. The AD5933 is a high precision impedance measurement device that combines an on-board frequency generator with a 12-bit, 1 MSPS, analog-to-digital converter (ADC). The frequency generator allows exciting external complex impedance with a known frequency. The response signal from the impedance is sampled by the on-board ADC and a discrete Fourier transform (DFT) is processed by an on-board DSP engine. The DFT algorithm returns a real (R) and imaginary (I)

data-word at each output frequency. Once calibrated, the magnitude of the impedance and relative phase of the impedance at each frequency point along the sweep is easily calculated. This is done off chip using the real and imaginary register contents, which can be read from the serial I2C interface. The block overview is shown in Fig. 5.30.

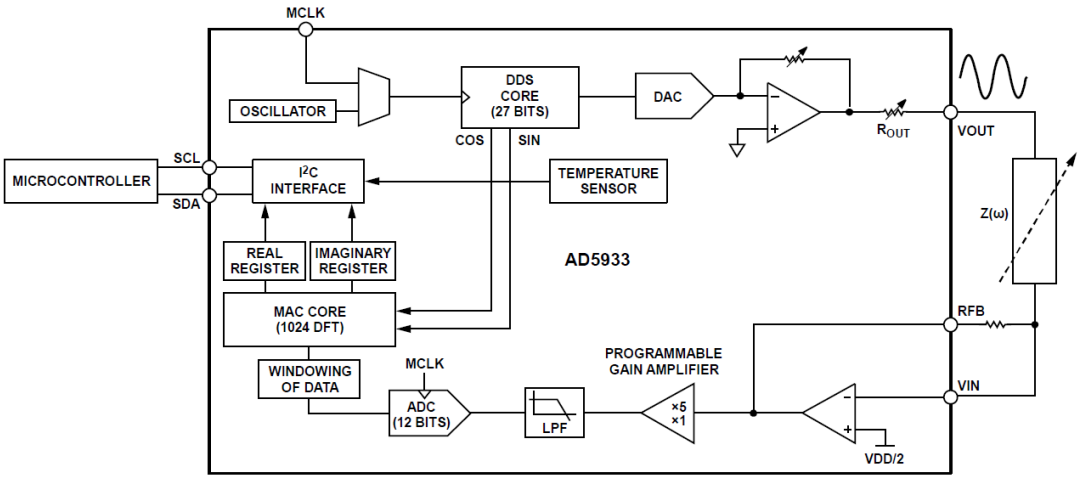

Figure 5.30. Block overview of AD5933

5.3.3 Selection of Frequency Ranges

The sensitivity of damage detection using NDE techniques is related to the frequency band selected. Initial damage in structure does not result in any measurable change in the structure's global stiffness properties. Hence, high frequency excitation is typically used. It was found that a frequency range with a high mode density covers more structural dynamic information. The range for a given structure typically used in the impedance methods is in the range of 30 kHz to 250 kHz and determined by a trial and error method. In the impedance-based method, numbers of peaks are usually chosen since there is a greater dynamic interaction over that frequency range. A higher frequency range (higher than 150 kHz) is found to be favorable in localizing the

sensing, while a lower frequency range (lower than 70 kHz) covers more sensing areas. [71, 131, 133].

Under the high frequency ranges used in this impedance-based method, the sensing region of the piezoelectric patch is localized to a region close to the sensor/actuator. Through various case studies in Esteban's work [134], it has been estimated that (depending on the material and density of the structure) the sensing area of a single PZT can vary anywhere from 0.4 m (sensing radius) on composite reinforced concrete structures, to 2 m on simple metal beams. The frequency ranges higher than 500 kHz have been found to be unfavorable, because the sensing region becomes extremely small and the PZT sensors show adverse sensitivity to their bonding conditions or PZT itself rather than behavior of a structure monitored.

CHAPHER 6 EXPERIMENTAL VERIFICATION

6.1 Introduction

In this chapter, this dissertation focused on the experimental study. When the theoretical basis of damage detection method and wireless SHM system based measuring system are completed, series experimental study are conducted to verify the proposed algorithm and system. First off all, the integrated WSN-based SHM system is verified involving sensor calibration, wireless communication quality, data losing, interference in material, power consumption. Subsequently, the proposed damage detection approach with proposed SHM system then investigated in a ¼ -scale six-storey steel structure that was designed by the National Center for Research on Earthquake Engineering (NCREE), Taiwan. Subsequently, the proposed wireless SHM system is employed in a bridge structure to test the feasibility in field.

6.2 Verification of Integrated WSN-Based SHM System

6.2.1 Verification of Sensing Node

In this test, the reliable data-sensing and transmission service is implemented on the sensing node and cluster head node. The sensing capability is calibrated compared to reference wire sensor. Two sensing nodes and a reference wire sensor (CXL01LF1) are attached on a Quanser shaking table to measure acceleration of table. The shaking table is excited by controller using Sin wave excitation input. Two sensing node and reference sensor are installed next to each other and the corresponding signals from those are expected to be identical. Measured dynamic responses were acquired by

sensing nodes and sent to the cluster head node connected to a host computer. Figure 6.1 compares the acceleration time history measured by two sensing nodes and reference sensor. The time history schemes of the wireless sensing nodes and reference sensor have identical shapes and magnitudes. This confirms good-quality data collection by the wireless sensing system. The same observation is made when the signals are compared in terms of FFT (Fig. 6.2) and power spectral density (Fig. 6.3). Moreover, the peak of FFT indicates the wireless sensing node can identify the shaking table is moving on 2 Hz Sin wave.

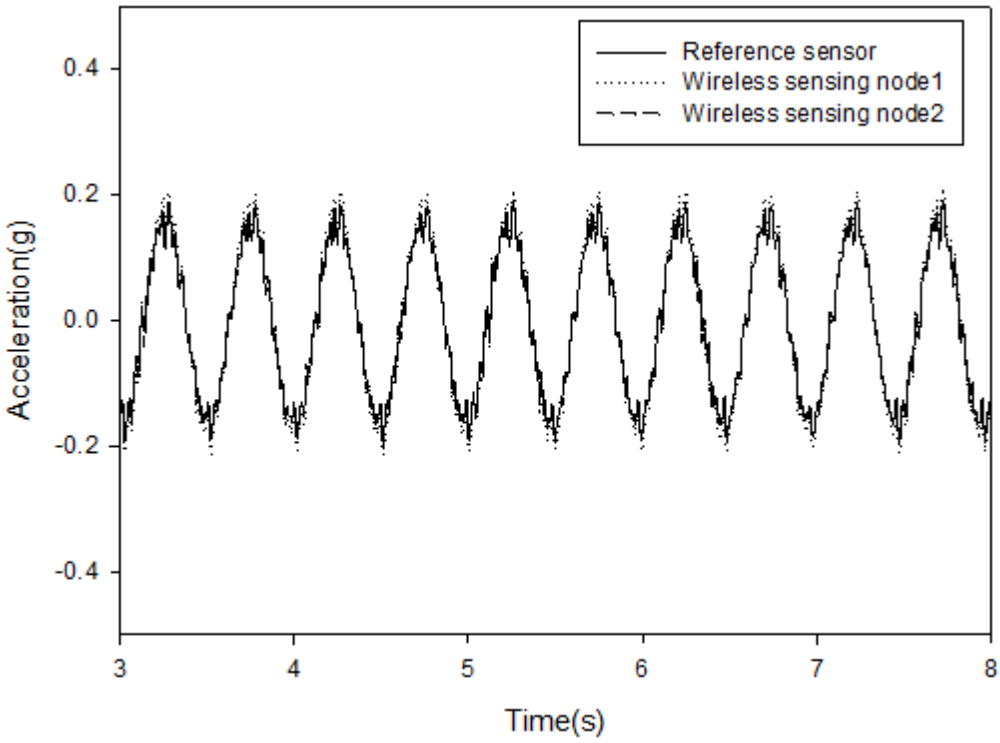

Figure 6.1 Acceleration record from wireless sensing nodes and reference sensor.

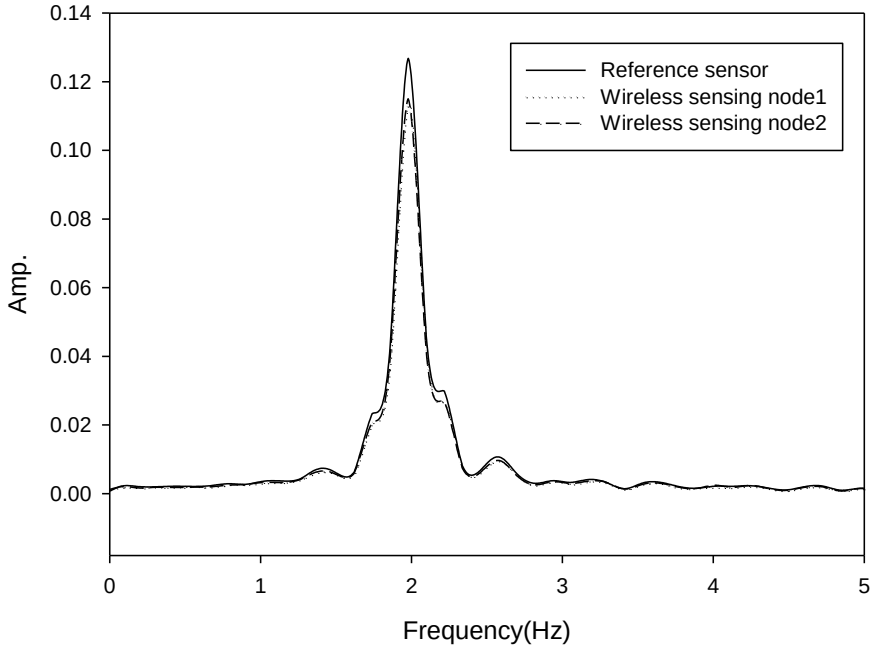

Figure 6.2 FFT of acceleration record from wireless sensing nodes and reference sensor.

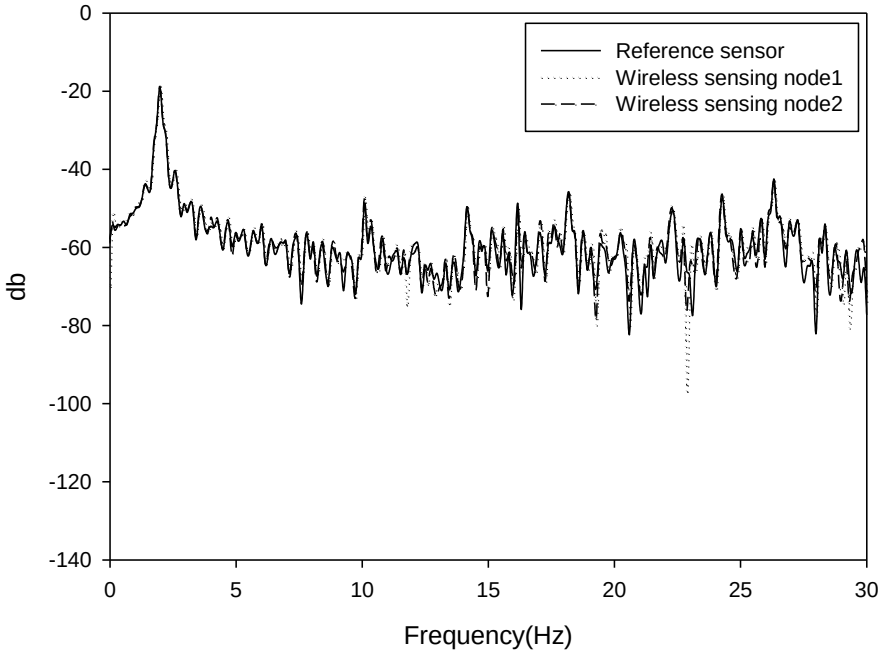

Figure 6.3 Power spectral density of acceleration record from wireless sensing nodes and reference sensor.

This experimental study then evaluated the feasibility and robustness of the proposed system in a 1/8-scaled three-storey steel frame model (Fig.6.4) was employed to verify the performance of the wireless sensing system placed on a Quanser shaking table. Each floor weighed about 3.8 kg and each column had a cross-sectional area of 80 mm^2 and was 440 mm in height. Wireless sensing nodes were deployed at the center of each floor. In this test, the model was excited by the Quanser shaking table using earthquake time history excitation data. The measurement period was 60 sec, during which data were oversampled. Oversampling, typically used for anti-aliasing, was based on the Nyquist theorem. Measurement data were sampled at 800Hz, and then down-sampled to a sampling rate of 200 Hz. Measured structural dynamic responses were acquired by sensing nodes and sent to the cluster head node connected to a host computer. Figure 6.5 shows the ground acceleration time history measured by wireless sensing nodes. Following, acceleration measurements from the wireless sensors identified natural frequencies by applying an ANN-based system identification (ANNSI) model [46]. The corresponding first three natural frequencies of the structure were 1.83, 5.42, and 7.96Hz. The modal parameters can be considered reasonable by comparing to FEM model.

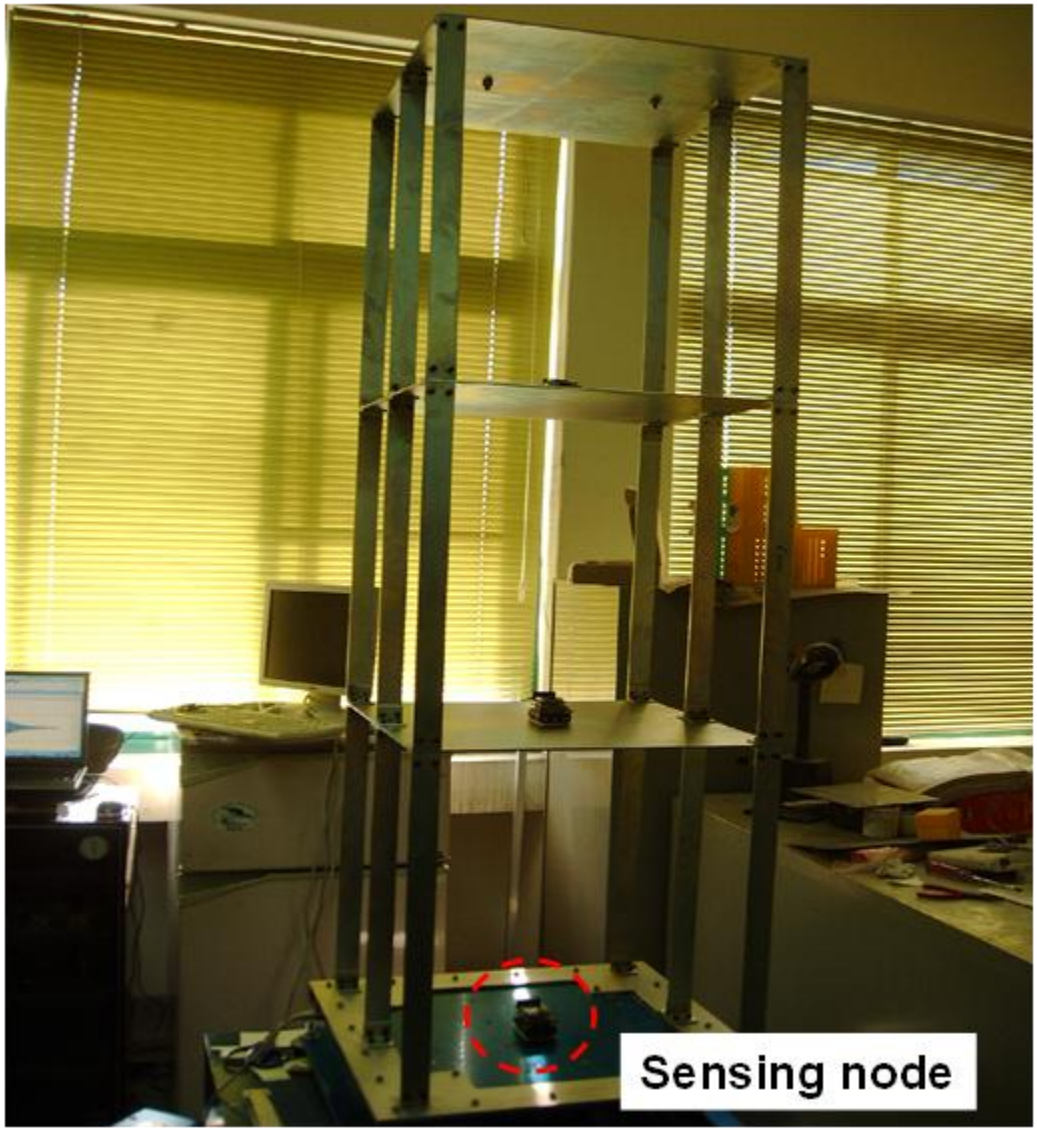

Figure 6.4 A 1/8-scaled three-storey steel frame model.

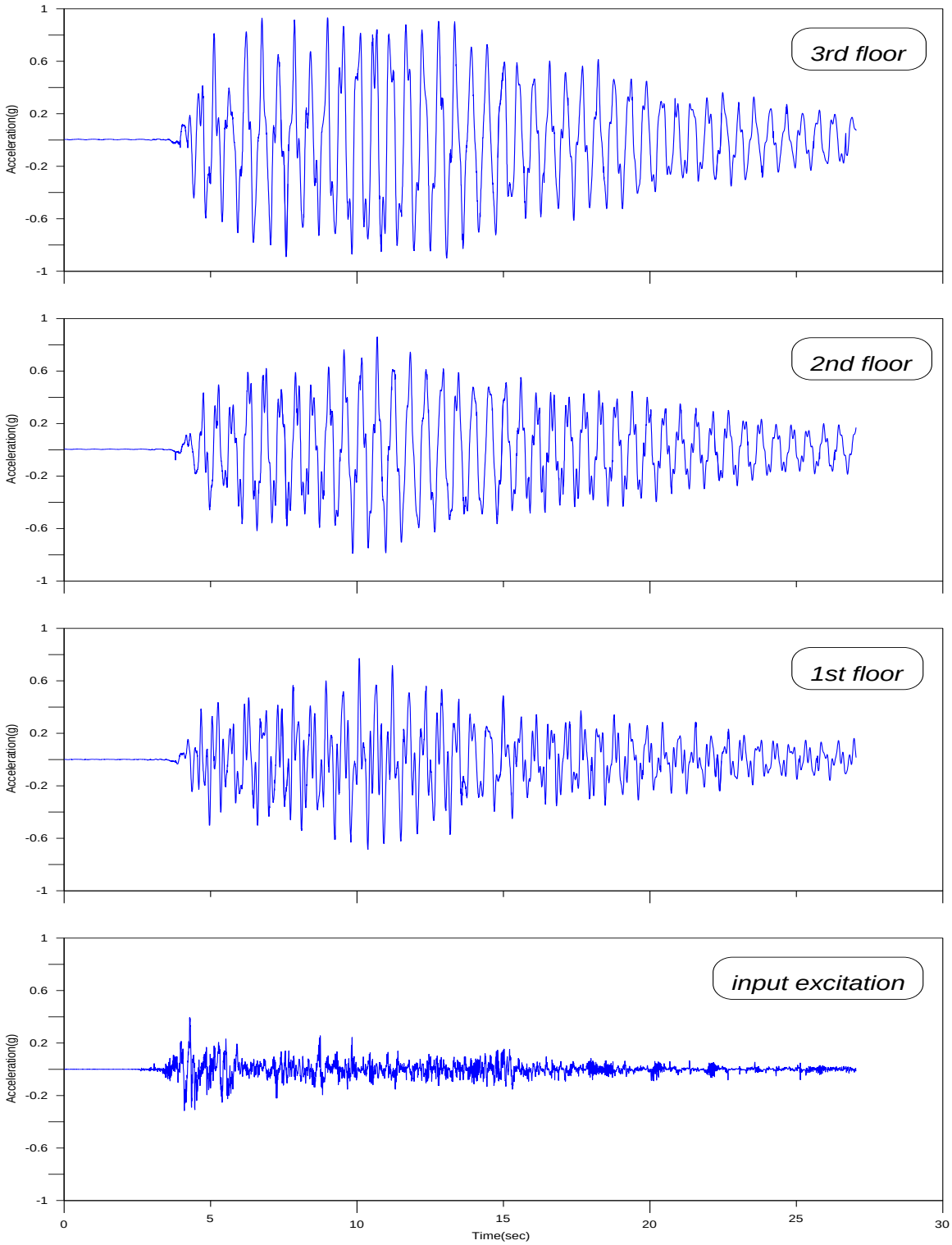

Figure 6.5 Acceleration record from wireless sensing nodes

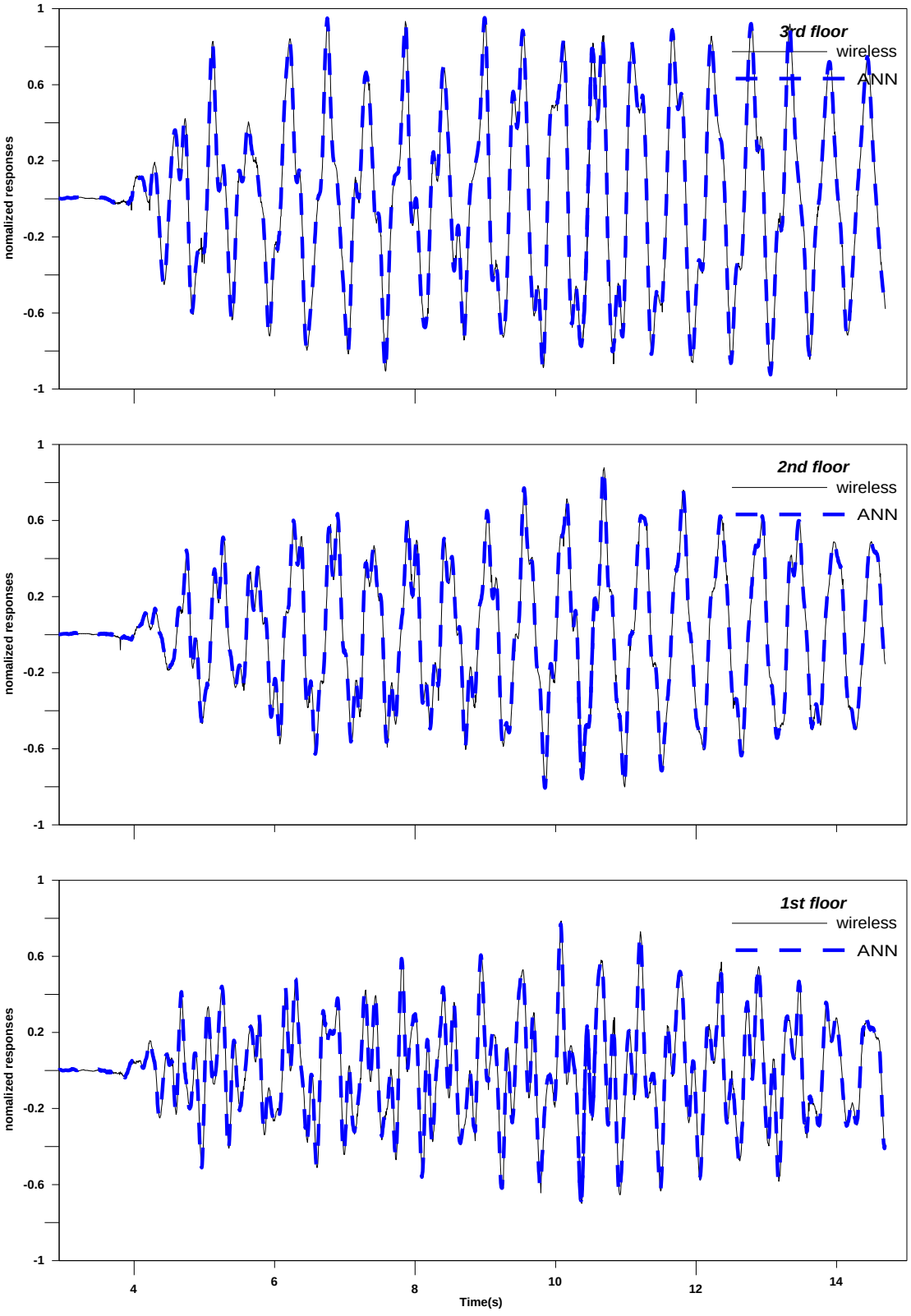

Figure 6.6. Response for ANN and wireless sensor node

6.2.2 Reliability of RF Communication Test

In a WSN, some packets may be lost during the RF communication. For instance, packets may collide with each other if multiple nodes attempt to send packets to the base station simultaneously. Packet loss may thus cause incomplete measurement signals. Herein, the successful packet received rate (SPRR) was utilized to evaluate the reliability of data transmission among nodes. The SPRR is defined as the number of successfully received packets divided by the number of sent packets. In practice, sensing nodes send a fixed number of packets to a base station. The base station can thus calculate the SPRR by using the number of sent and received packets.

The SPRR was used to evaluate the packet sent interval. In this study, the packet sent interval was 20 ms when the value of SPRR approached 1.0 whereas the SPRR declined as the packet sent interval decreased during the wireless communication test. In SHM, extended period measurement is necessary. In contrast with the conventionally adopted wired sensor system, the wireless sensor node runs an individual procedure on its CPU, with any exception event possibly disrupting node operations. Therefore, the stability and robustness for extended period measurement should be assessed. The measured period was set as 10, 30, 60 and 120 minutes, respectively. The sampling rate was 200Hz. The sensor nodes sample and transmit data to the base station via the proposed reliable data-sensing and transmission service. The base station then calculates the SPRR for data loss evaluation. Figure 6.7 indicates that the average SPRR is almost 99% for 10, 30, 60 and 120 minutes. This indicates that data loss was lower than 1% even in extended measuring period. It means that the proposed system is robust and stable for long term monitoring.

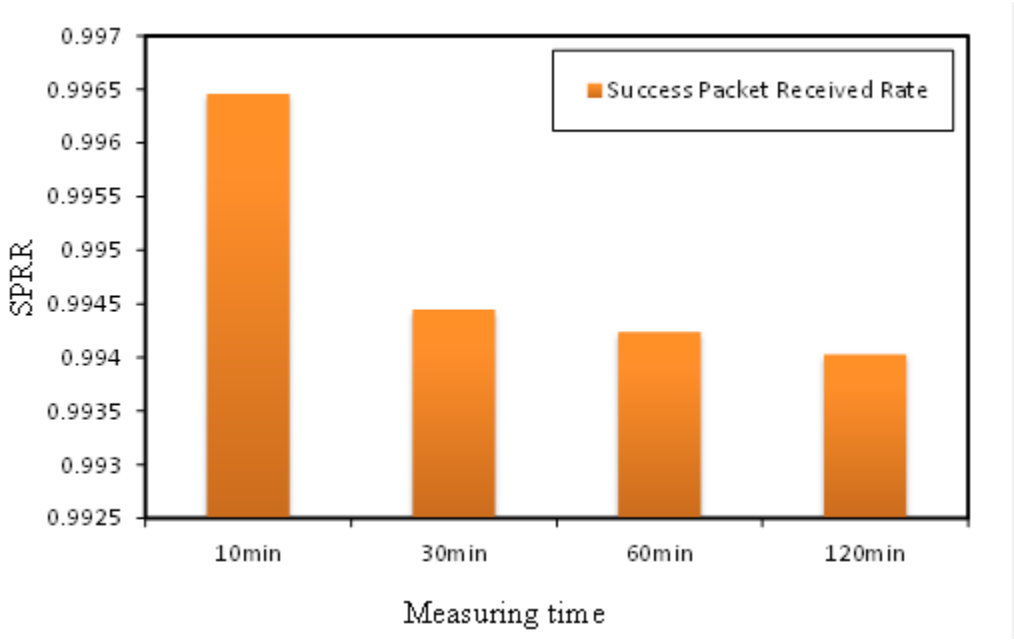

Figure 6.7 SPRR for various period measurement

As mentioned earlier, packets may collide with each other if multiple nodes attempt to send packets simultaneously. In this test, nodes with or without a time-scheduling data transmission procedure are designated to send 100 packets to the base station. The base station then calculates the SPRR to evaluate the data loss. With the time-scheduling procedure, the SPRR is close to 100% (Fig. 6.8). Without time-scheduling mechanism, if more than three nodes simultaneously send data to the base station, then the SPRR dramatically decreases to 50% (Fig. 6.8). These analytical results reveal that an effective time-scheduling procedure can increase the data transmission integrity.

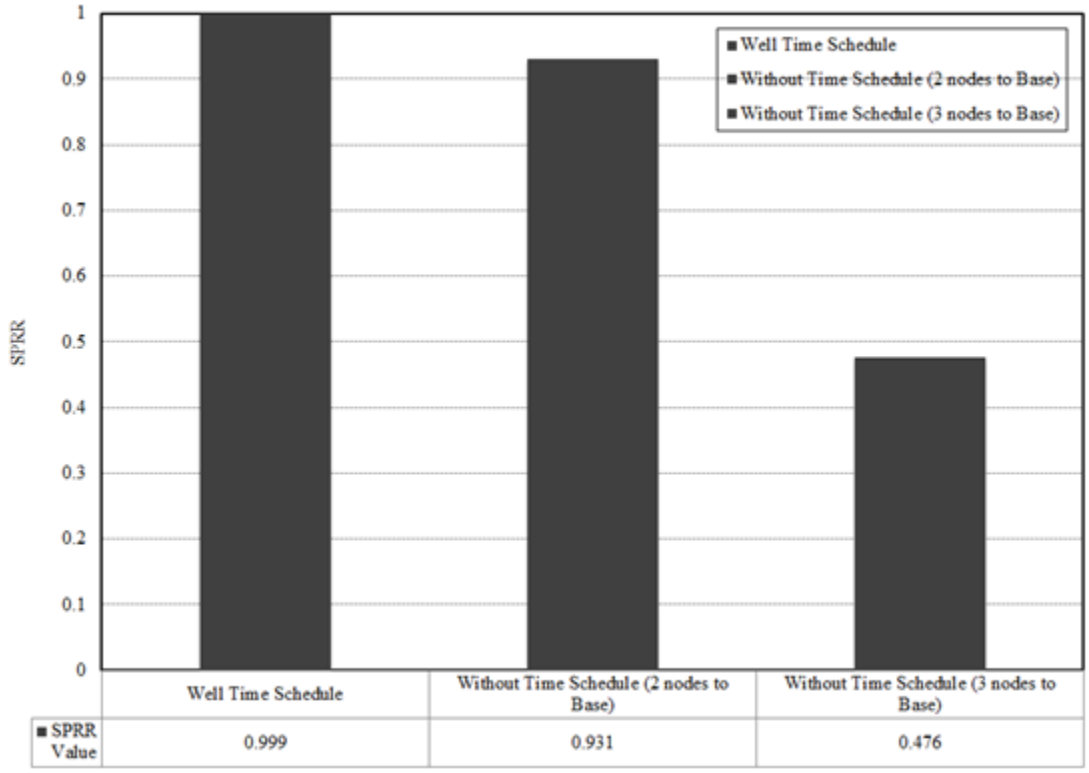

Figure 6.8 Comparison of success packets received rate(SPRR) for well Time Schedule and Non Time Schedule.

Figure 6.9 presents the relation between RF power and distance and the SPRR. Clearly, transmission range depends on RF power. A higher power output increases range but also increases power consumption. Therefore, Figure 6.9 is a useful reference when deploying the sensor nodes in the structure. Each node can be allocated a different transmission power to optimize power consumption for varying distance. In the experimental study, the farthest distance was 20m. Hence, power was set to -15dbm to reduce power consumption.

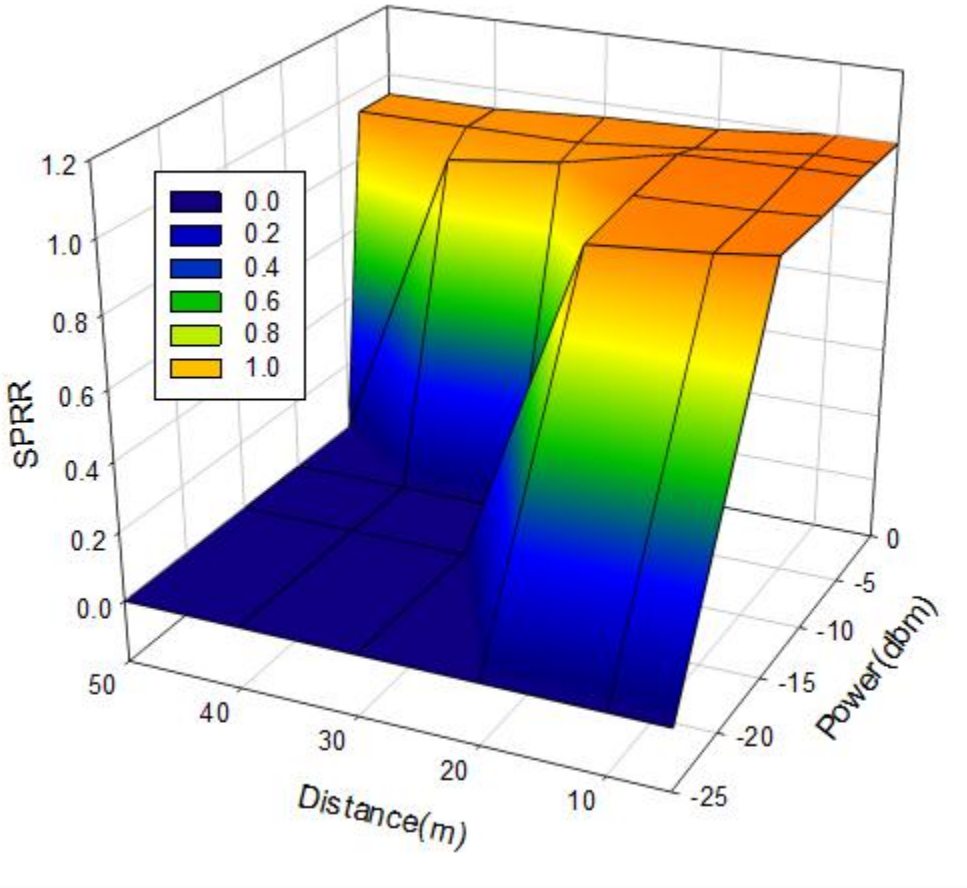

Figure 6.9. Successful packet received rate (SPRR) to RF Power and Distance

6.2.3 Field Test in Bridge Structure

In Taiwan, the typhoon cause great damage on bridge due to Bridge Scour. Hence, the monitoring of Bridge Scour has received considerable interest in the last decade. Traditional site investigation methods are expensive and time-consuming and may not always give a complete assessment. Geophysical methods can be used to determine the riverbed profile below the water in a river. A trial of ground penetrating radar (GPR) is a geophysical method that is particularly efficient in determining the sub-bottom geological structure in a shallow freshwater environment. Forde *et al.* [135] discussed a number of scour surveys using GPR. They concluded that GPR

surveys can be effective in determining both the water depth and sub-bottom geological structure near bridge piers and abutments. Yankielun *et al.* [136] conducted a laboratory experiment using time-domain reflectometry (TDR) for monitoring scour. Their system capable of continuous round-the-clock operation can be used to constantly monitor the extent of scour and can indicate changes in sediment depth of less than 5 cm. The fiber Bragg grating (FBG) was also an alternative technique for scour monitoring. Lin *et al.* [137] developed a FBG based monitoring system and tested in the laboratory. Their FBG scour-monitoring systems can be used to measure both the processes of scouring/deposition and the variations of water level. Several experimental runs have been conducted in the scaled flume to demonstrate the applicability of the system. Their experimental results indicate that the real-time FBG monitoring system has the potential monitor the scour. However, further applications in the field should be conducted. The robotic system was also presented for underwater inspection of bridge substructures. DeVault [138] developed an automated robotic system for underwater inspection of bridge substructures. This robotic system can detect scour, deterioration, or damage to support columns by two identical mobile robots designed to travel along opposite surfaces of the pier while connected to each another by a cable and winch system. It provides positional data and sensor information (video images) to the system operator for condition evaluation.

The conventional wired sensing system is expensive and infeasible. Characterized by its low manufacturing costs, low power requirements, miniaturized size, and no need for cabling, the wireless sensor networks (WSN) is an attractive sensing technology for deploying sensors for bridge scour monitoring. Hence, the developed integrated WSN-based SHM system was deployed in a bridge to test the feasibility and practicality in real civil structure.

The proposed system was deploying in Nioudou Bridge. A field free vibration test was conducted for obtaining dynamic response. Two piers were connected by a steel bar for free vibration test. The soil ground was excavated to 4m depth to simulate scouring. The free vibration test was performed twice for comparing intact and scouring case. Dynamic responses were record and send to base station via data-sensing and transmission service from wireless sensing nodes.

6.2.3.1 Experimental Setup

Figure 6.10 presents the experiment setup and sensor locations. The field experiment was conducted in Nioudou Bridge. Two piers were connected by a steel bar for a free vibration test. Hydraulic machinery was used to provide a tensile force on the steel bar. The tensile force was increasing till the weak part of the steel bar was broken. This broken energy forces the pier for free vibration. The maximum tensile force was previously examined by a Tensile Test in the laboratory. Figure 6.11 shows the maximum tensile force is 250kN. Three wireless sensing nodes were deployed on the top, center and bottom of the pier 1(P1), respectively. Dynamic responses were record and send to base station via reliable data-sensing and transmission service. The soil ground was excavated to 4m depth to simulate scouring. The free vibration test was performed twice for comparing intact and scouring case.

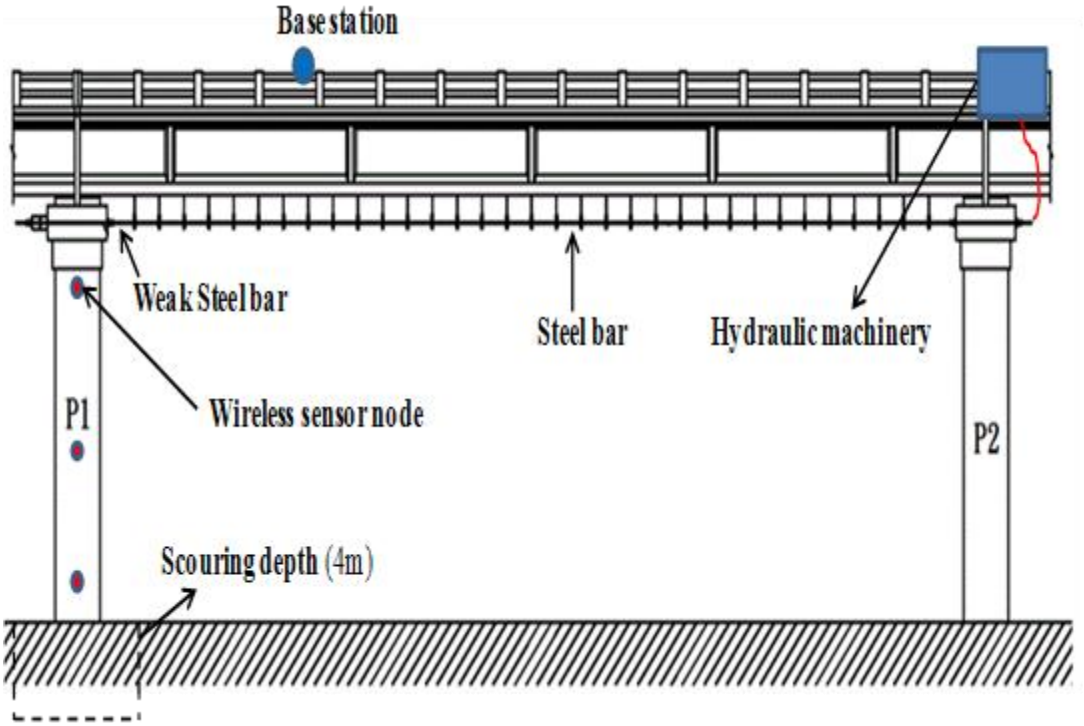

Figure 6.10. The experiment setup and sensor locations

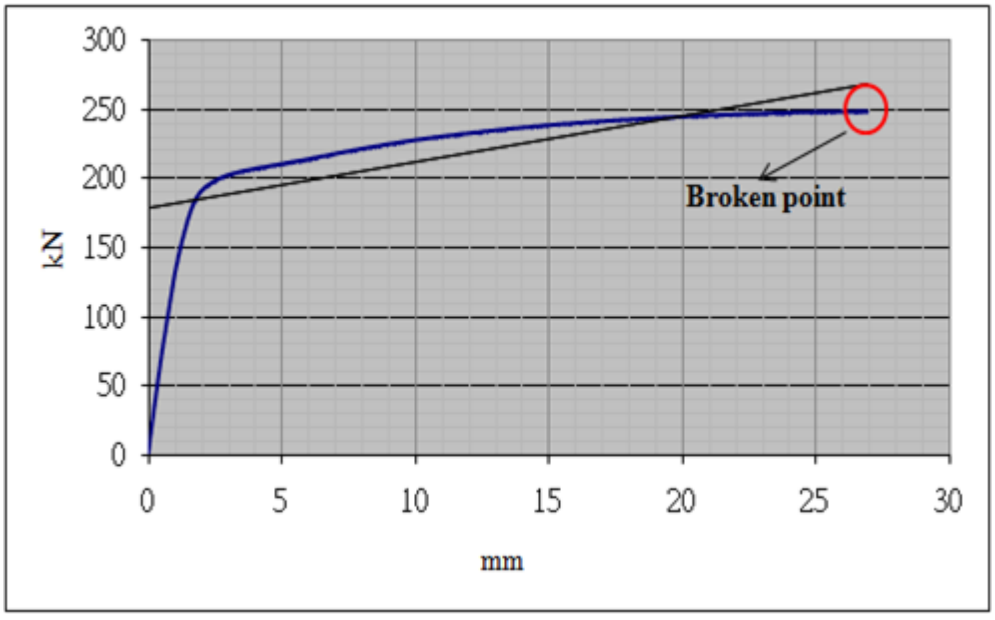

Figure 6.11 Previous Tensile Test

6.2.3.2 Experimental Results

Figure 6.12-6.15 shows the photograph of field experiment. Figure 6.12 shows the Nioudou Bridge. The expansion joint was previously removed to increase the displacement of pier when perform free vibration test. Figure 6.13 shows the weak part of the steel bar. Two weak steel bars were used in intact and scouring case. The steel bars were broken when the tensile force reach 180kN and 220kN respectively in intact and scouring case. Figure 6.14 demonstrates the excavation condition to simulate scouring. Figure 6.15 presents the location of wireless sensing node which is fixed in the pier.

Figure 6.12 Photo of Nioudou Bridge

Figure 6.13 Weak part of the steel bar

Figure 6.14 excavation of soil ground,

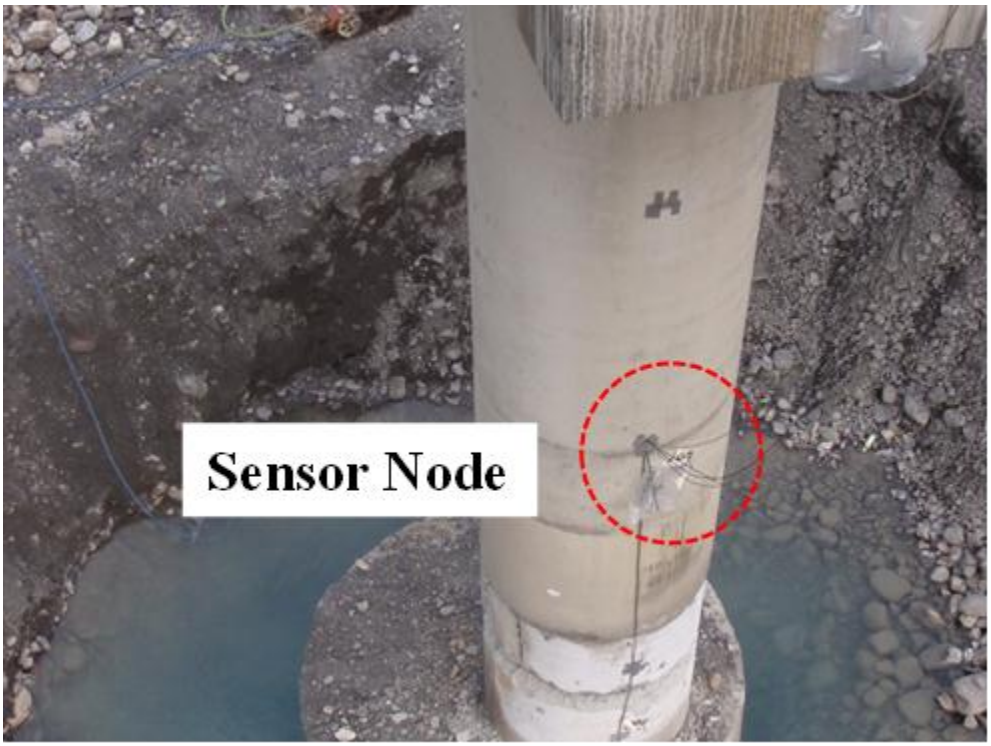

Figure 6.15 Wireless sensing node position.

In this experiment, the reliable data-sensing and transmission service which is proposed in chapter 4 were simply modified to implement in this test. Figure 6.16 shows the data transportation and sensing process. First, the sensing modes were deployed on the top, center and bottom of the pier. Next, after the sensing nodes and cluster head node are initialized, the cluster head node sends an inquiring packet to confirm whether the sensing nodes are ready. The cluster head node then broadcasted packets to synchronize all sensor nodes and to remote sensing nodes for sensing; sensors continued measuring and storing data in SDAM. The measurement period was 20 minute, during which data were sampled at 250Hz. Following the timeout, the Imote2 nodes sent data to the base station under a time-scheduling mechanism to avoid data collisions. Initially, the sensing nodes wait until a sending-delay time is equivalent to (total sampling time + total packet sending time)* (node ID). For instance, if the node ID is 0, the sensing node 0 transmits packet immediately since

the sending-delay equals zero. The data in each sensing node are then taken from the array, filled in a packet, and sent to the base station. Based on this procedure, each node sequentially sends the data to the base station with a respective sending-delay, which can avoid the packet collision.

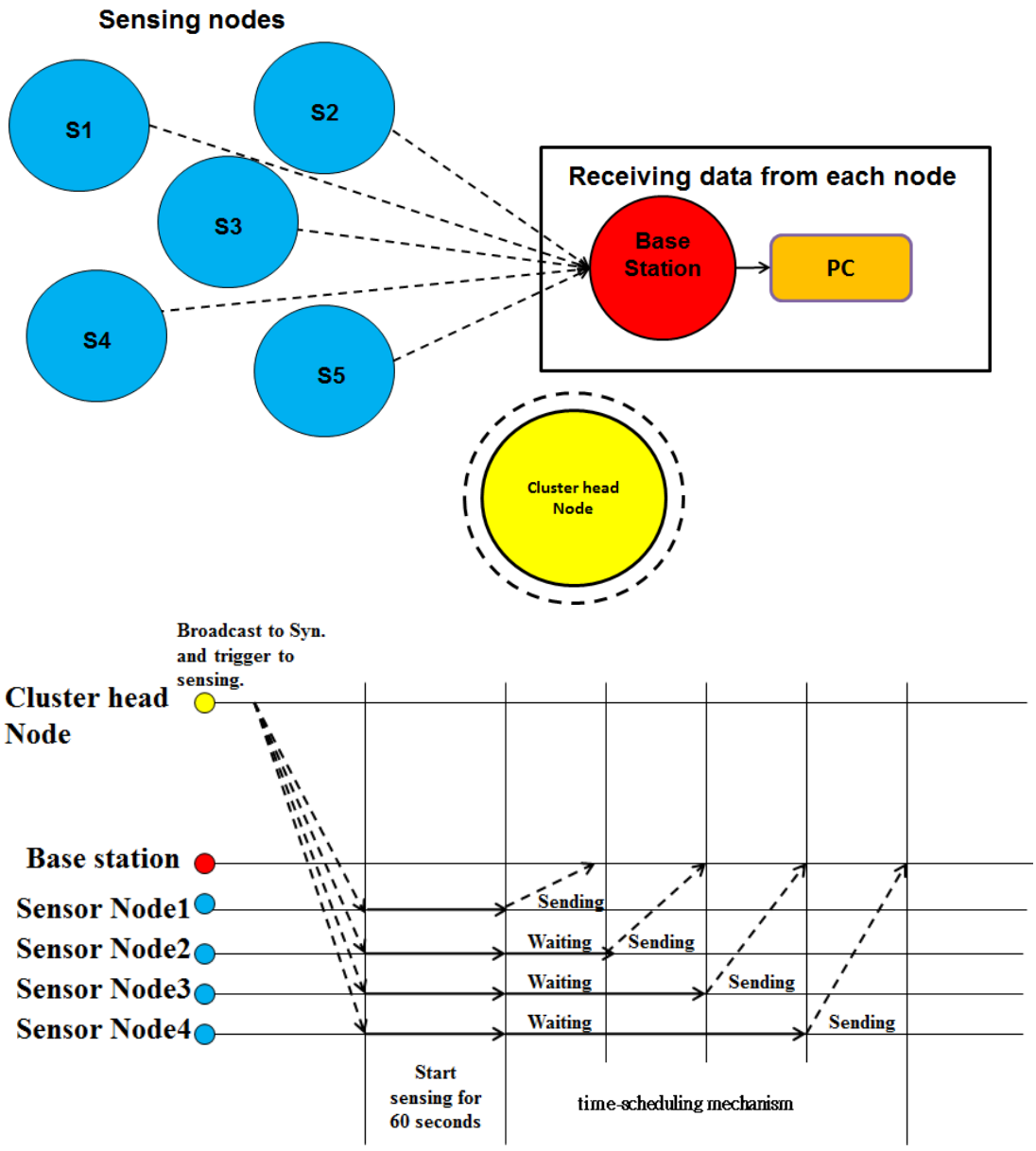

Figure 6.16 Modified reliable data-sensing and transmission service

Figure 6.17 shows the acceleration response measured by the sensing nodes. The good-quality data collection by the wireless sensing system successfully records a typical free vibration response of the pier. Figure 6.18 shows the responses on the top sensing node for comparing the intact and scouring case. Observing to the response of the free vibration, it indicates that the free vibration response for intact tend to stable faster than the scouring case. Figure 6.19 compares two FFTs for intact and scouring case. In frequency domain, the difference between intact and scouring case can be observed. The work indicates that the proposed wireless sensing system was a reliable technology for monitoring bridge structure.

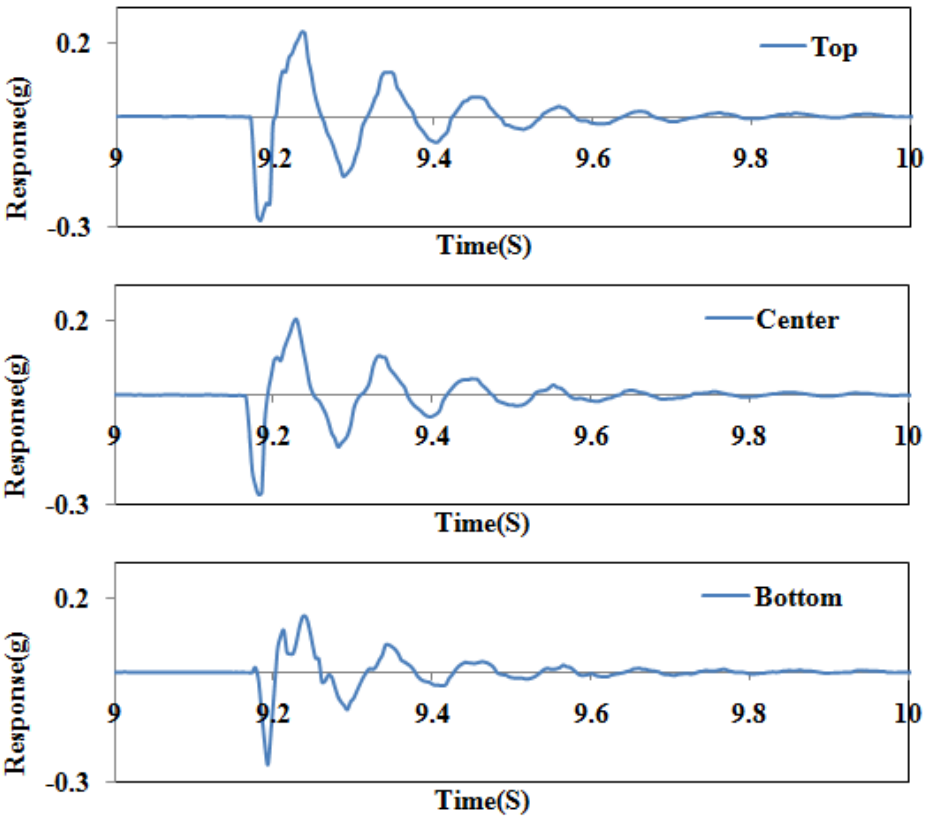

Figure 6.17 Responses of sensor nodes for intact case.

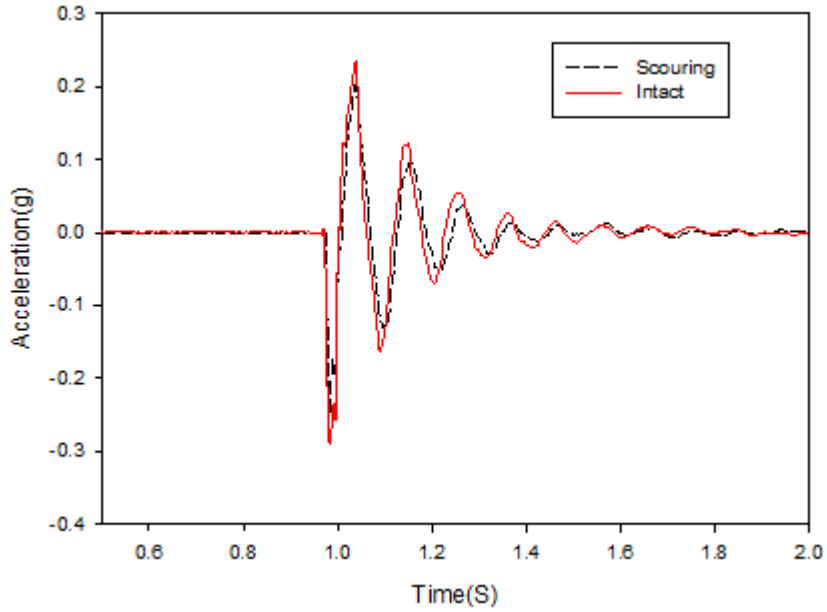

Figure 6.18 Comparison of scouring and intact bridge pier with free vibration response on the top node.

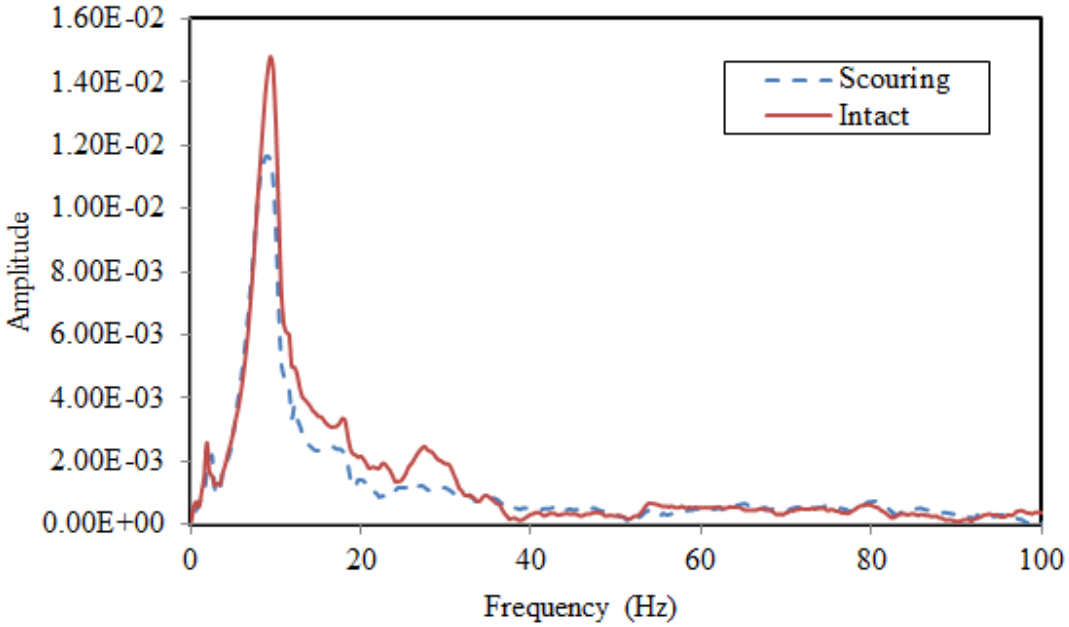

Figure 6.19 Comparison of FFT for scouring and intact bridge pie.

6.3 Experimental Study in Building Structure

This experimental study first exam the proposed damage detection approach in a four-storey steel frame model (Fig. 6.20) placed on a Quanser shaking table. Each floor weighed about 4 kg and each column had a cross-sectional area of 40 mm^2 and was 210 mm in height. Wireless sensing nodes were deployed at the center of each floor. Four PZT patches are respectively bonded to the joint of the columns in 1^{st} floor. After measuring the several baseline impedance signatures and acceleration, damage was introduced by completely loosening two bolts at joint 4 on first floor. In first stage, the proposed *SubFRFDI* were used to detect the damaged floor in global state. The identified result indicates that the proposed methods can detect the location of damage on first floor, as shown in Fig. 6.21.

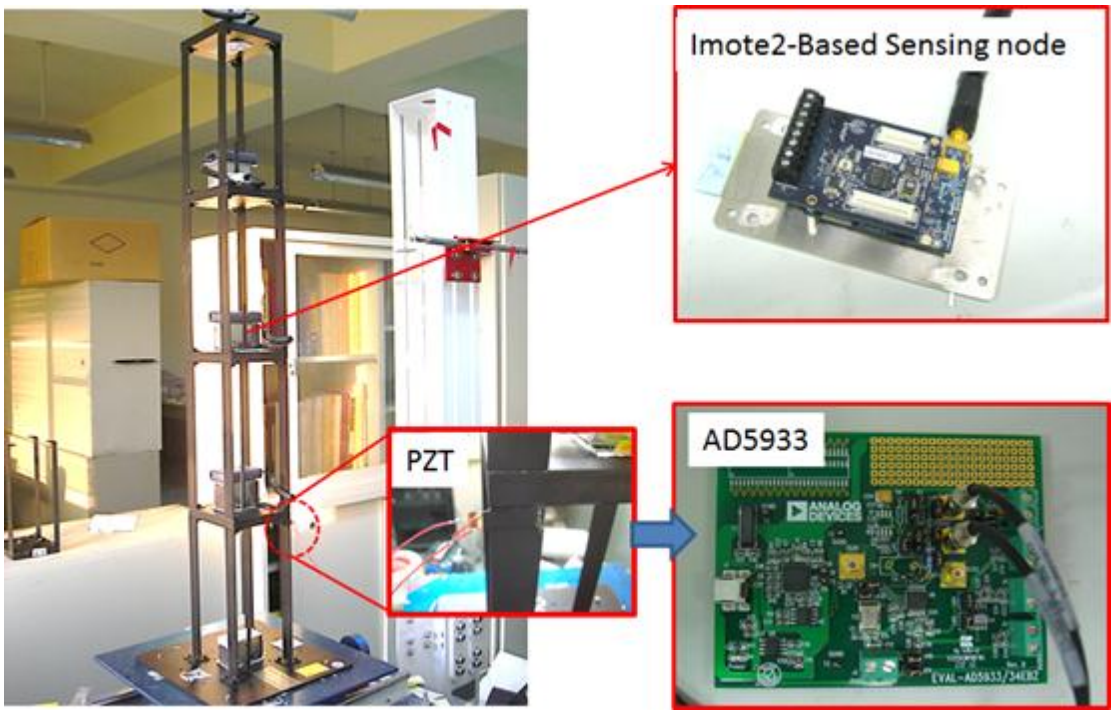

Figure 6.20 Experimental setup for wireless SHM system and impedance measurement device

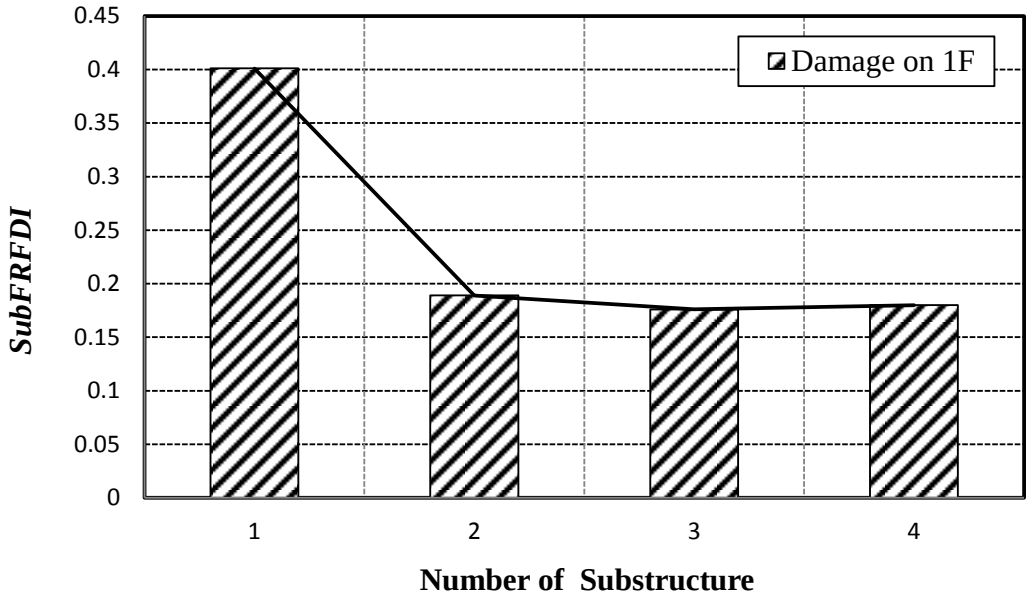

Figure 6.21 SubFRFDI value: damage on first floor.

After the global SHM approach, *SubFRFDI*, roughly indicate the location of damaged floor. The EMI based damage detection approach then check the component of building structure locally. The real part of impedance measurements of the PZT at joint 1 to joint 4 are shown in Fig. 6.22. Figure 6.22 shows a baseline of undamaged state and four damaged impedance curves. A damage metric chart is illustrated in Fig. 6.23. The damage metric chart based on *RMSD* is constructed to identify the local damage position of structure. As shown in Fig. 6.23, the highest value identifies the damage of joint 4 significantly.

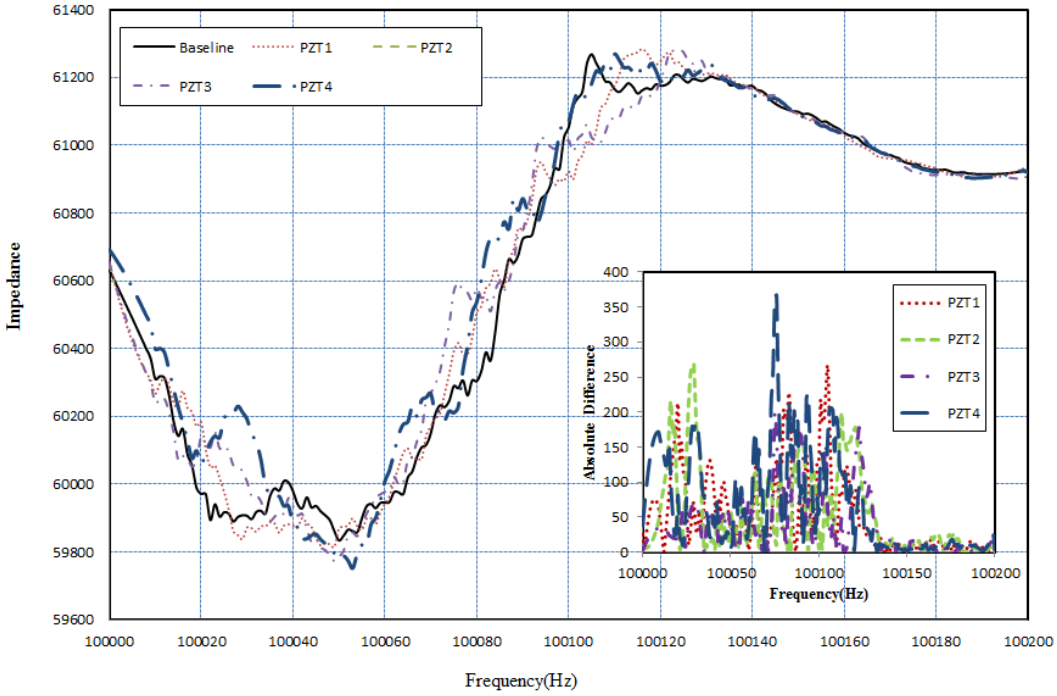

Figure 6.22 A baseline of undamaged state and four damaged impedance curves.

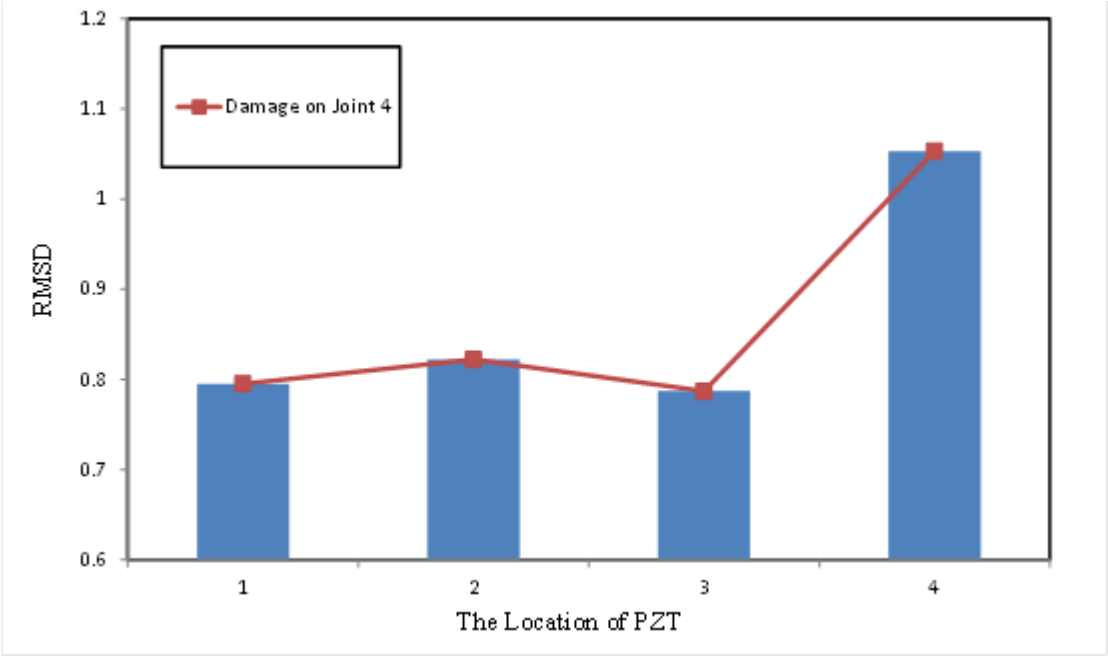

Figure 6.23 A damage metric chart of RMSD for damage on joint 4.

Subsequently, the proposed damage detection approach then test in a ¼ -scale six-storey steel structure that was designed by the National Center for Research on Earthquake Engineering (NCREE), Taiwan. Figure 6.24 shows an experimental setup of the test structure. The floors, beams, and columns were connected using bolts. Various measurement sensors, including 3-axes accelerometers, an LVDT, and velocity sensors, were deployed. Simultaneously, the wireless SHM system was deployed for sensing, logging, storing, processing, and analyzing thus obtained (Fig. 6.24). Four damage scenarios were considered to simulate states of damage to the steel frame model. Table 6.1 and Fig. 6.25 show the four damage scenarios in which the width and thickness of a column was reduced separately or simultaneously. All experiments involved excitation using a 100 gal El Centro earthquake input on a shaking table at NCREE.

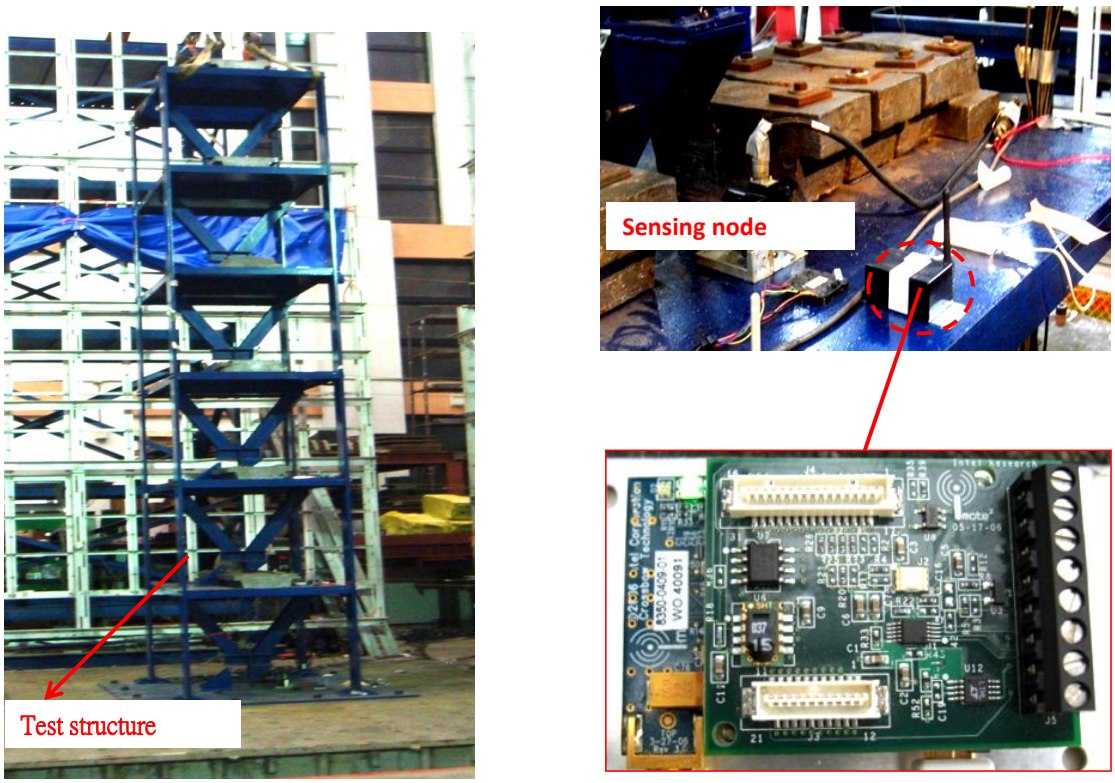

Figure 6.24 A photograph of the test structure. (b) The Imote2.NET-based sensing nodes fixed on the floor.

Table 6.1 Description damage scenarios for the steel-frame model.

Damage scenario case	Description
Damage scenario 1	Reduced 3.75 cm width in the medium height of each column at 1st floor.
Damage scenario 2	Reduced 7.5 cm width in the medium height of each column at 1st floor.
Damage scenario 3	Reduced 7.5 cm width and 6mm thickness in the medium height of each column at 1st floor.
Damage scenario 4	Reduced 12 cm width in the medium height of each column at 3rd floor.

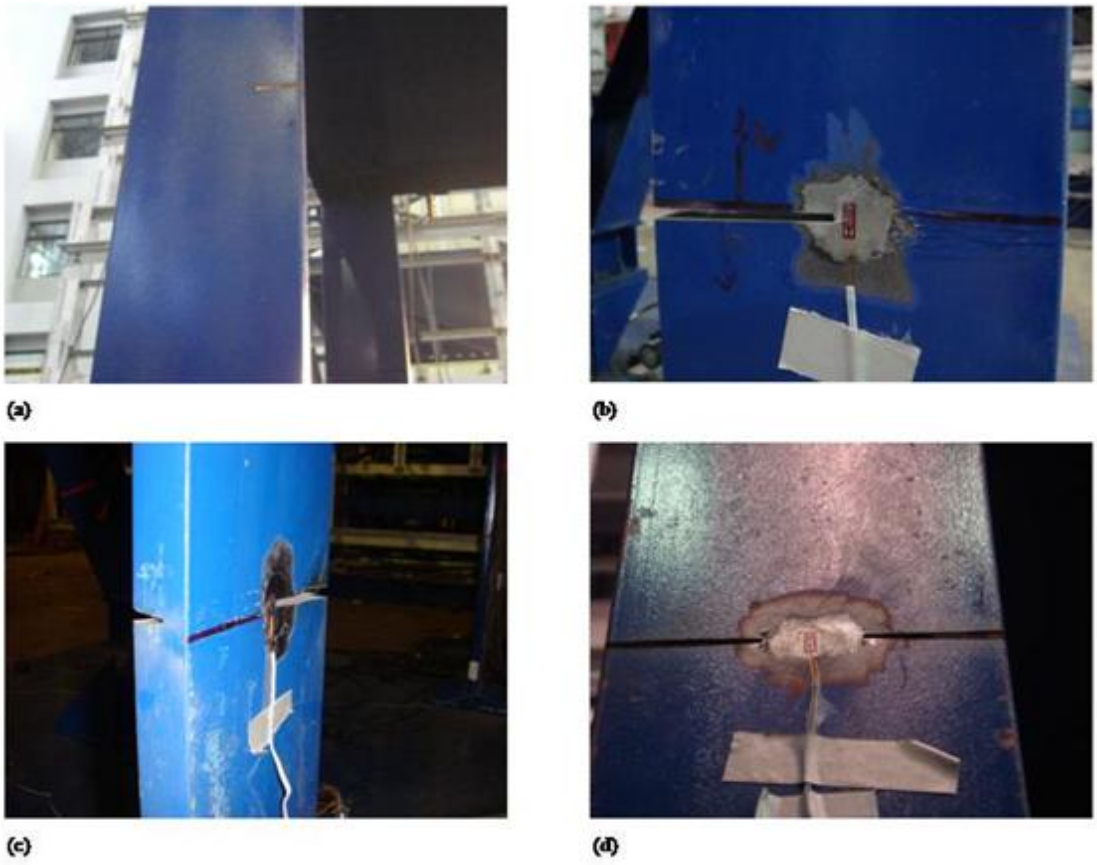

Figure 6.25 Photographer of damage scenario: (a) damage scenario 1. (b) damage scenario 2. (c) damage scenario 3. (d) damage scenario 4.

The proposed WSN-based SHM system was deployed on a steel frame model. The measurement period was 60s, during which data were sampled at 200 Hz. Besides using the proposed reliable data-sensing and transmission service, a time-scheduling data transmission procedure was used to transfer raw data to the base station. The reliable data-sensing and transmission service provides excellent data sensing and transmission quality for determining the structural dynamic properties. Measured dynamic responses were acquired by wireless sensing nodes and reference sensors. Figure 6.26 compares the acceleration time history measured by sensing nodes and reference sensor. Using the steel frame responses, modal properties were

identified by the system identification procedure. In Table 6.2, the modal parameters identified using the ANN-based system identification approach [139] were compared with the measured data obtained by wireless sensing nodes and conventional reference sensors. It is confirmed that the data obtained using the wireless sensing nodes possess good quality and can be utilized reasonably to calculate the modal parameters. Figure 6.27 (a)-(f) show the FRF of structure for 1^{st} floor to 6^{th} floor.

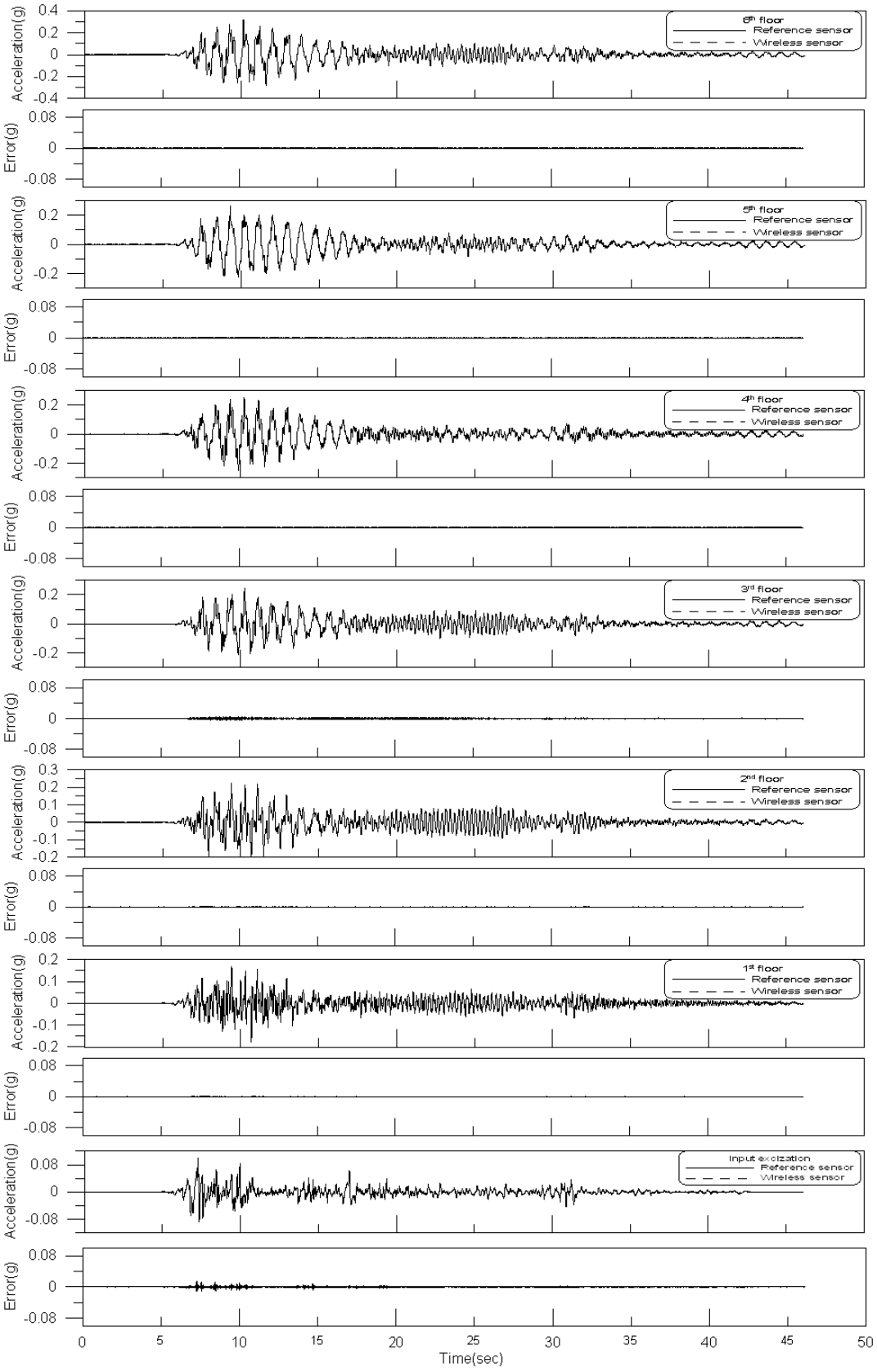

Figure 6.26 Acceleration of wireless sensor and reference sensor

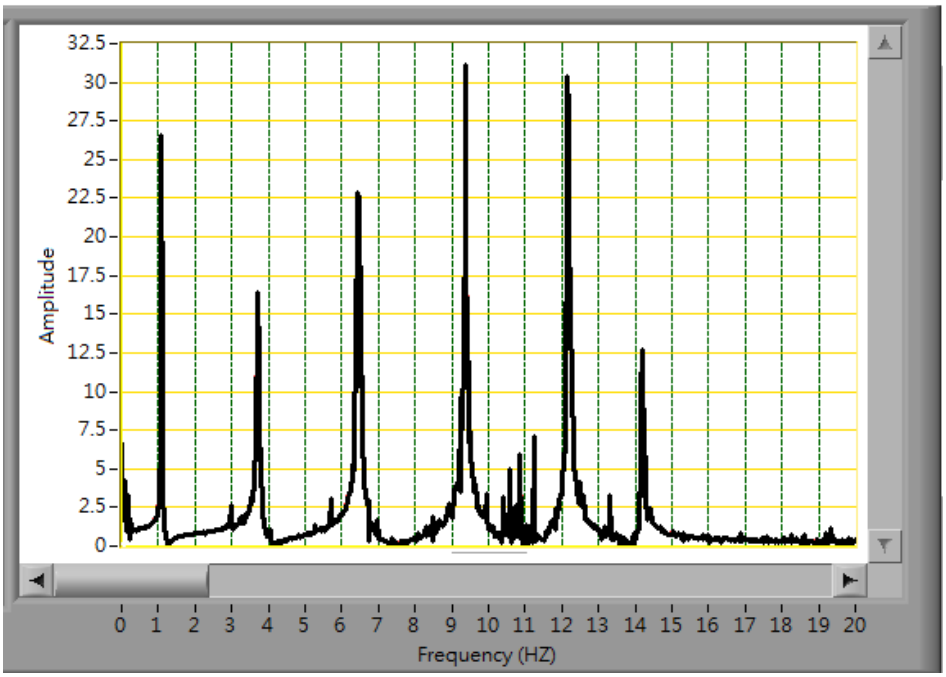
Amplitude
32.5
30
27.5
25
22.5
20
17.5
15
12.5
10
7.5
5
2.5
0
0 1 2 3 4 5 6 7 8 9 10 11 12 13 14 15 16 17 18 19 20
Frequency (HZ)

(a)

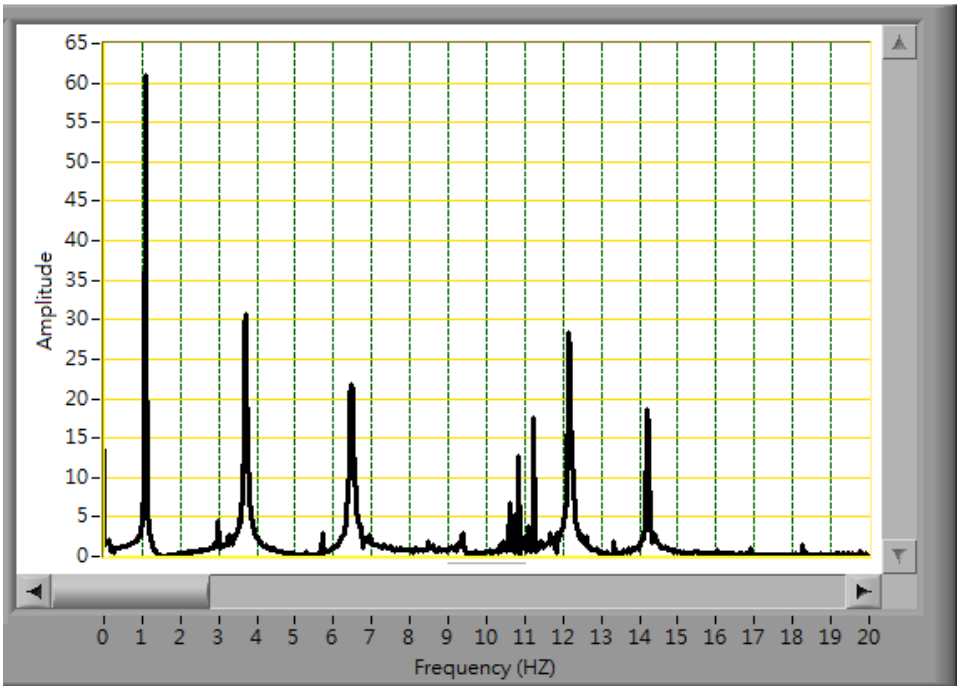
Amplitude
65
60
55
50
45
40
35
30
25
20
15
10
5
0
0 1 2 3 4 5 6 7 8 9 10 11 12 13 14 15 16 17 18 19 20
Frequency (HZ)

(b)

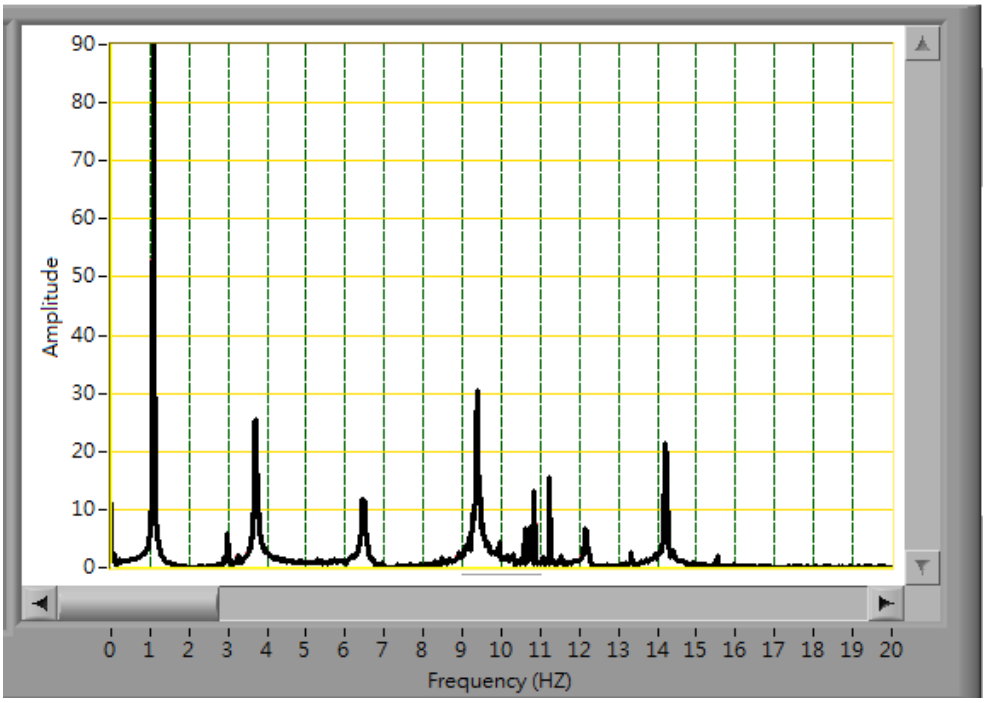
Amplitude
90
80
70
60
50
40
30
20
10
0
0 1 2 3 4 5 6 7 8 9 10 11 12 13 14 15 16 17 18 19 20
Frequency (HZ)

(c)

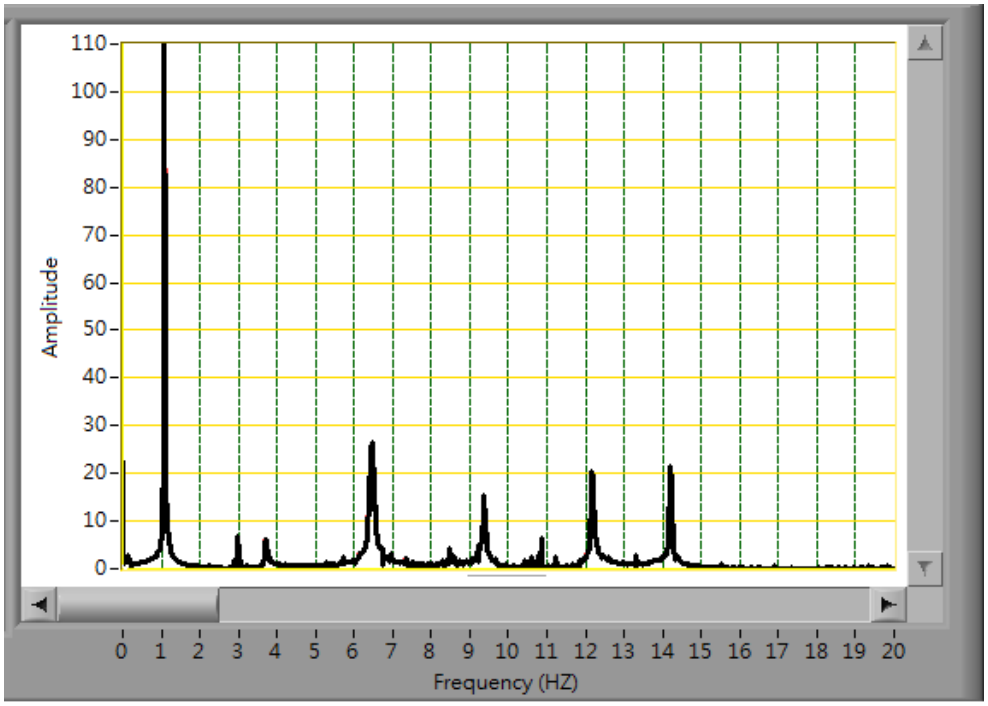
Amplitude
110
100
90
80
70
60
50
40
30
20
10
0
0 1 2 3 4 5 6 7 8 9 10 11 12 13 14 15 16 17 18 19 20
Frequency (HZ)

(d)

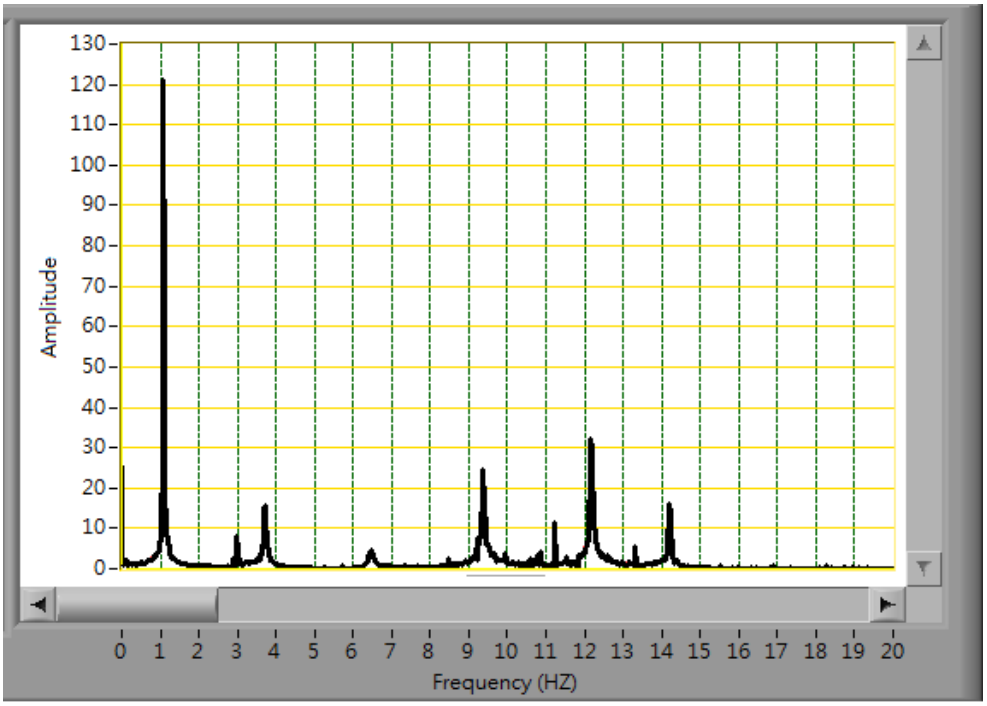

(e)

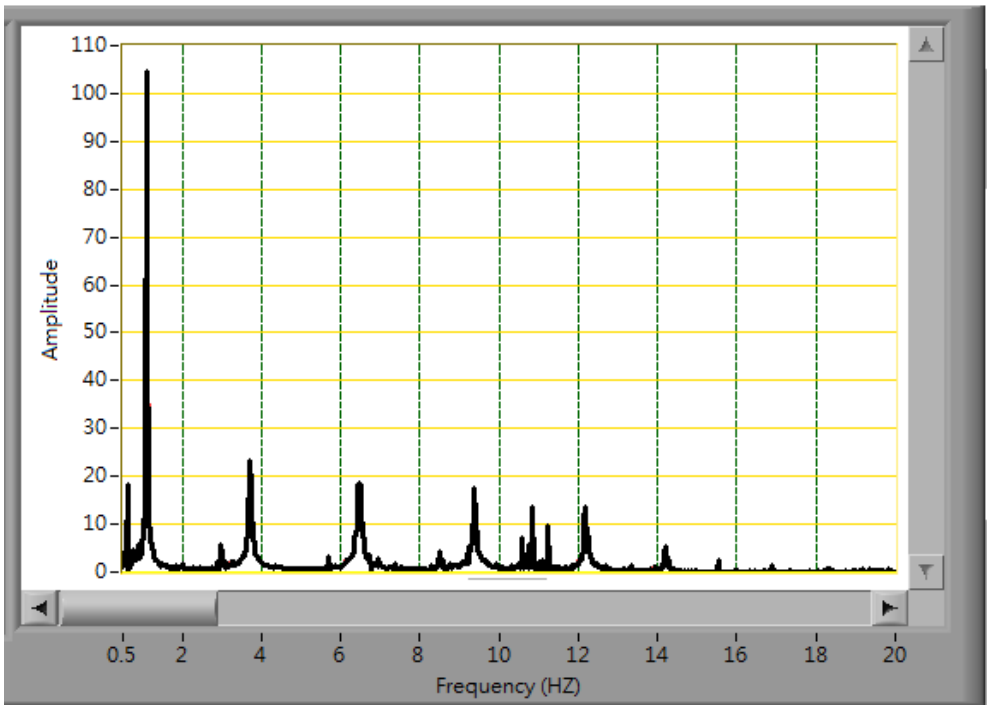

(f)

Figure 6.27. FRF of the structure: (a)1F, (b)2F, (c)3F, (d)4F, (e)5F, (d)6F

Table 6.2 Comparisons of modal parameters identified by wireless sensing nodes and conventional reference sensors.

	Frequency (Hz)			*Damping (%)*		
Mode	***Imote2***	***Conventional sensor***	***RMSE***	***Imote2***	***Conventional sensor***	***RMSE***
1	1.110	1.105	0.003	1.150	1.145	0.003
2	3.741	3.727	0.009	1.210	1.197	0.009
3	6.471	6.456	0.009	0.980	0.970	0.007
4	9.410	9.399	0.007	0.831	0.827	0.002
5	12.220	12.214	0.004	0.811	0.798	0.008
6	14.212	14.208	0.001	0.370	0.362	0.005

Figure 6.28 compares modal parameters identified using the Embedded FRF and ANN-based system identification (ANNSI) [46] approach with the measured raw data obtained by wireless sensing nodes. Comparisons demonstrate that the modal parameters identified by Embedded FRF approximate those identified by ANNSI. This comparison confirms that the proposed protocol is effective. Although the proposed protocol is reasonable for wireless-based SHM, a performance evaluation of embedded processing is essential. Table 6.3 shows the processing time of embedded FFT and FRF for different data lengths. Practically, the numbers of FFT data points was usually 1,024 or 2,048 points. The processing time for 1,024 points FFT and FRF are 0.193s and 0.064s respectively. The same code was also implemented in 200Mhz ARM processor-based .NET Micro Framework device. In this case, the processing time for 1,024 points FFT and FRF necessitate cost 0.8s and 0.25s. Obviously, the Imote2 with XScale processor and enhanced DSP core is sufficiently powerful for processing data in SHM.

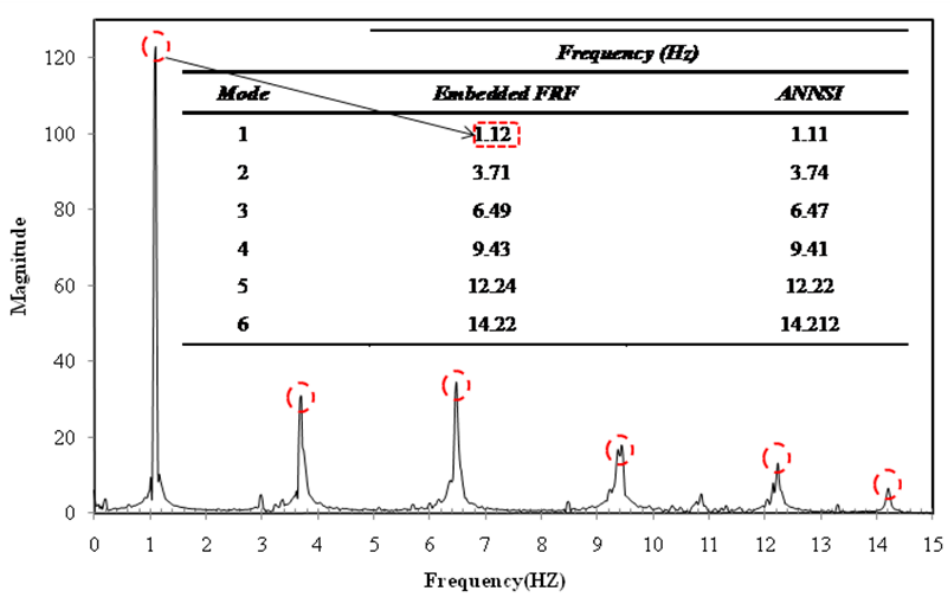

Figure 6.28 Comparisons of modal parameters identified by Embedded FRF and ANNSI.

Table 6.3 The processing time of embedded FFT and FRF for different data length.

	Data length			
	512	1024	2048	4096
FFT	0.089s	0. 193s	0. 442s	0.970s
FRF	0.032s	0.064s	0.130s	0.259s
Total	0.121s	0.256s	0.572s	1.229s

Numerically simulated responses demonstrate that the proposed *SubFRFDI* can be successfully used to identify the damage locations. The proposed *SubFRFDI* was further applied to identifying damage locations in the experimental frame. Figure 6.29 shows the *SubFRFDI* for damage scenarios 1–4. The highest *SubFRFDI* value indicates that the severest damage was located on the first floor in damage scenarios 1–3 (Figs. 6.29(a)– (c)). The *SubFRFDI* also indicates the damage location on the third floor in damage scenario 4 (Fig. 6.29(d)).

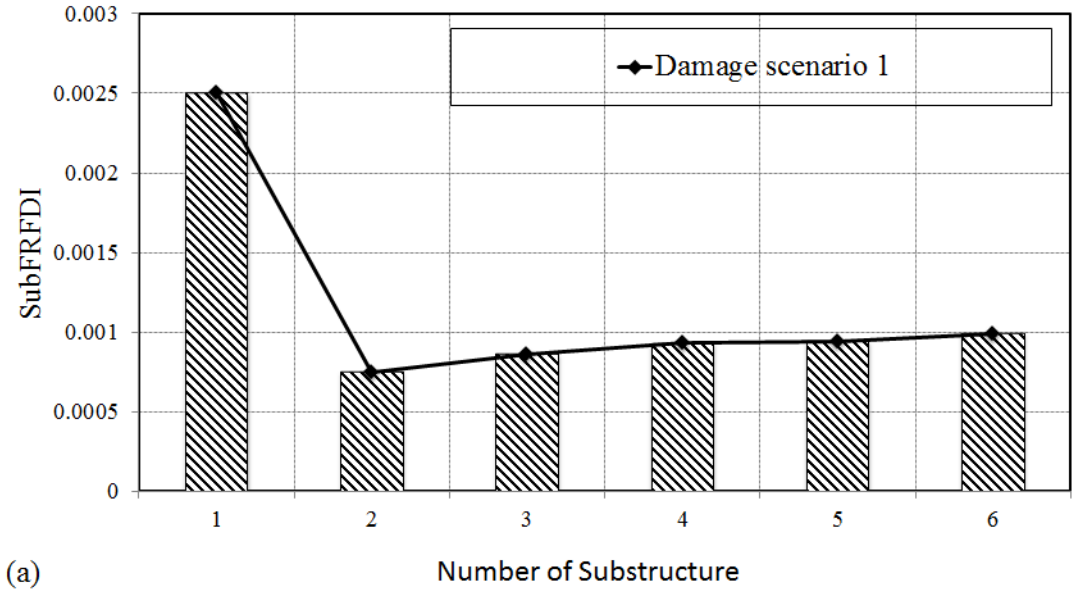
Damage scenario 1
SubFRFDI
0.003
0.0025
0.002
0.0015
0.001
0.0005
0
1
2
3
4
5
6
Number of Substructure

(a)

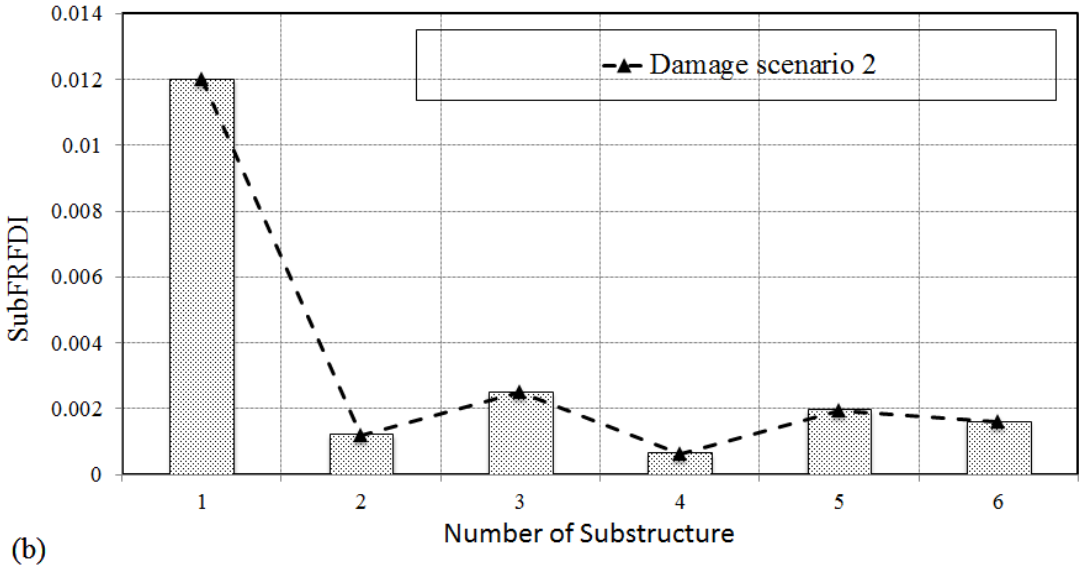
Damage scenario 2
SubFRFDI
0.014
0.012
0.01
0.008
0.006
0.004
0.002
0
1
2
3
4
5
6
Number of Substructure

(b)

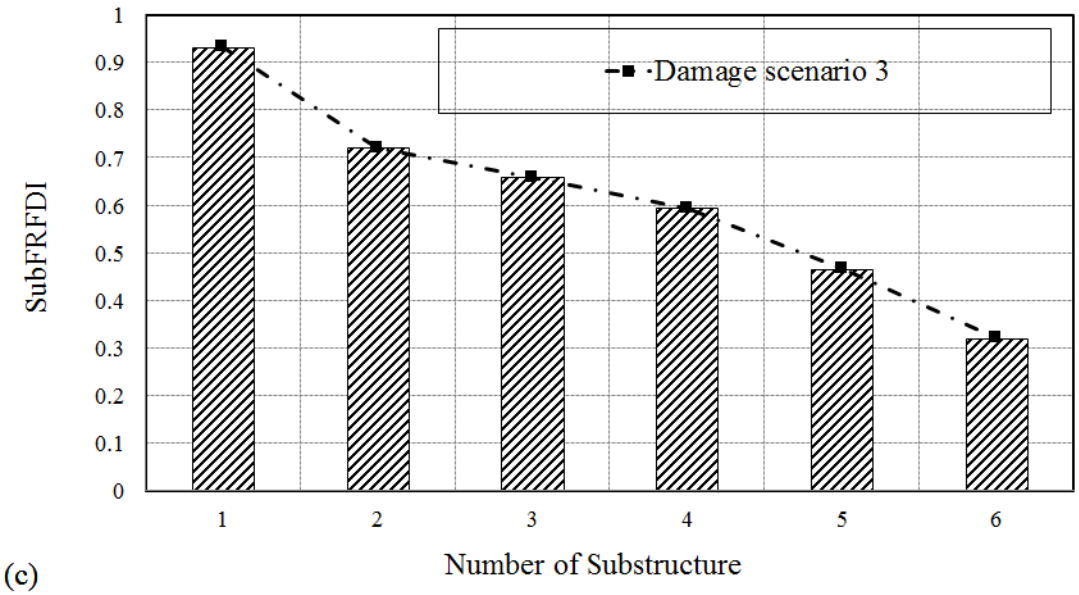

(c)

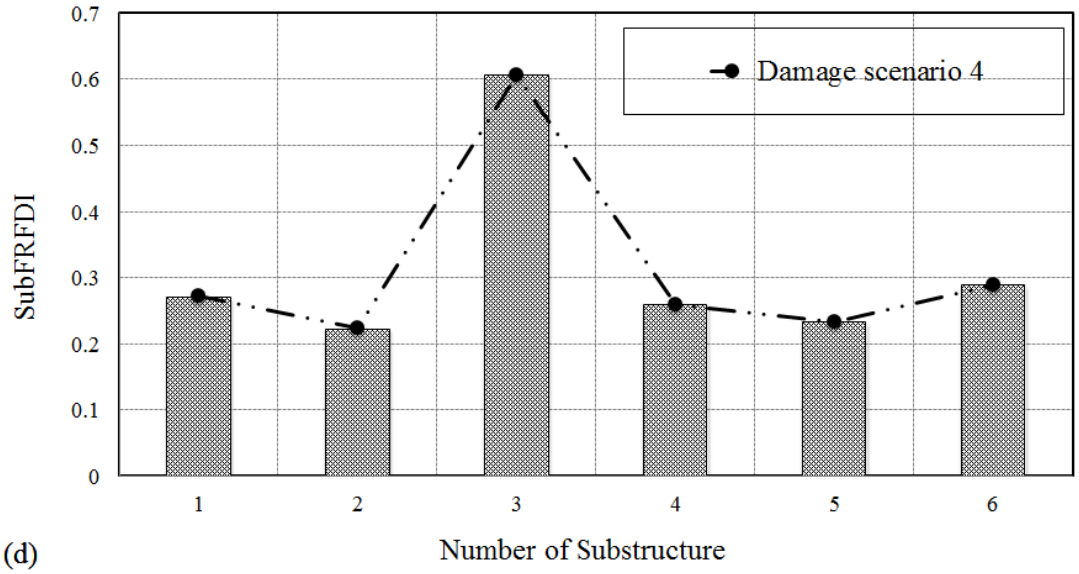

(d)

Figure 6.29 The *SubFRFDI* for damage scenarios 1–4.

Subsequently, the EMI based damage detection approach then check the component of building structure locally. Five PZT patches are respectively bonded to the the columns in 1st floor as shown in Figure 6.30. The damage metric chart based on RMSD is constructed to identify the local damage. As shown in Fig. 6.31-33, the highest value locates the damage of location 5 significantly. As can be seen in the Fig

6.34, with an increase in extent of damage, there is a corresponding increase in the damage metric values. Although the impedance method cannot exactly determine the exact extent of the damage, an increasing damage metric with increased severity of damage provides slightly quantitative information on the conditions of a structure.

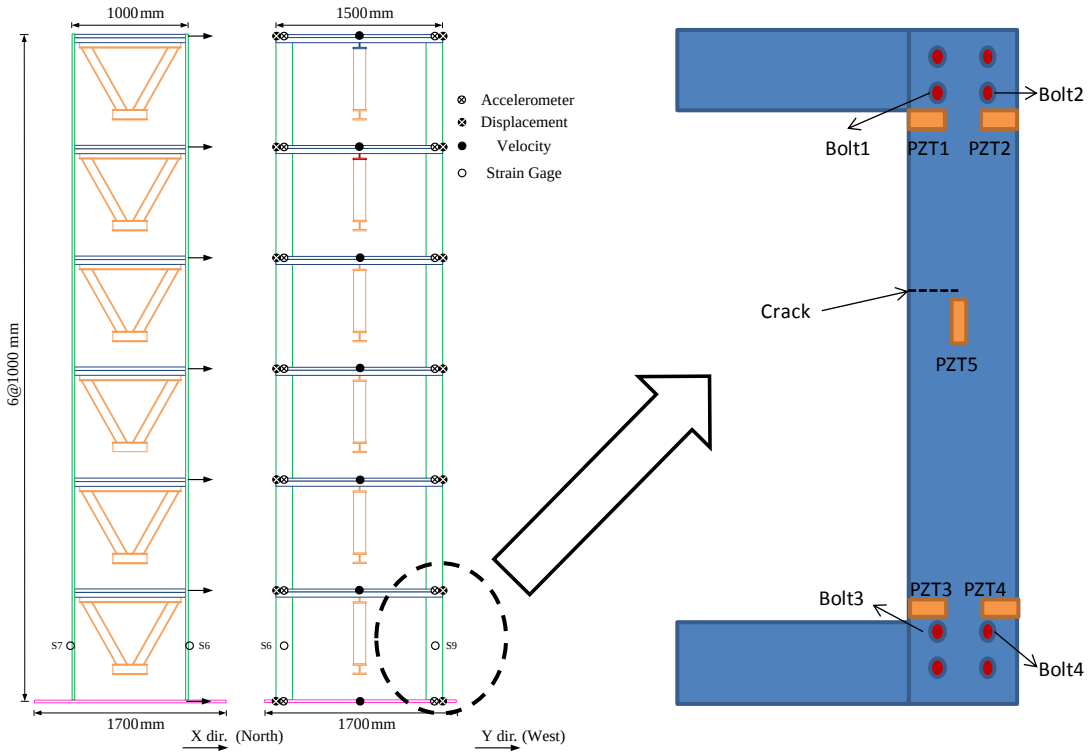

Figure 6.30 PZT setup on the test structure.

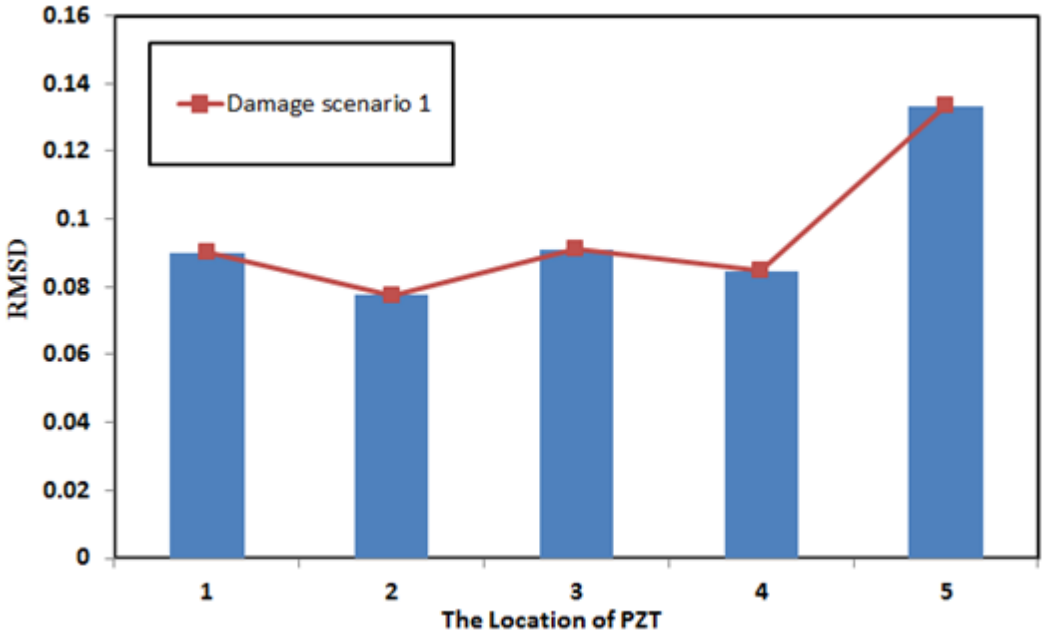

Figure 6.31 RMSD for damage scenario1

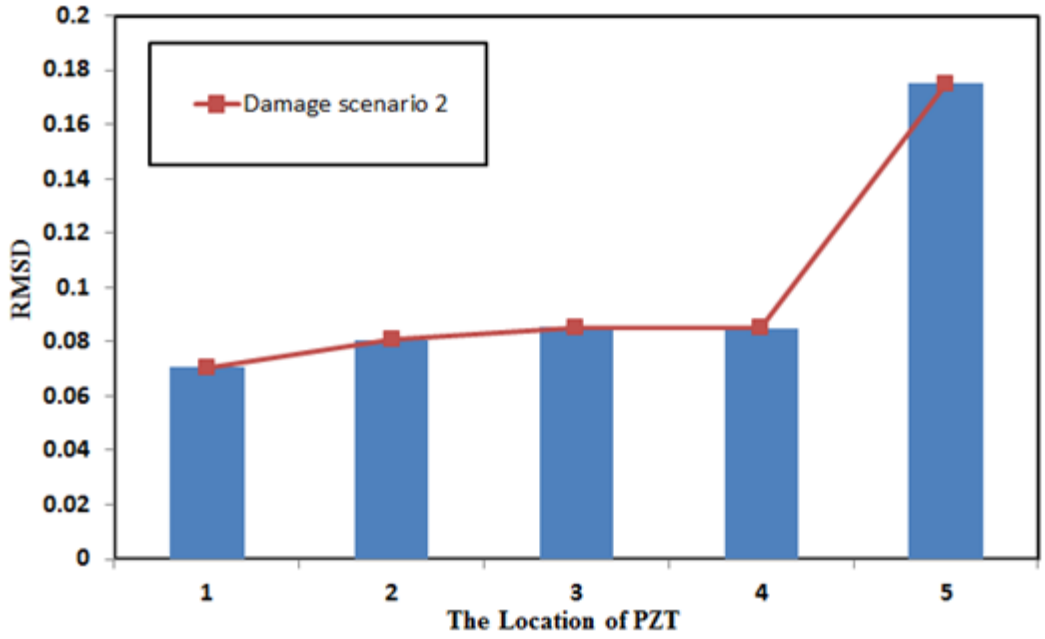

Figure 6.32 RMSD for damage scenario2

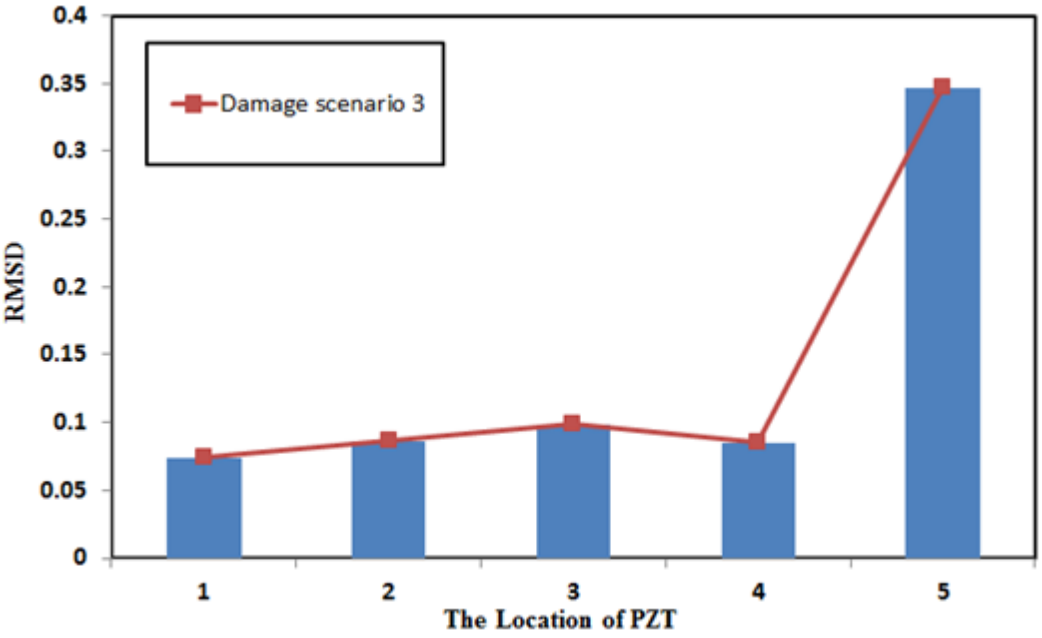

Figure 6.33 RMSD for damage scenario3

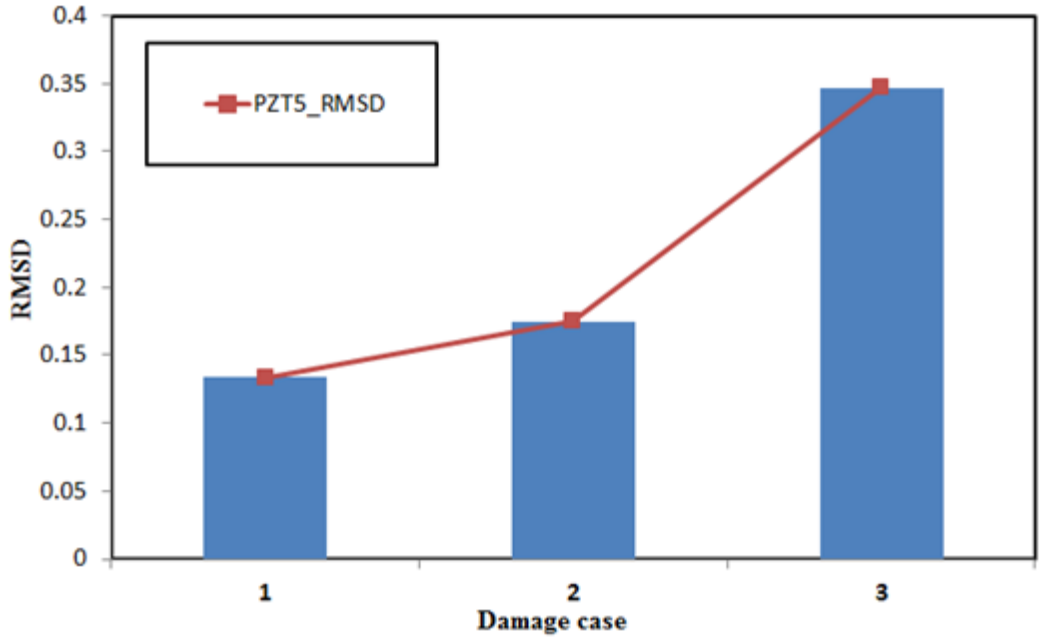

Figure 6.34 RMSD for three damage scenarios

CHAPHER 7 CONCLUSIONS REMARKS

7.1 Conclusion

A novel framework of an integrated wireless sensor network-based structural health monitoring system in buildings and civil infrastructures was developed in this study. The architecture of this SHM system was presented. A global-local-integrated damage detection approach was also developed for damage detection. Numerical and experimental studies were conducted to verify the applicability of the proposed approach. The following conclusions are drawn based on the integrated WSN-based SHM system, global-local-integrated damage detection approach and experimental results.

Integrated WSN-based SHM system

The Integrated WSN-based SHM system was developed in this study. This system architecture consists of sensing nodes, cluster head nodes, transfer node, and base station. Each sensing node is based on Imote2 platform which is comprised of a microprocessor, sensor module, and communication device. The cluster head is a dule core design which combine Imote2 platform and second embedded device. The cluster head has extra wireless module and GPS. The base station is the highest level end device that has largest memory, most powerful processor and highest communication capability.

A new sensor board was developed. This sensor board integrates a six degrees of freedom inertial measurement unit (6 DoF IMU) SD746 sensor chip and a GPS module. In this system, a novel windmill-magnet integrated piezoelectric (WMIP)

energy harvesting system was also developed.

The proposed software system of integrated WSN-based SHM system is a three-tier-framework, i.e., node, logging and processing tiers. The application functions are developed in a Microsoft NETMF environment. The NETMF and Crossbow's API, i.e., application interface provided by manufacturing company of Imote2, assist most libraries in dealing with all peripherals and drivers, allowing us to develop individual applications for the SHM efficiently. The proposed user interface shows how the sensor data can be represented in a Fig. chart and nodes distribution can also be conveniently observed.

WSN-based middleware services for SHM application are developed. The middleware services include reliable data-sensing and transmission, which are data aggregation, reliable communication, and synchronized sensing. These middleware services are implemented on the nodes running .NETMF and are generally applicable to SHM application.

Global-local-integrated damage detection approach

This study developed a global-local-integrated damage detection approach. In the first stage, the global approach detected changes in characteristics of the overall. After identifying the damage and its approximate location, the second stage used local detection method to identify the detailed conditions of the damage. Substructure-based frequency response function and wavelet energy distribution approaches are proposed for use in global damage detection. Local structural damage is detected using an EMI-based method. Numerical results confirm the effectiveness of the global-local-integrated damage detection approach for locating damage.

Experimental results

In experimental study, First off all, the integrated WSN-based SHM system is verified involving sensor calibration, wireless communication quality, data losing, interference in material, power consumption. The verification of sensing node indicates the good-quality data collection by the wireless sensing system and the modal parameters of structure can be correctly calculated by this system. In reliability of RF communication test indicates that the proposed system is robust and stable for long term monitoring via the proposed reliable data-sensing and transmission service.

This system was deployed in Nioudou Bridge. A field free vibration test was conducted for obtaining dynamic response. The good-quality data collection by the wireless sensing system successfully records a typical free vibration response of the pier. By comparing two FFTs for intact and scouring case, in frequency domain, the difference between intact and scouring case can be observed. The work indicates that the proposed wireless sensing system was a reliable technology for monitoring Bridge structure.

The proposed damage detection approach then was tested in a ¼ -scale six-storey steel structure. Experimental analysis using global SHM approach shows that, both *SubFRFDI* can indicates the approximate location of the damaged area, then the EMI-based damage detection approach can check the components of the building structure locally. The damage metric chart based on *RMSD* is constructed to identify the position of local damage to the structure.

7.2 Future Study

Following the unfinished works and the drawbacks of the proposed approaches, some potential directions on the future research are brought out.

In the proposed system, the main sensor on the sensing node is an accelerometer. However, the resolution of this accelerometer can works well on detection large vibration such as structural response excited by earthquake. For ambient vibration, new sensor board should be developed in the future work.

This study proposed a novel windmill-magnet integrated piezoelectric (WMIP) energy harvesting system. In the future work, the multiple energy harvesting methods such as solar, piezoelectric and wind should be integrated. The energy harvesting circuit needs to be included in the mote. Moreover, wireless power technology could be considered a feasible plan for WSN in SHM.

This works developed a structure of class libraries which is branch out into three basic class of NETMF, basic class library of Imote2, and SHM class. The SHM class, a specialized class, is developed by this study for SHM application. However, in this SHM class only FFT and FRF were included. In the future work, more embedded signal processing class like wavelet should be developed.

Substructure-based frequency response function approaches are proposed for use in global damage detection. However, these methods only focus on detecting and locating damage. Further study should be conducted in deciding the extent of damage in structure. EMI-based method was used to detect the local damage herein. In the future work, the EMI-based sensor node should be developed and the local damage index should be embedded in the node.

In experimental study, the developed integrated WSN-based SHM system was deployed in a steel structure and in a bridge. The experimental result indicates this system performs well either in Lab or in field test. In the future work, this system will be considered deploying in different civil structure. When deploying in a large scaled structure, the software and hardware of the system should be improved and modified. An optimization approach can also be applied for deploying great amount sensor nodes in the future works.

REFERENCE

1. **Adams, D.E.,** ***Health monitoring of structural materials and components.*** **Methods with Applications. Willey, New York, 2007.**

2. **Worden, K., Farrar, C.R., Haywood, J., and Todd, M.,** ***A review of nonlinear dynamics applications to structural health monitoring.*** **Structural Controal and Mealth Monitoring, 2008. 15(4): p. 540-567.**

3. **Sohn, H., Farrar, C.R., Hemez, F.M., Shunk, D.D., Stinemates, D.W., and Nadler, B.R.,** ***A review of structural health monitoring literature: 1996-2001*****. 2004, Los Alamos National Laboratory.**

4. **Doebling, S.W., Farrar, C.R., and Prime, M.B.,** ***A summary review of vibration-based damage identification methods.*** **Shock and Vibration Digest, 1998. 30(2): p. 91-105.**

5. **Sohn, H. and Laboratory, L.A.N.,** ***A review of structural health monitoring literature: 1996-2001*****. 2004: Los Alamos National Laboratory.**

6. **Inman, D.J.,** ***Damage prognosis for aerospace, civil and mechanical systems*****. 2005: John Wiley & Sons Inc.**

7. **Ansari, F.,** ***Sensing issues in civil structural health monitoring*****. 2005: Kluwer Academic Pub.**

8. **Chang, P., Flatau, A., and Liu, S.,** ***Review paper: health monitoring of civil infrastructure.*** **Structural Health Monitoring, 2003. 2(3): p. 257.**

9. **Farrar, C.,** ***Historical overview of structural health monitoring*****, in** ***Lecture notes on structural health monitoring using statistical pattern recognition*****. 2001, Los Alamos Dynamics, Los Alamos, NM.**

10. **Celebi, M.,** ***Seismic instrumentation of buildings (with emphasis on federal buildings)*****, in** ***Special GSA/USGS Project, an administrative report*****. 2002, United States Geological Survey: Menlo Park, CA.**

11. **Nagayama, T., Sim, S., Miyamori, Y., and Spencer Jr, B.,** ***Issues in structural health monitoring employing smart sensors.*** **Smart Structures and Systems, 2007. 3(3): p. 299-320.**

12. **Lynch, J.P. and Loh, K.J.,** ***A summary review of wireless sensors and sensor networks for structural health monitoring.*** **Shock and Vibration Digest, 2006.**

38(2): p. 91-130.

13. **Spencer Jr, B.F., Ruiz-Sandoval, M.E., and Kurata, N., *Smart sensing technology: opportunities and challenges.* Structural Control & Health Monitoring, 2004. 11(4): p. 349-368.**

14. **Chavali, M., Lin, T.H., Wu, R.J., Luk, H.N., and Hung, S.L., *Active 433 MHz-W UHF RF-powered chip integrated with a nanocomposite m-MWCNT/polypyrrole sensor for wireless monitoring of volatile anesthetic agent sevoflurane.* Sensors and Actuators a-Physical, 2008. 141(1): p. 109-119.**

15. **Xu, N., Rangwala, S., Chintalapudi, K., Ganesan, D., Broad, A., Govindan, R., and Estrin, D. *A wireless sensor network for structural monitoring*. Proceeding of 2nd international conference on Embedded networked sensor systems. 2004.**

16. **Yuan, S.F., Lai, X.S., Zhao, X., Xu, X., and Zhang, L., *Distributed structural health monitoring system based on smart wireless sensor and multi-agent technology.* Smart Materials & Structures, 2006. 15(1): p. 1-8.**

17. **Kurata, N., Spencer Jr, B., Ruiz-Sandoval, M., Miyamoto, Y., and Sako, Y., *A study on building risk monitoring using wireless sensor network MICA mote.* Strain, 2003. 1: p. 35.**

18. **Kim, S., Pakzad, S., Culler, D., Demmel, J., Fenves, G., Glaser, S., and Turon, M. *Health monitoring of civil infrastructures using wireless sensor networks*. Proceeding of 6th international conference on Information processing in sensor networks. 2007.**

19. **Doebling, S.W., Farrar, C.R., and Goodman, R.S. *Effects of measurement statistics on the detection of damage in the Alamosa Canyon Bridge*. Proceeding of Proceedings 15th International Modal Analysis Conference. 1997.**

20. **Farrar, C.R., Doebling, S.W., Cornwell, P.J., and Straser, E.G. *Variability of modal parameters measured on the Alamosa Canyon Bridge*. Proceeding of Proceedings 15th International Modal Analysis Conference. 1997.**

21. **Doebling, S.W., Farrar, C.R., Prime, M.B., and Shevitz, D.W., *Damage identification and health monitoring of structural and mechanical systems from changes in their vibration characteristics: a literature review*. 1996, Los Alamos National Lab., NM (United States).**

22. **Salawu, O., *Detection of structural damage through changes in frequency: a***

review. **Engineering Structures, 1997. 19(9): p. 718-723.**

23. **West, W.M.** ***Illustration of the use of modal assurance criterion to detect structural changes in an orbiter test specimen*****. Proceeding of Air Force Conference on Aircraft Structural Integrity. 1986.**

24. **Mayes, R.,** ***Error localization using mode shapes: An application to a two link robot arm*****, in** ***10th International Modal Analysis Conference*****. 1991, Sandia National Labs., Albuquerque, NM (United States): Albuquerque, NM.**

25. **Kam, T. and Lee, T.,** ***Detection of cracks in structures using modal test data.*** **Engineering fracture mechanics, 1992. 42(2): p. 381-387.**

26. **Ko, J., Wong, C., and Lam, H.** ***Damage detection in steel framed structures by vibration measurement approach*****. Proceeding of 12th International Modal Analysis Conference. 1994.**

27. **Farrar, C.R. and Doebling, S.W.** ***An overview of modal-based damage identification methods*****. Proceeding of DAMAS Conference. 1997.**

28. **Fox, C.** ***The location of defects in structures-A comparison of the use of natural frequency and mode shape data*****. Proceeding of the 10th International Modal Analysis Conference. 1992.**

29. **Pandey, A., Biswas, M., and Samman, M.,** ***Damage detection from changes in curvature mode shapes.*** **Journal of Sound and Vibration, 1991. 145(2): p. 321-332.**

30. **Topole, K.G. and Stubbs, N.,** ***Non destructive damage evaluation of a structure from limited modal parameters.*** **Earthquake Engineering & Structural Dynamics, 1995. 24(11): p. 1427-1436.**

31. **Chance, J., Tomlinson, G., and Worden, K.** ***A simplified approach to the numerical and experimental modelling of the dynamics of a cracked beam*****. Proceedings of the 12th International Modal Analysis Conference. 1994.**

32. **Chen, J.C. and Garbat, J.A.,** ***Analytical model improvement using modal test results.*** **Aiaa Journal, 1980. 18: p. 684-690.**

33. **SMITH, S.** ***Iterative use of direct matrix updates- Connectivity and convergence*****. Proceeding of 33rd AIAA Structures, Structural Dynamics and Materials Conference. 1992.**

34. **Liu, P.L.,** ***Identification and damage detection of trusses using modal data.***

Journal of Structural Engineering, 1995. 121(4): p. 599-608.

35. **KAOUK, M. and Zimmerman, D.C., *Structural damage assessment using a generalized minimum rank perturbation theory.* Aiaa Journal, 1994. 32(4): p. 836-842.**

36. **Hemez, F. and Farhat, C., *Structural damage detection via a finite element model updating methodology.* MODAL ANALYSIS-The International Journal of Analytical and Experimental Modal Analysis, 1995. 10(3): p. 152-166.**

37. **Norris, M.A. and Meirovitch, L., *On the problem of modelling for parameter identification in distributed structures.* International Journal for Numerical Methods in Engineering, 1989. 28(10): p. 2451-2463.**

38. **Haug, E. and Choi, K., *Structural design sensitivity analysis with generalized global stiffness and mass matrices.* Aiaa Journal, 1984. 22(9): p. 1299-1303.**

39. **Ricles, J. and Kosmatka, J., *Damage detection in elastic structures using vibratory residual forces and weighted sensitivity.* Aiaa Journal, 1992. 30(9): p. 2310-2316.**

40. **Lim, T.W. and Kashangaki, T.A.L., *Structural damage detection of space truss structures using best achievable eigenvectors.* Aiaa Journal, 1994. 32: p. 1049-1057.**

41. **Zimmerman, D.C. and MOHAMED, K., *Eigenstructure assignment approach for structural damage detection.* Aiaa Journal, 1992. 30(7): p. 1848-1855.**

42. **Sohn, H., Farrar, C.R., Hunter, N.F., and Worden, K., *Structural Health Monitoring Using Statistical Pattern Recognition Techniques.* Journal of Dynamic Systems, Measurement, and Control, 2001. 123(4): p. 706-711.**

43. **Lei, Y., Kiremidjian, A., Nair, K., Lynch, J., Law, K., Kenny, T., Carryer, E., and Kottapalli, A. *Statistical damage detection using time series analysis on a structural health monitoring benchmark problem*. Proceeding of 9th International Conference on Applications of Statistics and Probability in Civil Engineering. 2003.**

44. **Chen, H., Qi, G., Yang, J., and Amini, F., *Neural network for structural dynamic model identification.* Journal of engineering mechanics, 1995. 121: p. 1377.**

45. **Wu, X., Ghaboussi, J., and Garrett, J., *Use of neural networks in detection of structural damage.* Computers & Structures, 1992. 42(4): p. 649-659.**

46. **Wen, C.M., Hung, S.L., Huang, C.S., and Jan, J.C., *Unsupervised fuzzy neural networks for damage detection of structures.* Structural Controal and Mealth Monitoring, 2007. 14(1): p. 144-161.**

47. **Kudva, J., Munir, N., and Tan, P., *Damage detection in smart structures using neural networks and finite-element analyses.* Smart Materials and Structures, 1992. 1: p. 108.**

48. **Poudel, U., Fu, G., and Ye, J., *Structural damage detection using digital video imaging technique and wavelet transformation.* Journal of Sound and Vibration, 2005. 286(4-5): p. 869-895.**

49. **Kim, H. and Melhem, H., *Damage detection of structures by wavelet analysis.* Engineering Structures, 2004. 26(3): p. 347-362.**

50. **Ovanesova, A.V. and Suárez, L.E., *Applications of wavelet transforms to damage detection in frame structures.* Engineering Structures, 2004. 26(1): p. 39-49.**

51. **Huang, C.S. and Su, W.C., *Identification of modal parameters of a time invariant linear system by continuous wavelet transformation.* Mechanical Systems and Signal Processing, 2007. 21(4): p. 1642-1664.**

52. **Huang, C.S., Hung, S.L., Lin, C.I., and Su, W.C., *A wavelet-based approach to identifying structural modal parameters from seismic response and free vibration data.* Computer-Aided Civil and Infrastructure Engineering, 2005. 20(6): p. 408-423.**

53. **Wu, N. and Wang, Q., *Experimental studies on damage detection of beam structures with wavelet transform.* International Journal of Engineering Science, 2011. 49(3): p. 253-261.**

54. **Han, J.-G., Ren, W.-X., and Sun, Z.-S., *Wavelet packet based damage identification of beam structures.* International Journal of Solids and Structures, 2005. 42(26): p. 6610-6627.**

55. **Poornachandra, S., *Wavelet-based denoising using subband dependent threshold for ECG signals.* Digital Signal Processing, 2008. 18(1): p. 49-55.**

56. **Pasti, L., Walczak, B., Massart, D.L., and Reschiglian, P., *Optimization of signal denoising in discrete wavelet transform.* Chemometrics and Intelligent Laboratory Systems, 1999. 48(1): p. 21-34.**

57. **Lee, B. and Tarng, Y., *Drill fracture detection by the discrete wavelet transform.***

Journal of Materials Processing Technology, 2000. 99(1-3): p. 250-254.

58. **Prabhakar, S., Mohanty, A., and Sekhar, A., *Application of discrete wavelet transform for detection of ball bearing race faults.* Tribology International, 2002. 35(12): p. 793-800.**

59. **Sansalone, M., Carino, N.J., and Division, C.f.B.T.S., *Impact-echo: a method for flaw detection in concrete using transient stress waves*. 1986: US Dept. of Commerce, National Bureau of Standards, Center for Building Technology, Structures Division.**

60. **Davis, A.G., Evans, J.G., and Hertlein, B.H., *Nondestructive evaluation of concrete radioactive waste tanks.* Journal of performance of constructed facilities, 1997. 11: p. 161.**

61. **Chady, T., Enokizono, M., and Sikora, R., *Crack detection and recognition using an eddy current differential probe.* Magnetics, IEEE Transactions on, 1999. 35(3): p. 1849-1852.**

62. **Tian, G.Y., Sophian, A., Taylor, D., and Rudlin, J., *Multiple sensors on pulsed eddy-current detection for 3-D subsurface crack assessment.* Sensors Journal, IEEE, 2005. 5(1): p. 90-96.**

63. **Washer, G.A. *Detection of fatigue cracks in eyebars using time of flight diffraction*. Proceeding of Conf. on StructuralMaterials Technology and Nondestructive Testing. 1996.**

64. **Liang, C., Sun, F., and Rogers, C., *Coupled Electro-Mechanical Analysis of Adaptive Material Systems--Determination of the Actuator Power Consumption and System Energy Transfer.* Journal of Intelligent Material Systems and Structures, 1994. 5(1): p. 12.**

65. **Sun, F., Rogers, C.A., and Liang, C. *Structural frequency response function acquisition via electric impedance measurement of surface-bonded piezoelectric sensor/actuator*. Proceeding of Structures, Structural Dynamics, and Materials Conference. 1995.**

66. **Chaudhry, Z., Lalande, F., Ganino, A., and Rogers, C. *Monitoring the integrity of composite patch structural repair via piezoelectric actuators/sensors*. Proceeding of 36th AIAA/ASME/ASCE/AHS/ASC Structures, Structural Dynamics, and Materials Conference. 1995.**

67. **Park, G., Kabeya, K., Cudney, H.H., and Inman, D.J., *Impedance-based***

structural health monitoring for temperature varying applications. **JSME international journal. Series A, Solid mechanics and material engineering, 1999. 42(2): p. 249-258.**

68. **Park, G., Cudney, H.H., and Inman, D.J., *Impedance-based health monitoring of civil structural components.* Journal of Infrastructure Systems, 2000. 6(4): p. 153-160.**

69. **Yang, Y., Hu, Y., and Lu, Y., *Sensitivity of PZT impedance sensors for damage detection of concrete structures.* Sensors, 2008. 8(1): p. 327-346.**

70. **Kim, J., *Vibration and impedance monitoring for prestress-loss prediction in PSC girder bridges.* Smart Structures and Systems, 2009. 5(1): p. 81-94.**

71. **Park, G., Sohn, H., Farrar, C.R., and Inman, D.J., *Overview of piezoelectric impedance-based health monitoring and path forward.* Shock and Vibration Digest, 2003. 35(6): p. 451-464.**

72. **Mascarenas, D., Flynn, E., Todd, M., Park, G., and Farrar, C., *Wireless Sensor Technologies for Monitoring Civil Structures.* Sound and Vibration, 2008. 42(4): p. 16.**

73. **Kim, S., Pakzad, S., Culler, D., Demmel, J., Fenves, G., Glaser, S., and Turon, M. *Health monitoring of civil infrastructures using wireless sensor networks*. Proceeding of 6th international conference on Information processing in sensor networks 2007.**

74. **Cho, S., Jang, S.A., Jo, H., Mechitov, K., Rice, J.A., Jung, H.J., Yun, C.B., Spencer Jr, B.F., Nagayama, T., and Seo, J. *Structural health monitoring system of a cable-stayed bridge using a dense array of scalable smart sensor network*. Proceeding of Sensors and Smart Structures Technologies for Civil, Mechanical, and Aerospace Systems. 2010.**

75. **Hoult, N.A., Fidler, P.R.A., Hill, P.G., and Middleton, C.R., *Long-term wireless structural health monitoring of the Ferriby Road Bridge.* Journal of Bridge Engineering, 2010. 15: p. 153.**

76. **Kim, J., Lynch, J.P., Lee, J.J., and Lee, C.G., *Truck-based mobile wireless sensor networks for the experimental observation of vehicle¡Vbridge interaction.* Smart Materials and Structures, 2011. 20: p. 065009.**

77. **Castillo-Effer, M., Quintela, D.H., Moreno, W., Jordan, R., and Westhoff, W. *Wireless sensor networks for flash-flood alerting*. Proceeding of the Fifth IEEE**

International Caracas Conference on Devices. 2004.

78. **Simon, G., Maroti, M., Ledeczi, A., Balogh, G., Kusy, B., Nadas, A., Pap, G., Sallai, J., and Frampton, K. *Sensor network-based countersniper system*. Proceeding of the 2nd international conference on Embedded networked sensor systems 2004.**

79. **Werner-Allen, G., Lorincz, K., Welsh, M., Marcillo, O., Johnson, J., Ruiz, M., and Lees, J., *Deploying a wireless sensor network on an active volcano.* Ieee Internet Computing, 2006: p. 18-25.**

80. **Akyildiz, I.F., Su, W., Sankarasubramaniam, Y., and Cayirci, E., *Wireless sensor networks: a survey.* Computer Networks-the International Journal of Computer and Telecommunications Networking, 2002. 38(4): p. 393-422.**

81. **Yick, J., Mukherjee, B., and Ghosal, D., *Wireless sensor network survey.* Computer Networks, 2008. 52(12): p. 2292-2330.**

82. **Younis, M. and Akkaya, K., *Strategies and techniques for node placement in wireless sensor networks: A survey.* Ad Hoc Networks, 2008. 6(4): p. 621-655.**

83. **Nagayama, T., Spencer Jr, B.F., Mechitov, K.A., and Agha, G.A., *Middleware services for structural health monitoring using smart sensors.* Smart Structures and Systems, 2009. 5(2): p. 119-137.**

84. **Lynch, J.P., *An overview of wireless structural health monitoring for civil structures.* Philosophical Transactions of the Royal Society a-Mathematical Physical and Engineering Sciences, 2007. 365(1851): p. 345-372.**

85. **Cho, S., Yun, C.B., Lynch, J.P., Zimmerman, A.T., Spencer, B.F., and Nagayama, T., *Smart Wireless Sensor Technology for Structural Health Monitoring of Civil Structures.* International Journal of Steel Structures, 2008. 8(4): p. 267-275.**

86. **Paek, J., Chintalapudi, K., Govindan, R., Caffrey, J., and Masri, S. *A wireless sensor network for structural health monitoring: Performance and experience*. Proceeding of The Second IEEE Workshop on Embedded Networked Sensors (EmNetS-II). 2005.**

87. **Straser, E.G., Kiremidjian, A.S., and Center, J.A.B.E.E., *A modular, wireless damage monitoring system for structures*. 1998: The John A. Blume Earthquake Engineering Center.**

88. **Lynch, J.P., Law, K.H., Kiremidjian, A.S., Kenny, T.W., Carryer, E., and**

Partridge, A. ***The design of a wireless sensing unit for structural health monitoring*****. Proceeding of 3rd Int'l Ws. Structural Health Monitoring. 2001.**

89. Wang, Y., Lynch, J.P., and Law, K.H., ***Validation of an integrated network system for real-time wireless monitoring of civil structures.*** **Structural health monitoring, 2005: advancements and challenges for implementation, 2005. 1050(48109): p. 275.**

90. Aoki, S., Fujino, Y., and Abe, M. ***Intelligent bridge maintenance system using MEMS and network technology*****. Proceeding of SPIE Conf. 2003.**

91. Chung, H.C., Enomoto, T., Shinozuka, M., Chou, P., Park, C., Yokoi, I., and Morishita, S. ***Real-time visualization of structural response with wireless MEMS sensors*****. Proceeding of 13th world conf. Earthquake Engineering. 2004.**

92. Farrar, C.R., Allen, D.W., Park, G., Ball, S., and Masquelier, M.P., ***Coupling sensing hardware with data interrogation software for structural health monitoring.*** **Shock and Vibration, 2006. 13(4): p. 519-530.**

93. Chen, B. and Liu, W., ***Mobile agent computing paradigm for building a flexible structural health monitoring sensor network.*** **Computer Aided Civil and Infrastructure Engineering, 2010. 25(7): p. 504-516.**

94. Xu, N., Rangwala, S., Chintalapudi, K.K., Ganesan, D., Broad, A., Govindan, R., and Estrin, D., ***A wireless sensor network For structural monitoring.*** **Proceedings of the 2nd international conference on Embedded networked sensor systems, 2004: p. 13-24.**

95. ShenfangYuan, X.L., Zhao, X., Xu, X., and Zhang, L., ***Distributed structural health monitoring system based on smart wireless sensor and multi-agent technology.*** **Smart Mater. Struct, 2006. 15: p. 1-8.**

96. Kurata, N., Spencer Jr, B.F., Ruiz-Sandoval, M., Miyamoto, Y., and Sako, Y., ***A study on building risk monitoring using wireless sensor network MICA mote.*** **Strain. 1: p. 35.**

97. Hoblos, G., Staroswiecki, M., and Aitouche, A. ***Optimal design of fault tolerant sensor networks*****. Proceeding of IEEE International Conference on Control Applications. 2000.**

98. Cho, S.H. and Chandrakasan, A.P. ***Energy efficient protocols for low duty cycle wireless microsensor networks*****. Proceeding of 33rd Annual Hawaii**

International Conference on System Sciences. 2001.

99. Rabaey, J.M., Ammer, M.J., da Silva Jr, J.L., Patel, D., and Roundy, S., *PicoRadio supports ad hoc ultra-low power wireless networking.* Computer, 2000. 33(7): p. 42-48.

100. Intanagonwiwat, C., Govindan, R., and Estrin, D. *Directed diffusion: A scalable and robust communication paradigm for sensor networks*. Proceeding of ACM Mobi-Com'00. 2000.

101. Kahn, J.M., Katz, R.H., and Pister, K.S.J. *Next century challenges: mobile networking for smart dust*. Proceeding of ACM MobiCom'99. 1999.

102. Alliance, Z.B., *ZigBee Specifications Version 1.0., San Ramon, CA, USA, December. 2004*. 2004.

103. Gutierrez, J.A., Naeve, M., Callaway, E., Bourgeois, M., Mitter, V., and Heile, B., *IEEE 802.15. 4: a developing standard for low-power low-cost wireless personal area networks.* Network, IEEE, 2001. 15(5): p. 12-19.

104. Woo, A., Madden, S., and Govindan, R., *Networking support for query processing in sensor networks.* Communications of the Acm, 2004. 47(6): p. 47-52.

105. Kopetz, H., Damm, A., Koza, C., Mulazzani, M., Schwabl, W., Senft, C., and Zainlinger, R., *Distributed fault-tolerant real-time systems: The Mars approach.* Micro, IEEE, 1989. 9(1): p. 25-40.

106. Horauer, M., Schossmaier, K., Schmid, U., Holler, R., Kero, N., and ., V.U.O.T. *PSynUTC-Evaluation of a High-Precision Time Synchronization Prototype System for Ethernet LANs*. Proceeding of 34th Annual Precise Time and Time Interval Meeting (PTTI). 2002.

107. Mills, D.L., *Internet time synchronization: The network time protocol.* Communications, IEEE Transactions on, 1991. 39(10): p. 1482-1493.

108. Syed, A. and Heidemann, J. *Time synchronization for high latency acoustic networks*. Proceeding of IEEE Infocom. 2006.

109. Nagayama, T., Spencer, B.F., and Rice, J.A., *Autonomous decentralized structural health monitoring using smart sensors.* Structural Control & Health Monitoring, 2009. 16(7-8): p. 842-859.

110. Lanzara, G., Feng, J., and Chang, F.K., *Design of micro-scale highly*

expandable networks of polymer-based substrates for macro-scale applications. **Smart Materials & Structures, 2010. 19(4): p. 045013.**

111. Gratzel, M., ***Solar energy conversion by dye-sensitized photovoltaic cells.*** **Inorg. Chem, 2005. 44(20): p. 6841-6851.**

112. Sodano, H., Simmers, G., Dereux, R., and Inman, D., ***Recharging batteries using energy harvested from thermal gradients.*** **Journal of Intelligent Material Systems and Structures, 2007. 18(1): p. 3.**

113. Beeby, S., Tudor, M., and White, N., ***Energy harvesting vibration sources for microsystems applications.*** **Measurement Science and Technology, 2006. 17: p. R175.**

114. Ottman, G., Hofmann, H., Bhatt, A., and Lesieutre, G., ***Adaptive piezoelectric energy harvesting circuit for wireless remote power supply.*** **IEEE Transactions on Power Electronics, 2002. 17(5): p. 669-676.**

115. Ganeriwal, S., Kumar, R., and Srivastava, M. ***Timing-sync protocol for sensor networks.*** **Proceeding of 1st international conference on Embedded networked sensor systems. 2003.**

116. Cauberghe, B., Guillaume, P., Verboven, P., Vanlanduit, S., and Parloo, E., ***Frequency response function-based parameter identification from short data sequences.*** **Mechanical Systems and Signal Processing, 2004. 18(5): p. 1097-1116.**

117. Celic, D. and Boltezar, M., ***Identification of the dynamic properties of joints using frequency-response functions.*** **Journal of Sound and Vibration, 2008. 317(1-2): p. 158-174.**

118. Wang, Z., Lin, R.M., and Lim, M.K., ***Structural damage detection using measured FRF data.*** **Computer Methods in Applied Mechanics and Engineering, 1997. 147(1-2): p. 187-197.**

119. Lee, U. and Shin, J., ***A frequency-domain method of structural damage identification formulated from the dynamic stiffness equation of motion.*** **Journal of Sound and Vibration, 2002. 257(4): p. 615-634.**

120. Thyagarajan, S.K., Schulz, M.J., Pai, P.F., and Chung, J., ***Detecting structural damage using frequency response functions.*** **Journal of Sound and Vibration, 1998. 210(1): p. 162-170.**

121. Lee, U. and Shin, J., ***A frequency response function-based structural damage***

identification method. **Computers and Structures, 2002. 80(2): p. 117-132.**

122. Sampaio, R.P.C., Maia, N.M.M., and Silva, J.M.M., *Damage detection using the frequency-response-function curvature method.* Journal of Sound and Vibration, 1999. 226(5): p. 1029-1042.

123. Maia, N.M.M., Silva, J.M.M., Almas, E.A.M., and Sampaio, R.P.C., *Damage detection in structures: from mode shape to frequency response function methods.* Mechanical Systems and Signal Processing, 2003. 17(3): p. 489-498.

124. Liu, X., Lieven, N.A.J., and Escamilla-Ambrosio, P.J., *Frequency response function shape-based methods for structural damage localisation.* Mechanical Systems and Signal Processing, 2009. 23(4): p. 1243-1259.

125. Ni, Y.Q., Zhou, X.T., and Ko, J.M., *Experimental investigation of seismic damage identification using PCA-compressed frequency response functions and neural networks.* Journal of Sound and Vibration, 2006. 290(1-2): p. 242-263.

126. Furukawa, A., Otsuka, H., and Kiyono, J., *Structural damage detection method using uncertain frequency response functions.* Computer-Aided Civil and Infrastructure Engineering, 2006. 21(4): p. 292-305.

127. Kanwar, V.S., Kwatra, N., Aggarwal, P., and Gambir, M.L., *Health monitoring of RCC building model experimentally and its analytical validation.* Engineering Computations, 2008. 25(7-8): p. 677-693.

128. Hsu, T. and Loh, C. *Damage detection using frequency response functions under ground excitation*. Proceeding of Sensors and Smart Structures Technologies for Civil, Mechanical, and Aerospace Systems. 2009.

129. Park, G. and Inman, D., *Structural health monitoring using piezoelectric impedance measurements.* Philosophical Transactions of the Royal Society A: Mathematical, Physical and Engineering Sciences, 2007. 365(1851): p. 373.

130. Liang, C., Sun, F., and Rogers, C., *Coupled electro-mechanical analysis of adaptive material systems¡Xdetermination of the actuator power consumption and system energy transfer.* Journal of Intelligent Material Systems and Structures, 1994. 5(1): p. 12.

131. Sun, F., Chaudhry, Z., Liang, C., and Rogers, C., *Truss structure integrity identification using PZT sensor-actuator.* Journal of Intelligent Material Systems and Structures, 1995. 6(1): p. 134-139.

132. Peairs, D.M., Park, G., and Inman, D.J., *Improving accessibility of the*

impedance-based structural health monitoring method. **Journal of Intelligent Material Systems and Structures, 2004. 15(2): p. 129.**

133. Nokes, J. and Cloud, G., ***The application of interferometric techniques to the nondestructive inspection of fiber-reinforced materials.*** **Experimental Mechanics, 1993. 33(4): p. 314-319.**

134. Esteban, J., ***Modeling of the sensing region of a piezoelectric actuator/sensor*****. 1996, Ph. D. Dissertation, Virginia Polytechnic Institute and State University, Blacksburg, VA.**

135. Forde, M., McCann, D., Clark, M., Broughton, K., Fenning, P., and Brown, A., ***Radar measurement of bridge scour.*** **Ndt & E International, 1999. 32(8): p. 481-492.**

136. Yankielun, N. and Zabilansky, L., ***Laboratory investigation of time-domain reflectometry system for monitoring bridge scour.*** **Journal of Hydraulic engineering, 1999. 125(12): p. 1279-1284.**

137. Lin, Y., Chen, J., Chang, K., Chern, J., and Lai, J., ***Real-time monitoring of local scour by using fiber Bragg grating sensors.*** **Smart Materials and Structures, 2005. 14: p. 664.**

138. DeVault, J., ***Robotic system for underwater inspection of bridge piers.*** **Instrumentation & Measurement Magazine, IEEE, 2002. 3(3): p. 32-37.**

139. Huang, C.S., Hung, S.L., Wen, C.M., and Tu, T.T., ***A neural network approach for structural identification and diagnosis of a building from seismic response data.*** **Earthquake Engineering & Structural Dynamics, 2003. 32(2): p. 187-206.**

Vita

林子軒 (Tzu-Hsuan Lin)

個人資料

生日：1978/06/05
性別：男性
住址：新竹市東大路二段172巷1弄7號1樓
電話：03-5712121#54965, 0963354403
Email: cornetlin@gmail.com
兵役：役畢

現職

國立交通大學土木工程系博士候選人(指導教授:洪士林教授)

國立交通大學電機與控制工程研究所碩士班(指導教授:廖德誠教授)

學歷

2009.7~2009.9	**東京大學**訪問學生(Host: Professor Yozo Fujino)
2005.9 ~Now	國立交通大學土木工程研究所博士班結構組
2007.6~ Now	**雙主修**國立交通大學電機與控制工程研究所碩士班
2001.9 ~ 2003.6	國立交通大學土木工程研究所碩士
2001.9 ~ 2003.6	國立交通大學資訊管理研究所輔所
1997.9 ~ 2001.6	國立台北科技大學土木系**(第一名畢業)**

榮譽

2009.7~9	**日本交流協會**暑期交換學生獎學金(兩個月共，72 萬日幣)赴東京大學研究，**並獲選為得獎代表**，上台致謝。(全國 18 名，唯一的土木領域)
2010	中華顧問工程司，工程科技獎學金，博士班獎學金 10 萬元。
2007~2009	中興工程研究發展基金會博士班獎助學金 (**土木領域全國最高獎學金**，每年 30 萬元)，連續三年獲獎
2006	中興工程顧問社優秀學生獎

研究成果目錄：論文及著述

A. 學位論文

林子軒，”土木工程結構修復補強知識管理與支援決策輔助系統之研究”碩士論文，國立交通大學土木工程系，2003。

B. 期刊論文

[1] **T. H. Lin**, S. L. Hung, Y. C. Lu, T. Nagayama and Y. Fujino (2011), Development of An Embedded Damage Detection Approach Using Imote2.net-Based Wireless Structural Health Monitoring, *Structural health monitoring-an international journal*. (Reviewing)

[2] **T. H. Lin**, S. L. Hung, C. S. Huang, and T. K. Lin (2012), Detection of damage location using a novel substructure-based frequency response function approach with a wireless sensing system, *International Journal of Structural Stability and Dynamics*, has been accepted for publication in Vol. 12, No. 3 (June 2012) ***IF:0.721***

[3] **T. H. Lin**, S. L. Hung, M. Chavali, R. J. Wu, H. N. Luk and Q. Fei (2010), Towards Development of Wireless Sensor System For Monitoring Anesthetic Agents, *Sensor Letters*. 8, 767-776. ***IF:0.626***

[4] R. J. Wu, Y. C. Huang, M. R. Yu, **T. H. Lin**, S. L. Hung (2008), Application of m-CNTs/NaClO4/Ppy to A Fast Response, Room Working Temperature Ethanol Sensor”. *Sensors and Actuators B: Chemical*, 134(1), 213-218. ***IF:3.083***

[5] Murthy Chavali , **T. H. Lin**, R.J. Wu, H.N. Luk and S.L. Hung (2008), “Active 433 MHz-W UHF RF powered chip integrated with a nano composite *m*-MWCNT/Polypyrrole sensor for wireless monitoring of anesthetic agent Sevoflurane”, *Sensors & Actuators: A. Physical*, 141(1), 109-119 ***IF:1.674***

[6] R.J. Wu, Y.C. Huang, M. Chavali, **T.H. Lin**, S.L. Hung and H.N. Liud (2007), “New sensing technology for detection of the common inhalational anesthetic agent sevoflurane using conducting polypyrrole films”, *Sensors & Actuators: B. Chemical* 126 (2), 387-393. ***IF:3.083***

[7] 吳仁彰， 余明儒， **林子軒**， 洪士林 (2008/12/1)。CuO-ZnO 材料於半導體型快速酒精感測之研究。 科儀新知，第 30 卷，第 3 期，第 167 輯，頁 48 -55 。

[8] 吳仁彰， 黃裕清， **林子軒**， 龍彥先， 吳登峻， 梁元豪 (2008/5/1)。CNT/NaClO4/Ppy 材料於快速酒精感測之研究。 量測資訊，第 121 期，頁 58-63。

[9] **林子軒**、洪士林、吳仁彰、黃裕清、陸翔寧、柴梅熙，「無線感測網路應用

於醫院建築環境之監測」，科儀新知，第 28 卷，第 2 期，76－84 頁，民國 95 年 10 月。

[10] 吳仁彰, 黃裕清, 陸翔寧, **林子軒**, 洪士林, 柴梅熙，「麻醉氣體七氟烷的量測技術研究」，科儀新知，第 27 卷，第 6 期，87－93 頁(2006)。

[11] 李有豐、刁健原、**林子軒**，「碳纖維強化高分子複合材料(CFRP)補強建築物 RC 構件簡易查圖法」，結構工程，第十七卷，第一期，第 43-60 頁(2002)。

C.研討會論文

[1] **T. H. Lin,** Y. C. Lu and S. L. Hung, Field Study of Bridge Scour Using Imote2.NET−Based Wireless Monitoring System, 6th International Workshop on Advanced Smart Materials and Smart Structures Technology, Dalian, China, July 25-26, 2011.(Accepted)

[2] C. S. Hsieh, D. C. Liaw and **T. H. Lin**, Optimal Filtering Method to Structural Damage Estimation Under Ground Excitation (I): Kalman Filtering Approach, The 8th Asian Control Conference (ASCC 2011), Kaohsiung, Taiwan, May15-18, 2011. (Accepted)

[3] C. S. Hsieh, D. C. Liaw and **T. H. Lin**, Optimal Filtering Method to Structural Damage Estimation Under Ground Excitation (II): Constrained Optimization Approach, The 8th Asian Control Conference (ASCC 2011), Kaohsiung, Taiwan, May15-18, 2011. (Accepted)

[4] **T. H. Lin**, S. L. Hung, T. Nagayama andY. Fujino, Study of Energy Harvesting Technology in Structural Health Monitoring, Proceeding of Fifth World Conference on Structural Control and Monitoring, Tokyo, Japan, July 11-13, 2010.

[5] D. C. Liaw, S. L. Hung, Y. H. Hsie, **T. H. Lin** and T. Y. Lu, Developing of Adaptive Wireless Sensor Platform for Structural Health Monitoring , Proceeding of Fifth World Conference on Structural Control and Monitoring, Tokyo, Japan, July 11-13, 2010.

[6] M. R. Yu, R. J. Wu, **T. H. Lin** and S. L. Hung, Application of Semiconductor Type CuO-ZnO Material in Room Working Temperature for Ethanol Sensor, Proceeding of 8th Asian Conference on Chemical Sensors, Daegu, Korea, November 11-14,2009.

[7] S. L. Hung , **T. H. LIN** , and F. QIN, Developing of .NET Based Imote2 Data Logging and Signal Processing System for Wireless Structural Health Monitoring Sensor Networks, Proceeding of Eleventh East Asia-Pacific Conference on Structural Engineering & Construction (EASEC-11), Taipei, TAIWAN, November 19-21, 2008.

[8] S. L. Hung, **T. H. Lin**, D. C. Liaw and Y. H. Hsieh, Study of Wireless Sensor Networks Based Structural Health Monitoring in Buildings and Civil Infrastructures, Proceeding of CACS International Automatic Control Conference, Tainan, Taiwan, November 21-23, 2008.

[9] **T. H. Lin** ,S. L. Hung ,and Q. Fei, "TinyOS Tutorial and Experimental Experience for Applying Wireless Sensor Networks in Civil Engineering", Proceeding of 12th International conference on Computing in Civil and Building Engineering, Bejin, China, October 16-18, 2008.

[10]**T. H. Lin** and S. L. Hung, Pilot Study of Wireless Sensor Platform for Existing Tunnel Environment Monitoring, Proceeding of Computing in Civil Engineering, Pittsburgh, *USA*, July 24-27, 2007.

[11]**T. H. Lin**, S. L. Hung, Development of Wireless Sensor Device for Rapid Deploying in Buildings and Civil Infrastructures, Proceeding of The 3rd International Conference on Structural Health Monitoring of Intelligent Infrastructure, Vancouver, Canada November 13-16, 2007.

[12]**林子軒**、洪士林、溫俊明、洪冠豪、閆世賢，「基於無線感測網路之結構健康監測系統架構與實驗分析」，98 年電子計算機於土木水利工程應用研討會論文集，新竹，台灣，2009 年九月。

[13]廖德誠、洪士林、**林子軒**、王世昌、吳立祥，「應用於土木工程結構健康監測之智慧型無線感應器系統平臺開發」，系統科學與工程會議論文集，宜蘭，台灣，2008 年 6 月。

[14]**林子軒**、洪士林、溫俊明，「案例式推理(Case Based Reasoning)系統於土木工程結構補強之應用」，台灣混凝土學會 2007 年混凝土工程研討會論文集，台北，台灣，2007 年 11 月。

[15]**林子軒**、洪士林、張瀞云，「無線感測網路應用於智慧型建築之防災系統與網路查詢介面之開發」，96 年電子計算機於土木水利工程應用研討會論文集，淡水，台灣，2007 年 9 月。

[16]**林子軒**、洪士林、吳仁彰、陸翔寧、柴梅熙(Murthy)，「無線感測網路應用於醫院建築中麻醉氣體之感測」，96 年電子計算機於土木水利工程應用研討會論文集，淡水，台灣，2007 年 9 月。

[17]柴梅熙、**林子軒**、吳仁彰、黃裕清、陸翔寧、洪士林，"An active 433 MHz-W UHF RF powered chip sensor for wireless monitoring of anesthetic agent Sevoflurane"，中華民國第一屆生醫檢測理論及應用研討會，台中，台灣，2006 年 11 月。

[18]**林子軒**、洪士林，「無線感測網路平台 MICA 於土木工程監測之應用」，第八屆結構工程研討會論文集，南投，台灣，2006 年 9 月。

[19]黃裕清、吳仁彰、**林子軒**、洪士林、柴梅熙(Murthy)、陸翔寧，「導電性高分子應用於麻醉氣體之量測與理論模擬 」，中華民國化學年會論文集，高雄，台灣，2005 年 11 月。

[20]**林子軒**、洪士林，「RFID(Radio Frequency Identification)射頻辨識於土木工程之應用」，九十四年電子計算機於土木水利工程應用研討會論文集，台南，台灣，2005 年 9 月。

[21]洪士林、**林子軒**、史頌恩，「土木結構補強知識管理與支援輔助決策系統之研究」，中華民國第七屆結構工程研討會論文集，桃園，台灣，2004 年 8 月。

[22]李有豐、刁健原、**林子軒**，「碳纖維強化高分子複合材料(CFRP)補強建築物 RC 構件簡易查圖法究」，第六屆結構工程研討會論文集，屏東，台灣，2002 年 8 月。

E.專利

1. 感測及無線傳輸功能之結合件,中華民國新型專利，專利證書號 M319403。
2. 電阻量測式麻醉氣體感測元件及其製造方法,中華民國發明專利,公開號 200823453。